

# **GENERATION AND CHARACTERIZATION OF FREE AND METAL ASSOCIATED AMINO ACID RADICALS IN RIBONUCLEOTIDE REDUCTASE USING EPR TECHNIQUES**

vorgelegt von  
Candidatus Scientiarum  
**Matthias Kolberg**  
aus Sofiemyr, Norwegen

Von der  
Fakultät II – Mathematik und Naturwissenschaften  
der Technischen Universität Berlin  
zur Erlangung des akademischen Grades  
Doktor der Naturwissenschaften  
– Dr. rer. nat. –  
genehmigte Dissertation

Promotionsausschuss:

Vorsitzender:

Berichter:

Berichter:

Tag der mündlichen Prüfung:

Prof. Dr. R. Schomäcker

Prof. Dr. W. Lubitz

Priv.-Doz. Dr. G. Lassmann

24. September 2001

Berlin, 2001

D 83



## **ABSTRACT**

Ribonucleotide reductase (RNR) is responsible for the supply of precursors for DNA in every known organism. The class I RNR's contain a diiron cofactor, which generates a stable tyrosyl radical in the protein subunit R2 upon oxygen activation. During the catalytic turnover in RNR, the tyrosyl radical is postulated to generate a thiyl radical on a cysteine residue at the active site in the protein subunit R1 using a long-range electron-proton transfer chain. So far, no thiyl radical has been detected directly by EPR, neither in RNR, nor in fact, in any other protein.

In this thesis, three methods are described for artificial generation of thiyl radicals in model systems, as well as in R1: (i) photolysis by UV irradiation, (ii) thiol oxidation using cerium(IV), and (iii) visual light photolysis of nitrosylated thiol groups. The radicals generated by UV irradiation of frozen solutions were detected directly by EPR at low temperature, and through the combination of the *g*-tensors and the strongly anisotropic relaxation behavior of the unpaired spin, the presence of thiyl radicals in R1 was confirmed. These are the first EPR characterizations of a non-metal-coupled thiyl radical in a protein. Due to the superposition of several thiyl radicals and *g*-strain, the broad *g*<sub>||</sub> component could be visualized favorably in the absorption display by integration of the first derivative EPR spectrum.

The chemical oxidation of thiols by Ce<sup>IV</sup>/nitrotriacetate (NTA), and laser photolysis of nitric oxide (NO) from nitrosylated cysteines represent two methods for radical generation at room temperature in the liquid state, which may be suitable for RNR activity assays. In both cases, EPR spin trapping using phenyl-N-t-butyl nitron (PBN) and controls with chemically blocked cysteines, have shown that the observed spin adduct originates from thiyl radicals. The EPR lineshape of the protein-bound spin adduct is typical for slow motion of the nitroxide moiety, which indicates that the majority of trapped thiyl radicals are localized in a folded region of R1. In aerobic R1 samples without spin trap that were frozen after treatment with Ce<sup>IV</sup>/NTA or laser photolysis, we observed sulfinyl radicals (R-S<sup>•</sup>=O) which are formed when thiyl radicals react with molecular oxygen. These experiments open the way for detection and characterization of protein-associated thiyl radicals.

The second part of this thesis concerns the characterization of a paramagnetic center in the mutant R2-Y122H of the small RNR subunit. This mutant had been prepared to investigate alternate functions for the oxygen activation reaction of the diiron center by modifying the site of the normal tyrosyl radical. The purified protein contains an unknown unusually stable center with an isotropic EPR signal, termed center H. The *g*-tensor anisotropy of center H was resolved by high-field EPR at W-band. The smallest *g*-tensor value, the temperature dependence, as well as the relaxation behavior, pointed towards a metal-associated paramagnetic center with *S* = ½. From two <sup>57</sup>Fe hfs-tensors observed in both CW and pulsed ENDOR spectra of a sample labeled with <sup>57</sup>Fe, we obtained clear evidence for a diferric system, which however had to be coupled to a third spin to obtain the observed *S* = ½ ground state. From pulsed ENDOR spectra of R2-Y122H labeled with Phe-*d*<sub>8</sub>, we obtained significant evidence for a phenoxyl radical on residue F208. The best spectrum fit was obtained assuming a phenoxyl type radical at the C<sub>4</sub>-carbon of the phenyl ring, like a tyrosyl radical, directly ligated to the iron center. Interestingly, in other R2 mutants, hydroxylation at the C<sub>3</sub>-carbon of F208 has been observed. This is, however, a two-electron oxidation similar to the catalytic hydroxylation activity that is performed by another diiron-oxygen protein, methane monooxygenase (MMO), which can hydroxylate small hydrocarbons, e.g. benzene to phenol *in vivo*. Therefore, the long-lived paramagnetic center H in R2-Y122H, represents a previously not described possibility for such a diiron center since the formation of a phenoxyl radical involves a three-electron oxidation. This work has shown that an introduced perturbation of the surroundings of the diiron center leads to a distinctly new enzymatic function of the diiron center.

## KURZFASSUNG

Ribonukleotid-Reduktase (RNR) ist für die Produktion von DNA-Vorläufern in allen bekannten Organismen verantwortlich. Die RNR-Proteine der Klasse I enthalten einen zweikernigen Eisen-Kofaktor, der nach einer Sauerstoffaktivierung ein stabiles Tyrosinradikal in der Proteinuntereinheit R2 erzeugt. Im Laufe des katalytischen Zyklus ist dieses Tyrosinradikal für die Erzeugung eines Thiylradikals in der Substratbindungstasche der Proteinuntereinheit R1 über eine Elektronen-Protonen-Transferkette verantwortlich. Bis heute wurde protein-assoziierte Thiylradikale weder in R1 noch in anderen Proteinen mit EPR beobachtet.

In dieser Arbeit wurden drei verschiedene Methoden eingesetzt, um Thiylradikale in sowohl R1 als auch Modellsystemen künstlich zu erzeugen: (i) Photolyse durch UV-Bestrahlung, (ii) Thiol-Oxidation mittels  $\text{Ce}^{\text{IV}}$ , und (iii) Photolyse von nitrosylierten Thiolgruppen mit sichtbarem Laser-Licht. Die Radikale, die durch UV-Bestrahlung gefrorene Lösungen erzeugt wurden, wurden direkt mittels EPR bei tiefer Temperatur nachgewiesen, und konnten durch die Kombination der  $g$ -Faktoren und des stark anisotropen Relaxationsverhaltens des ungepaarten Spins, eindeutig identifiziert werden. Es handelt sich hierbei um die erste EPR-Charakterisierung von nicht-metallgekoppelten Thiylradikalen in einem Protein. Aufgrund der Überlagerung mehrerer Thiylradikale und  $g$ -Strain der breiten  $g_{\parallel}$ -Komponente, konnte das EPR-Spektrum am besten im Absorptionsmodus beobachtet werden.

Die chemische Oxidation von Thiole mittels  $\text{Ce}^{\text{IV}}$ / Nitrilotriessigsäure (NTA) oder die Laser-Photolyse von nitrosyliertem Cystein ermöglichen Radikalerzeugung bei Zimmertemperatur in flüssiger Lösung und sind daher für RNR-Aktivitätsstudien geeignet. In beiden Fällen haben EPR Spin-Trap-Versuche mit Phenyl-N-t-Butylnitron (PBN) und Kontrollen mit chemisch blockierten Cysteinen, gezeigt, dass die beobachteten Spinaddukte von Thiylradikalen stammen. Die EPR-Linienform der proteingebundenen Spinaddukten ist typisch für eine langsame Bewegung des Spinaddukts. Dies weist darauf hin, dass die Mehrheit der spingetrapten Thiylradikale sich in den gefalteten, inneren Bereichen von R1 befinden. In aeroben R1-Proben ohne Spintrap, die nach der  $\text{Ce}^{\text{IV}}$ /NTA-Behandlung bzw. Laserphotolyse eingefroren wurden, wurden Sulfinylradikale ( $\text{R-S}^{\bullet}=\text{O}$ ) beobachtet. Sulfinylradikale sind die Reaktionsprodukte von Sauerstoff und Thiylradikalen. Diese Experimente könnten als Grundlage für weitere Untersuchungen von proteinassoziierten Thiylradikalen dienen.

Der zweite Teil dieser Arbeit beschreibt die Charakterisierung eines paramagnetischen Zentrums in der Mutante R2-Y122H des kleinen RNR Protein-Untereinheit. Diese Mutante wurde erzeugt durch eine Modifizierung an der Stelle des normalen Tyrosinradikals, um alternative Funktionen für die Sauerstoffaktivierung des Zwei-Eisen-Zentrums untersuchen. Das isolierte Protein enthält ein neuartiges ungewöhnlich stabiles Radikal mit einem isotropischen EPR-Signal, genannt Zentrum H. Die  $g$ -Tensoranisotropie dieses Zentrums konnte mittels Hochfeld-EPR bei W-Band aufgelöst werden. Die kleinste  $g$ -Tensorkomponente, die Temperaturabhängigkeit, sowie das Relaxationsverhalten deuteten auf ein metallassoziertes paramagnetisches Zentrum mit einem  $S = \frac{1}{2}$  Grundzustand. In CW und Puls-ENDOR-Spektren von  $^{57}\text{Fe}$ -markiertem R2-Y122H, geben die zwei observierten  $^{57}\text{Fe}$ -hfs-Tensoren einen klaren Hinweis auf ein Zwei-Fe<sup>III</sup>-System, das wiederum zu einem dritten Spin gekoppelt sein muss, um einen  $S = \frac{1}{2}$  Grundzustand zu bilden. Die Puls-ENDOR-Spektren von Phe- $d_8$ -markiertem R2-Y122H liefern eindeutige Hinweise, dass dieser dritte Spin ein Phenoxylradikal in der Position F208. Diese Spektren konnten am besten unter der Annahme simuliert werden, dass ein Phenoxylradikal in der *para*-Position des F208-Phenylrings gebildet worden ist. Dies entspricht also einem Tyrosinradikal, das einen direkten Ligand zum Eisenzentrum bildet. Interessanterweise sind Hydroxylierungen in der *meta*-Position von F208 in anderen R2-Mutanten beobachtet worden. Hydroxylierung handelt sich um eine Zwei-Elektronen-Oxidation, ähnlich wie die katalytische Hydroxylierungsaktivität in dem strukturell verwandten Zwei-Eisen-Sauerstoff-Protein, Methan-Monooxygenase (MMO), wo z.B. Benzen in Phenol umgesetzt werden kann. Das langlebige paramagnetische Zentrum H in R2-Y122H stellt eine bislang unbekannte Möglichkeit für die Sauerstoffaktivierung des Zweieisenzentrums dar. Die Erzeugung eines Phenoxylradikals erfolgt durch eine Drei-Elektronen-Oxidation im Gegensatz zu der Hydroxylierungsreaktion in MMO und anderen R2-Mutanten. Wir haben gezeigt, dass die eingeführte Änderung in der Eisenumgebung zu einer neuartigen enzymatischen Funktion des Eisenzentrums geführt hat.

## LIST OF PUBLICATIONS

- [1] Günther Bleifuss, Matthias Kolberg, Stephan Pötsch, Wulf Hofbauer, Wolfgang Lubitz, Astrid Gräslund, Günter Lassmann, and Friedhelm Lendzian (2001) Tryptophan and Tyrosine Radicals in Ribonucleotide Reductase: A Comparative High-Field EPR Study at 94 GHz. *Biochemistry*, *in press*
- [2] Matthias Kolberg, Günther Bleifuss, Stephan Pötsch, Astrid Gräslund, Wolfgang Lubitz, Günter Lassmann, and Friedhelm Lendzian (2000) A New Stable High-Valent Diiron Center in R2 Mutant Y122H of *E. coli* Ribonucleotide Reductase Studied by High-Field EPR and  $^{57}\text{Fe}$ -ENDOR. *J. Am. Chem. Soc.*, **122**, 9856-9857
- [3] Matthias Kolberg, Günther Bleifuss, Britt-Marie Sjöberg, Astrid Gräslund, Wolfgang Lubitz, Friedhelm Lendzian, and Günter Lassmann (2001) Generation and EPR Spin Trapping Detection of Thiyl Radicals in Model Proteins and the R1 Protein of *E. coli* Ribonucleotide Reductase. *Arch. Biochem. Biophys.*, *in press*
- [4] Matthias Kolberg, Günther Bleifuss, Astrid Gräslund, Britt-Marie Sjöberg, Wolfgang Lubitz, Friedhelm Lendzian, and Günter Lassmann (2001) Protein Thiyl Radicals Observed Directly by EPR Spectroscopy. *Submitted to J. Am. Chem. Soc.*
- [5] Günter Lassmann, Friedhelm Lendzian, Stephan Pötsch, Günther Bleifuss, Wulf Hofbauer, Matthias Kolberg, Lars Thelander, Astrid Gräslund, Wolfgang Lubitz (1999) Structure of Tryptophan Radicals in Mutants of Protein R2 of Ribonucleotide Reductase Studied by X-band EPR /ENDOR and by High-Field EPR. *J. Inorg. Biochem.*, **74**, 201
- [6] Günter Lassmann, Friedhelm Lendzian, Matthias Kolberg, Günther Bleifuss, and Wolfgang Lubitz (2000) Spin Trapping of a Protein Thiyl Radical in the Catalytic Subunit R1 of *E. coli* RNR. *Proceedings of the 6<sup>th</sup> International Symposium on Spin Trapping, Aug 27 - 31, Marseille, France*, p 70
- [7] Günter Lassmann, Matthias Kolberg, Günther Bleifuss, Friedhelm Lendzian, Britt-Marie Sjöberg, Astrid Gräslund, and Wolfgang Lubitz (2001) EPR Analysis of Artificially Generated Protein Thiyl Radicals in BSA and R1 Protein of *E. coli* Ribonucleotide Reductase. *Proceedings of the 9<sup>th</sup> Chianti Workshop on Magnetic Resonance, May 26 - Jun 1, Tirrenia (Pisa), Italy*, p 88
- [8] Friedhelm Lendzian, Günther Bleifuss, Matthias Kolberg, Stephan Pötsch, Astrid Gräslund, Wolfgang Lubitz, Günter Lassmann (2000) A New Stable Paramagnetic State of the Di-Iron Diiron Center in Mutant Y122H Ribonucleotide Reductase R2 of *E. coli* Studied by High-Field EPR and  $^{57}\text{Fe}$ -ENDOR. *Proceedings of the 5<sup>th</sup> European Biological Inorganic Chemistry Conference, July 17-20, Toulouse, France*
- [9] Friedhelm Lendzian, Günther Bleifuss, Matthias Kolberg, Stephan Pötsch, Astrid Gräslund, Wolfgang Lubitz, Günter Lassmann (2000) High-Field EPR and  $^{57}\text{Fe}$ -ENDOR on a New Mixed-Valence Di-Iron Center in Mutant Y<sub>122</sub>H Ribonucleotide Reductase R<sub>2</sub> of *E. coli*. *Proceedings of the 30<sup>th</sup> Congress Ampere on Magnetic Resonance and related Phenomena, July 23-28, Lisbon, Portugal*
- [10] Friedhelm Lendzian, Matthias Kolberg, Günther Bleifuss, Günter Lassmann, Astrid Gräslund, and Wolfgang Lubitz, (2001) A Strongly Coupled Diiron/Radical State in Ribonucleotide Reductase Mutant Y122H of *E. coli* Studied by  $^{57}\text{Fe}$ -ENDOR and  $^1\text{H}/^2\text{H}$ -ENDOR. *J. Inorg. Biochem.*, **86**(1), 314

## LECTURES AT CONFERENCES AND FOREIGN UNIVERSITIES

Matthias Kolberg, Günther Bleifuss, Britt-Marie Sjöberg, Astrid Gräslund, Wolfgang Lubitz, Friedhelm Lenzian, and Günter Lassmann

“Artificial Generation of Thiyl Radicals in the R1 Subunit of *E. coli* Class Ia RNR”

Department of Molecular Biology University of Stockholm, Sweden, June 13, 2000.

Matthias Kolberg, Günther Bleifuss, Wolfgang Lubitz, Friedhelm Lenzian, Britt-Marie Sjöberg, Astrid Gräslund, and Günter Lassmann

“EPR of Artificially Generated Protein Thiyl Radicals in Model Proteins and in R1”

Enzymes in Deoxyribonucleotide Synthesis 2000, Engeltofta, Sweden, August 20, 2000.

Matthias Kolberg, Günther Bleifuss, Britt-Marie Sjöberg, Astrid Gräslund, Günter Lassmann, Wolfgang Lubitz, and Friedhelm Lenzian

“EPR and Pulsed ENDOR Characterization of the Stable Paramagnetic Diiron Center H in Mutant R2-Y122H of *E. coli* RNR”

The Annual Iron-Oxygen-Protein TMR Network Meeting, Les Arcs, France, March 5, 2001.

# INDEX

<b>Abstract.....</b>	<b>i</b>
<b>Kurzfassung.....</b>	<b>ii</b>
<b>List of Publications .....</b>	<b>iii</b>
<b>1 Introduction .....</b>	<b>1</b>
1.1 Ribonucleotide Reductase .....	1
1.2 The R1 Subunit- the Active Site of RNR .....	5
1.2.1 The Catalytic Cycle .....	5
1.2.2 Active Thiols in R1 .....	9
1.3 The R2 Subunit – a Diiron and Radical Protein .....	9
1.3.1 Diiron-Oxygen Proteins.....	10
1.3.2 Oxygen Activation of the Iron Center and Generation of the Tyrosyl Radical in R2 .....	12
1.4 Aim .....	15
<b>2 Materials and Methods .....</b>	<b>17</b>
2.1 Preparation of the RNR Proteins .....	17
2.1.1 Over-Expression of RNR in <i>E. coli</i> .....	17
2.1.2 Purification of R1 and R2 .....	19
2.1.3 Activity Assay .....	19
2.1.4 The Azido-CDP Assay .....	20
2.1.5 Dephosphorylation of Azido-CTP .....	21
2.2 Methods Used for Characterization of the R1 Subunit.....	22
2.2.1 Quantification of Protein Thiols .....	22
2.2.2 Thiol Blocking.....	24
2.2.3 Sulfur Centered Radicals .....	24
2.2.4 Generation of Thiyl Radicals By UV Irradiation .....	27
2.2.5 Generation of Thiyl Radicals by Oxidation of Thiols with Cerium(IV) .....	28
2.2.6 Nitrosylation of Thiols.....	28
2.2.7 Photochemical Generation of Thiyl Radicals .....	29
2.2.8 Detection of Thiyl Radicals by Spin Trapping .....	29
2.3 Methods Used for Characterization of the R2 subunit .....	30

2.3.1	Extraction of Iron from R2 .....	30
2.3.2	Reconstitution of the Metal Center .....	31
2.3.3	Redox Chemistry .....	31
2.3.4	Iron Quantification Assay .....	32
2.3.5	Deuterium Exchange .....	33
2.4	Spectroscopic Techniques: EPR/ENDOR .....	33
2.4.1	Theoretical Background for EPR .....	33
2.4.2	EPR .....	38
2.4.3	ENDOR .....	41
2.4.4	Pulsed Davies ENDOR .....	43
<b>3</b>	<b>Artificially Generated Thiyl Radicals in the Catalytic Subunit R1 of RNR .....</b>	<b>45</b>
3.1	Generation of Thiyl Radicals by UV-Irradiation – Direct EPR Detection .....	46
3.1.1	UV Irradiated Cysteine .....	46
3.1.2	UV irradiated BSA and R1 .....	49
3.2	Chemical Generation of Protein-Thiyl Radicals Using Cerium (IV) – Spin Trap Detection .....	52
3.2.1	Thiol Oxidation in Model Systems – Glutathion and BSA .....	55
3.2.2	Thiol Oxidation in Protein R1 .....	55
3.3	Photochemical Generation of Protein-Thiyl Radicals by Light Induced Release of Nitric Oxide from Nitrosothiols – Spin Trap Detection .....	58
3.3.1	Nitrosylation of Protein Thiols .....	59
3.3.2	Laser Photolysis of Nitrosothiols .....	59
3.4	EPR Detection of Thiyl Radical Successors in R1 without Spin Traps .....	61
3.5	EPR Lineshape Analysis .....	63
3.6	Activity Tests of Artificially Generated Thiyl Radicals .....	67
3.6.1	Azido-CDP .....	67
3.6.2	Reverse Radical Transfer .....	71
3.7	Discussion .....	72
<b>4</b>	<b>Stable and Transient Paramagnetic Centers in R2-Y122H .....</b>	<b>77</b>
4.1	The Crystal Structure of R2-Y122H .....	79
4.2	The New Stable Paramagnetic Species – EPR Data of Center H .....	81
4.3	Spectroscopical Characterization of R2-Y122H .....	84
4.3.1	Optical Properties of the Metal Center .....	84
4.3.2	Reduction and Oxidation of the Diiron Center – A Mixed Valence Fe <sup>II</sup> -Fe <sup>III</sup> Center in R2-Y122H .....	86
4.4	EPR and ENDOR Spectroscopical Characterization of Center H in R2-Y122H .....	89
4.4.1	CW EPR on <sup>57</sup> Fe R2-Y122H – Evidence for an Iron Center .....	89
4.4.2	Pulsed and CW ENDOR on <sup>57</sup> Fe R2-Y122H – Evidence for a Diiron Center .....	91
4.4.3	The Spin Density Distribution in Center H .....	93



4.4.4	Pulsed Davies ENDOR on Phe- $d_8$ Labeled R2-Y122H – Evidence for a Ligand Radical on F208.....	94
4.5	Discussion – Possible Mechanisms for the Formation of Center H.....	101
<b>5</b>	<b>Summary and Outlook.....</b>	<b>107</b>
<b>6</b>	<b>Zusammenfassung und Ausblick .....</b>	<b>111</b>
<b>7</b>	<b>Abbreviations .....</b>	<b>117</b>
<b>8</b>	<b>References.....</b>	<b>121</b>
	<b>Acknowledgements .....</b>	<b>133</b>
	<b>Curriculum .....</b>	<b>135</b>

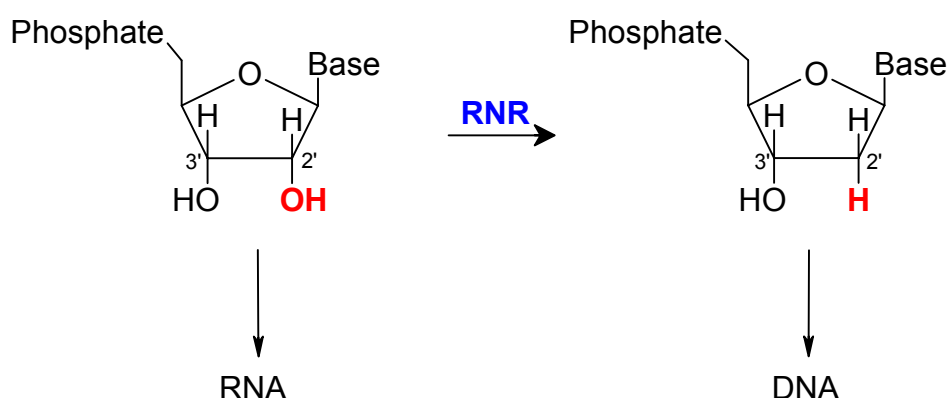


# 1

## INTRODUCTION

### 1.1 RIBONUCLEOTIDE REDUCTASE

Ribonucleotide reductase (RNR) is the enzyme responsible for the conversion of the four standard ribonucleotides – adenosine, cytidine, guanosine, and uridine – to their deoxyribonucleotide counterparts (Scheme 1-1), and thereby provides the precursors needed for both the synthesis and repair of DNA.



**Scheme 1-1 The reduction of a ribonucleotide in RNR**

As all known cellular life-forms store their genetic information as DNA, RNR is likely to be found in all growing cells of every living organism, a fact that has been confirmed by a rapidly increasing number of genomic screenings (Jordan and Reichard, 1998). Even several species of viruses carry their own copy of RNR, probably to ensure faster proliferation in the infected host cell. The reduction of ribonucleotides is the rate-limiting step of DNA synthesis, which makes RNR an important target for cell growth control, and several RNR inhibitors are being used, or have been proposed, as drugs for chemotherapeutic treatment of cancer (Pötsch *et al.*, 1994, Nocentini, 1996) and AIDS (Bianchi *et al.*, 1994). The understanding of the catalytic mechanism of RNR on a molecular level is therefore important for the

development of new strategies in the treatment of cancer, as well as bacterial and viral infections, where the inhibition of cell growth is needed.

The universal requirement for RNR brought up the idea that all RNR's have evolved from a common ancient enzyme leading the way from an early RNA world, in which the relatively unstable RNA polymer was the only existing carrier of genetic information, to the DNA world as we know it today (Reichard, 1997, Stubbe *et al.*, 2001). Several features of the RNR's support this theory. (i) All known RNR's use radical based chemistry to reduce the substrate, including sulfur centered radicals at the active site. (ii) The enzyme is multi-functional accepting all of the four standard ribonucleotides, either as diphosphates, ADP, CDP, GDP, and UDP (NDP's), or in several cases, as triphosphates (NTP's). (iii) The product dUDP (or dUTP) is not a building block for DNA and must be converted to dTTP by a second enzyme called thymidylate synthase, which is also found in all organisms investigated so far. Finally, (iv) the RNR's undergo feedback regulation to ensure that there is always a balanced pool of the four deoxyribonucleotides. Despite these similarities, three different classes of RNR have been found, classified by their different metallic cofactors (see Table 1-1). Many bacteria, e.g. *Escherichia (E.) coli*, can express two or even three different RNR's depending on their current environment, but higher organisms only have class I reductase. The three classes have very little amino acid sequence homology, they have a slightly different allosteric regulation pattern, and they differ in their tolerance for oxygen. While class III is completely inactive in the presence of oxygen, class I requires oxygen for activation. Based on this fact, it is believed that class I could only have evolved after the photosynthetic reactions started to produce an atmosphere with a surplus of oxygen, and is therefore the youngest class. There is, however, still dispute on which one of the two classes, II or III, was the first to evolve.

Class I enzymes are found in practically all eukaryotic organisms, from yeast and algae to plants and mammals, and some prokaryotes and viruses also express this type. Class I can be divided into two subclasses, Ia and Ib, which differ in the number of effector sites reflected in the different overall regulation pattern (see Table 1-1). In *E. coli*, only the class Ia enzyme is expressed under standard aerobic growth conditions, and most of the knowledge on class I RNR's stem from this protein. Class I RNR's are tetrameric ( $\alpha_2\beta_2$ ) enzymes (Sjöberg, 1995); the active site is located in the large  $\alpha_2$ -homodimer called the R1 subunit, and the small  $\beta_2$ -homodimer, called the R2 subunit, harbors one diiron center in each polypeptide chain. After an oxygen dependent activation reaction (see Section 1.3.3), both iron centers are in the  $\mu$ -oxo bridged diferric state, and a stable tyrosyl radical is generated near one of these centers. There is a conserved pathway of hydrogen bonded side chains leading from this tyrosine residue to a cysteine residue at the active site in R1, about 35-40 Å long (see Figure 1-1). The radical character is believed to be transferred from the tyrosine to the cysteine during the catalytic turnover, which is best described as a coupled electron/proton transfer in the opposite direction (Ekberg *et al.*, 1998, Siegbahn *et al.*, 1998, Ehrenberg, 1999). During the substrate turnover, a disulfide bridge that must be reduced before a new substrate can bind is formed at the active site in R1. This is accomplished by the hydrogen

**TABLE 1-1 THE CLASSES OF RIBONUCLEOTIDE REDUCTASE IN OVERVIEW**

	Class Ia	Class Ib	Class II	Class III
Metal cofactor	Fe-O-Fe	Fe-O-Fe	Co	4Fe-4S
Subunit structure	$\alpha_2\beta_2$	$\alpha_2\beta_2$	$\alpha$ or $\alpha_2$	$\alpha_2\beta_2$
Radicals involved in turnover	Tyr, Cys	Tyr, Cys	Cobalamin, Cys	AdoMet, Gly, Cys
Oxygen dependence	Aerobic	Aerobic	No dependency	Anaerobic
Substrates <sup>a</sup>	NDP	NDP	NDP/NTP	NTP
Reductant	Thioredoxin Glutaredoxin	NrdH-redoxin Glutaredoxin	Thioredoxin	Formate
Allosteric sites	2	1	1	2
Occurrence	Eukaryotes  Eubacteria, e.g. <i>Escherichia coli</i>  Bacteriophages  Viruses	Eubacteria	Archaeobacteria  Eubacteria, e.g. <i>Lactobacillus leichmannii</i>	Archaeobacteria  Eubacteria, e.g. <i>Escherichia coli</i>  Bacteriophages

<sup>a</sup> N represents any of the four ribonucleotide bases, A, C, G, or U.

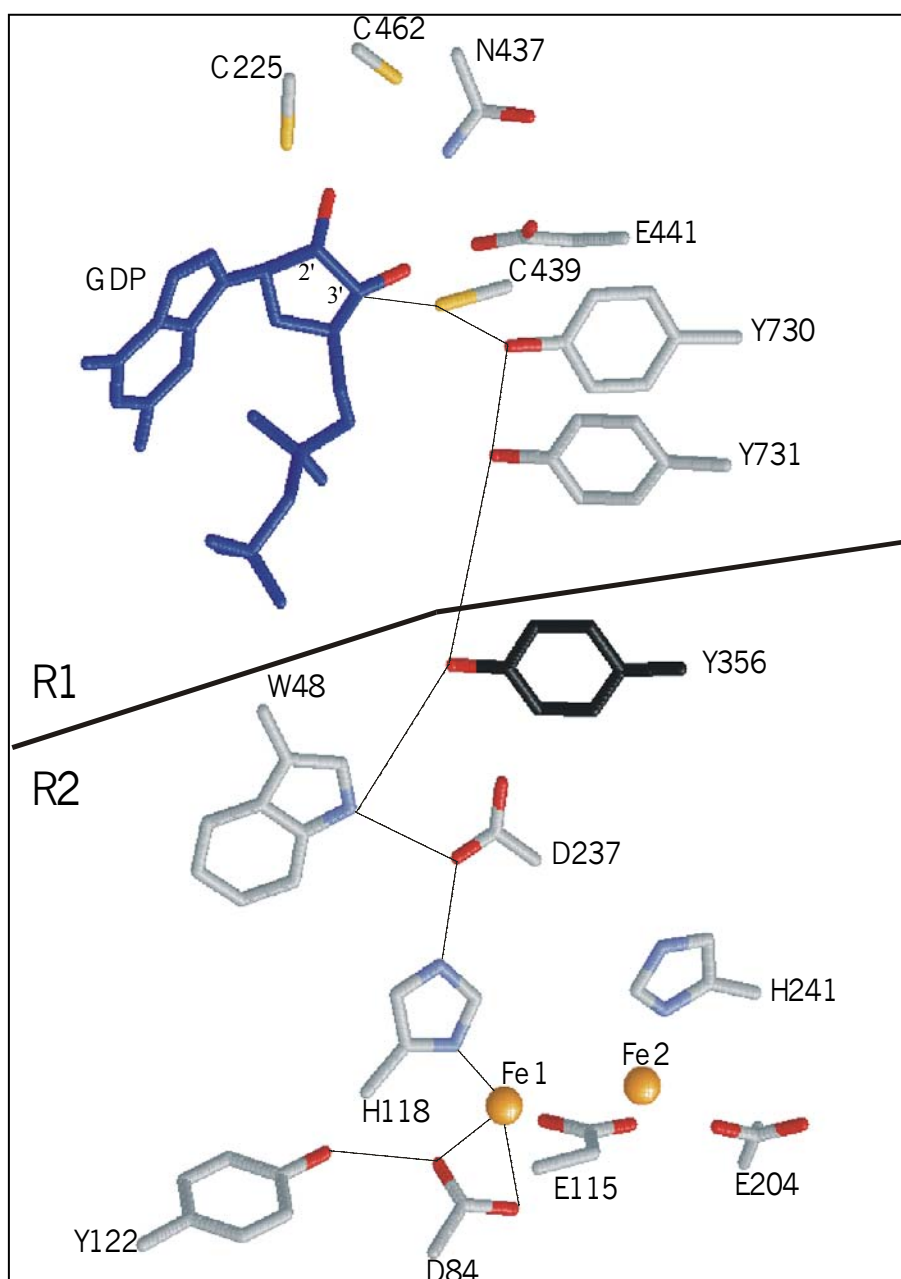


**FIGURE 1-1 THE RADICAL TRANSFER CHAIN IN CLASS I RNR**

*Scheme of the amino acid side chains involved in the radical transfer chain of R1 and R2, which connects the site of the stable tyrosyl radical, Y122, and the substrate binding site with the postulated thiyl radical site C439. The colors indicate the type of atom; oxygen: red, nitrogen: light blue, sulfur: yellow, carbon: light gray, and iron: orange spheres. The substrate GDP is colored blue, with the 2'- and 3'-hydroxyl groups in red. Y356 is not resolved in the crystal structure, and is indicated in the R1/R2 interface in black with the hydroxyl oxygen in red. Coordinates from R1: 4r1r.pdb (Eriksson et al., 1997) and R2: 1rib.pdb (Nordlund et al., 1993).*

donor proteins, thioredoxin or glutaredoxin, via a second disulfide bridge located on the surface of R1. For a detailed description of the two protein subunits, see Sections 1.2 and 1.3 below.

In this work, thiyl radicals in R1 as well as intermediate paramagnetic iron states in a mutant of R2 of the class Ia RNR from *E. coli* will be studied.

## 1.2 THE R1 SUBUNIT- THE ACTIVE SITE OF RNR

The binding and reduction of ribonucleotides in class I RNR takes place on the large subunit, R1, which is a dimer of  $2 \times 85.5$  kDa in *E. coli*. R1 is also the place where the allosteric effectors bind, and it has docking sites for both the small subunit R2 and the small hydrogen donor proteins thioredoxin or glutaredoxin, which are needed for the reduction of the active site disulfide bridges which are generated during the turnover. The crystal structure of the R1 subunit has been resolved with a resolution of 2.5 Å by Uhlin and Eklund, 1994, and later more structures with different substrates and effectors have been published with slightly lower resolution (2.9-3.2 Å) (Eriksson *et al.*, 1997) (see Figure 1-2). The crystal structure in Figure 1-2 is oriented in an angle looking down into the active site cleft of one half of R1 (in white). From this view, the binding of the substrate GDP is clearly visible (stick model in blue). By rotating the structure upwards around a horizontal axis in the paper plane, the active site of the second half of R1 (in yellow) would be visible as well as a GDP molecule coordinated in a complimentary fashion. However, as only one half of R2 is believed to generate a tyrosyl radical (Sjöberg *et al.*, 1987), the turnover in R1 can also only take place on one half, even if the substrate can bind at both halves of R1. The origin of this half-site activity is still unclear, but it is a widespread phenomenon in nature, found in several dimeric enzymes.

As pointed out above, RNR is a multi-substrate enzyme responsible for the conversion of all of the four deoxyribonucleotides needed for the assembly of a DNA chain. In all DNA chains, the total number of each nucleic base is evenly distributed, which requires a balanced supply of dNTP's. This is accomplished through a feedback control mechanism of RNR via two different allosteric effector sites on the R1 subunit, a low affinity so-called activity site that turns the enzyme on and off depending on the level of ATP or dATP in the cell, and a high affinity specificity site that determines which one of the four substrates will bind to the catalytic site (Thelander and Reichard, 1978, Thelander, 1979). An assay of enzyme activity therefore requires the right set of substrate and activators.

### 1.2.1 THE CATALYTIC CYCLE

The triggering of the radical transfer from the tyrosyl radical Y122<sup>•</sup> to the cysteine C439 at the active site of R1 (*E. coli* numbering) is not fully understood, but joining R1 and R2, and binding of the substrate in the reduced form of R1 is essential. A scheme for the catalytic cycle in R1 starting from a thiyl radical at C439 (Figure 1-3) has been proposed by Stubbe and van der Donk, 1998, and is based on experimental data from several biochemical studies, active site mutants, as well as advanced EPR methods. The thiyl radical as a starting point of the catalysis is a

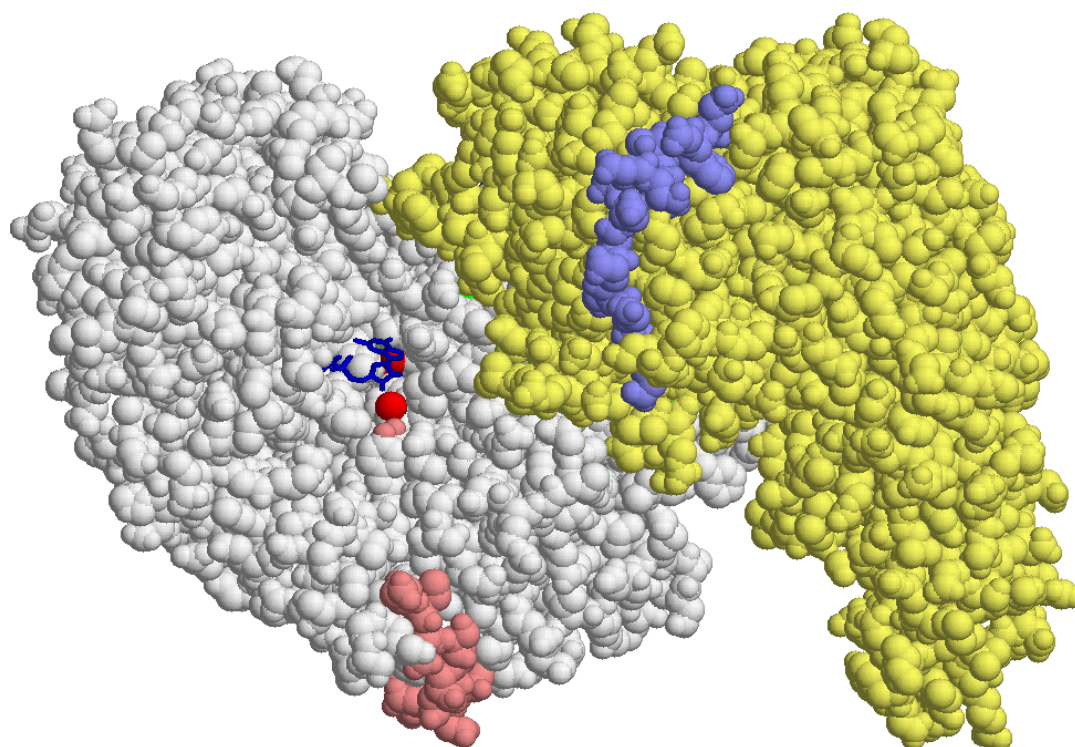


**FIGURE 1-2    STRUCTURE OF THE R1 DIMER SUBUNIT OF RNR**

*The two R1 monomers are colored white and yellow, and the cocrystallized C-terminal peptide of R2 is shown in pink and light blue. A stick model of a GDP substrate (in blue) is bound in the catalytic cleft of both subunits, only one is seen from this view. In this model, all cysteine sulfur atoms are colored red, but only the catalytically active C439 and C225 are visible from the outside in the space filling mode. The C439 is located above and C225 below the GDP in the catalytic cleft. The hydroxyl oxygen atoms of the two tyrosine residues Y730 and Y731 are colored pink as the C-terminal peptide of R2, indicating their role in the radical transfer pathway. This space filling model is based on data from the Brookhaven Databank (4r1r.pdb from Eriksson et al. 1997).*



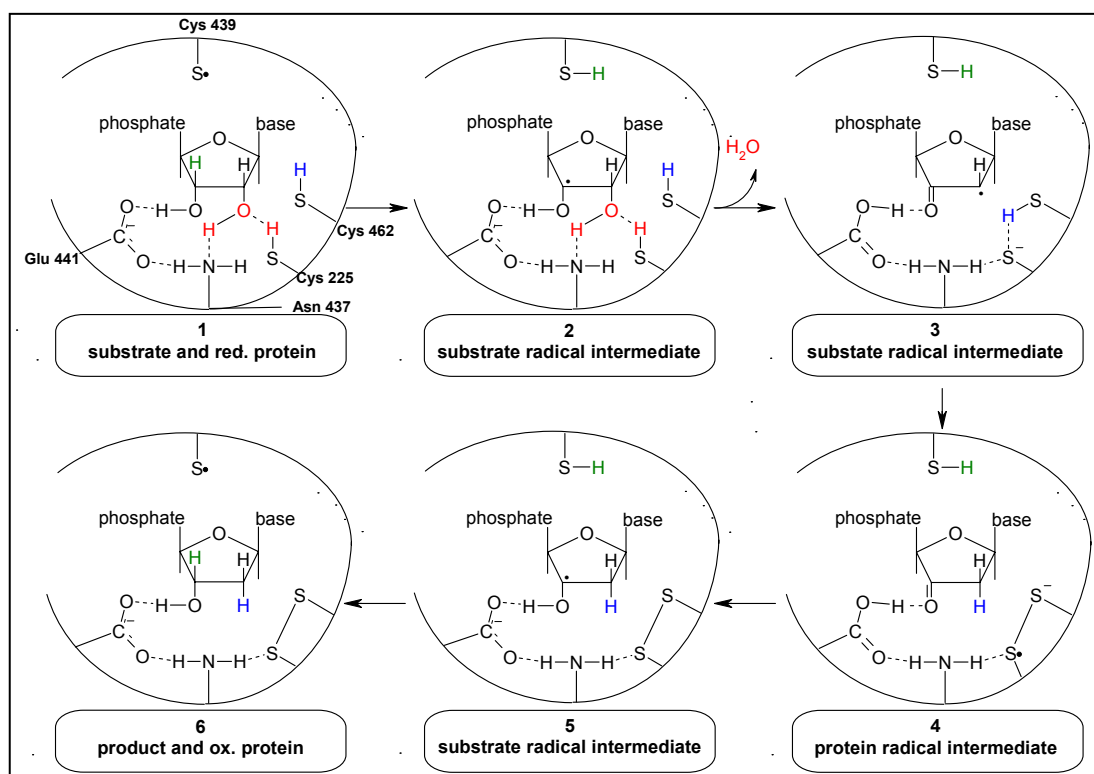


**FIGURE 1-3 THE CATALYTIC CYCLE OF CLASS I RNase H**

*The reduction of a ribonucleotide substrate is postulated to be accompanied by the formation of at least five different transient radical species. Only the protein disulfide anion radical has been observed spectroscopically. See text for details.*

central point of the reaction mechanism. It is believed to be a common feature of all the three known classes of RNR (Stubbe *et al.*, 2001), and theoretical studies confirm its importance (Siegbahn, 1998). It is therefore of great interest to obtain conclusive evidence for the existence of the thiyl radical and its catalytic competence. So far, a thiyl radical has only been observed in the class II RNR from *Lactobacillus leichmannii*, strongly coupled to the cobalt cofactor (Gerfen *et al.*, 1996b), whereas in the class I RNR's from *E. coli* there is no spectroscopic evidence for the existence of a catalytic thiyl radical at C439.

In the first step of the substrate turnover cycle (Figure 1-3), the thiyl radical C439 (state 1) will abstract the 3'-hydrogen from the ribose ring of the substrate and thereby generate a substrate radical (state 2). The abstraction of the 3'-hydrogen has been verified by  $^3\text{H}$ -labeling of a substrate analogue, where a  $^3\text{H}$  label was found on the protein after an interrupted turnover (Stubbe and Ackles, 1980). 3'-Hydrogen abstraction from ribose by thiyl radicals has also been mimicked in model compounds (Lenz and Giese, 1997, Robins and Ewing, 1999). The ribose radical makes the 2'-OH-group more nucleophilic, and abstracts one hydrogen atom from C225 and then leaves as a water molecule. The substrate is thereby converted to a 2' ketyl radical (state 3). The two cysteine residues C225 and C462 are then oxidized to a disulfide anion radical loosing the second hydrogen to the substrate (state 4). This radical was first observed by X-band EPR in an interrupted turnover in the mutant E441Q of R1 (Persson *et al.*, 1997, Persson *et al.*, 1998). These authors recognized the nature of this radical as a sulfur centered species on cysteine, but the position in R1 could not be unambiguously determined due to the overlap of at least two other radical species, namely the bulk tyrosyl radical in R2 and a weak substrate radical signal. Later, the identity as a disulfide anion radical was evidenced by high-field pulsed EPR, where the different radical signals could be isolated based on their different spin relaxation behavior (Lawrence *et al.*, 1999). In the proposed reaction scheme for the wild type, the electron is then transferred via a chain of hydrogen bonded active site residues, including E441, to the substrate 2'- position, thereby generating a substrate radical (state 5) which finally abstracts the hydrogen from C439 and leaves as a deoxyribonucleotide product. For a complete turnover, the C439 thiyl radical regains its hydrogen and the Y122 in R2 its unpaired electron via the radical transfer chain. The disulfide bridge at C225 and C462 is indirectly reduced by NADPH via a cysteine pair at the surface of R1, thioredoxin (or glutaredoxin), and finally the NADPH binding flavoprotein thioredoxin reductase (Holmgren, 1988).

The class II RNR's have a very similar reaction mechanism, including the three active site cysteines (Licht *et al.*, 1996), whereas in the class III RNR's, an equivalent to C462 is missing. This indicates that a disulfide bridge cannot be formed. Instead, a formate ion takes over the function as the hydrogen donor, being reduced to carbon dioxide during the turnover reaction (Eklund and Fontecave, 1999). However, the thiol group carrying the thiyl radical as initiator of the substrate turnover is conserved in all classes of RNR.

### 1.2.2 ACTIVE THIOLS IN R1

The involvement of cysteine residues in the reduction of ribonucleotides was recognized by Thelander, 1974, who showed that one disulfide bridge is formed for each ribonucleotide reduced, and that two ribonucleotides can be reduced by the fully reduced protein in the absence of external reductants, indicating the involvement of two disulfide bridges in the active monomer of R1. Later, these two cysteine pairs were identified by the combination of genomic sequencing (Carlson *et al.*, 1984, Nilsson *et al.*, 1988) thiol-labeling experiments (Lin *et al.*, 1987), site directed mutagenesis (Åberg *et al.*, 1989, Mao *et al.*, 1992a,b,c), and finally the crystal structure (Uhlén and Eklund, 1994). One cysteine pair, C225 and C462, is located at the active site (see Figures 1-1 and 1-3) and the second pair, C754 and C759, is located on the flexible C-terminal tail of R1, and is therefore not resolved in the crystal structure. A model peptide of the C-terminal of R1, including C754 and C759, has been shown to interact with thioredoxin using structure resolving NMR spectroscopy (Berardi *et al.*, 1998).

After the two active site cysteines are oxidized during substrate turnover, the disulfide bridge is transferred to the exposed C-terminal cysteine pair, which in turn can be reduced by external reductants, thioredoxin or glutaredoxin. For *in vitro* experiments, the disulfide bridges can also be reduced by small thiol compounds such as dithiothreitol (DTT), which, however, gives only half of the specific activity (Åberg *et al.*, 1989).

Already at an early stage, it was realized that the well-known tyrosyl radical in R2 could not be directly involved in catalysis, and that a different protein radical at the active site in R1 had to be the one responsible for abstracting the 3' hydrogen from the substrate (Stubbe and Ackles, 1980). The biochemical, structural, and sequence analysis of R1 revealed that this radical had to be positioned on the conserved cysteine residue C439 (Mao *et al.*, 1992a). The crystal structure confirmed its proximity to the expected 3'-position of the substrate (Eriksson *et al.*, 1997) (see Figure 1-1). An active site cysteine complementary to C439 in *E. coli* is also conserved in all the other classes of RNR.

Apart from the active site cysteines, the cysteine C292 is located at the low affinity allosteric site. In the mutant R1-C292A, the activity was reduced with 50 % compared to the wild type using thioredoxin as reductant (Åberg *et al.*, 1989). This can be explained by the distorted binding of the positive effector ATP, but the actual mechanism for the involvement of C292 is still unclear (Ormö *et al.*, 1996).

There are five more cysteines in the *E. coli* R1 protein, which are not conserved and are therefore not believed to be essential for the catalytic function. They must, however, be taken into consideration for the thiol modification experiments described in Section 3 of this thesis.

## 1.3 THE R2 SUBUNIT – A DIIRON AND RADICAL PROTEIN

The R2 subunit of RNR is, analogous to R1, a dimer of two polypeptide chains consisting of 375 amino acid residues in *E. coli*, and adding up to a total mass of 2×43.4 kDa. Each polypeptide chain carries a binuclear iron site coordinated by

histidines and acidic amino acid residues. Similar diiron centers are found in a series of other proteins that are classified as diiron-oxygen proteins. Close to the diiron site, a tyrosine residue carries a stable tyrosyl radical in the active state of R2, independently of the R1 subunit.

The system that is investigated in this thesis is a R2 mutant where the tyrosyl residue Y122 close to the iron site has been modified to histidine. It is therefore of interest to look closer on the different possible actions of the diiron center that are known from the members of the diiron-oxygen protein family.

### 1.3.1 DIIRON-OXYGEN PROTEINS

Proteins carrying iron cofactors are widespread in biological systems, as iron is the most abundant of the transition metal elements in nature. The commonly best known iron proteins are the heme proteins, which are mononuclear iron proteins, e.g. hemoglobin and cytochromes (for a recent review on spectroscopic properties, see Walker, 1999). The iron-sulfur proteins form another large group, where the number of irons in the cluster can vary from two to four, and in some cases even more (reviewed in Johnson, 1998). The small subunit of the class III RNR, with its Fe<sub>4</sub>S<sub>4</sub> cluster, is a member of this family. The R2 subunit of the class I RNR, however, belongs to another distinct protein family, the oxygen bridged binuclear iron, or diiron, proteins. The oxygen bridge can be either an oxo ion, a hydroxo ion, or water, depending on the protein and/or the oxidation state. This group includes several structurally related proteins, but with quite diverse functions (Feig and Lippard, 1994, Andersson and Gräslund, 1995, Kurtz, 1997).

As stated above, the diiron center in the R2 subunit of RNR is responsible for the generation of the essential tyrosyl radical, which is a one electron oxidation; in methanotrophic bacteria, the enzyme methane monooxygenase (MMO) utilizes the diiron site for a two electron oxidation as methane gas is hydroxylized to methanol, which enables the organism to grow with methane as its sole source of carbon and energy; hemerythrin found in marine invertebrates can bind and release O<sub>2</sub> reversibly, and functions as an oxygen carrier protein comparable to hemoglobin in vertebrates; and in stearoyl-acyl carrier protein  $\Delta^9$ -desaturase in higher plants, the diiron site is also involved in a two electron oxidation in which double-bonds are formed in long chain fatty acids.

The functional differences between these proteins, and several other members of this group, can be ascribed to the fine-tuning of the oxygen activation process of the diiron center. The reaction between ferrous iron and oxygen is not a unique reaction for a protein, but the stabilization of high-valence intermediates, and specific oxidation of substrates, can only occur in a highly optimized protein frame. From the different diiron proteins, it is obvious that even very small changes in the iron coordination will have large effects on the outcome of the oxygen activation reaction.

In Figure 1-4, the structures of the reduced and oxidized forms of R2 and the hydroxylase component (MMOH) of methane monooxygenase are presented for comparison. These two proteins both undergo activation by binding of molecular oxygen to the diferrous form, but in MMOH this enables the protein to hydroxylate

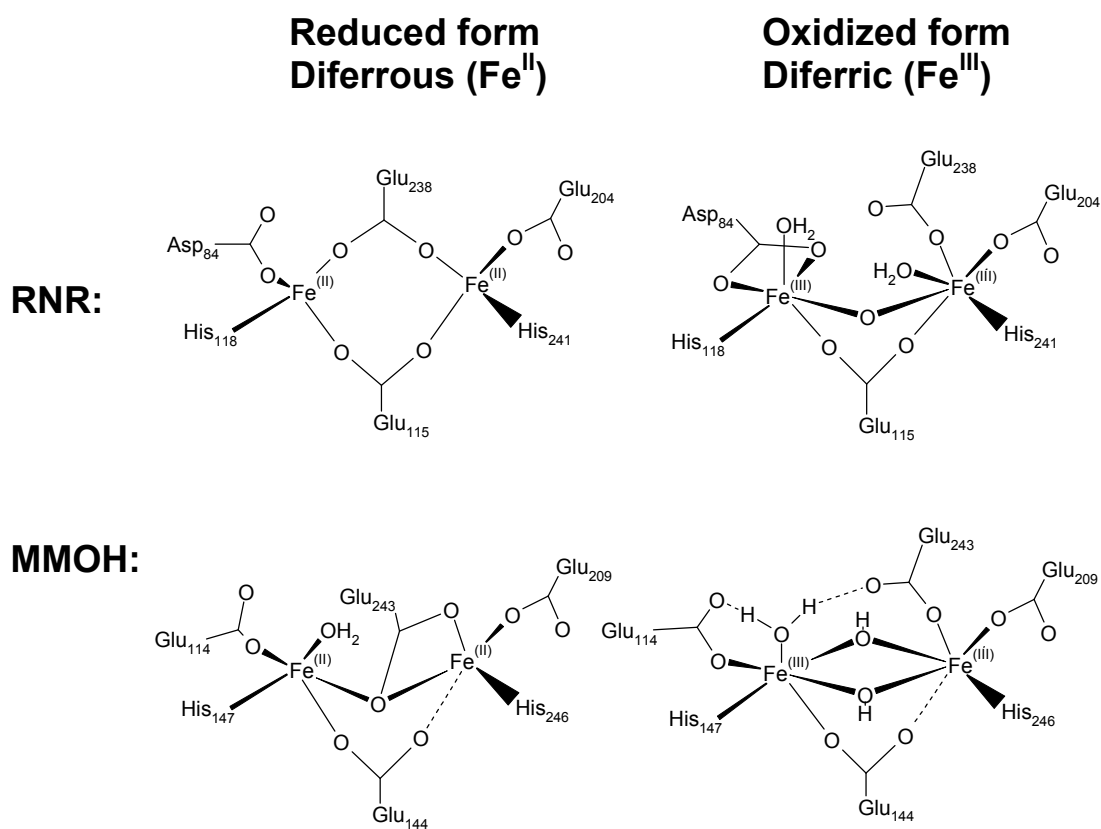


**FIGURE 1-4 THE DIIRON-OXYGEN CENTERS OF RNR R2 AND THE HYDROXYLASE COMPONENT OF METHANE MONOOXYGENASE (MMOH)**

*Comparison of the reduced (left) and oxidized (right) forms of the diiron centers in R2 from *E. coli* RNR (top), and MMOH from *M. trichosporium* OB3b (bottom).*

small hydrocarbons, whereas in R2 a stable tyrosyl radical is formed on the protein itself. The actual amino acid residues involved in the coordination of the diiron center are exactly the same in MMOH and R2, with the exception of the position of aspartate-84 in R2, which is replaced by glutamate-114 in MMOH, both of which are, however, carboxylic side chains. The backbone positions of the amino acids residues are also remarkably similar. In both proteins, the diiron centers are coordinated by the inwards pointing amino acids of a four-helix bundle, and in the oxidized form, the coordination number is six for both irons in both proteins. However, in the R2 protein the diferric irons are  $\mu$ -oxo bridged, whereas they are  $\mu$ -hydroxo bridged in MMOH, and in the reduced form, the ferrous irons of R2 are four coordinated, whereas they are five coordinated in MMOH. There are also some noticeable differences in the oxygen activation reaction, which is described in the following section.

### 1.3.2 OXYGEN ACTIVATION OF THE IRON CENTER AND GENERATION OF THE TYROSYL RADICAL IN R2

The incorporation of iron into the R2 subunit and the oxygen activation *in vivo* is still poorly understood and little data are available. In isolated *E. coli* R2 samples, however, it has been studied in detail. It was shown in a process called the "reconstitution reaction", that adding of a  $6\times$  molar excess of a ferrous iron-ascorbate complex to the apo protein will give the reduced diferrous ( $\text{Fe}^{\text{II}}\text{Fe}^{\text{II}}$ ) form of the diiron center in both subunits (Atkin *et al.*, 1973) (step 1 in Figure 1-5). The diferrous form is stable under anaerobic conditions, which has allowed the growth of crystals suitable for X-ray structure analysis with 1.7 Å resolution (Logan *et al.*, 1996). The ferrous iron atoms have fourfold ligand coordination and they are bridged by two bidentately ligated carboxylates from glutamic acid residues. The intrinsic electron spins of the two irons are antiferromagnetically coupled to a net diamagnetic ground state with  $S = 0$ , which is not observable by EPR. In the diferrous form of mouse R2, however, an integer high spin state,  $S = 2$ , has been observed using parallel mode EPR in the presence of azide which is a small iron ligand (Atta *et al.*, 1996).

If molecular oxygen is allowed to enter the diferrous R2, it will spontaneously oxidize the diiron site through a series of intermediate states, leading to the diferric iron center ( $\text{Fe}^{\text{III}}\text{Fe}^{\text{III}}$ ) and a stable tyrosyl radical (steps 2 to 4 in Figure 1-5). The two oxygen atoms are reduced in a four-electron process from formally  $\text{O}^0$  in molecular oxygen, via an  $\text{O}^-$  peroxy state, to  $\text{O}^{2-}$  as water and the oxid ion in the  $\mu$ -oxo-bridge, respectively. Not all of these intermediates have been observed, but they have been proposed based on analogous activation reaction in other diiron proteins (Solomon *et al.*, 2000, Andersson *et al.*, 1999).

The first step of the oxygen reaction after formation of a short-lived diferrous-oxygen complex ( $\text{Fe}^{\text{II}}\text{Fe}^{\text{II}}/\text{O}^0=\text{O}^0$ ), which has so far not been observed. The oxygen atoms immediately abstract one electron from each iron to form a diferric-peroxy intermediate ( $\text{Fe}^{\text{III}}\text{Fe}^{\text{III}}/\text{O}^-\text{O}^-$ ), which has been observed in MMOH. In the R2 protein, the peroxo intermediate has only been observed in the mutants R2-D84E and R2-W48F/D84E, which thereby has exactly the same iron ligands as MMOH (Bollinger *et al.*, 1998, Moënne-Loccoz *et al.*, 1998).

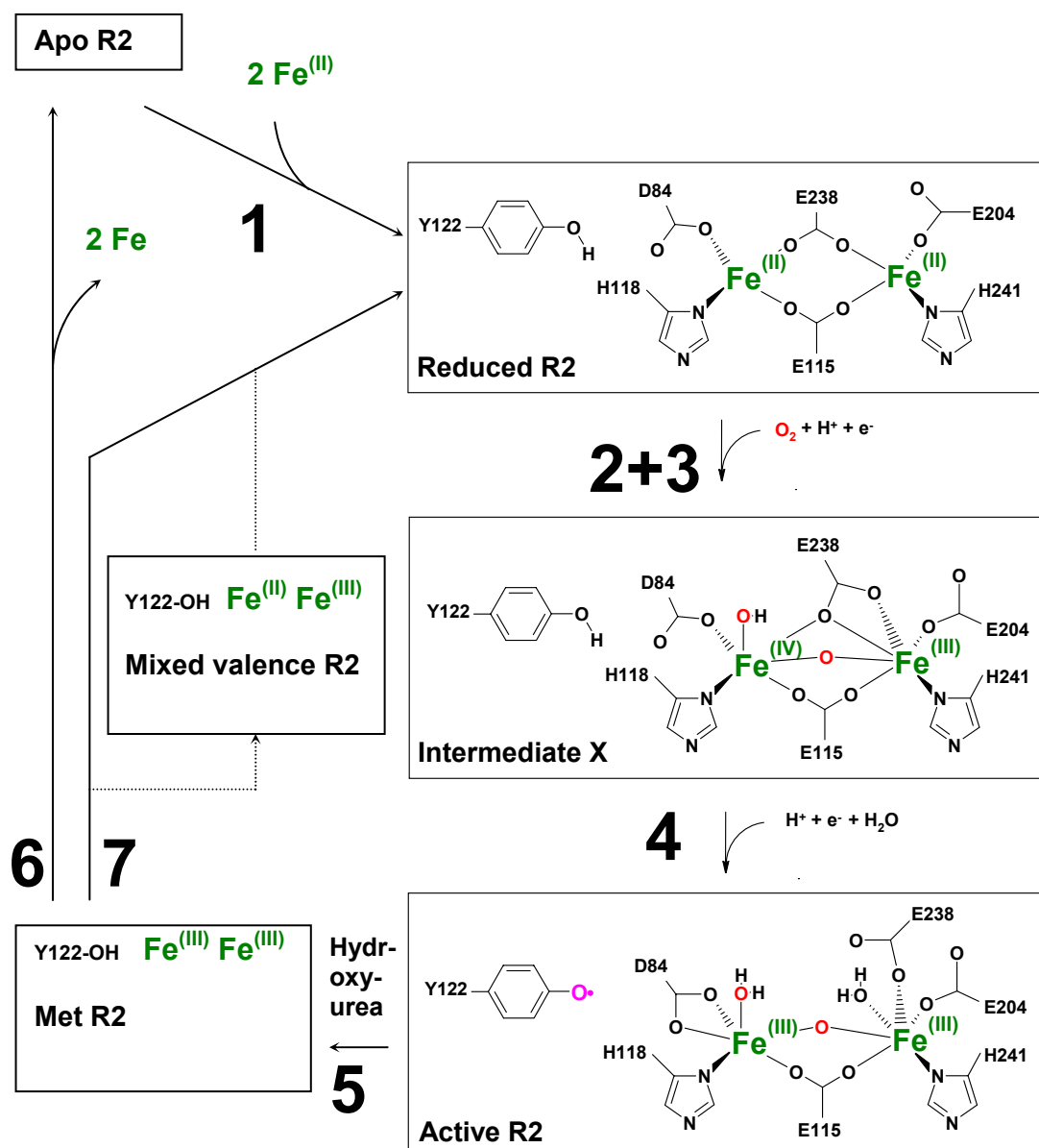


FIGURE 1-5 THE OXYGEN ACTIVATION REACTION PATHWAY IN R2

*Adapted from Andersson et al. 1999. See text for details.*

If the reconstitution reaction is carried out under limiting iron supply (less than 2.4 irons per R2), a distinct intermediate called "U", has been observed in the wild type R2 by its optical absorption band  $\epsilon_{\text{max}}$  at 560 nm (Bollinger *et al.*, 1994b). This intermediate has been shown to be a protonated tryptophan radical on the electron transfer chain residue W48 (Baldwin *et al.*, 2000, Krebs *et al.*, 2001). It is believed that the radical-transfer chain is involved in transporting an electron from the iron site to an externally docked ferrous iron in the medium (Coves *et al.*, 1997), and the tryptophan radical could be an intermediate during this transfer, "waiting" for an external ferrous iron to dock. Another suggestion is that the target for this electron is a ferrous iron in the diiron site of the second dimer half (Miller *et al.*, 1999).

If the reconstitution of apo R2 is performed with excess of iron (more than 5 irons per R2) the lifetime of the intermediate U is too short to be observed (Bollinger *et al.*, 1994b). Instead, its successor called intermediate "X" is observed directly. Intermediate X is formally described as an  $\text{Fe}^{\text{III}}\text{Fe}^{\text{IV}}$  mixed valence state (Sturgeon *et al.*, 1996) (Figure 1-5). At this stage the two oxygen atoms are fully reduced ( $\text{O}^{2-}$ ), having accepted one electron from the  $\text{Fe}^{\text{IV}}$  iron and one from the external source. From EXAFS studies of intermediate X, it has been suggested that the diiron center forms a diamond core with a very short iron-iron distance, 2.5 Å, compared to 3.2-3.4 Å measured for the diferric met R2 form, and 3.4-3.7 for the diferrous reduced form (Riggs-Gelasco *et al.*, 1998). Intermediate X is stable on a few seconds time-scale, and in mutants where the essential tyrosyl is substituted with non-oxidizable amino acids, such as R2-Y122F, the lifetime of intermediate X is doubled, allowing for freeze-quenching and spectroscopic characterization (Bollinger *et al.*, 1991, Bollinger *et al.*, 1994a,b, Ravi *et al.*, 1994, Tong *et al.*, 1996, Burdi *et al.*, 1996, Burdi *et al.*, 1998, Willems *et al.*, 1997, Veselov and Scholes, 1996). These studies suggest that both irons are six-coordinated in intermediate X, one oxygen atom is forming a terminal hydroxo ligand to one iron, whereas the second oxygen atom is engaged in a  $\mu$ -oxo bridge between the irons (Figure 1-5). Due to the mixed valence state, the antiferromagnetically coupled high-spin irons  $\text{Fe}^{\text{III}}$  ( $S = 5/2$ ) and  $\text{Fe}^{\text{IV}}$  ( $S = 2$ ) form an  $S = 1/2$  ground state that is paramagnetic and suitable for EPR characterization. For spectroscopic data, see Section 4. This state is not believed to be significant in the activation of MMOH, but it can be generated by reduction of the  $\text{Fe}^{\text{IV}}\text{Fe}^{\text{IV}}$  intermediate Q (Valentine *et al.*, 1998).

In the final step of the activation process (step 4 in Figure 1-5), the intermediate X oxidizes the nearby tyrosyl residue Y122 to a stable tyrosyl radical, and the iron site is left in a  $\mu$ -oxo bridged diferric form ( $\text{Fe}^{\text{III}}\text{Fe}^{\text{III}}$ ), with a water ligand on both irons. The tyrosyl radical can be observed by optical spectroscopy by a characteristic peak at 410 nm (Petersson *et al.*, 1980), and it can be observed by EPR giving rise to a doublet spectrum with an isotropic  $g$ -value of 2.0047 (Sjöberg *et al.*, 1978), typical for an organic radical, but with a microwave saturation behavior clearly influenced by the nearby diiron site, which leads to fast relaxation. The antiferromagnetically coupled diferric iron center itself is EPR silent, but it gives rise to a characteristic optical spectrum with broad maxima at 325 and 370 nm (Petersson *et al.*, 1980). The total yield of the Y122 radical is often measured to be 1.2 per R2 dimer, i.e. a little more than expected for half site occupancy, the reason for this is still unclear.



In addition to the iron intermediates involved in the reconstitution process (right side of Figure 1-5), two reduced states can also be generated *in vitro*, see Section 2.3. These include the stable inactive met-R2, which is formed by mild reduction using e.g. hydroxyurea (step 5 in Figure 1-5), and an intermediate mixed valence  $\text{Fe}^{\text{II}}\text{Fe}^{\text{III}}$  state, which can be observed during reduction to the diferrous state using e.g. dithionite (step 7 in Figure 1-5) (Atta *et al.*, 1994). In the wild-type *E. coli* R2, this mixed valence state has only been observed after radiolytic reduction (Davydov *et al.*, 1999). The first crystal structure of R2, with 2.2 Å resolution, was obtained from met-R2 (Nordlund and Eklund, 1993), and still, no crystals have been obtained in which the tyrosyl radical is present.

## 1.4 AIM

The goal of the first part of this work was to set up an approach for finding spectroscopic evidence for the catalytic role of the thiyl radical in RNR. So far, there are no EPR spectroscopic data for isolated thiyl radicals in any protein, in general, and particularly in RNR, where they have been postulated to play a catalytic role. Therefore, it was necessary to establish methods for artificial generation and EPR detection of thiyl radicals in the R1 subunit of RNR. To determine under what conditions thiyl radicals are observable by EPR, and to get information about their lifetimes and spectroscopic properties, studies on low molecular weight thiol compounds and model proteins in addition to R1, were indispensable. Direct detection by EPR and characterization of sulfur centered radicals generated by UV-irradiation in R1 and model systems as well as spin trapping of thiyl radicals generated by oxidation with cerium(IV) and photolysis of NO from nitrosylated cysteines is the topic of chapter 3 of this thesis.

The second part of this thesis deals with the characterization of a new, unusually stable, paramagnetic species called center H in the R2 mutant Y122H from *E. coli*. The aim of this work was to determine the nature, electronic structure, and the biochemical mechanism of generation of center H, by combining advanced EPR spectroscopic and biochemical methods, including pulsed ENDOR on selectively isotopic labeled R2-Y122H proteins.

The investigation of this mutant should provide new information on the versatile applications of this type of diiron center, as well as give insight into the fine-tuning of the oxygen activation reaction, which is known from several different proteins with remarkably diverse functions.

Parts of this work were done in close collaboration with Günther Bleifuss, who presented his work in his own doctoral thesis. His work focussed on the spectroscopic techniques and simulations of spectroscopic data.



## 2

# MATERIALS AND METHODS

## 2.1 PREPARATION OF THE RNR PROTEINS

### 2.1.1 OVER-EXPRESSION OF RNR IN *E. COLI*

The bacterial strains used for the over-expression of the ribonucleotide reductase proteins are based on the commercially available *Escherichia coli* strain MC1009 (Amersham Pharmacia Biotech). They were all supplied with a plasmid, pGP1-2, carrying a heat inducible gene for the T7 polymerase (Tabor and Richardson, 1985), and a second plasmid carrying the gene for the protein to be over-expressed attached downstream from a T7 promoter. The two plasmids also carry a kanamycin and ampicillin resistance gene, respectively, to ensure that the bacterium retains both plasmids as long as the medium is supplied with these antibiotics, or their analogues. In the case of the wild-type R1 protein, the second plasmid is called pTB1 carrying the R1 gene *nrda* (Åberg *et al.*, 1989), the R1 mutant R1-C439A was generated by site-directed mutagenesis of the *nrda* gene and the plasmid is referred to as pTB1-C439A (Åberg *et al.*, 1989).

The wild-type R2 producing strain carries the R2 gene *nrdb* in a plasmid called pTB2 (Persson *et al.*, 1996). These three strains were kindly provided to us by Prof. Britt-Marie Sjöberg of the University of Stockholm. The R2 mutant Y122H was also made in her laboratory by Dr. Stephan Pötsch by site directed mutagenesis of the *nrdb* gene using a primer where the codon for Y122 is exchanged for a histidine codon by the method described by Kunkel, 1985. The plasmid is referred to as pTB2-Y122H. As we are expressing *E. coli* genes in *E. coli* bacteria, it should be noted that all preparations of RNR mutants will contain traces of chromosomally encoded wild-type RNR, although usually less than 1 percent.

The standard procedure for the expression of recombinant wild-type proteins R1 and R2, and the mutants R1-C439A and R2-Y122H, was to grow the respective *E. coli* strains in an incubator shaker in 5 l Erlenmeyer flasks with 1.2 l Luria Broth (LB) medium supplied with the plasmid selection antibiotics carbenicillin and kanamycin. Carbenicillin is an ampicillin analogue with higher temperature stability

and is therefore preferred. In some preparations, neomycin was used instead of kanamycin, these antibiotics are degraded by the same resistance gene product and they can therefore replace each other. When the optimal cell density of the bacterial culture is reached, i.e.  $OD_{640nm} = 0.5 - 0.7$ , the temperature is raised from 30 to 42°C to induce the over-expression, as described by Sjöberg *et al.*, 1986. After three hours, when the growth has stopped at an OD of 2.0 to 2.5, the cells are harvested by centrifugation. The yield of cell paste is normally 2-3 g/l. Bacto agar, yeast extract, and bacto tryptone used for the rich growth medium were from Difco Inc. Carbenicillin and kanamycin were from Sigma, neomycin from Roth.

For isotope labeling and preparation of iron depleted apo protein of the R2 protein, the cells were originally grown in an iron free minimal medium as described by Åberg *et al.*, 1993. Later, a minimal medium containing iron was introduced to enable the specific incorporation of iron-56 or iron-57 in the R2-Y122H protein during cell growth. This medium equals the medium described in Åberg *et al.*, 1993, except that the "trace metal solution" containing EDTA complexes of calcium, cobalt, copper, manganese, and zinc, was omitted and substituted with a ferric chloride solution. It was also of interest to reduce the copper signal background of the EPR spectra, which we had found in all earlier preparations from the iron free minimal medium. As the new iron containing minimal medium proved successful, this medium was later also applied for isotopic labeling of specific amino acid residues.

#### Iron Containing Minimal Medium

45 mM	potassium phosphate
7.6 mM	ammonium sulfate
0.61 mM	<i>L</i> -leucine
0.41 mM	magnesium sulfate
5.9 µM	thiamin hydrochloride (vitamin B <sub>1</sub> )
22 mM	glucose (0.4 %)
118 µM	carbenicillin (50 µg/ml)
85 µM	kanamycin (50 µg/ml)
18.5 µM	ferric chloride

The amino acids with stable isotopes, Phe-*d*<sub>5</sub>, Phe-*d*<sub>8</sub>, and their negative control, protonated Phe, were added in 160 µM concentration, and for the global <sup>15</sup>N labeling, 7.6 mM ammonium(<sup>15</sup>N) sulfate was added. The yield of cell paste from the minimal medium was around 1 g/l.

Vitamin B<sub>1</sub>, *L*-leucine, and *L*-phenylalanine were obtained from Sigma, and the inorganic salts and glucose from Merck. The isotope labeled compounds, Phe-*d*<sub>5</sub>, Phe-*d*<sub>8</sub>, and <sup>15</sup>N-ammoniumsulfate were from Isotec. For the growth in <sup>57</sup>Fe enriched medium, 10 mg metallic <sup>57</sup>Fe (95.85% from Chemotrade, Düsseldorf) was dissolved in boiling concentrated hydrochloric acid, and the dry ferric chloride was dissolved in an 8 ml 0.1 M aqueous solution of hydrochloric acid. The iron content in the stock solution was determined to be 18.0 mM by the bathophenanthroline assay (see Section 2.3.4).

### 2.1.2 PURIFICATION OF R1 AND R2

Three different methods were used for cell disruption. The preferred method was to pass the frozen cell pellets through a precooled ( $-70^{\circ}\text{C}$ ) X-Press under high pressure. Alternatively, the pellets were suspended in an equal volume (1 ml/g) of cold buffer, and passed through a French Press three times, or the dissolved cell pellets were pulse-sonified in four volumes of buffer (4 ml/g) for five minutes at maximum output energy using a Branson Sonifier. All methods gave about the same protein yield and specific activity.

The proteins were purified as described by Sjöberg *et al.*, 1986, for the R2 subunit, and Larsson *et al.*, 1988, for R1. The purification steps included streptomycin precipitation of DNA, ammonium sulfate precipitation of the protein, gel filtration on a Sephadex G25 column, ion exchange on a Whatman DE52 column (see refs. for details).

The R2 protein was utilized after the DE52 ion exchange step with a purity of  $> 95\%$  estimated from SDS-PAGE on an Amersham Pharmacia Phast Gradient Gel (10-15 %), using Commassie Brilliant Blue staining (Laemmli, 1970). Before the first gel filtration step, the R2 preparations were provided with an iron(II)/ascorbate solution to ensure a fully developed diiron center in the protein (Atkin *et al.*, 1973). For crystallization, the protein was purified further on a Pharmacia Mono Q or Poros 20HQ ion exchange column, with a 0 – 0.6 M NaCl gradient in 50 mM TrisHCl pH 7.6, and finally a gel filtration step on a Pharmacia Superdex 200.

For the R1 protein, the second ion exchange step, using the POROS 20HQ column, was always performed to remove thioredoxins. Dithiothreitol (DTT) was present during the whole purification process of R1 to keep the thiol groups reduced, which has a stabilizing effect on the specific activity of R1.

Concentration of protein was performed in Amicon 8400 or 8050 stirred ultrafiltration cells with a 30 kDa cut-off membrane under 4 bar argon pressure, and subsequently Amicon Centricon or Microcon cells (30 kDa cut-off for R2, and 50 kDa cut-off for R1). Typical concentrations used for EPR experiments were 0.1 - 0.7 mM R1 and 0.2 - 3.0 mM R2. For ENDOR experiments, only the higher end concentrations were used. The buffer components and salts were obtained from Merck, streptomycin sulfate and DTT were from Fluka and Sigma, respectively.

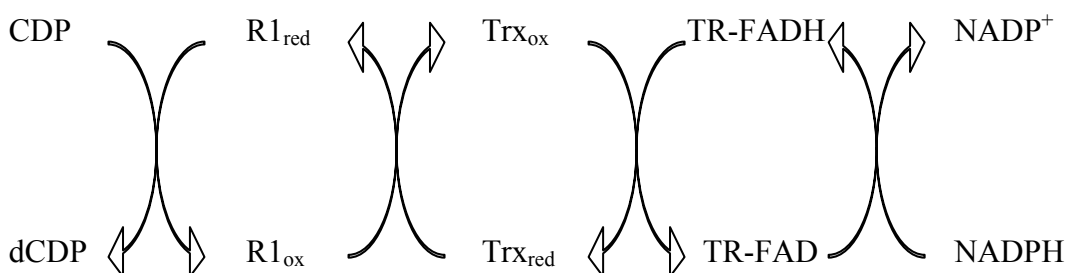
The protein concentrations were calculated from the optical absorption spectra using  $\epsilon_{280-310} = 180.000 \text{ M}^{-1}\text{cm}^{-1}$  and  $\text{MW} = 171.500 \text{ Da}$  for the R1 dimer, and  $\epsilon_{280-310} = 120.000 \text{ M}^{-1}\text{cm}^{-1}$  and  $\text{MW} = 86.800$  for the R2 dimer (Ormö and Sjöberg, 1990)

### 2.1.3 ACTIVITY ASSAY

The substrate turnover in RNR follows the redox-scheme shown below (Scheme 2-1) (Thelander *et al.*, 1976), where one of the four ribonucleotides is reduced to deoxyribonucleotide, in this case CDP is reduced to dCDP. Thereby, the active site cysteines are oxidized into a disulfide bridge, which are reduced by a chain of thiol bridge exchanges starting with an intra-protein exchange to a cysteine pair at the surface of R1. This pair is reduced by a cysteine pair on the multipurpose

protein thioredoxin (Trx), which again is reduced by a flavin (FADH) in the specialized enzyme thioredoxin reductase (TR). The TR flavin is finally reduced by NADPH.

The standard procedure for measuring activity in the RNR components is by mixing a cocktail of all these proteins together with substrate (CDP), allosteric activators (ATP or dTTP, which are activators for pyrimidine reduction), and Mg-acetate, and monitoring the time dependent decay of the optical absorption 340 nm at 25 °C as NADPH is reduced to NADP<sup>+</sup>. For detailed description see (Thelander *et al.*, 1978). To measure activity of R1 a tenfold excess of R2 is added and vice versa.



**Scheme 2-1 The redox scheme of the substrate turnover in RNR**

Thioredoxin and thioredoxin reductase was obtained from IMCO, Stockholm, NADPH, ATP, and dTTP from Sigma. The optical time sweeps were recorded by a Varian Cary 5 UV-Vis-NIR spectrophotometer.

### 2.1.4 THE AZIDO-CDP ASSAY

2'-Azido-2'-deoxycytosine 5'-diphosphate (azido-CDP) is a substrate analogue that allows the triggering of the radical transfer from Y122 in the R2 subunit to the active site of R1, but due to its modified 2'-group the radical state is trapped, thereby destroying the enzyme (Thelander *et al.*, 1976, Salowe *et al.*, 1993). The first steps of this inactivation reaction correspond to the normal turnover reaction (Salowe *et al.*, 1993, Eriksson, 1998): the thiyl radical, C439<sup>•</sup> in R1 abstracts the 3'-H from the ribose of azido-CDP, forming a substrate radical that abstracts an hydrogen atom from C225 (see Section 1.2.1). In the normal case, this hydrogen is taken up by the 2'-hydroxyl group of the substrate, which then leaves as a water molecule. In the case of azido-CDP, the leaving group is the far more unstable HN<sub>3</sub>, which does not leave the active site. By cleaving off N<sub>2</sub> the remaining HN is added on to the protein radical on C225 forming a new relatively stable EPR observable nitrogen centered sulfinylimine radical, R-S-N<sup>•</sup>-H (Salowe *et al.*, 1993). After a few minutes, this radical decays, and the protein is irreversibly inactivated with a covalently bound amino group on C225.

In a standard turnover reaction, no changes in the signal amplitude of the characteristic EPR doublet signal of the tyrosyl radical can be observed. In the case of the substrate analogue reaction with azido-CDP, however, the radical state does not return to Y122 in R2, and R2 is thereby converted to met R2, which is EPR silent. The decay of the tyrosyl radical in R2 and the formation of sulfinylimine radical can be followed kinetically by EPR, and the rate constants indicate that these

processes are correlated (Persson *et al.*, 1997). The azido-CDP assay can therefore be used as a test of the activity of RNR, where the rate constants for tyrosyl radical decay and/or formation of the sulfinylimine radical contain measures of the specific activity of the protein.

When experiments with substrate analogs are performed, the same activators are used as for the standard substrates. Since only single turnovers are possible, the thioredoxin reactivation system can not be used, but the R1 protein must be in the reduced form for successful binding of the substrate. For this reason, DTT is added to the reaction mixture. The assay conditions used were 50  $\mu$ M R1, 50  $\mu$ M R2, 50  $\mu$ M dTTP, 1 mM azido-CDP, 15 mM Mg-acetate, 1.25 mM DTT in 50 mM Tris-HCl pH 7.6. 160  $\mu$ l reaction mix was filled in 4 mm o.d. EPR tubes and frozen after 1 min incubation time at room temperature. Control spectra were made with samples without azido-CDP, which represents the full amount of Y122 $\cdot$  from R2, defining the zero-point of the reaction.

This assay was also used for testing if another substrate analogue 2'-arabino-furanosyl-cytosine 5'-diphosphate (ara-CDP), which is based on a furanose sugar ring with the 2'-hydroxyl group pointing in the opposite direction as in the ribose ring of CDP. This, and other arabinoside compounds are known to inhibit R1 (Ludwig and Follmann, 1978), but so far there were no reports on EPR experiments for detection of intermediate radical formation using this inhibitor.

### 2.1.5 DEPHOSPHORYLATION OF AZIDO-CTP

The 5'-diphosphate form of the 2'-azidonucleotide required for binding to the active site of R1 of class I RNR's, is not commercially available. However, the 5'-triphosphate can be obtained as this compound is also used for labeling experiments of RNA or DNA (i.e. from Trilink Biotechnologies, San Diego, CA).

To cleave of the terminal phosphate group an enzymatic assay was used, based on myosin (Persson *et al.*, 1997). 5 mM Azido-CTP was incubated with 5 mM  $\text{CaCl}_2$  and 0.65  $\mu$ M myosin (65  $\mu$ l/ml) in 50 mM Tris HCl, pH 8.0, for 9 hours at 37°C. The standard assay volume is totally 1 ml. The reaction is stopped by placing the mixture on ice, and then the precipitated calcium phosphate is spun down.

For isolation of the nucleotide, the myosin protein is separated by centrifugation in a Centricon 10 ultrafiltration cell twice for one hour, with addition of 1 ml fresh 50 mM Tris HCl pH 7.6 after the first round.

The protein free filtrate containing the nucleotide (~2 ml) is then frozen in a 15 ml plastic tube placed horizontally, and then freeze dried for about three hours. The dry nucleotide is then dissolved in 1 ml 50 mM Tris HCl pH 7.6. To check the concentration 1  $\mu$ l is transferred to 1 ml 0.01 M HCl in an optical cuvette and the optical absorption at 279 nm is measured.  $\epsilon_{279 \text{ nm (pH 2.0)}} = 13\,700 \text{ M}^{-1}\text{cm}^{-1}$ .

The efficiency of the cleavage reaction is checked by thin layer chromatography (TLC) using PEI-Cellulose F (Merck 5579) as stationary phase and 0.3 M  $(\text{NH}_4)_2\text{CO}_3$  as mobile phase, which performs a good separation of the di- and triphosphates. The separation is detected in UV-illumination. The total yield of diphosphate is normally around 80 %, and the purity close to 100 % (no traces of triphosphates observable on the TLC sheet).

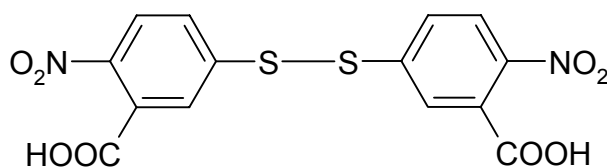
Due to sterical hindrance of the 2'-OH group of 2'-arabino-furanosyl-cytosine 5'-tridiphosphate (ara-CTP), this compound is a very poor substrate for myosin. The ara-CDP therefore had to be synthesized by chemical phosphorylation. The ara-CDP was kindly provided by Dr. von Janta-Lipinski, Max-Delbrück-Center, Berlin.

## 2.2 METHODS USED FOR CHARACTERIZATION OF THE R1 SUBUNIT

### 2.2.1 QUANTIFICATION OF PROTEIN THIOLS

Thiols play an important role in maintaining the appropriate oxidation-reduction state of proteins, cells and organisms. In proteins, thiol groups, also called sulfhydryls, are found on the cysteine residues. Thiols are quite susceptible to oxidation, leading to the formation of disulfides, if another thiol is nearby, or higher oxidation products ( $-SO_x$ ), often with loss of biological activity. Measuring the oxidation state of thiols within living cells is complicated due to the extraordinarily high concentration of reduced glutathione (GSH), a cysteine-containing tripeptide. However, good reagents and methods have been described for the quantitative assay of thiols (and disulfides) *in vitro*.

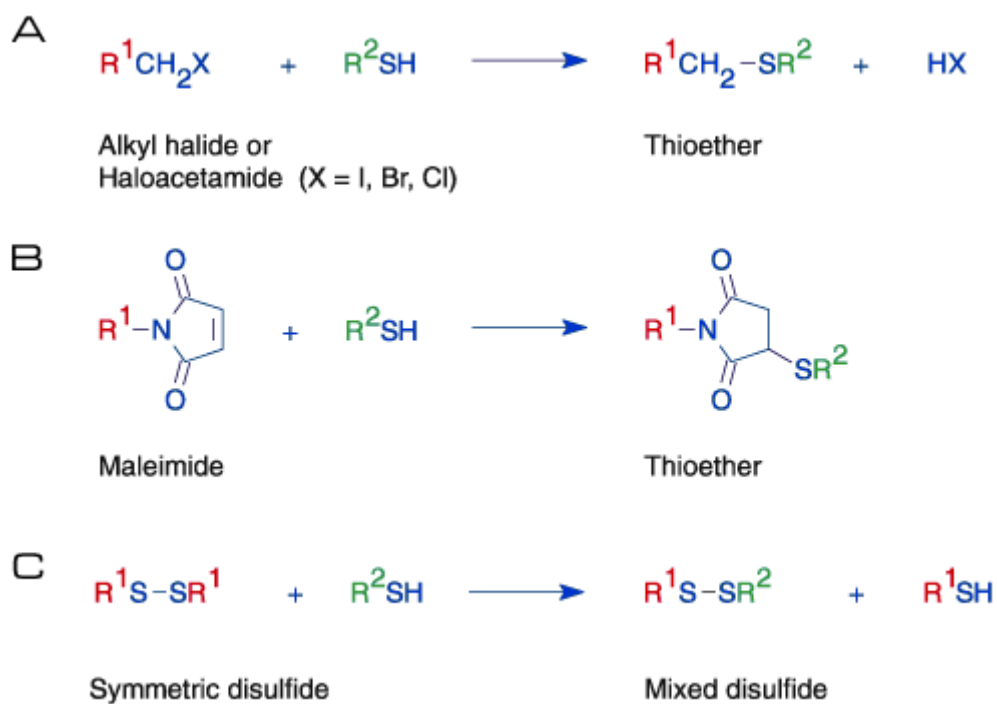
The best established method for thiol quantification is the Ellman assay, which was used in this work for R1 and BSA. The Ellman assay is based on a homodithiol compound called 5,5'-dithiobis(2-nitrobenzoic acid) (DTNB) or simply Ellman's reagent (Scheme 2-2, and Figure 2-1C). When DTNB is allowed to react with a free thiol, its disulfide bond will break, one half will form a heterodisulfide bond, and the remaining second half gives an intense color with absorption maximum at 412 nm,  $\epsilon_{412\text{nm}} = 13.6 \text{ mM}^{-1} \text{ cm}^{-1}$  at pH 8.0 (Ellman, 1959, Krauth-Siegel *et al.*, 1995). This assay will only modify the cysteines that are accessible to the solvent. Inaccessible thiols can usually be quantified by carrying out the titration in the presence of 6 M guanidinium chloride, which unfolds the protein. In an early study, 20 of the totally 22 cysteines in the R1 dimer were recognized at a time where the sequence was still unresolved (Thelander, 1974).



**Scheme 2-2**      **5,5'-Dithiobis(2-nitrobenzoic acid) (DTNB)**

As the dithiol, DTT, is present in the R1 preparations, the samples had to be gel filtrated on a Sephadex G25 column prior to treatment with DTNB. The number of free cysteines in the oxidized R1 was determined after oxidizing the R1 disulfide bridges by incubation under turnover conditions with R2 protein, ATP, CDP, and Mg-acetate, as described by Lin *et al.*, 1987.



**FIGURE 2-1** CHEMICAL BLOCKING AGENTS FOR THIOL GROUPS

Blocking with A) an haloacetamide, B) a maleimide and C) a symmetric disulfide (e.g., DTNB)

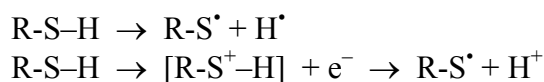
### 2.2.2 THIOL BLOCKING

Chemical blocking of protein thiol groups, i.e. cysteines, can be performed by at least three different groups of molecules. The haloacetamides, especially iodoacetamide, form thioethers by liberating the halide ion (Figure 2-1A). These compounds are however not selective for cysteine as reaction with methionine, histidine can occur. The iodoacetamide is also known to be light sensitive. The maleimides have a higher selectivity for thiols. They also form thioethers by donating a ring electron to the thiol (Figure 2-1B).

The thiol blocking experiments were performed by adding a 40x molar excess, 16 mM to 400  $\mu$ M protein, of either N-ethylmaleimide (NEM) (Torchinski, 1974) or DTNB (see Figure 2-1C, and Scheme 2-2) (Ellman, 1959), both of which bind specifically to free thiol groups and thereby prevent the generation of thiyl radicals. After incubating the protein at 4°C overnight with NEM or 1 hour with DTNB, the solution was gel filtrated to remove excess NEM or DTNB.

### 2.2.3 SULFUR CENTERED RADICALS

Thiyl radicals are generated when a thiol group (R-SH) loses the hydrogen by a homolytical cleavage of the S-H bond, or if the sulfur loses an electron to an oxidant and subsequently the proton:



These two processes are stoichiometrically equivalent and usually hard to distinguish experimentally in aqueous solution since the proton-transfer to water is rapid. The difference of these schemes might well only be defined by the time the electron and the proton are separated. In controlled *in vitro* experiments, however, one can make use of both ways of radical generation, selectively. One-electron oxidation is facilitated by adding a suitable oxidant, and homolytical cleavage can be generated when an energy quantum larger than the dissociation energy for the S-H bond is provided. The energy supplied by a UV lamp (Windle *et al.*, 1964) or a  $\gamma$ -radiation source (Truby, 1962) is sufficiently large for such a cleavage.

There are several problems associated with the EPR detection of thiyl radicals. As expected for a radical, thiyl radicals are highly reactive. Even at low temperatures, the thiyl radicals will combine with nearby molecules and form secondary radicals, or if two radicals combine, diamagnetic molecules. When, for example, a thiyl radical combines with a thiol group it can form a dithiyl radical, RS-S'R', or a perthiyl radical, RS-S', and when oxygen is present, the thiyl radical will be converted into a sulfinyl, sulfonyl, or thiyl peroxy radicals, see Figure 2-2 (Sevilla *et al.*, 1987, Sevilla, *et al.*, 1988). The *g*-values and hyperfine coupling constants of these radicals are known and presented in Table 2-2.

**TABLE 2-1 RANGES OF G-VALUES AND HYPERFINE COUPLINGS OBSERVED FOR SULFUR CENTERED RADICALS AND SULFUR CONTAINING OXO RADICALS**

Radical	Structure	Range of observed g-tensor components			Hyperfine couplings (mT)	Refs.
		$g_x$	$g_y$	$g_z$		
Thiyl	$R-S^\bullet$	2.134 - 2.321	1.99 - 2.03	1.92 - 1.99	1.2-1.6 and 2.8-3.9	b, c, d
Perthiyl	$R-S-S^\bullet$	2.052 - 2.062	2.023 - 2.027	1.998 - 2.006	0.5-1.1	e, f, g
Dithiyl anion	$[R-S-S^\bullet-R']^-$	2.017 - 2.024	2.014 - 2.020	2.002	0.8-1.1	h, i
Sulfinyl	$R-S^\bullet=O$	2.0203	2.0080 - 2.0082	2.0027 - 2.0050	1.4	j, k
Sulfonyl	$R-S=O$   $O^\bullet$		2.0056 <sup>a</sup>			j
Thiyl peroxy	$R-S-O-O^\bullet$	2.0350	2.0090	2.0027	-	l

<sup>a</sup> average g-value. <sup>b</sup> Nelson *et al.*, 1977. <sup>c</sup> Kennedy *et al.*, 1997. <sup>d</sup> Kou and Box, 1976. <sup>e</sup> Bonazzola *et al.*, 1984. <sup>f</sup> Covès *et al.*, 1996. <sup>g</sup> Parast *et al.*, 1995. <sup>h</sup> Lawrence *et al.*, 1999. <sup>i</sup> Rao *et al.*, 1990. <sup>j</sup> Sevilla *et al.*, 1987. <sup>k</sup> Reddy *et al.*, 1998. <sup>l</sup> Sevilla *et al.*, 1988

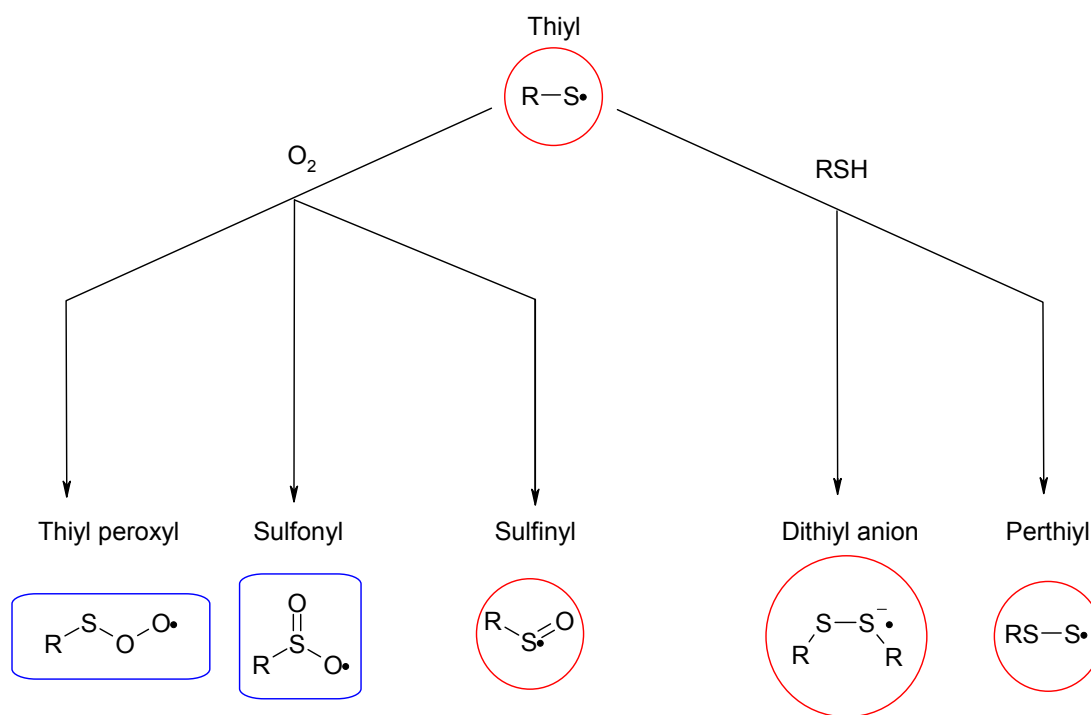


**FIGURE 2-2 FORMATION OF SECONDARY RADICALS FROM THE THIYL RADICAL**

*The blue rounded rectangles indicate oxygen centered radicals, and the red circles sulfur centered radicals*

The detection of thiyl radicals,  $R-S^\bullet$ , by EPR is further complicated by the atomic properties of sulfur. Compared to other elements that are biologically important radical sites, sulfur has a large spin-orbit coupling constant ( $\zeta$ ) (see Section 2.4.1):  $382\text{ cm}^{-1}$ ,  $151\text{ cm}^{-1}$ ,  $76\text{ cm}^{-1}$  and  $28\text{ cm}^{-1}$  for sulfur, oxygen, nitrogen and carbon, respectively (Carrington, A. and McLachlan, D. M., 1969). Accordingly, the thiyl radicals have exceptionally large  $g_{\parallel}$ -values ( $\cong 2.1 - 2.3$ ), oriented along the C-S ( $x$ ) axis. The  $g_{\perp}$ -value of the almost axially symmetric  $g$ -tensor is in the typical range for an organic radical ( $g_{\perp} \cong 2.00$ ). In most cases, however, particularly in disordered systems, i.e. powder or frozen solution, the  $g_{\parallel}$  component is very broad and only detectable if the sulfur atom has a defined H-bond (Nelson and Symons, 1975, Nelson *et al.*, 1977, Becker *et al.*, 1988). The H-bond lifts the degeneracy of the two symmetric lone pair orbitals of sulfur in the  $xy$ -plane, which leads to a reduced  $g$ -strain of the  $g_{\parallel}$ -component making the linewidth narrow enough for detection (Nelson and Symons, 1975, Nelson *et al.*, 1977).

The  $g_x$  shifting of 0.13 of thiyl radicals due to H-bonding effects has also been described for the tyrosyl radical in both photosystem II and R2 of RNR, however, in these cases the shift in the  $g_x$  component is less than 0.01, which can only be resolved by high-field EPR (Un *et al.*, 1996, Ivancich *et al.*, 1999). The direct detectability of thiyl radicals by EPR, therefore, strongly depends on the environment even at low temperature. However, the axial symmetry and the exceptionally large  $g_{\parallel}$  value are "EPR fingerprints", which make the identification of thiyl radicals unambiguous.

Furthermore, the large spin-orbit coupling constant influences the spin-lattice relaxation, i.e. giving a short  $T_1$ , leading to a large linewidth of the EPR spectrum. The linewidth of the thiyl radical is strongly temperature dependent, increasing with increasing temperature, and therefore, thiyl radicals are undetectable directly by EPR in the liquid state at room temperature (Saxeboel and Herskedal, 1975).

Other sulfur-centered radicals with non-axial symmetry, like the perthiyl radical, the disulfide anion radical, and the sulfinyl radical, do not have these restrictions and are easier to detect by EPR. Their rhombic  $g$ -tensor values are characteristic for each of them, and the  $g$ -anisotropy and proton hyperfine splitting are large enough to be resolved even by X-band EPR (see Table 2-1).

#### 2.2.4 GENERATION OF THIYL RADICALS BY UV IRRADIATION

Three methods were used to generate the thiyl radicals. The first method was UV irradiation. UV irradiation induces homolytic cleavage of the S-H group of e.g. cysteine and other thiol compounds (Box *et al.*, 1966). In this work, thiyl radical generation by UV irradiation was performed using a 500 W Hg lamp. An 0.2 - 1 mL sample of cysteine, or the proteins BSA and R1 were made anaerobic in a 3 mL septum sealed vial by repeated argon flushing and evacuation ( $P \geq 0.05\text{ mbar}$ ). Then the sample was transferred to a septum sealed 3 mm I.D. EPR tube using a gastight syringe with a long needle. The sample was frozen in the EPR tube and placed into a "cold finger" transparent quartz dewar filled with liquid nitrogen, which was mounted in the focus of a UV light source, a 500 W mercury lamp. The lamp was equipped with a water filter which removes infra red radiation to prevent heating of

the sample. For irradiation at temperatures below 77 K, the UV lamp was mounted with the light beam directed through the grid of the standard EPR cavity with the focus on the sample inside the quartz helium cryostat. The cryostat is capable of cooling the sample down to ~4 K, and for the experiments described here, the temperature was set to 10 K. The samples were irradiated in four steps and rotated by an angle of 90 degrees between each step. The total irradiation time was varied from 2 to 8 minutes.

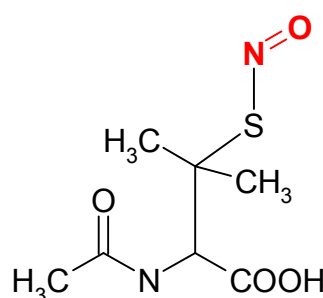
### 2.2.5 GENERATION OF THIYL RADICALS BY OXIDATION OF THIOLS WITH CERIV(IV)

The second method for generation of thiyl radicals was oxidation of cysteine thiols using a cerium( $\text{Ce}^{\text{IV}}$ )/nitrilotriacetate(NTA) complex (Graceffa, 1983, Mullins *et al.*, 1992). To remove the low molecular weight thiol compound DTT, which is present during purification of R1, the protein samples were gel filtrated on a 1 ml Penefsky centrifuged column (Penefsky, 1979) equilibrated with 0.5 M MOPS, pH 7.0 and 1 mM diethylenetriamine pentaacetate (DTPA). DTPA was added in order to chelate traces of transition metals, which may cause radicals from undesired Fenton reaction. To protect the thiyl radicals from oxygen, the protein was collected in a sealable Wheaton vial and deaerated by repeatedly evacuating and argon flushing while stirring gently. Then, an anaerobic spin trap solution (PBN) was added (final conc. 10 mM) and finally an anaerobic  $\text{Ce}^{\text{IV}}$ /NTA solution that was 10-fold the protein concentration. A 250 mM  $\text{Ce}^{\text{IV}}$  stock solution was prepared by dissolving  $\text{Ce}^{\text{IV}}\text{SO}_4 \times 4\text{H}_2\text{O}$  in 0.1 M HCl, from which one volume was transferred into 10 volumes of 50 mM NTA in 0.5 M MOPS, pH 7.0. The NTA was dissolved in NaOH before adding MOPS. After mixing the protein/spin trap solution with the  $\text{Ce}^{\text{IV}}$ /NTA solution anaerobically, the sample was transferred to an EPR flat cell for room temperature measurements, or to a 4 mm o.d. (3 mm i.d.) quartz tube for low temperature measurements. For direct EPR detection of radicals generated by  $\text{Ce}^{\text{IV}}$ /NTA, the spin trap was omitted and the protein/  $\text{Ce}^{\text{IV}}$ /NTA solution was frozen in cold liquid isopentane ( $T \sim 150$  K) 60 seconds after mixing. BSA was prereduced at pH 6.0 with 10 mM DTT in 200 mM potassium phosphate buffer and then desalted over a 1 ml Penefsky column equilibrated with 0.5 M MOPS pH 7.0, 1 mM DTPA. When BSA is reduced by DTT at pH 6.0, only mixed disulfide bridges on C34, that is disulfide bridges involving a low molecular weight thiol and the C34 thiol of BSA, will be reduced, while all the other cysteines in BSA will remain as intra protein disulfide bridges (Katchalski *et al.*, 1957).

### 2.2.6 NITROSYLATION OF THIOLS

The third method for generation of thiyl radicals was photolysis of nitrosothiols (R-S-NO) using a 355 nm laser beam. This method requires a specific nitrosylation of the cysteine residues prior to laser treatment. Nitrosylation of BSA and R1 was performed in 200 mM potassium phosphate buffer pH 8.0 and 0.2 mM EDTA by adding 5-15 molar excess of S-nitrosoacetylpenicillamine (SNAP) (see Scheme 2-3) (Barnett *et al.* 1994). EDTA is added to prevent unspecific cleavage of the S-NO bond by traces of copper or other transition metal ions (Askew *et al.*,

1995). During this transnitrosylation, the local absorption maximum is shifted from 590 (SNAP:  $\epsilon_{590\text{nm}} = 47 \text{ M}^{-1} \text{ cm}^{-1}$ ) to 545 nm (NO-BSA:  $\epsilon_{545\text{nm}} = 15 \text{ M}^{-1} \text{ cm}^{-1}$ ), and can be followed in a spectrophotometer. Both S-NO species have a 70 fold stronger absorption band around 340 nm (SNAP:  $\epsilon_{340\text{nm}} = 3550 \text{ M}^{-1} \text{ cm}^{-1}$ ) which is used for quantifying the degree of nitrosylation after removing SNAP by gel filtration using  $\epsilon_{334\text{nm}} = 870 \text{ M}^{-1} \text{ cm}^{-1}$  for NO-BSA (Meyer *et al.*, 1994); the same value was used for R1. Prior to transnitrosylation, 1 mM BSA was dissolved and reduced in 200 mM potassium phosphate, pH 6.0, and 10 mM DTT, and then desalted by gel filtrating over a 10 ml Pharmacia NAP10 column equilibrated by 200 mM potassium phosphate pH 8.0 and 0.2 mM EDTA. All optical spectra were recorded by a Varian Cary 5 UV-Vis-NIR spectrophotometer.



**Scheme 2-3 S-Nitroso-Acetylpenicillamine(SNAP)**

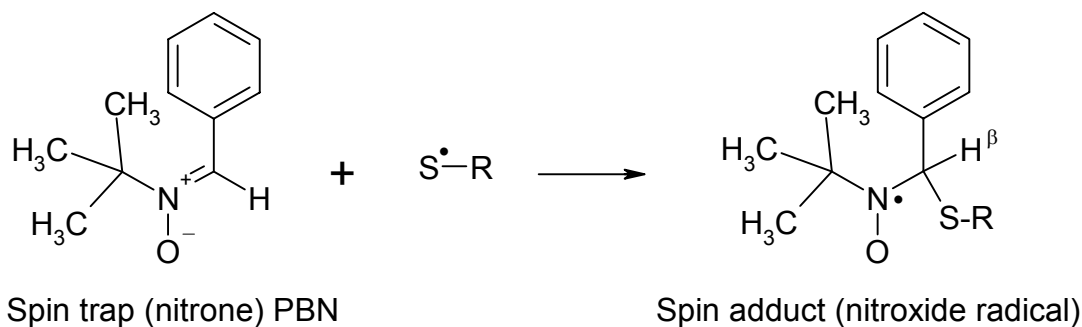
### 2.2.7 PHOTOCHEMICAL GENERATION OF THIYL RADICALS

The cleavage of S-nitrosothiols in GSNO and NO-BSA by light is described in Wood *et al.*, 1996. The photochemical release of nitric oxide and generation of thiyl radicals were performed by illuminating the protein sample using an Nd:YAG laser (GCR 130, Spectra Physics) at 355 nm (100 mJ for each 8 ns pulse). The samples were excited in the liquid state by the unfocussed laser beam (about 8 mm diameter) directed either on an optical cuvette (1 cm optical length), or for EPR, on a flat cell (0.3 mm) for room temperature measurements, or on a 4 mm quartz tube for EPR (3 mm i.d.) for low temperature EPR measurements. For spin trap experiments, 10 mM PBN was added before illuminating the sample. The samples for EPR at low temperature were rapidly frozen (within 2 s) in cold liquid isopentane (150 K) after illumination in the liquid phase.

### 2.2.8 DETECTION OF THIYL RADICALS BY SPIN TRAPPING

Thiyl radicals can be detected indirectly by EPR with high sensitivity at room temperature in the liquid state as spin adducts by addition to a nitron spin traps such as 5,5'-dimethyl-1-pyrroline N-oxide (DMPO) or phenyl-N-t-butyl nitron (PBN) (Büttner, 1987) (see Scheme 2-4). The reaction of a nitron spin trap with R-S<sup>•</sup> leads to a chemical addition at the double bond of the nitron yielding a radical spin adduct, a nitroxide radical, that is a totally different type of radical than thiyl radicals. Nitroxide radicals can easily be detected at room temperature, and they have a lifetime of several minutes, or longer. Due to the hyperfine interaction of a nitrogen,

which has a nuclear spin  $I_{14\text{N}} = 1$ , and in the case of PBN, also a  $\beta$ -proton, which has  $I_{1\text{H}} = 1/2$ , the EPR spectrum of the nitroxide radical has a characteristic hyperfine splitting pattern. The magnitude of the isotropic hyperfine coupling constant of the  $\beta$ -proton can be used to identify the origin of the trapped radical (Buettner, 1987).



#### Scheme 2-4 Spin trapping of a thiyl radical by phenyl-t-butyl-nitrone (PBN)

These spin adducts are stable for minutes, or longer, in liquid solution at room temperature, and there are reports on spin trapped thiyl radicals in proteins (i.e. Graceffa, 1983, Maples *et al.*, 1990). However, by using spin traps the information about  $g$ -values, hyperfine couplings, kinetics, and relaxation of the trapped radical itself is lost.

## 2.3 METHODS USED FOR CHARACTERIZATION OF THE R2 SUBUNIT

The R2 protein can exist in four stable forms, as (i) apo R2, (ii) reduced R2, the diferrous form, (iii) active R2, the diferric form with tyrosyl radical, and (iv) met-R2, the diferric form without radical. In addition, several intermediate states have been observed, like the semimet  $\text{Fe}^{\text{II}}\text{Fe}^{\text{III}}$  form, the high valence intermediate  $\text{X Fe}^{\text{III}}\text{Fe}^{\text{IV}}$ , and the diferric peroxo form. Some of these are shown in Figure 1-5. Here, the apo, diferrous, active, met, and semimet forms of the protein were prepared using the following techniques.

### 2.3.1 EXTRACTION OF IRON FROM R2

Iron free apo R2 can be produced by growing the over-expressing cells in iron-free medium (Åberg *et al.*, 1993), or, starting from active R2, by treating the protein with a strong iron chelator under mildly denaturing conditions (Atkin *et al.*, 1973) (step 6 in Figure 1-5). In that case, the protein is dialyzed against a solution of 0.2 M lithium-8-hydroxyquinoline-5-sulfonate (Li-HQS) and 1.0 M imidazole. This method was also applied for the R2-Y122H mutant, but in this case, the imidazole concentration had to be reduced from 1 M to 0.7 M to prevent irreversible precipitation. After three hours, the protein is removed from the dialysis bag and the hydroxyquinoline complexes and imidazole are removed by gel filtration (Penefsky, 1979).



The remaining iron in the protein in the apo protein was quantified by the bathophenanthroline assay (see Section 2.3.4). The apo R2 produced by both methods, growth in minimal medium and iron chelation, still contain ~0.2 iron ions per R2 dimer, which represents 5% of the maximum amount with fully occupied iron sites, i.e. four iron atoms.

Lithium-8-hydroxyquinoline-5-sulfonate was prepared by dissolving 8-hydroxy-quinoline-5-sulfonate in lithiumhydroxide. The solution was neutralized by adding imidazole. These chemicals were all obtained from Sigma.

### 2.3.2 RECONSTITUTION OF THE METAL CENTER

The diiron center and the tyrosyl radical can be generated from the apo protein by adding 6× excess of ferrous iron complexed with ascorbate to an aerobic protein solution (Atkin *et al.*, 1973). During this reconstitution reaction, a small amount of the transient intermediate X can be observed if the mixture is freeze quenched rapidly after mixing, but to obtain larger amounts of X, the mutant R2-Y122F has proved to be valuable as the lifetime of X is prolonged to 2 min in this case.

The reduced diferrous form of R2 is stable if the iron/ascorbate complex is added anaerobically. The protein solution can be made anaerobic by placing the solution in a septum sealed vial, and repeatedly evacuating the vial and refilling with argon while stirring.

### 2.3.3 REDOX CHEMISTRY

The R2 protein of RNR can be stabilized in several oxidation states of the diiron center and at the tyrosine radical site (see Figure 1-5). The different states can be generated *in vitro* by adding a reductant, or oxidant, and a suitable mediator that can access the interior of the protein (Silva *et al.*, 1995). If the partial concentrations of the reduced and oxidized states can be quantified, the redoxpotential ( $E_0$ ) can be determined from the Nernst equation:

$$E = E_0 + (RT/n\mathcal{F}) \ln [\text{ox}]/[\text{red}]$$

Methods for the determination of midpoint potentials are described in several textbooks (e.g. Clark, 1960, Dutton, 1978).

The met-R2 was generated by selectively reducing the tyrosyl radical of the active form of R2 by adding a 10-fold excess of hydroxyurea (Ehrenberg and Reichard, 1972, Karlsson *et al.*, 1992). The redox potential of hydroxyurea has been determined to be  $E_0' = + 724 \text{ mV}^1$  which is between that of the tyrosyl radical, ( $E_0'' = + 1000 \pm 100 \text{ mV}$ ) and that of the diiron center ( $E_0'' = - 115 \pm 2 \text{ mV}$ ) (Silva *et al.*, 1995). This way, only the tyrosyl radical will be reduced and the diiron center remains in the diferric state.

<sup>1</sup>  $E_0'$  in the standard reduction potential measured vs. the standard hydrogen electrode (SHE) at pH 7.0 and 25 °C,

$E_0''$  in the standard reduction potential measured at pH 7.6 and 4 °C from Silva *et al.*, 1995

By adding stronger reductants, such as dithionite ( $E_0' = -460$  mV) and a redox mediator, even the diiron center will be reduced (Sahlin *et al.*, 1989, Silva *et al.*, 1995). In the wild-type R2 from *E. coli*, the iron center becomes fully reduced to the diferrous form by this treatment, whereas in the mouse R2 and also several *E. coli* R2 mutants, the intermediate paramagnetic mixed-valence  $\text{Fe}^{\text{II}}\text{Fe}^{\text{III}}$  can be observed on a time-scale of several minutes, up to half an hour, due to different accessibility of the two irons (Atta *et al.*, 1994).

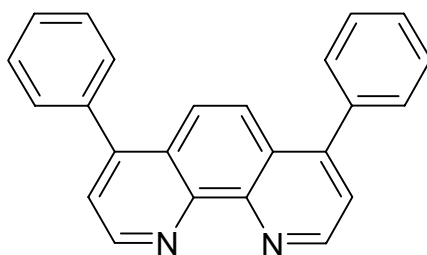
Here, phenazinemethosulfate (PMS) ( $E_0' \sim -270$  mV) was used as mediator, as described in Atta *et al.*, 1994. The reaction conditions for the reduction of R2-Y122H were addition of an equal amount of PMS to R2-Y122H, ranging from 0.2 to 1 mM, and then a four times excess of dithionite. Anaerobic stock solutions of dithionite and PMS were made by adding deaerated, argon saturated buffer to a sealed vial with dry dithionite, or PMS, previously evacuated and refilled with argon gas. The protein solution was deaerated before addition of the reducing agents by repeatedly evacuating and refilling with argon under gentle stirring. The spectroscopic characterization of the mixed valence intermediate of R2-Y122H was performed by freezing the sample within 10 min after addition of dithionite and PMS. The same procedure was also used with ascorbate and PMS as reducing agents.

The active form of R2 was generated from met R2 by adding an excess of hydrogen peroxide ( $E_0' = 1.3$  V), which will regenerate the tyrosyl radical (Fontecave *et al.*, 1990, Sahlin *et al.*, 1990). The standard procedure was to add 10 mM  $\text{H}_2\text{O}_2$  to 1 mM protein. This treatment was also tried out for R2-Y122H, both in the as isolated form, and after prereduction with dithionite/PMS.

Dithionite and 30 % hydrogenperoxide was obtained from Merck, hydroxyurea and phenazinemethosulfate was from Sigma, and the trisodium ascorbate was from Fluka.

### 2.3.4 IRON QUANTIFICATION ASSAY

The total iron content in the R2 proteins was determined by a bathophenanthroline assay described by Massey, 1957. The assay procedure has been modified for the R2 protein by Atkin *et al.*, 1973, and Sahlin *et al.*, 1990, including acid denaturation of R2 and down scaling to 120  $\mu\text{l}$  microcuvettes. Bathophenanthroline, or its water soluble disulfonic acid derivative, is a highly selective photometric reagent for Fe determination (Scheme 2-5), it forms a red complex with ferrous iron in the pH range of 2 to 9 with an extinction coefficient  $\epsilon_{535-650} = 21700 \text{ M}^{-1}\text{cm}^{-1}$ . By the addition of large excess of ascorbate, ferric iron is reduced and can also be accounted for.



Scheme 2-5

Bathophenanthroline

The protein was first denaturated with 0.4 M HCl for 10 min at room temperature. To 50  $\mu$ l of this solution, 45  $\mu$ l water, 19  $\mu$ l 0.1 % bathophenanthroline, 6  $\mu$ l 60 mM sodium ascorbate and 5  $\mu$ l saturated ammoniumacetate is added. The final sample should contain 10 to 300  $\mu$ M iron, i.e. 2.5 to 75  $\mu$ M of active R2 protein with four irons per dimer.

The bathophenanthroline sulfonate was obtained from Sigma, sodium ascorbate was from Fluka, ammonium acetate and hydrochloric acid were from Merck.

### 2.3.5 DEUTERIUM EXCHANGE

To exchange the acidic protons of the R2-Y122H protein with deuterons, the protein was concentrated to 200  $\mu$ l in a Centricon-30 ultrafiltration cell and diluted to 2 ml with deuterium buffer (50 mM Tris DCl, pD 7.6 in D<sub>2</sub>O). After 24 hours at 4 °C, the protein was concentrated again and diluted in fresh deuterium buffer. This procedure was repeated twice, i.e. 72 hours incubation time. The Tris DCl buffer was prepared by freeze drying Tris HCl and dissolving in D<sub>2</sub>O three times. To obtain a pD of 7.6 the pH meter reading was adjusted to 7.2 using 2 M DCl (Glasoe and Long, 1960). The D<sub>2</sub>O (99.8%) was purchased from Isotec.

## 2.4 SPECTROSCOPIC TECHNIQUES: EPR/ENDOR

Electron paramagnetic resonance (EPR), also called electron spin resonance (ESR), is a powerful, selective, and sensitive tool for studying systems with unpaired electrons, e.g. radicals and paramagnetic transition metals. Stable paramagnetic centers and transient radical species play functionally important roles in several biological systems, where they can be found involved in enzymatic reactions and single electron transfer reactions, e.g. in metallo-proteins. With EPR spectroscopy, detailed information about the nature, location, and the electronic structure ( $g$  and  $hfs$ ) and electrostatic environment (H-bonds) of the unpaired spin can be obtained, and thereby contribute to the understanding of the biological function mechanism of the protein (Pilbrow and Hanson, 1993). As ribonucleotide reductase contains an iron center, a stable protein radical, an electron transfer pathway, and a catalytic reaction involving transient substrate and protein radicals, this enzyme is an ideal object for EPR studies (Gräslund and Sahlin, 1996). It has therefore often been used as a model system for pioneering spectroscopical analysis (e.g. Bar *et al.*, 2001).

### 2.4.1 THEORETICAL BACKGROUND FOR EPR

Electron paramagnetic resonance spectroscopy is based on the interaction of the magnetic dipole moment of an unpaired electron with an external magnetic field. This interaction is called the Zeeman-interaction, which results in a splitting of the energy level of the electron spin ( $S$ ) into two different levels given by the magnetic spin quantum number ( $m_S = \pm 1/2$ ) (Figure 2-3). The energy difference ( $\Delta E$ ) between these levels is in the microwave region (e.g. the X- or W-band) and is proportional to the magnitude of the external magnetic field ( $B_0$ ),

$$\Delta E = g \beta B_0 \quad (2.1)$$

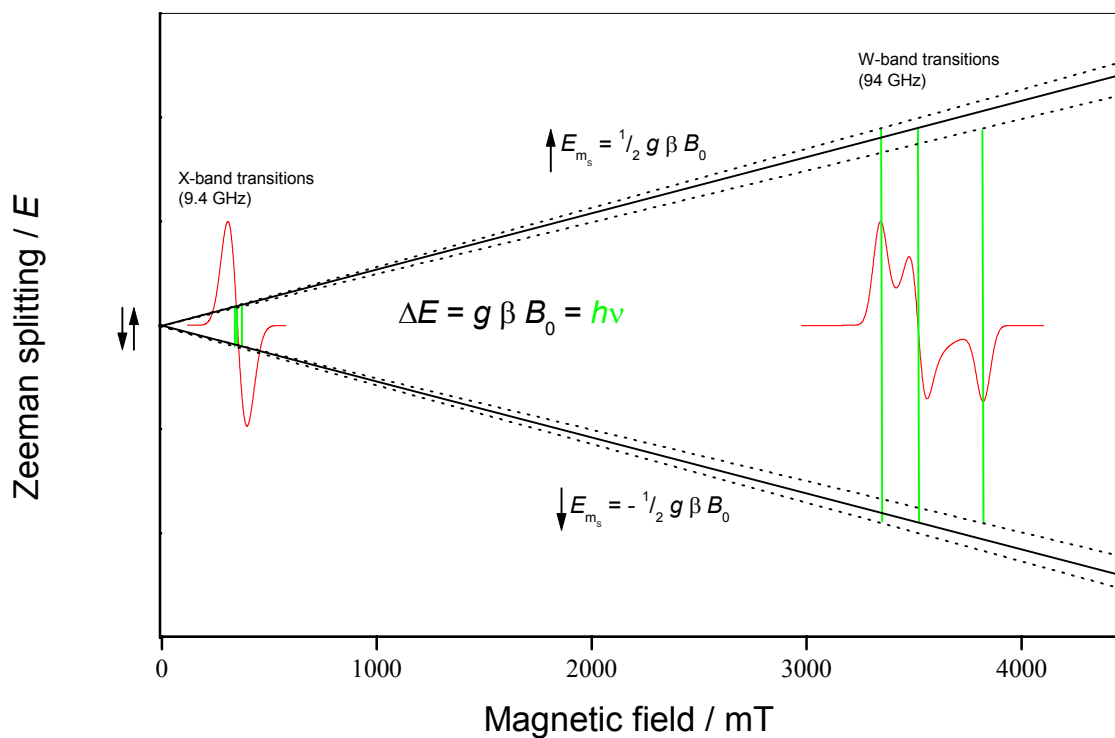


**FIGURE 2-3 MAGNETIC FIELD DEPENDENCY OF THE G-TENSOR ANISOTROPY**

*Schematic diagram showing the Zeeman effect. At zero field, the two energy levels of an electron spin (indicated by arrows up and down) have the same energy, unless they are influenced by a closely located second spin giving rise to zero-field splitting. When a magnetic field is applied, these levels are split. If the environment of the spin is anisotropic, each orientation will have slightly different splitting giving rise to a splitting of the three spatial g-tensor components.*

*The EPR spectra in this diagram are stretched out along the field axis for clarity.*

where  $\beta$  is the Bohr magneton and  $g$  is a proportionality factor that is characteristic for the paramagnetic species and its surroundings. For a free electron the  $g$  factor,  $g_e$ , is 2.002319 (Atherton, 1993). The number of spins ( $N$ ) in the upper, excited, and lower, ground state level is depending on the temperature ( $T$ ), according to the Boltzmann factor:

$$N_{\text{Upper}}/N_{\text{Lower}} = e^{-\Delta E / kT} \quad (2.2)$$

When a sample is exposed to microwave energy, i.e.

$$g \beta B_0 = h\nu \quad (2.3)$$

where  $h$  is the Planck constant and  $\nu$  is the frequency of the microwave field, transitions between the two energy levels are induced (see Figure 2-3).

In a molecule, the unpaired electron spin occupies an orbital and will interact with spins from other closely surrounded electrons and nuclei. These interactions will lead to further splitting of the energy levels (see Figure 2-4), and the different types of interactions can be expressed as distinct terms in the spin hamiltonian ( $\mathcal{H}$ ), from which the spin energy levels can be obtained:

$$\mathcal{H} = \mathcal{H}_{\text{EZ}} + \mathcal{H}_{\text{HF}} + \mathcal{H}_{\text{NZ}} + \mathcal{H}_{\text{Q}} \quad (2.4)$$

The *electron-Zeeman* term describes the interaction between the electron spin operator ( $\mathbf{S}$ ) and the applied external magnetic field vector ( $\mathbf{B}_0$ ).

$$\mathcal{H}_{\text{EZ}} = g \beta \mathbf{B}_0 \mathbf{S} \quad (2.5)$$

Here, the  $g$ -value is the observable, and any deviations from  $g_e$  results from the so-called spin-orbit coupling between the unpaired spin ( $\mathbf{S}$ ) and the orbital angular momentum ( $\mathbf{L}$ ). This coupling can be described by the Hamiltonian

$$\mathcal{H} = \lambda \mathbf{L} \mathbf{S} \quad (2.6)$$

where  $\lambda$  is called the spin-orbit coupling constant, sometimes termed as  $\zeta$  ( $= 2S \lambda$ ).  $\lambda$  is constant for a particular shell in a particular atom, increasing sharply with the atomic mass (Atherton, 1993). The spin orbit coupling is influenced by the admixture of other orbitals, e.g. lone pair orbitals, to the singly occupied orbital. For organic radicals on carbon or oxygen the spin-orbit coupling is usually small and therefore the  $g$  anisotropy is small, as in the oxygen centered tyrosyl radical Y122\* in RNR R2 where the  $g$ -anisotropy is not resolved in the X-band EPR spectrum (Sjöberg *et al.*, 1978). Sulfur is located beneath oxygen in the periodic table, and the orbitals have similar orientations, however, due to the larger mass, the larger  $\lambda$  leads to larger  $g$  anisotropy. In transition metals, the low energy separation between the partly filled  $d$ -orbitals can lead to even larger deviations from  $g_e$ .

However, perturbations of the lone pair orbitals of the oxygen due to H-bonding, will lead shifts of the  $g$ -components (Burghaus *et al.*, 1993).

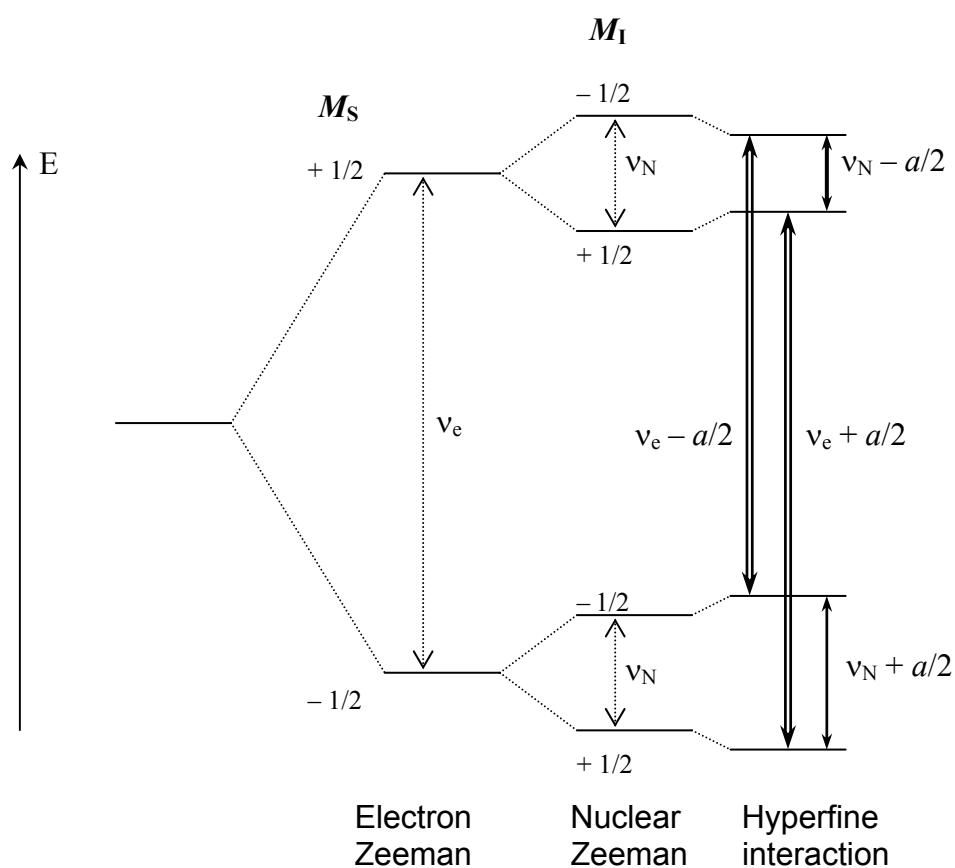


**FIGURE 2-4 ENERGY LEVEL DIAGRAM OF HYPERFINE INTERACTIONS ON A SYSTEM WITH ONE UNPAIRED ELECTRON AND ONE NUCLEUS WITH  $I = 1/2$  AND  $a_{\text{ISO}} > 0$ ,  $a_{\text{ISO}}/2 < \nu_N$**

*In an applied magnetic field, the Zeeman interactions lead to a splitting of the energy levels of both the electron spin and nuclear spin, where  $\nu_e \gg \nu_N$  (marked with dashed arrows). The EPR transitions ( $\nu_e \pm a/2$ ) are indicated by double line arrows, and the ENDOR transitions ( $\nu_N \pm a/2$ ) by single line arrows.*

*Hyperfine interactions* are the interactions between the magnetic moment of the electron spin and the magnetic moment of a nucleus in the vicinity. A prerequisite for hyperfine interactions is that the nuclear spin ( $I$ ) of these nuclei is different from zero, which is the case for protons ( $^1\text{H}$ ), nitrogen ( $^{14}\text{N}$ ), and phosphorus ( $^{31}\text{P}$ ) in unlabeled biological samples, as well as for certain transition metals like copper ( $^{63}\text{Cu}/^{65}\text{Cu}$ ) and manganese ( $^{55}\text{Mn}$ ), and others. The specific incorporation of stable isotopes, like  $^2\text{H}$ ,  $^{13}\text{C}$ ,  $^{15}\text{N}$ ,  $^{17}\text{O}$ , and  $^{57}\text{Fe}$  is therefore a useful approach in the EPR and ENDOR analysis to identify the nature of a paramagnetic center.

In an EPR spectrum, the hyperfine interactions give rise to resolved splitting of the EPR line into  $2I + 1$  lines (see Figure 2-4 for the  $I = \frac{1}{2}$  case). However, in cases where the EPR linewidth is large, e.g. due to a fast spin relaxation (see Section 2.4.2), or if many nuclei contribute to the EPR line, the hyperfine interaction is often not resolved. Here, ENDOR spectroscopy is the preferred method to determine the hyperfine couplings, see Section 2.4.3.

The hyperfine interactions between the electron spin momentum ( $\mu_e$ ) and the nuclear spin momentum ( $\mu_N$ ) are expressed by the Spin Hamiltonian

$$\mathcal{H}_{\text{HF}} = -8\pi/3 \mu_e \mu_N \delta(\mathbf{r}) + 1/r^3 [ \mu_e \mu_N - 3/r^2 (\mu_e \mathbf{r})(\mu_N \mathbf{r}) ] \quad (2.7)$$

where ( $\mathbf{r}$ ) is the distance vector between the two spins and  $\delta(\mathbf{r})$  is the spin density a distance  $r$  from the nucleus. This interaction can also be expressed by

$$\mathcal{H}_{\text{HF}} = \mathbf{S} \mathbf{A} \mathbf{I} \quad (2.8)$$

containing the vector operators  $\mathbf{S}$  for the electron spin and  $\mathbf{I}$  the nuclear spin, and the hyperfine coupling (hfc) tensor  $\mathbf{A}$ . The hfc tensor can be separated into an isotropic hfc constant ( $a_{\text{iso}}$ ) and the anisotropic hfc tensor ( $\mathbf{A}'$ )

$$\mathcal{H}_{\text{HF}} = a_{\text{iso}} \mathbf{S} \mathbf{I} + \mathbf{S} \mathbf{A}' \mathbf{I} \quad (2.9)$$

The isotropic term, also called the Fermi contact term, accounts for the interaction between the nucleus and the unpaired electron spin density contribution with  $r = 0$ , i.e. the  $s$ -orbital contribution. The energy of the isotropic hyperfine interaction is given by

$$E_{\text{HFiso}} = -8/r^3 |\psi(0)|^2 \langle \mu_e \mu_N \rangle \quad (2.10)$$

where  $|\psi(0)|^2$  is the probability for the unpaired electron to be located at a distance  $r = 0$  from the nucleus.

The anisotropic term, sums up the orientation dependent interactions, and contains information about the distance and angle between the unpaired electron spin and the nuclear spin. For purely dipolar interactions, i.e. when  $r$  is large, the energy of the anisotropic hyperfine interactions can be simplified to the following expression

$$E_{\text{HFdipolar}} = -1/r^3 (\mu_e \mu_N) (3 \cos^2 \gamma - 1) \quad (2.11)$$

where  $\gamma$  is defined as the angle between the axis between the electron magnetic moment ( $\mu_e$ ) and nuclear magnetic moment ( $\mu_N$ ), and the external field axis ( $\mathbf{B}_0$ ), and  $r$  is the distance between the electron and nuclear spins (Bertini and Luchinat, 1996).

Analogous to the electron spins, *Nuclear-Zeeman interactions* split the energy of nuclear spins ( $I \neq 0$ ) into two levels when a magnetic field is applied, which is also the basis for performing NMR experiments. This interaction can be expressed in a similar fashion as the electron Zeeman interaction by using a nuclear magneton constant  $\beta_N$  and a nuclear  $g_N$  tensor for the nuclear spin operator ( $\mathbf{I}$ )

$$\mathcal{H}_{\text{NZ}} = -g_N \beta_N \mathbf{B}_0 \mathbf{I} \quad (2.12)$$

Since the charge of the nucleus is opposite of the electron, this term is given a negative sign. The nuclear-Zeeman interactions apply for the same elements as the hyperfine interactions, and their contributions are often in the same order of magnitude (see Figure 2-4).

The *nuclear quadrupole* term is only relevant for nuclei with a spin  $I \geq 1$ , typically  $^{14}\text{N}$  in biological samples, or  $^2\text{H}$  in labeled samples. These nuclei have a non-spherical distribution of their nuclear charge namely a so-called electric quadrupole moment ( $Q$ ) which interacts with the electric field gradient generated by all the electrons and nuclei surrounding the nucleus. The Hamilton term for the quadrupole interaction is

$$\mathcal{H}_Q = \mathbf{I} \mathbf{Q} \mathbf{I} \quad (2.13)$$

where  $\mathbf{Q}$  is the quadrupole tensor.

### 2.4.2 EPR

A continuous wave (CW) EPR spectrum is obtained by placing a sample in a microwave resonator where it is exposed to constant, instrument specific, microwave radiation, as well as a variable magnetic field, which in most cases is oriented perpendicular to the magnetic microwave field component. A net absorption of microwave energy due to induced spin transitions will occur as long as the spin population in the ground state level is higher than in the excited level. The EPR signal is recorded using field modulation and phase sensitive detection, which results in a first derivative absorption spectrum.

In an applied magnetic field, the electron populations in the excited and ground energy levels are given by the temperature dependent Boltzman distribution, with the highest population in the ground state level (see above). When extra energy is fed into the system by microwave radiation, transitions between the levels are



induced, disturbing the equilibrium. The absorption of the microwave energy by the electron spins is the basis for the EPR signal.

There are two distinct mechanisms involved in the spin *relaxation*, spin-lattice relaxation (longitudinal relaxation) and spin-spin relaxation (transversal relaxation), which are measured by the two relaxation times  $T_1$  and  $T_2$ , respectively. The magnitude of  $T_1$  increases with lower temperature, however, the relation between these parameters vary for different spin systems and is most prominent for transition metals. The spin-spin relaxation describes the dephasing of the spins in the plane that is perpendicular to the microwave field, and the energy is kept in the system, whereas spin-lattice relaxation leads to a net loss of energy. The magnitude of  $T_1$  and  $T_2$  is characteristic for the environment of the electron, which means that different paramagnetic species can be differentiated not only by their  $g$ -values, but also by their different relaxation behavior. The *linewidth* of the EPR line is also dependent on the magnitude of  $T_1$  and  $T_2$ . If  $T_2 \gg T_1$ , the spin dephasing (spin-spin relaxation) can be neglected, which leads to a narrow Lorentzian shaped EPR line. The linewidth is, however, also influenced by unresolved hfs as well as hfs- and  $g$ -anisotropy and  $g$ -strain, which cause inhomogeneous line broadening (see below).

As long as the population in the ground state is higher than in the excited level, a net absorption of microwave energy will occur, proportional to the square root of the applied microwave power. However, as more power is used, the spin system will approach a situation where the populations of the two levels are equal, the system is then said to be saturated. The microwave power needed for *half-saturation*,  $P_{1/2}$ , is a temperature dependent characteristic quantity for the paramagnetic species. This constant can be determined from a semiempirical formula (Ohnishi, 1987):

$$\frac{I}{\sqrt{P}} = \frac{\frac{I_0}{\sqrt{P_0}}}{\left(1 + \frac{P}{P_{1/2}}\right)^{b/2}} \quad (2.14)$$

where  $I$  is the EPR signal intensity,  $P$  the power of the applied microwave, and  $b$  an empirical inhomogeneity parameter.  $I_0/(P_0)^{1/2}$  is a the constant ratio at non-saturating conditions. When the signal intensity,  $I$ , is measured as the area of the EPR absorption spectrum,  $b$  can take values ranging between the extremes 1 and 2, or, if  $I$  is measured as the amplitude of the first derivative EPR spectrum,  $b$  can take values ranging between 1 and 3 (Sahlin *et al.*, 1986). The magnitude of  $b$  depends on the spin relaxation mechanism, which is described by  $T_1$  and  $T_2$ . If  $T_2 \gg T_1$ , i.e. the system has mainly spin-lattice relaxation and the EPR spectrum has a Lorentzian shape, the microwave power dependent line broadening is homogeneous, which gives  $b$  the maximum value, 2 (or 3 for a first derivative spectrum). On the other hand, if  $T_2 \approx T_1$ , i.e. the spin-spin and spin-lattice relaxation contribute equally and the EPR lineshape is Gaussian, the line broadening is inhomogeneous, which gives the minimum value,  $b = 1$  (Sahlin *et al.*, 1986). In exchange coupled systems, e.g. dinuclear iron centers, the  $T_2$  can become very small. Therefore, if the power

saturation curve can only be fitted using a value of  $b$  that is smaller than 1, this is diagnostic for an exchange coupled system (Galli *et al.*, 1996).

The estimation of  $P_{1/2}$  from mathematical simulation of power saturation data using the formula above, therefore, requires knowledge of the spin relaxation mechanism, due to the large variations in the inhomogeneity parameter  $b$ .

Of the spin Hamiltonian terms listed in Section 2.4.1, only the electron and nuclear Zeeman terms scale with the magnetic field, whereas the hyperfine, quadrupole, and zero-field splitting terms can be regarded as field independent. This means that by enhancing the *microwave frequency* band, where a higher magnetic field strength is required for fulfilling the resonance condition, the resolution of the spectrum will be improved due to increased  $g$ -anisotropy (Figure 2-3). Due to instrumental reasons, EPR experiments are carried out by using distinct constant energy sources in the microwave region (e.g. X-band 9.5 GHz, Q-band 35 GHz, or W-band 95 GHz). For a free electron, which has an isotropic  $g$  value of 2.00232 ( $g_e$ ), the resonance condition is fulfilled at a magnetic field strength of about 350 mT at X-band, and 3500 mT in W-band with the 10-fold higher microwave frequency. At higher frequencies, anisotropic  $g$ -components are more separated, and therefore hyperfine and quadrupole interactions on the individual  $g$ -components are better resolved.

Another large advantage of going to higher frequencies, using standard cylindrical cavities, is that the sensitive sample volume is scaled down, due to the shorter wavelength of the microwave. The X-band wavelength is about 30 mm and the typical sample volume is ~100-200  $\mu$ l, whereas the W-band wavelength is 3 mm, and thus, less than 1  $\mu$ l sample volume can be used. This is a large benefit for biological protein samples where the preparations often give low yields, and in particular, the small sample volume allows the analysis of protein single crystals as they are used also for X-ray diffraction studies.

The *signal intensity*, or the integral of the EPR absorption spectrum, is proportional to the number of spins in the sample, and can therefore be used as estimation for the concentration of the paramagnetic species (Aasa and Vänngård, 1975). However, due to baseline errors, and sample filling factors, the error of this quantitation method is 5-10 %, or more, when the integral absorption of the unknown sample is compared with that of a sample of known spin concentration, measured under exactly the same, non-saturating, conditions. In this work, 0.2 mM Cu(II)ClO<sub>4</sub> or 0.33 mM TEMPOL were used as reference samples.

The X-band EPR measurements were performed on a Bruker ESP 300E Spectrometer equipped with a 9.7 GHz microwave bridge. The exact microwave frequency was monitored by a Hewlett-Packard 5352B microwave frequency counter. The sample was placed in a standard rectangular cavity, Bruker ER 4102 ST TE<sub>102</sub>. The magnet used was a Bruker E25 electromagnet capable of generating fields from 5 to 1400 mT. For low temperature measurements, the sample was kept at a constant temperature between 4 and ~120 K by using an ESR900 helium Flow cryostat from Oxford Instruments, monitored by an ITC4 temperature controller. The

temperature setting at the actual helium flow was calibrated by a thermocouple against a reference of liquid nitrogen.

The low temperature samples were filled into 4 mm o.d. (3 mm i.d.) quartz EPR tubes and frozen in liquid nitrogen or cold isopentane ( $\sim 150$  K) prior to the EPR measurement. The room temperature EPR spectra of aqueous solutions were recorded on samples in 200  $\mu$ l quartz flat cells of 0.3 mm thickness.

The W-band EPR measurements were performed on a Bruker Elexsys ESP 680E Spectrometer with a 9 GHz microwave source that is mixed with 84 GHz to obtain 94 GHz. The superconducting split-coil magnet can reach up to 6000 mT, but for our measurements only 60 mT sweeps around 3500 mT were performed, using the room temperature coils ("persistent mode"). The samples were filled in 0.7 mm i.d. quartz tubes. All W-band measurements were performed at low temperature, from 10 to 80 K using a helium flow cryostat.

For the determination of  $g$ -values, the resonance field positions in both X- and W-band EPR were calibrated using a standard reference sample with a known  $g$ -value, Li:LiF, ( $g = 2.002293$  (Stesmans and van Gorp, 1989)).

### 2.4.3 ENDOR

Electron nuclear double resonance (ENDOR) spectroscopy is a combined EPR and NMR experiment, hence double resonance, where the EPR transitions are saturated by microwave power and NMR transitions of the nuclear spins ( $I$ ) are induced by a radio frequency source (Feher, 1956). This method is used to get a better resolution of the hyperfine interactions between the unpaired electron in a radical or metal center and the surrounding atomic nuclei that have nuclear spin (Table 2-2). By monitoring the intensity of the saturated EPR line at a fixed microwave frequency and magnetic field, and then sweeping the radio frequency to induce nuclear spin transitions, only the nuclear spin excitation that are in coupling distance of the electron spin will be observed, in contrast to an NMR experiment.

The Hamilton operator for an ENDOR experiment is reduced to include only the nuclear terms (see Section 2.4.1):

$$\mathcal{H} = \mathcal{H}_{\text{HF}} + \mathcal{H}_{\text{NZ}} + \mathcal{H}_{\text{Q}} = \hat{\mathbf{S}} \mathbf{A} \hat{\mathbf{I}} - g_{\text{N}} \beta_{\text{N}} \mathbf{B}_0 \hat{\mathbf{I}} + \hat{\mathbf{I}} \mathbf{Q} \hat{\mathbf{I}} \quad (2.15)$$

and since the magnetic field is kept at a constant value, the nuclear-Zeeman term is also constant. The resonance frequency for the nucleus at the given magnetic field strength can thus be calculated. This frequency is called the Zeeman frequency, or Larmor frequency  $\nu_{\text{N}}$  (see Table 2-2). The resonance condition, the observed ENDOR frequency, is

$$\nu_{\text{ENDOR}} = | \nu_{\text{N}} \pm A/2 | \quad (2.16)$$

if we consider a simple case with only one  $I = 1/2$  nucleus, thus having no quadrupole splitting, and the position of the ENDOR lines depends only on the magnitude of the hyperfine coupling tensor,  $A$  ( $= |\mathbf{A}|$ ).

Based on the first order perturbation theory, if the Larmor frequency is larger than  $A/2$ , which is often the case for protons, the ENDOR transitions will appear at

$$\nu_{\text{ENDOR}} = \nu_{\text{N}} + A/2 \quad (2.17)$$

and

$$\nu_{\text{ENDOR}} = \nu_{\text{N}} - A/2 \quad (2.18)$$

If, on the other hand,  $A/2$  is larger than the Larmor frequency, which is the case if there is a large coupling on nitrogen or  $^{57}\text{Fe}$

$$\nu_{\text{ENDOR}} = A/2 + \nu_{\text{N}} \quad (2.19)$$

and

$$\nu_{\text{ENDOR}} = A/2 - \nu_{\text{N}} \quad (2.20)$$

In the case of an anisotropic hyperfine tensor in a powder, the two symmetrical lines will be replaced by a broader structure, which shows narrow features at the positions corresponding to the three principal values of the tensor in the first derivative spectrum

$$|\mathbf{A}| = A_x + A_y + A_z \quad (2.21)$$

**TABLE 2-2** SELECTED ENDOR NUCLEI WITH RESPECTIVE NUCLEAR SPIN,  $g_{\text{N}}$ , AND LARMOR FREQUENCY

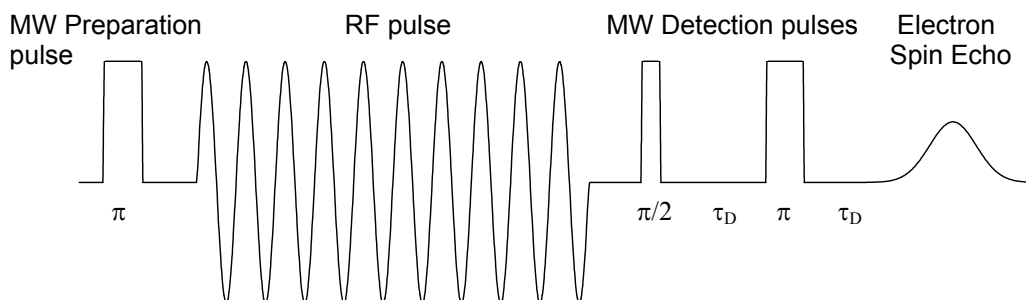
Nucleus	Spin ( $I$ )	$g_{\text{N}}$	$\nu_{\text{N}}$ at 330 mT (MHz)
$^1\text{H}$	$\frac{1}{2}$	5.5857	14.05
$^2\text{H}$ (D)	1	0.8574	2.16
$^{14}\text{N}$	1	0.4038	1.02
$^{15}\text{N}$	$\frac{1}{2}$	-0.5664	1.42
$^{57}\text{Fe}$	$\frac{1}{2}$	0.1806	0.45

In CW ENDOR, both the microwaves and the radio waves are supplied continuously, and the spectrum appears as the first derivative absorption spectrum of the radio waves due to the field modulation of the radio frequency (Kurreck *et al.*, 1988).

The X-band CW ENDOR experiments were performed on a Bruker ESP 300E Spectrometer and a self-built ENDOR cavity of the type TM110 (Zweygart *et al.*, 1994). The sample is cooled by an Oxford ESR910 helium flow cryostat using an Oxford ITC4 temperature controller. The radio frequency signal is provided by a SMT Rhode & Schwarz frequency synthesizer.

### 2.4.4 PULSED DAVIES ENDOR

In a pulsed ENDOR experiment, in contrast to CW-ENDOR, the microwave and radio frequency fields are applied in short discrete time intervals, i.e. pulses. This leads to the generation of strong magnetic fields,  $B_1$ , at the position of the sample. In this work, the so-called Davies pulse sequence was used (Davies, 1974).



**Scheme 2-6 The Davies pulsed ENDOR sequence**

Each sequence starts with a so-called preparation microwave pulse, or  $\pi$  pulse, followed by a radio frequency pulse, and finally two microwave detection pulses ( $\pi/2$  and  $\pi$ ). The preparation pulse inverts the electron spin polarization with an angle of  $180^\circ$ , hence  $\pi$ -pulse, from  $m_S = -1/2$  to  $m_S = +1/2$  (e.g.  $\Delta E = \nu_e - a/2$ ) (see Figure 2-4) within a narrow microwave frequency region of the broad EPR transition domain. The width of this region is proportional to the inverse preparation pulse length,  $1/\tau_{MW}$ , which is normally around 200 ns.

The radio frequency (rf) pulse, which induces the ENDOR transitions, is applied with gradually increasing frequency for each pulse sequence. When the radio frequency reaches an ENDOR transition frequency,  $\Delta E = \nu_N \pm a/2$  (see Figure 2-4), the induced nuclear transitions change the populations of the connected spin energy levels leading to a change of the EPR echo intensity. The length of the rf pulse,  $\tau_{rf}$ , should be set shorter than the electron spin  $T_1$  and should correspond to the  $\pi$  pulse for the NMR transition, to minimize spin depolarization due to electron spin relaxation, which would reduce the signal intensity. A variation of  $\tau_{rf}$  can thus be used for estimating  $T_1$  as well as for selective observation of different paramagnetic species in one sample if these species have different relaxation behavior. For the fast relaxing center H in R2-Y122H,  $\tau_{rf}$  was set to 8  $\mu s$ .

After the rf pulse, two microwave pulses  $\pi/2$  and  $\pi$  are used for detection. The first of these pulses flips the spins into a plane that is perpendicular ( $\pi/2$ ) to the static magnetic field ( $B_0$ ). Due to inhomogeneous broadening, the spins will diffuse, or dephase, in this plane during a defined time period  $\tau_D$  before the next pulse. The second pulse flips the spins  $180^\circ$ , still within the plane perpendicular to the magnetic field, which will lead to reversion of the dephasing process. A spin echo will therefore occur at a time period  $\tau_D$  after the last pulse as the spins are polarized again. The intensity of the echo reflects the number of spins involved, and after a pulse sequence where the radio frequency induced ENDOR transitions, the number of electron spins will be reduced and the spin echo will therefore also be smaller. The

pulsed ENDOR spectra are recorded as the inverse spin echo intensity as a function of the radio frequency, and is therefore an absorption spectrum.

The *repetition rate* is also an important parameter in pulse EPR and pulse ENDOR; it determines the time span between two pulse sequences. It is important to set this rate so slow that the spins can restore the Boltzmann distribution completely between each sequence, which is depending on the electron spin relaxation time  $T_1$ . At the same time, it is desirable to enhance the repetition rate, to reduce the overall spectrum accumulation time.

Pulsed ENDOR spectroscopy has several advantages over the conventional CW-technique:

- it requires no critical balance of electron and nuclear relaxation times, a condition which has to be met in CW-ENDOR
- it is less susceptible to artifacts as there is no rf and no microwave field applied during the detection period
- it gives access to all relaxation times of a spin system (electron  $T_1$  and  $T_2$ , nuclear  $T_1$  and  $T_2$ , and cross relaxation)
- it allows the manipulation of the spin system to observe one particular spin property with high selectivity and sensitivity if these have different relaxation behavior
- the ENDOR effect can be as large as the electron spin echo intensity itself

The X-band pulse ENDOR, and pulse EPR (ESE), experiments were performed on a Bruker ESP 380E Spectrometer supplemented with an ESP 360D-P Pulse ENDOR module, an ENI A500 radio frequency amplifier, and a Bruker ER 035 NMR-Teslameter. For low temperature measurements, the sample was kept at a constant temperature using a CF935 helium Flow cryostat from Oxford Instruments, monitored by an ITC4 temperature controller.

The CW and Pulsed Davies ENDOR spectra were simulated using the program SPLEEN, which was written by Dr. Christof Gessner, a former PhD student at the Max-Volmer-Institute, TU-Berlin (Gessner *et al.*, 1999).

### 3

## ARTIFICIALLY GENERATED THIYL RADICALS IN THE CATALYTIC SUBUNIT R1 OF RNR

Thiyl radicals are believed to be involved in a variety of enzymatic reactions, including electron transfer, addition reactions, and, as in RNR, hydrogen abstraction (Kalyanaraman, 1994, DeGray and Mason, 1995). Despite its frequent appearance, direct EPR detection of thiyl radicals in proteins have so far only been reported in cases where they are directly associated with metals. In an Fe-S-cluster of aconitase, a long-living thiyl radical was formed after enzyme inactivation by nitric oxide (Kennedy *et al.*, 1997). The observed line-shape and  $g$ -values ( $g_{\parallel} = 2.11$  and  $g_{\perp} = 2.03$ ) are similar to those of thiyl radicals in small molecules. A thiyl radical associated with a paramagnetic  $\text{Co}^{2+}$ -complex has been found in freeze-quenched mixtures of class II RNR and its cofactor adenosyl-cobalamin; the line shape of the thiyl radical, however, was completely dominated by the interaction with the cobalt metal (Gerfen *et al.*, 1996b). Otherwise, there are no reports on isolated thiyl radicals in proteins detected directly by EPR.

The first step in the enzymatic reduction of ribonucleotides to deoxyribonucleotides by RNR involves the abstraction of the 3'-hydrogen of the substrate ribose by a protein thiyl radical (Stubbe and van der Donk, 1998) (see Section 1.2.1). Several radical species are postulated to be formed during the following steps of the substrate turnover, on the substrate itself and on amino acid residues at the active site of R1, but none of these radicals have been observed by means of EPR spectroscopy in the wild-type enzyme using a standard substrate. The aim of this study was to establish a system in which transient thiyl radicals, and primarily that on C439 in R1, could be generated selectively and characterized by spectroscopic methods to give information on spectroscopic properties and electronic structure. Before looking at the R1 protein, initial model studies were performed on low molecular weight thiol compounds and bovine serum albumin (BSA) to optimize the conditions under which protein thiyl radicals can be generated and detected.

### 3.1 GENERATION OF THIYL RADICALS BY UV-IRRADIATION – DIRECT EPR DETECTION

The first method employed for generation of thiyl radicals was UV-irradiation of different thiol containing compounds at low temperature in the solid state. Fortunately, the S-H bond is weaker than most other covalent bonds found in a protein and UV irradiation will therefore preferably break this bond (Box *et al.*, 1966). However, with this crude method, other bonds are also likely to be broken, forming other types of radicals, which might possibly destroy the enzymatic function of the protein. The UV-irradiation experiments were therefore mainly performed to obtain high yields of thiyl radicals which were used for establishing conditions for direct observation and characterization by EPR spectroscopy. Since both radical generation and detection is performed in the solid state, no mixing processes can take place. Due to the high reactivity of thiyl radicals with oxygen, all samples were made anaerobic by argon flushing in a sealed vial.

#### 3.1.1 UV IRRADIATED CYSTEINE

The first experiments were performed on free cysteine as a model for the cysteine residues in proteins. Figure 3-1 shows an annealing series of EPR spectra of an anaerobic cysteine solution (300 mM) in phosphate buffer irradiated with UV light for 8 minutes at 10 K. The spectra were recorded at 10 K after 10 minutes incubation at sequentially increasing temperatures, which allows irreversible partial decay of the radical signals. Due to their different temperature stability in the frozen ice matrix, we were able to isolate the EPR spectra of four different radical species from this annealing series,  $H^\bullet$ ,  $R-C^\bullet$ ,  $R-S^\bullet$ , and  $R-S-S^\bullet$ . In Figure 3-2, the temperature dependence of each species is shown.

The first spectrum, before annealing, (Figure 3-1, lower spectrum) contains a doublet signal split by 50 mT around the  $g_e$  value for the free electron. This is characteristic for the hyperfine splitting of a hydrogen atom (marked with  $H^\bullet$  in Figure 3-1, left), which is expected to be generated concomitantly with the thiyl radical. Due to its small size and high reactivity, it disappeared already after heating to 80 K (see Figure 3-2).

The multi-line signal, most dominantly between 340 and 355 mT, derives from a carbon-centered species with hfs from three protons. In earlier studies of irradiated cysteine samples, this has been characterized as decarboxylated cysteine (Box *et al.*, 1966). This signal is half saturated at 2.5 mW ( $= P_{1/2}$ ) at 80 K. Half of the signal intensity is irreversibly lost by annealing at 140 K, and above 180 K it is no longer measurable (see Figure 3-2).

At higher temperatures, practically only one radical species remain, which is therefore the most stable one. By spectrum simulation the  $g$ -tensor components  $g_x = 2.056$ ,  $g_y = 2.024$ , and  $g_z = 2.000$ , as well as an isotropic hyperfine coupling of  $A_{iso} = 0.6$  mT were determined (the position of the  $g$ -components are indicated in Figure 3-1, right upper spectrum). These values fit well with those reported for perthiyl radicals,  $R-S-S^\bullet$  (see Table 2-1), which are formed when a thiyl radical reacts with another thiol group. In Figure 3-2, we can observe that the perthiyl signal increases



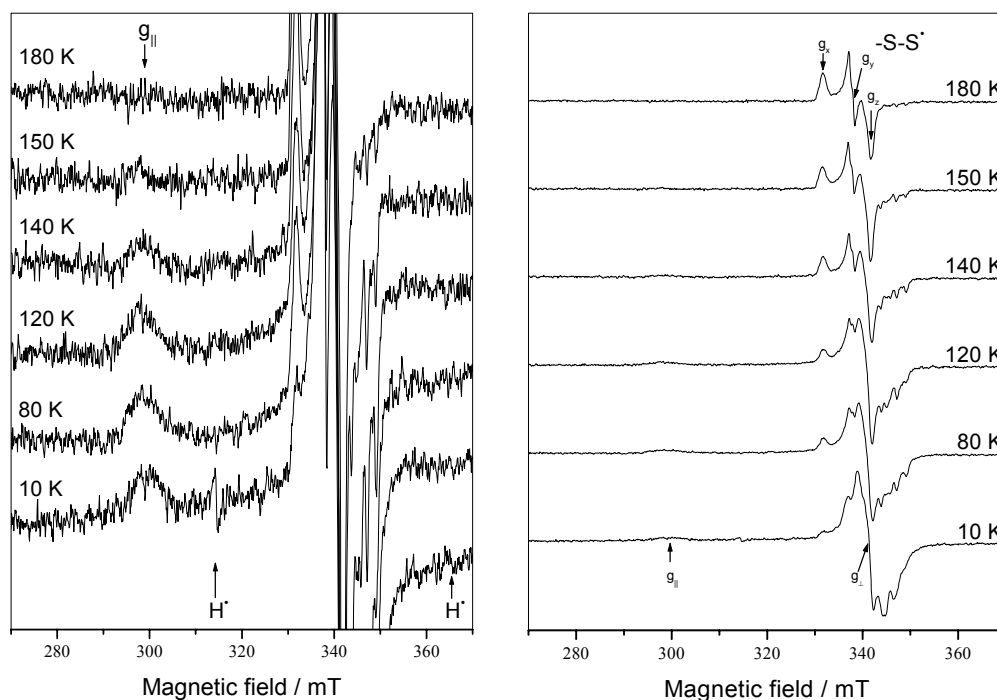


**FIGURE 3-1 ANNEALING SERIES OF AN UV IRRADIATED FROZEN SOLUTION OF CYSTEINE**

*X-band EPR spectra recorded at 10 K (left: 15 $\times$  magnification) showing the temperature stability of different radical species generated in an anaerobic solution of 300 mM cysteine in 200 mM potassium phosphate buffer, pH 7.0, irradiated 4  $\times$  2 min (90 $^\circ$  rotation between each step) by UV light at 10 K. The axial  $g$ -tensor components,  $g_{||}$  and  $g_{\perp}$ , of the thiyl radical are indicated, as well as the rhombic  $g$ -tensor components  $g_x$ ,  $g_y$ , and  $g_z$  of a perthiyl radical. The EPR spectra were recorded using 10 mW microwave power, 0.4 mT modulation amplitude, time constant 40 ms, 5 scans. Annealing was performed by 10 min incubation at the indicated temperature before cooling back to 10 K for the EPR measurement.*

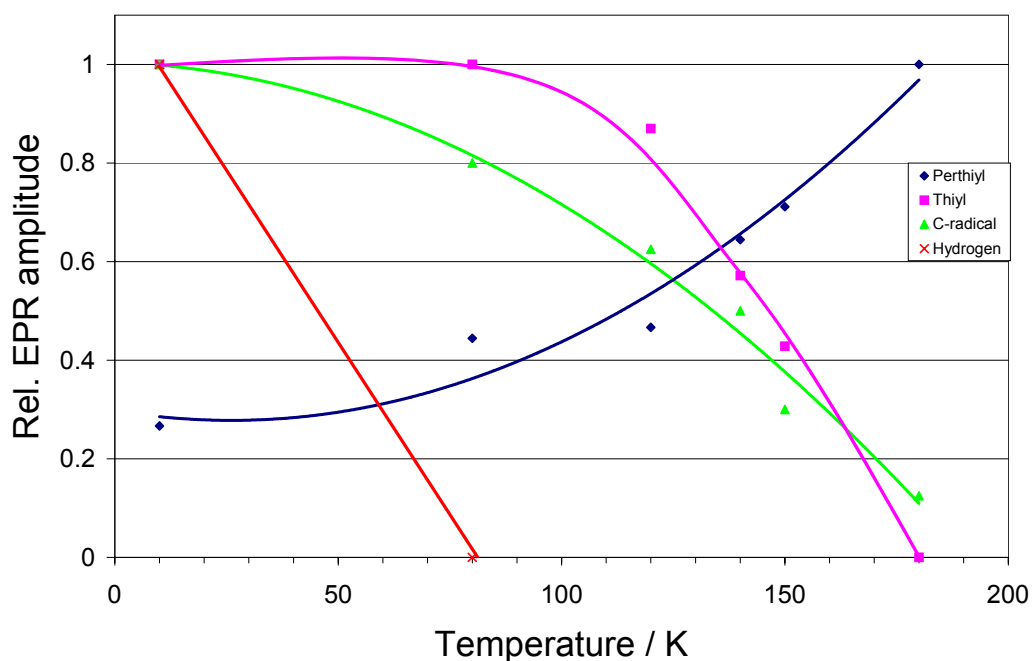


**FIGURE 3-2 TEMPERATURE STABILITY OF DIFFERENT RADICAL SPECIES GENERATED AFTER UV IRRADIATION OF CYSTEINE**

*The diagram shows the relative EPR amplitude at 80 K after the sample has been heated sequentially for 10 min to the indicated temperature, and cooled back to 80 K for EPR measurement. The sample and data correspond to the EPR spectra in Figure 3-1.*

as the other signals decrease. First, the carbon centered radicals decay to form thiyl radicals, which again form perthiyl radicals. The half saturation power of the perthiyl radical at 80 K was determined to be  $P_{1/2} = 1$  mW.

By subtraction of the perthiyl spectrum recorded after annealing to 180 K from the original spectrum before annealing (upper and lower spectrum in Figure 3-1), two lines remain unaccounted. This is an axial signal with one broad weak component at a low magnetic field 300 mT ( $g_{\parallel} = 2.29$ ) and a strong narrower line at 340 mT ( $g_{\perp} = 2.008$ ), which are characteristic for the axial signal of the thiyl radical. The thiyl radical in the frozen cysteine solution is visible up to 140 K, but above 150 K the signal is irreversibly lost.

### 3.1.2 UV IRRADIATED BSA AND R1

After the initial experiments with free cysteine, we wanted to observe thiyl radicals in the model protein BSA and the R1 subunit of RNR. In the oxidized state, BSA has one isolated cysteine residue, C34, where a thiyl radical can be formed. All the remaining cysteine residues in BSA are engaged in 17 disulfide bridges. In R1 there are 11 cysteine residues per monomer, 4 of which can form disulfide bridges. However, since the reduced form of R1 is the substrate binding form, the experiments with R1 was performed on the reduced form. In Figure 3-3, the EPR spectra of UV irradiated anaerobic frozen solutions of BSA (B), and R1 (C) are compared with the cysteine spectrum (A) taken from Figure 3-1. The amount of perthiyl radicals is noticeably lower in the R1 sample, where the possibilities for interaction between thiols are sterically hindered. The  $g_{\parallel}$ -component at 2.29 seen in the cysteine spectrum is visible neither in BSA nor in R1. In the BSA spectrum we see a new broad weak maximum at  $g = 2.18$ , which is typical for the  $g_{\parallel}$  in case of a strong defined hydrogen bond to the sulfur in a thiyl radical (Nelson and Symons, 1975, Nelson *et al.*, 1977). The corresponding  $g_{\perp}$  component at 2.008, however, is visible in all samples, but this alone is not an unambiguous evidence for a thiyl radical since most organic radicals have components in that region.

The  $g_{\parallel}$ -component of the thiyl radical in R1 is not visible in the normal first derivative display of the EPR spectrum. However, if we integrate the spectrum, a broad shoulder appeared at low magnetic field (Figure 3-4). In this absorption display, it becomes obvious that all three samples, cysteine (Figure 3-4A), BSA (3-4B), and R1 (3-4C), have broad  $g_{\parallel}$ -components, but only in the cysteine spectrum, a defined edge is visible. This means that in cysteine, all the thiyl radicals seem to be ordered in a framework with uniformly oriented, weak, hydrogen bonds in the frozen matrix, whereas in the two protein samples, there must be a larger heterogeneity of the H-bonds, leading to a larger  $g$ -strain and a broader shoulder. Still, in BSA we have one orientation dominating, since we do observe a maximum at  $g_{\parallel} = 2.18$ , whereas in R1, the larger number of free thiol groups, each with different environments, most likely contribute further to a broadening of the  $g_{\parallel}$ -value.

The amplitude of the broad shoulders of both proteins can be quantified after careful subtraction of the spectrum baseline recorded before UV irradiation. We performed an annealing experiment on the thiyl radicals in R1 in order to get information on the stability in frozen aqueous solution at elevated temperatures

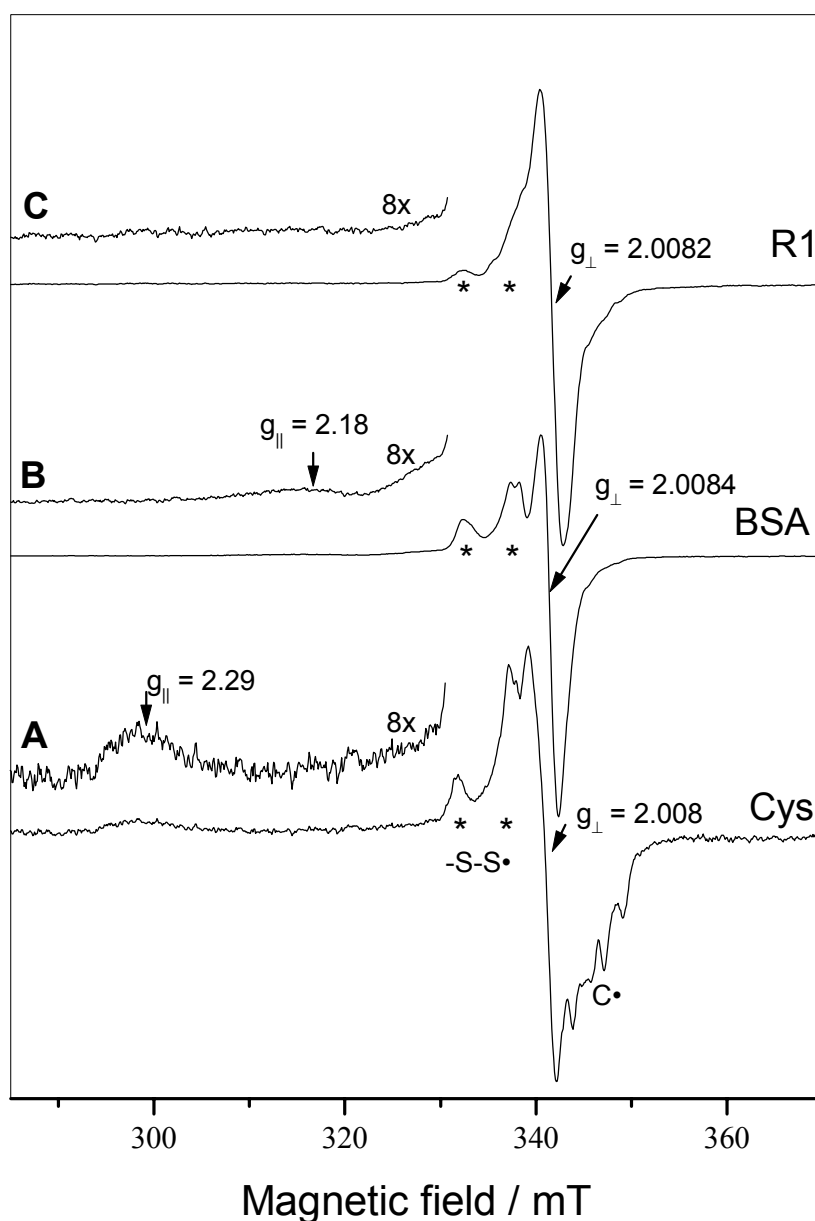


**FIGURE 3-3 FIRST DERIVATIVE EPR SPECTRA OF UV IRRADIATED ANAEROBIC SOLUTIONS OF R1, BSA, AND CYSTEINE**

(A) Cysteine 300 mM in 200 mM potassium phosphate buffer, pH 7.0. irradiated 4 min by UV light at 10 K. EPR spectra recorded at 10 K, 10 mW microwave power 0.4 mT modulation amplitude, 5 scans, time constant 40 ms.

(B) BSA 4 mM in 200 mM potassium phosphate buffer pH 7.0. 8 min UV at 80 K. EPR: recorded at 80 K, microwave power: 200 mW, modulation amplitude: 10 G, 4 scans. Background subtracted.

(C) R1 0.5 mM in 200 mM potassium phosphate buffer pH 7.0. 8min UV at 80 K. EPR: recorded at 80 K, microwave power: 200 mW, modulation amplitude: 10 G, 4 scans. Background subtracted. All preparations were made anaerobic to prevent formation of sulfinyl, peroxy, and sulfonyl radicals.

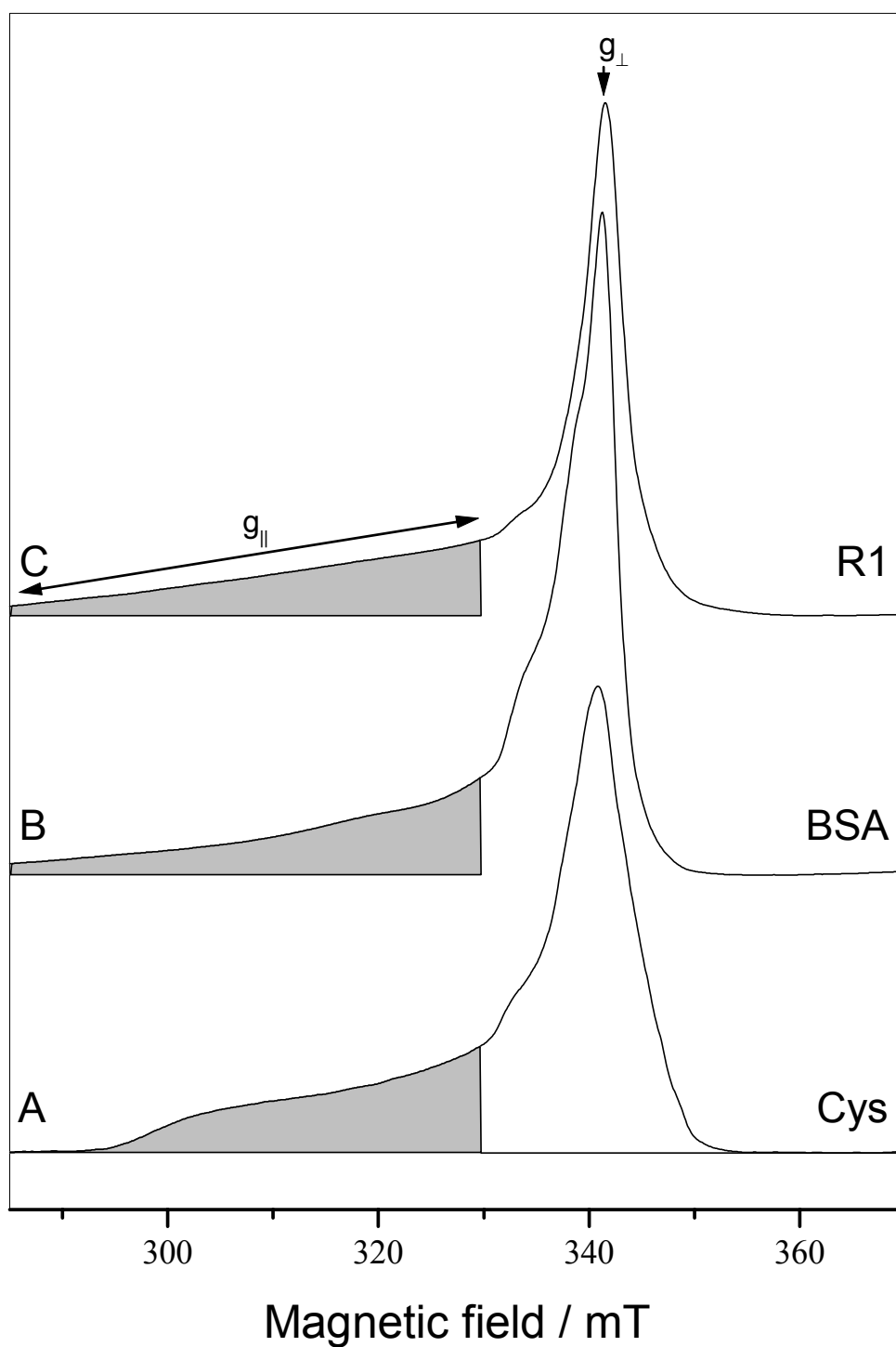


**FIGURE 3-4** INTEGRATED FIRST DERIVATIVE EPR SPECTRA (ABSORPTION SPECTRA) OF UV IRRADIATED PROTEINS AND CYSTEINE

*EPR spectra as in figure 3-3, after numerical integration. The broad range of the  $g_{\parallel}$  component is indicated by an arrow.*

(Figure 3-5). This way, we found a clear correlation of the signal intensity between the broad  $g_{\parallel}$  and the narrow  $g_{\perp}$  component which is a strong indication that these components derive from the same radical species.

The different radical species generated by UV irradiation can also be characterized by their different microwave power saturation behavior, which is directly correlated with the spin-lattice relaxation of the unpaired radical spins. At low temperature, 10 K, the perthiyl as well as the C-centered species are easily saturated, and at a microwave power above 20 mW we do practically only observe the thiyl radical alone (compare the EPR spectrum in Figure 3-6 recorded with 200 mW and spectrum (C) in Figure 3-4 recorded with 10 mW). The two  $g$ -components of the thiyl radical, however, do display an anisotropic relaxation pattern, which differs by two orders of magnitude (Figure 3-6, insert). The  $g_{\parallel}$ -component has an unusually large  $P_{1/2} = 3.8$  mW at 10 K, which is more similar to a metal-complex than to an organic radical, and at 80 K, this component cannot be saturated even at 200 mW, which is the instrumental limit for our microwave bridge. In contrast, the  $g_{\perp}$  component of the thiyl radical has  $P_{1/2} = 33$   $\mu$ W at 10 K, which is more in the normal range of an organic radical. This large anisotropy of relaxation corresponds to the equally large  $g$ -anisotropy of the thiyl radical. Both power saturation curves were simulated using equation 2.14 in Section 2.4.2, and a homogeneity factor  $b = 1$ , which is consistent with a Gaussian shaped EPR signal.

## 3.2 CHEMICAL GENERATION OF PROTEIN-THIYL RADICALS USING CERIUM (IV) – SPIN TRAP DETECTION

The second strategy for generation of thiyl radicals is the abstraction of an electron from the thiyl sulfur atom using a chemical oxidant. Cerium ( $\text{Ce}^{\text{IV}}$ ) is known as a strong one-electron oxidant, which, chelated with nitrilotriacetate (NTA), can be utilized for generating thiyl radicals at neutral pH on both low molecular weight thiols and proteins (Graceffa, 1983, Mullins *et al.*, 1992, Davies *et al.*, 1993). The oxidation reaction requires diffusion of the reactants involved and must therefore be carried out in liquid solution. As discussed in Section 2.2.3, thiyl radicals are not detectable by EPR in the liquid state at room temperature. They can, however, be detected indirectly by EPR with high sensitivity as spin adducts after addition of nitron spin traps such as DMPO or PBN (see Scheme 2-4) (Buettner, 1987). Since PBN spin adducts are more stable than DMPO adducts in the presence of  $\text{Ce}^{\text{IV}}$ /NTA (Graceffa, 1983, Mullins *et al.*, 1992), we preferred PBN for all spin trap experiments. The longer lifetime of the PBN spin adduct allows longer time for accumulation of the EPR spectra, which therefore gives a better signal-to-noise ratio. Furthermore, we found that a 5 to 10 fold concentration of cerium with respect to the protein gave the strongest EPR signals.

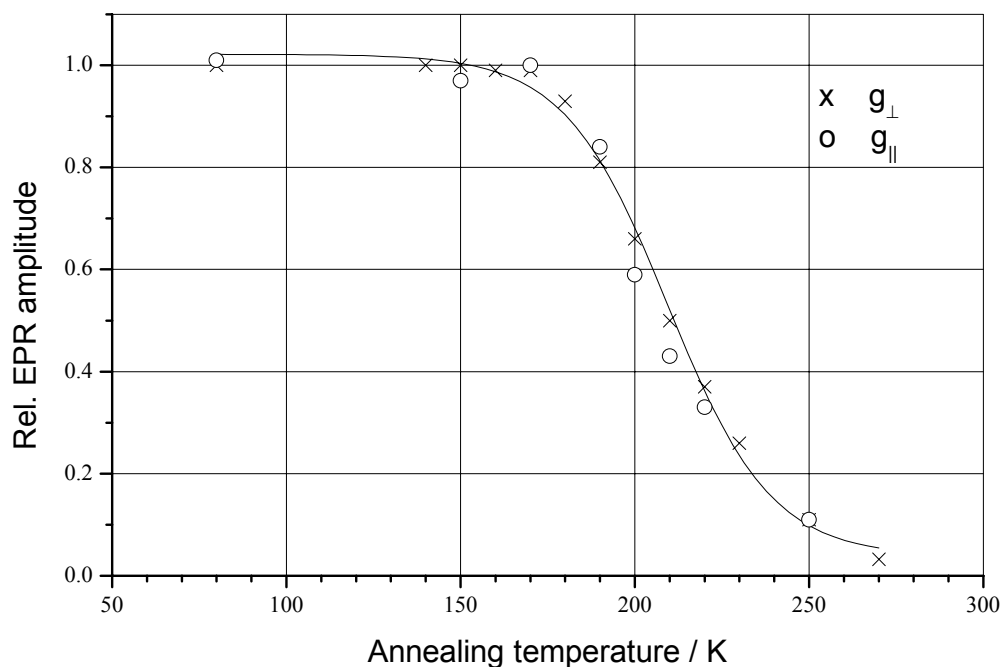


**FIGURE 3-5 TEMPERATURE DEPENDENCE OF THE G-COMPONENTS ( $G_{\perp}$  AND  $G_{\parallel}$ ) OF THE THIYL RADICAL IN R1**

The sample was irradiated by UV at 80 K, and after recording an EPR spectrum, it was incubated for 10 min at the indicated temperature before cooling back to 80 K for recording the next spectrum. The signal intensity factor was determined by scaling up the spectrum until it overlapped the original spectrum at 80 K. The EPR spectra were recorded at 80 K using 1 mT modulation amplitude and 200 mW microwave power.

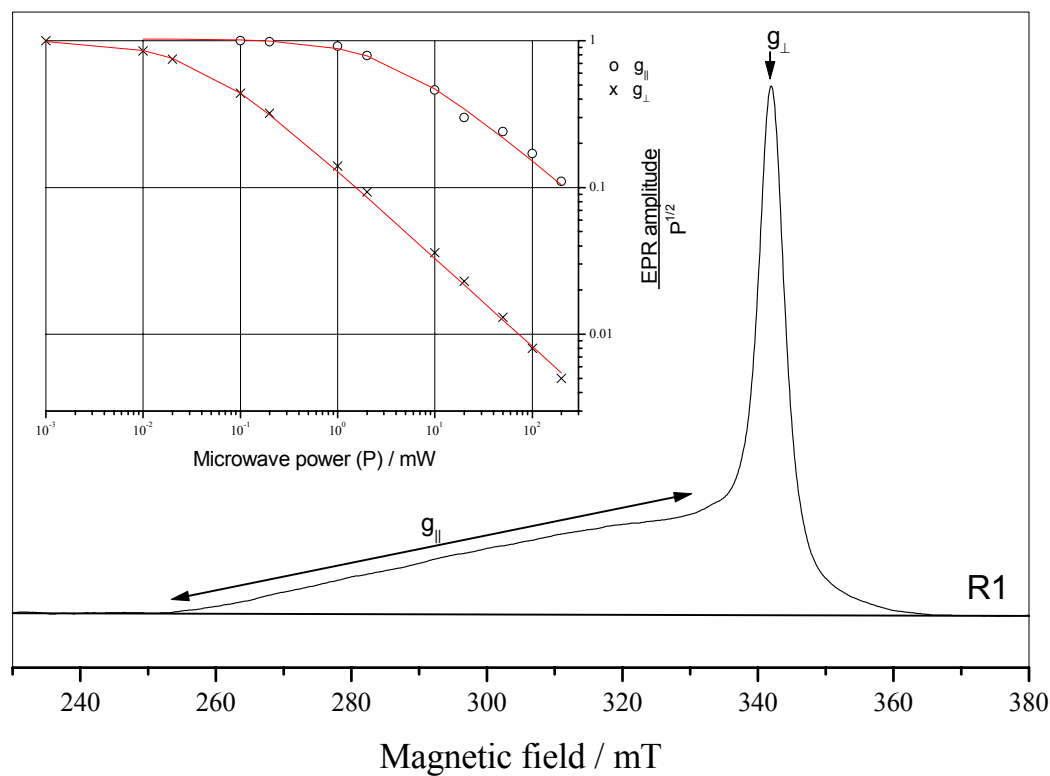


**FIGURE 3-6 ABSORPTION SPECTRUM OF A THIYL RADICAL IN R1 AND ITS RELAXATION BEHAVIOR AT 10 K**

*Integrated first derivative EPR spectrum recorded at 10 K, 200 mW and 1 mT modulation amplitude, showing only features from the thiyl radical.*

*Insert: Power saturation curve of the two g-components of the axial EPR spectrum of the thiyl radical in R1 at 10 K*



### 3.2.1 THIOL OXIDATION IN MODEL SYSTEMS – GLUTATHION AND BSA

Reduced glutathion (GSH), a tripeptide containing a cysteine residue, was used as a model substance for generation of thiyl radicals with  $\text{Ce}^{\text{IV}}/\text{NTA}$  in the liquid state, and the thiyl radicals were detected using the spin trap PBN. Due to its small size (MW = 307 Da), GSH should have small rotational restrictions in the liquid phase, which greatly influences the shape of the EPR spectrum of the spin adduct. The hyperfine interactions from both a nitrogen and a proton are resolved in the EPR spectrum at room temperature (Figure 3-7A). It shows a triplet hyperfine splitting from the nitroxide  $^{14}\text{N}$  ( $A_{\text{iso}}(\text{N}) = 1.53 \text{ mT}$ ) and a doublet subsplitting from the  $\beta$ -proton ( $A_{\text{iso}}(\text{H}) = 0.31 \text{ mT}$ ), which corresponds to a trapped thiyl radical (Buettner, 1987). This experiment confirmed that we were able to generate thiyl radicals by cerium(IV) oxidation, and that these radicals are trapped by PBN. The lineshape indicates that the spin adduct is rotating freely in the solution (see Section 3.6 for a lineshape analysis). The half-life of the PBN-GSH spin adduct was 3 minutes.

BSA was chosen as a model for a thiyl spin adduct located in a globular protein. This protein has a total of 35 cysteine residues, but beside 17 disulfide bridges, BSA has only one free thiol group, namely C34. The EPR spectrum of the PBN-BSA spin adduct in the liquid state, formed after oxidation by  $\text{Ce}^{\text{IV}}/\text{NTA}$ , exhibits two spectral parts (Figure 3-7B): the major part (marked with arrows) has a line shape resembling the powder spectrum of the frozen solution (Figure 3-7E) and is typical for slow isotropic rotational motion, and the minor part of the spin adduct spectrum (marked with an asterisk) is typical for faster isotropic rotational fluctuations. By comparison of the apparent nitrogen hfs (termed  $A'_{\text{zz}}(\text{N})$ ) with the nitrogen hfs obtained from the frozen solution spectrum ( $A_{\text{zz}}(\text{N})$ ), which are indicated in Figure 3-7B and 3-7E, the rotational correlation times can be calculated (see section 3-5, below). Quantification by integration of the spectrum yielded ~20 % of the spin adduct with fast motion and ~80 % with slow motion. The small proton splitting seen in the GSH-PBN adduct in Figure 3-7A is no longer resolved for any of the spectral parts. The minor part has a faster decay (half-life time 3 min) than the major part with slow motion (5 min), so that the minor part could be separated by subtraction of spectra recorded after different incubation times (Figure 3-7C). This difference spectrum exhibits the isotropic  $^{14}\text{N}$ -coupling as in Figure 3-7A, but has a broader linewidth. By subtracting the minor part, Figure 3-7C, from the original spectrum, Figure 3-7B, only the major part remains (Figure 3-7D). This spectrum implies an almost rigid attachment of the spin adduct to the globular protein.

### 3.2.2 THIOL OXIDATION IN PROTEIN R1

After optimization of the conditions for thiol oxidation by  $\text{Ce}^{\text{IV}}/\text{NTA}$  in model proteins and PBN detection of thiyl radicals, protein R1 of RNR was studied. Figure 3-8A shows the EPR spectrum at room temperature (4 min after mixing) of the PBN spin adduct formed after oxidation of thiols in R1 by  $\text{Ce}^{\text{IV}}/\text{NTA}$ , and Figure 3-8G the frozen state spectrum for comparison. Control experiments with two different thiol blocking agents (DTNB, Figure 3-8B; and NEM, Figure 3-8C) clearly

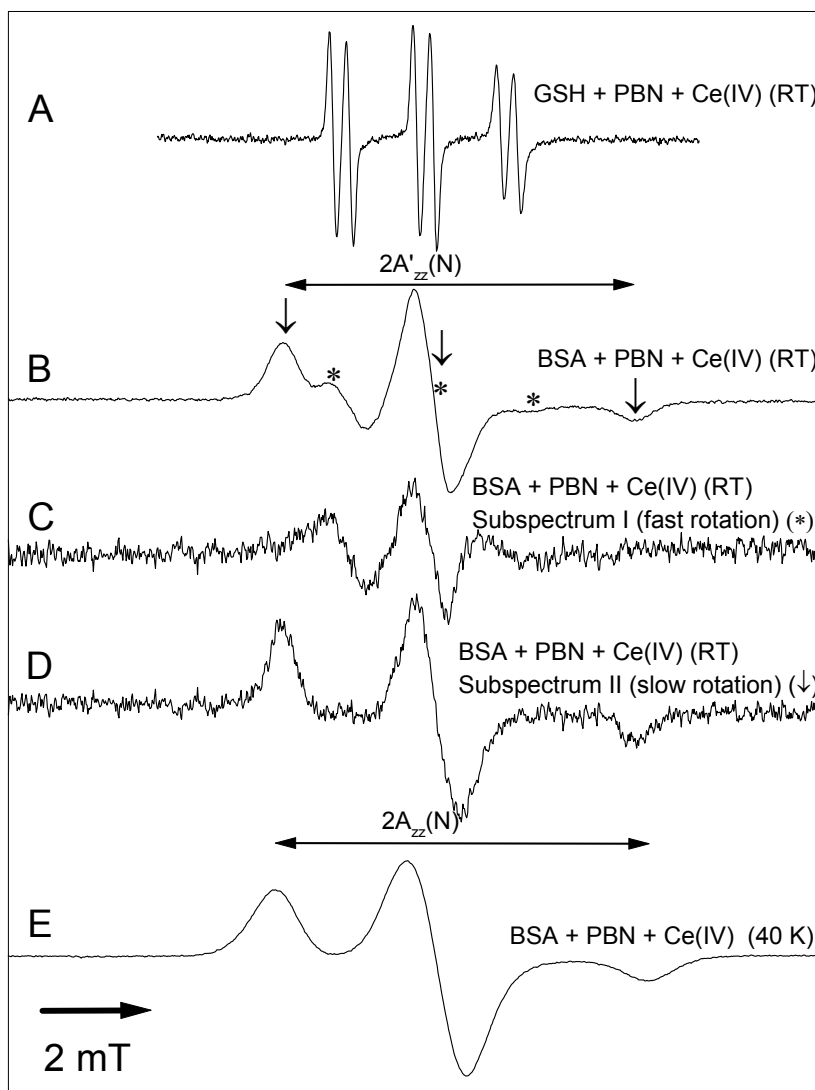


**FIGURE 3-7 EPR SPECTRA OF THE PBN SPIN ADDUCT FORMED AFTER OXIDATION OF THIOLS BY  $\text{Ce}^{\text{IV}}$ /NTA**

(A) Reduced glutathion (GSH), recorded at room temperature 2 min after mixing. Assay: GSH (2mM)/ PBN (5mM)/ DTPA (1 mM)/ MOPS (0.5 M) pH 7.0 + CeIV (4mM)/ NTA (8mM). EPR: MW: 20 mW; mod. amp.: 0.1 mT; time constant: 20 ms; scan time: 20 s; 8 scans.

(B) Bovine serum albumin (BSA), recorded at room temperature 1 min after mixing. Assay: BSA (700  $\mu\text{M}$ )/ PBN (9 mM)/ DTPA (1 mM)/ MOPS (0.5 M) pH 7.0 + CeIV (7.5 mM)/ NTA (15 mM). EPR: MW: 20 mW; modul.amp.: 0.2 mT; time const.: 40 ms; scan time: 40 s; 6 scans. Faster rotating parts indicated by (\*)

(C) Difference spectrum of spectrum (B) ,1 min incubation time, and the spectrum of the same sample after 5 min; only the faster rotating part is visible.

(D) Spectrum (B) after subtraction of spectrum (C); only the slowly rotating part is visible.

(E) BSA as (B), frozen in cold isopentane ( $T = 150 \text{ K}$ ) 60 s after mixing, recorded at  $T = 40 \text{ K}$ . EPR: MW: 0.1 mW; modul. amp.: 0.4 mT; time const.: 40 ms; scan time: 40 s; 5 scans.

The apparent hfs  $2A'_{zz}(\text{N})$  for spectrum (B) and the powder hfs  $2A_{zz}(\text{N})$  for spectrum (C) are indicated by horizontal arrows, see section 3.5.

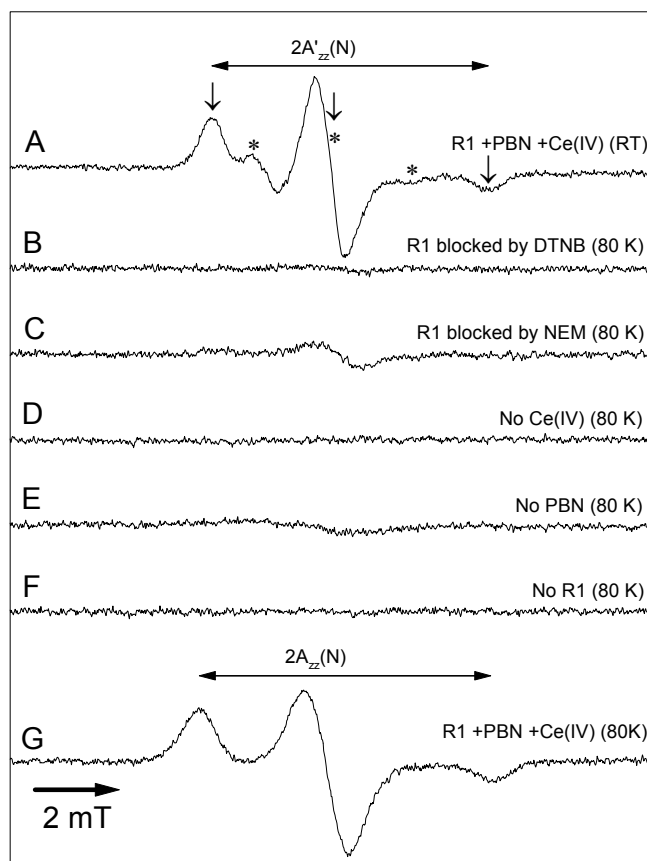


**FIGURE 3-8 EPR SPECTRA OF THE PBN SPIN ADDUCT FROM PROTEIN R1 OF *E. COLI* RNR AFTER OXIDATION BY  $\text{Ce}^{\text{IV}}$ /NTA**

(A) R1 recorded at room temperature in a flat cell 4 min after mixing. Assay conditions: R1 (650  $\mu\text{M}$ )/ PBN (9.3 mM)/ DTPA (1 mM)/ MOPS (0.5 M) pH 7.0 +  $\text{Ce}^{\text{IV}}$  (5.4 mM)/ NTA (11 mM). EPR conditions: microwave power: 20 mW; modulation amplitude: 0.2 mT; time constant: 40 ms; scan time: 40 s; 3 scans. The spectral part with fast rotation of the nitroxide spin adduct is indicated by an asterisk, with slow rotation by an arrow.

The control spectra (B to F) refer to spectrum G:

(B) Control: R1 preincubation with DTNB

(C) Control: R1 preincubation with NEM

(D) Control:  $\text{Ce}^{\text{IV}}$ /NTA is omitted in assay

(E) Control: PBN is omitted

(F) Control: R1 is omitted.

Assay conditions (B to F): R1 (350  $\mu\text{M}$ )/ PBN (8.3 mM)/ DTPA (1 mM)/ MOPS (0.5 M) pH 7.0 +  $\text{Ce}^{\text{IV}}$  (1.9 mM)/ NTA (3.8 mM). Samples frozen 1 min after mixing. EPR conditions: recorded at 80 K; microwave power: 0.1 mW; modulation amplitude: 0.4 mT; time constant: 40 ms; scan time: 40 s; 10 scans.

(G) R1 as (A) but recorded at 80 K, the sample is frozen 1 min after mixing. Assay conditions: R1 (350  $\mu\text{M}$ )/ PBN (8.3 mM)/ DTPA (1 mM)/ MOPS (0.5 M) pH 7.0 +  $\text{Ce}^{\text{IV}}$  (1.9 mM) / NTA (3.8 mM). EPR conditions as (B-F).

The apparent hfs  $2A'_{zz}(\text{N})$  for spectrum (A) and the powder hfs  $2A_{zz}(\text{N})$  for (G) are indicated by horizontal arrows, see section 3.5.

indicate that the EPR spectrum in Figure 3-8A originates from thiyl radical spin adducts. The further controls, omitting one of the three reactants,  $\text{Ce}^{\text{IV}}/\text{NTA}$  (Figure 3-8D), PBN (Figure 3-8E), or R1 (Figure 3-8F), show that the trapped thiyl radicals are generated in protein R1 only in the presence of  $\text{Ce}^{\text{IV}}/\text{NTA}$  and PBN. All control experiments (Figure 3-8B-F) were performed with samples frozen 1 min after mixing, and EPR spectra were recorded at low temperature allowing a longer accumulation of the spectrum, due to the limited lifetime of the spin adduct at room temperature.

The EPR spectrum of the thiyl PBN spin adduct in R1 (Figure 3-8A) is very similar to that of the BSA-PBN spin adduct (see Figure 3-7B). It does also display a superposition of two spectral parts, a fast motion spectrum, marked with an asterisk contributing ~20 % of the total spin, and a slow motion one, marked with an arrow, which contributes ~80%.

As a negative control experiment for the generation of a thiyl radical on the catalytically essential C439 of R1, we also performed the oxidation by  $\text{Ce}^{\text{IV}}/\text{NTA}$  on the R1 mutant C439A. The EPR signal intensity of the PBN spin adduct of this mutant was however not significantly lower. In case the thiyl radical is generated exclusively on C439, or only on a very limited number of other cysteines, we would expect to see a loss of intensity of using this mutant. If, however, a larger number of cysteines are involved (more than 4 or 5) the quantification of the PBN spin adduct based on the EPR signal intensity is too uncertain to make predictions based on single mutants. Except from the inherent difficulties with quantification of EPR spectra (Aasa and Vänngård, 1975), this uncertainty is also due to (i) the short lifetime of the thiyl radical itself, (ii) the limited accessibility of some thiyl radicals for PBN, and (iii) the fact that the thiyl spin adduct is unstable and decays on a minute time scale.

### 3.3 PHOTOCHEMICAL GENERATION OF PROTEIN-THIYL RADICALS BY LIGHT INDUCED RELEASE OF NITRIC OXIDE FROM NITROSTHIOLS – SPIN TRAP DETECTION

The homolytical cleavage of the S–H bond requires relatively high energy (~365 kJ/mole (Nicovich *et al.*, 1992)) and when UV-irradiation is applied, other bonds such as C–COOH will also be broken to some extent, as shown above in Section 3.1. This is obviously undesirable if one wants to preserve an intact active site environment. On the other hand, thiol oxidation by the strong oxidant  $\text{Ce}^{\text{IV}}$  could also damage the protein.

By substitution of the thiol hydrogen with nitric oxide, the bond strength is significantly lower so that visible light is sufficient to break the RS–NO bond (Sexton *et al.*, 1994, Wood *et al.*, 1996). Fortunately, nitric oxide can be easily attached to thiol groups (Stamler *et al.*, 1992a), and we used laser-light induced photolysis of nitrosothiols as a third method for generation of thiyl radicals.

Nitric oxide is a small gas molecule and a free radical that will bind selectively to thiol groups or metal atoms like iron. In the last years, the function of

nitric oxide as an intracellular messenger has been the subject for intensive investigation, and biological thiols like glutathione are thought to function as storage and transporters of NO (Stamler *et al.*, 1992b, Sheu *et al.*, 2000). It has even been suggested that nitric oxide has regulatory effects on the R2 subunit of RNR, because of the observation of reversible binding to the iron site or the tyrosyl radical (Lepoivre *et al.*, 1991).

### 3.3.1 NITROSYLATION OF PROTEIN THIOLS

The nitrosylation of thiol groups in BSA and in R1 was performed using S-NO-acetyl-penicillamine (SNAP) as transnitrosylating agent, as described in Section 2.2.6. Incubation of SNAP with BSA and R1, respectively, leads to a transfer of the loosely bound NO from SNAP to the protein thiols (Barnett *et al.*, 1994). This process was monitored quantitatively by the decrease of the S-NO absorption from SNAP at 590 nm and a simultaneous increase of the S-NO absorption of NO-BSA or NO-R1 at 545 nm (Figure 3-9). The degree of nitrosylation monitored at 340 nm after removing excess SNAP by gel filtration was 0.6 NO per BSA and 10 NO per R1-dimer.

### 3.3.2 LASER PHOTOLYSIS OF NITROSOTHIOLS

The oxidation of thiols by  $\text{Ce}^{\text{IV}}$ /NTA can only take place in the liquid state allowing diffusion of the compounds involved, whereas photolysis of nitrosylated thiols may, in principle, also be performed in frozen samples. Laser photolysis of NO-BSA was therefore performed both in frozen and in liquid solution, with subsequent freezing. To optimize the quantum yield, experiments were also performed in frozen solutions with 70 % glycerol, which gives the sample a glassy transparent character. The laser photolysis experiments at low temperature were, however, troublesome. The EPR spectra recorded at 40 K (not shown) revealed EPR signals from released NO molecules trapped in the ice matrix (Musci *et al.*, 1991). These signals are not resolved above 80 K where they only contribute to a line broadening. The yield of sulfur-centered radicals in the frozen sample was very low. Probably, NO is restricted from escaping and may recombine with the formed thiyl radicals. In the following, we therefore focussed on laser photolysis at room temperature.

BSA. The release of NO from NO-BSA after laser treatment was monitored by changes in the optical absorption band at 340 nm, and the degree of nitrosylation decreased from 0.6 to 0.1 NO per BSA depending on the number of laser shots (Figure 3-10). The optical yield was determined in the following way: The OD of the sample at 355 nm was about 0.1 for the optical cuvette, 0.03 for the 3 mm i.d. EPR tube, and 0.003 for the EPR flat cell. The percentage of photons absorbed per flash was determined from the optical density of an illuminated sample NO-BSA in the optical cuvette (optical length 1 cm). Comparison with the total photon number per laser flash yields the total number of absorbed photons for one laser flash. It was determined that after 10 flashes about 50% of the bound NO was released, and the total number of molecules having lost the NO after these flashes is set into correlation with the total number of absorbed photons in 10 laser flashes, giving a quantum yield of 0.08.

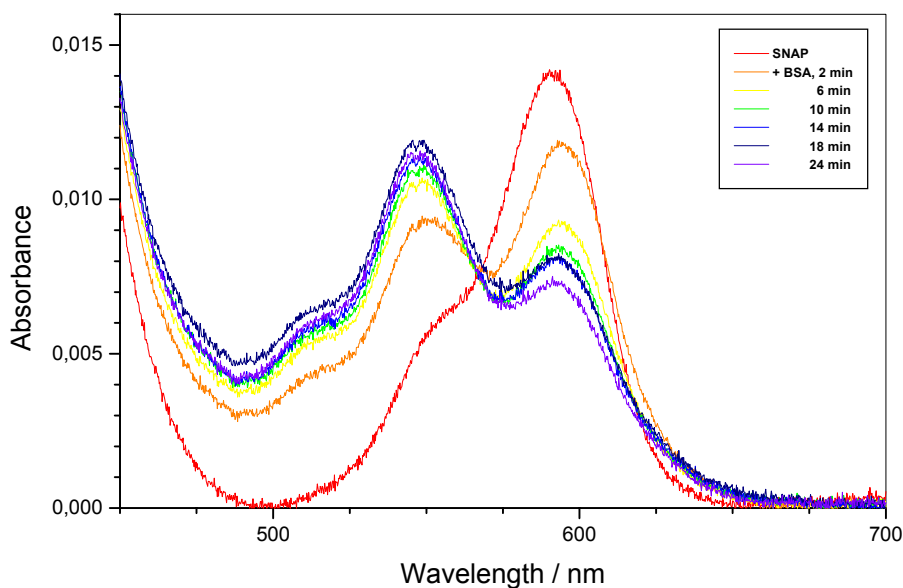


**FIGURE 3-9 TRANSNITROSYLATION FROM SNAP TO BSA**

Optical absorption spectra showing the decay of SNAP at 590 nm and increase of NO-BSA at 545 nm. The sample contained 1.5 mM SNAP (red spectrum) and 1.5 mM SNAP + 0.8 mM BSA after the indicated incubation time

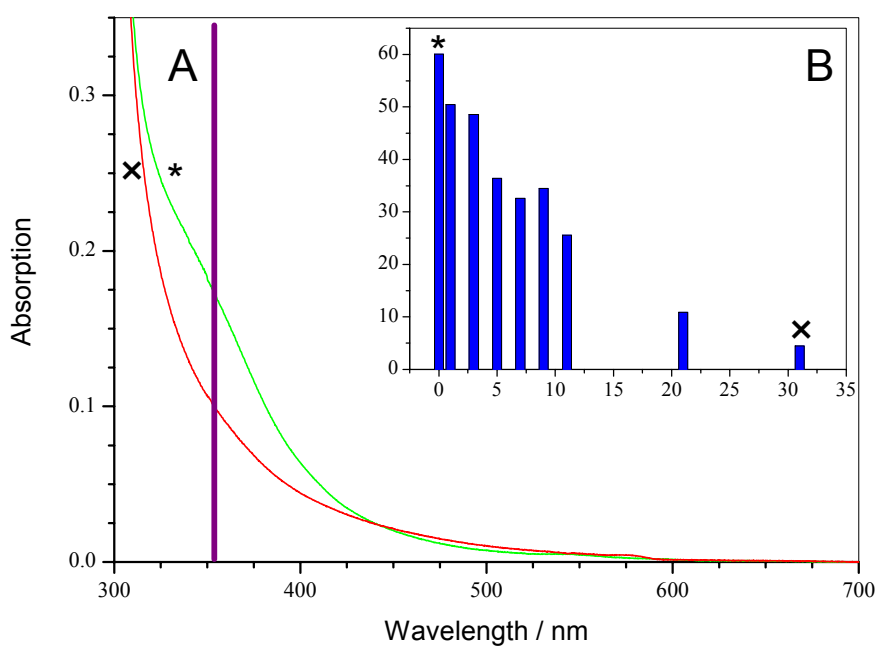


**FIGURE 3-10 LASER PHOTOLYSIS AT 355 NM OF NITRIC OXIDE (NO) FROM BSA**

(A) Optical absorption spectra of NO-BSA before (green) and after (red) 30 laser flashes. The laser light wavelength is indicated by a purple vertical line.

(B) Decay of the 340 nm band of NO-BSA correlated with the number of laser shots. The sample contained 1 mM BSA with 0.6 NO per BSA before laser treatment.

For the EPR tube and flat cell, the yield was significantly lower, due to the shorter optical length. Considering the estimated error margins, this value is very similar to the quantum yield 0.09 reported previously for NO-BSA (Wood *et al.*, 1996).

The photochemical generation of thiyl radicals in protein thiols in the presence of PBN using laser-induced release of NO from nitrosothiols at 355 nm was optimized with the model protein BSA, analogously to the case of chemical thiol oxidation using  $\text{Ce}^{\text{IV}}/\text{NTA}$ . The maximum signal intensity of a thiyl-PBN spin adduct EPR spectrum from NO-BSA was found after 20-30 laser flashes in the liquid state. The EPR spectra were recorded in a flat cell at room temperature immediately after laser excitation (Figure 3-11A).

The EPR spectrum of the thiyl-PBN spin adduct of BSA formed after photolysis is dominated by a line shape indicative for slow isotropic motion (Figure 3-11A) - similar to the case of oxidation by  $\text{Ce}^{\text{IV}}/\text{NTA}$ . The half-life time of the nitroxide radical in the thiyl-PBN spin adduct in BSA is 5 min which is comparable to the half-life time found for the spin adduct in the presence of  $\text{Ce}^{\text{IV}}/\text{NTA}$ . In Figure 3-11A, only a very small contribution from a fast motion spectrum is visible. An EPR spectrum at 40 K was also recorded from the same preparation illuminated at room temperature in a 4 mm tube and then frozen to 77 K (Figure 3-11B).

**R1.** Figure 3-11C shows the EPR spectrum at room temperature of the PBN spin adduct in NO-R1 after 30 laser flashes at 355 nm. The lifetime of the thiyl-PBN spin adduct was 4 min, and it showed a lineshape indicative for slow rotation, similar to R1 oxidized by  $\text{Ce}^{\text{IV}}/\text{NTA}$ . There is also a small fraction of faster moving adducts. The corresponding EPR spectrum acquired at 40 K of the illuminated NO-R1 sample frozen immediately after laser treatment in a 4 mm (o.d.) tube (Figure 3-11D) shows the rigid limit spectrum for a fully immobilized nitroxide spin adduct. The quantification yielded ~3 % PBN adduct per R1, which represents a lower limit for the generated intermediate thiyl radicals because not every thiyl radical formed will be trapped due to the difficulties outlined in Section 3.2.2.

A control experiment was performed with non-nitrosylated R1 protein which was illuminated in the presence of PBN under the same conditions as for NO-R1, and the EPR spectrum was recorded at 40 K (Figure 3-11E). The comparison of Figure 3-11E with Figure 3-11D clearly shows that there is no PBN spin adduct spectrum in the non-nitrosylated R1 sample. This indicates that the PBN spin adduct visible in Figure 3-11D originates exclusively from photorelease of NO, i.e. from a selective formation of thiyl radicals in R1.

### 3.4 EPR DETECTION OF THIYL RADICAL SUCCESSORS IN R1 WITHOUT SPIN TRAPS

Spin trapping is a sensitive method for the detection of short-lived radicals, like thiyl radicals. This method can, however, not provide any information on the *g*- and hyperfine coupling tensors, relaxation times, or the lifetime of protein thiyl radicals, which can only be obtained by direct EPR detection. Therefore, we investigated radicals formed in the absence of PBN after laser photolysis of nitrosylated R1 as well as after  $\text{Ce}^{\text{IV}}/\text{NTA}$  oxidation, using EPR at low temperature.

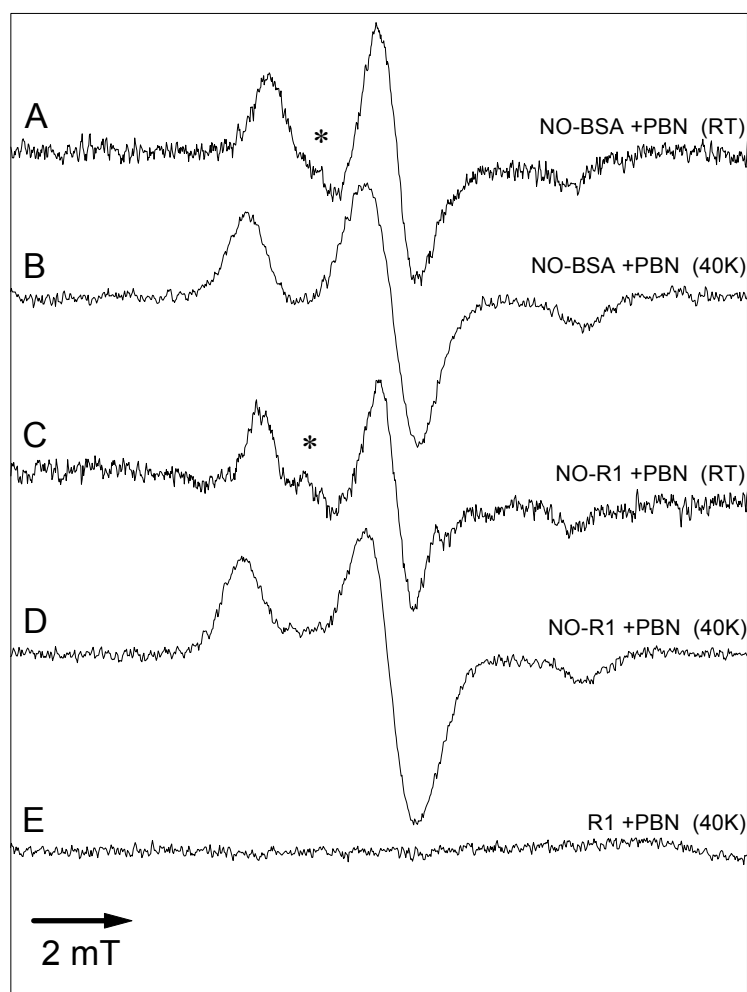


**FIGURE 3-11 EPR SPECTRA OF THE PBN SPIN ADDUCT FORMED BY LASER FLASHING OF NITROSYLATED PROTEIN.**

(A) Room temperature spectrum of NO-BSA after 40 laser flashes in an EPR flat cell. BSA: 360  $\mu$ M, (nitrosylation: 0.5 NO/ BSA), PBN: 9 mM, potassium phosphate 200 mM, pH 8.0. EPR conditions: microwave power: 20 mW; modulation amplitude: 0.4 mT; time constant: 40ms; sweep time: 40 s; 3 scans.

(B) 40 K spectrum of NO-BSA after 10 laser flashes at room temperature in 3 mm EPR tube. The sample was frozen to 77 K within 1 s. BSA: 360  $\mu$ M (nitrosylation: 0.5 NO / BSA), PBN: 9mM, potassium phosphate 200 mM, pH 8.0. EPR conditions: microwave power: 0.1 mW, modulation amplitude: 0.4 mT, time constant: 40ms, sweep time: 40 s, 4 scans.

(C) Room temperature spectrum of NO-R1 after 30 flashes laser flashes in a flat cell. R1: 100  $\mu$ M (nitrosylation: 10 NO per R1), PBN: 9 mM, potassium phosphate 200 mM, pH 8.0. EPR conditions: microwave power: 20 mW, modulation amplitude: 0.2 mT, time constant: 40ms, scan time: 40 s, 7 scans.

(D) 40 K spectrum of NO-R1 after 30 flashes in a 3 mm EPR tube at room temperature. The sample was frozen to 77 K within 1 s. R1: 500  $\mu$ M, (nitrosylation: 10 NO/R1), PBN: 9 mM, potassium phosphate 200 mM, pH 8.0. EPR conditions: as in (A), 6 scans.

(E) 40 K spectrum of non-nitrosylated R1 after 30 laser flashes in a 3 mm EPR tube at room temperature (control for spectrum 4D). The sample was frozen to 77 K within 1 s. Assay and EPR conditions as in (D), 6 scans.



The EPR spectrum at 40 K of NO-R1 after 10 laser shots at room temperature in a 4 mm EPR tube under aerobic conditions, and freezing within 2 - 3 s to 77 K, is shown in Figure 3-12A. The simulation of the spectrum (dotted line in Figure 3-12A) using a linewidth of 0.7 mT, reveals a rhombic  $g$ -tensor with  $g_x = 2.0213(4)$ ,  $g_y = 2.0094(4)$  and  $g_z = 2.0018(4)$  (errors in the last digit in parenthesis), and a hyperfine splitting (hfs) due to one proton with  $A_x = 1.0$  mT,  $A_y = 1.1$  mT and  $A_z = 0.9$  mT. These values are typical for a sulfinyl radical of the type  $R-CH_2-S^{\bullet}=O$ . The nearly isotropic proton splitting originates from one of the two  $\beta$ -protons. Thiyl radicals ( $R-S^{\bullet}$ ) and perthiyl radicals ( $R-S-S^{\bullet}$ ), which have their largest  $g$ -values at 2.1 - 2.3 (Nelson and Symons, 1975, Nelson *et al.*, 1977, Becker *et al.*, 1988) and 2.057 - 2.062 (Parast *et al.*, 1995, Covès *et al.*, 1996), respectively, can be excluded as candidates. Thiyl peroxy radicals ( $R-S-O-O^{\bullet}$ ) can also be ruled out since they have quite different  $g$ -values (2.0350, 2.0090, 2.0027) and do not exhibit any proton hfs (Sevilla *et al.*, 1988). In the anaerobic enzyme pyruvate formate lyase (PFL), a sulfinyl radical with the  $g$ -values 2.0204, 2.0082, and 2.0050, and  $A_{iso}(H) = 0.9$  mT, was observed after inactivation of PFL by oxygen (Reddy *et al.*, 1998). These values are close to the values obtained from the simulation of the spectrum in Figure 3-12. In an oxygen saturated frozen solution of cysteine-HCl, sulfinyl radicals have also been observed by EPR after  $\gamma$ -irradiation at 77 K ( $g_x = 2.0203$ ,  $g_y = 2.0080$ ,  $g_z = 2.0027$ , and  $A_{iso}(H) = 1.4$  mT). The sulfinyl radicals were shown to be successors of thiyl radicals after a reaction of thiyl radicals with dissolved oxygen in the sample (Sevilla *et al.*, 1987).

Oxidation of R1 by  $Ce^{IV}/NTA$  in the presence of oxygen leads to the formation of an EPR spectrum detected at 40 K (Figure 3-12B) that exhibits a similar lineshape to the spectrum recorded after photolysis of NO-R1 (Figure 3-12A). Although the width of the hfs components are slightly larger in the sample treated with  $Ce^{IV}/NTA$ , it most likely the same sulfinyl radical. When the R1 sample is pretreated with the thiol-blocking agent DTNB, no sulfinyl radicals are observed after oxidation by  $Ce^{IV}/NTA$  (Figure 3-12C). Though, it is evident that the more stable sulfinyl radicals found in R1 are the successors of the shorter living thiyl radicals. The lifetime of the sulfinyl radical in R1 was rather long, thawing of the sample and holding it at room temperature for 2 min did not change the shape and amplitude of the EPR spectrum, which was recorded after refreezing to 40 K. From EPR studies of oxidized low-molecular weight thiols, it is known that sulfinyl radicals are observable even at room temperature in the liquid state (Gilbert *et al.*, 1975).

### 3.5 EPR LINESHAPE ANALYSIS

Rotational fluctuations of a spherical molecule in a liquid medium can be described by a term called the rotational correlation time  $\tau_R$ , which is defined as the time it takes the molecule to rotate an angle of 1 rad, i.e.  $57^\circ$ . Given the molecular radius  $r$  and the viscosity  $\eta$  of the medium, this value can be estimated from the Einstein-Debye expression (Equation 3.1) (Carrington and McLachlan, 1969):

$$\tau_R = \frac{4\pi r^3 \eta}{3kT} \quad (3.1)$$

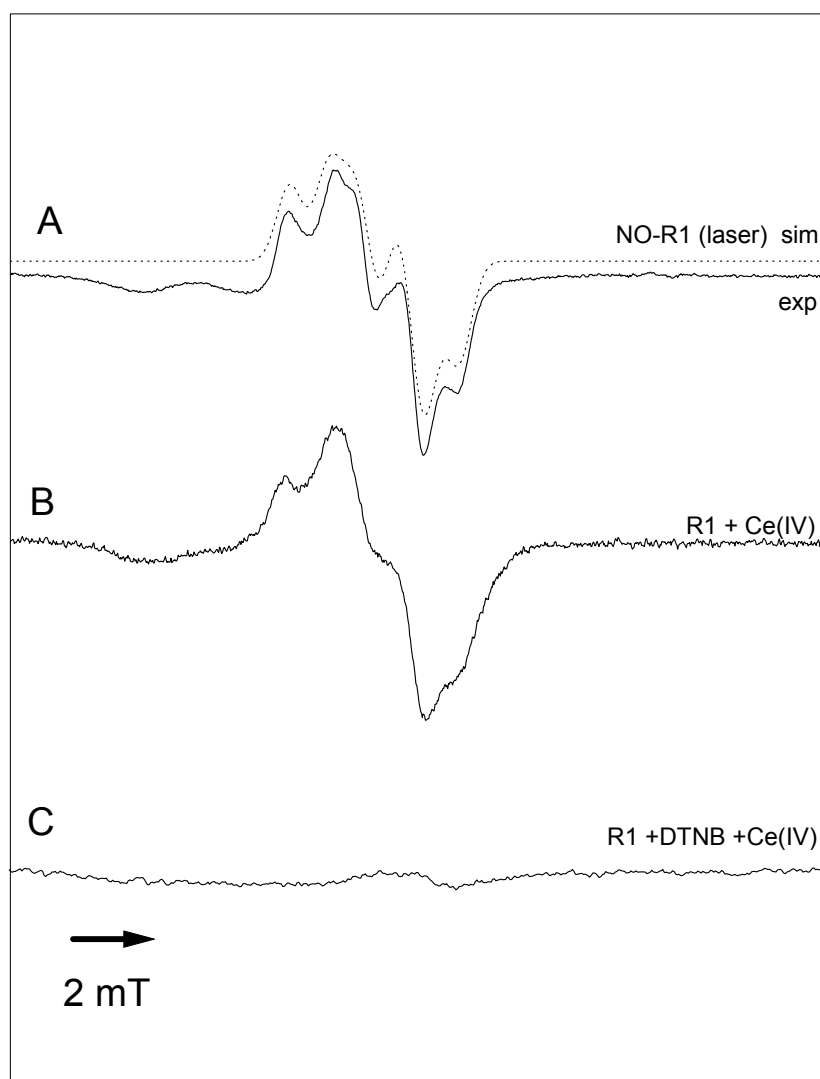


**FIGURE 3-12 EPR SPECTRA OF SULFINYL RADICALS FORMED IN R1 PROTEIN AFTER PHOTOLYTICAL OR CHEMICAL OXIDATION OF THIOLS UNDER AEROBIC CONDITIONS IN THE ABSENCE OF SPIN TRAPS**

(A) EPR spectrum at 40 K of NO-R1 protein (700 $\mu$ M) after laser illumination. EPR conditions: microwave power: 0.1 mW; modulation amplitude: 0.4 mT; time constant: 40 ms; scan time: 40 s; 100 scans. Dotted line: simulated spectrum, gaussian lineshape ( $\Delta H = 0.72$  mT),  $g_x = 2.0213(4)$ ,  $g_y = 2.0094(4)$ ,  $g_z = 2.0018(4)$  (errors in the last digit in parenthesis),  $A_x = 1.0$  mT,  $A_y = 1.1$  mT,  $A_z = 0.9$  mT.

(B) EPR spectrum at 40 K of R1 oxidized by  $Ce^{IV}$ /NTA. Assay conditions: R1 (400 $\mu$ M), DTPA (1 mM), MOPS (0.5 M) pH 7.0, +  $Ce^{IV}$  (1.9 mM)/NTA (3.8 mM), frozen to 77 K after 1 min incubation time. EPR conditions: as in (A), 10 scans.

(C) Assay conditions as in (B), but R1 is preincubated with DTNB prior to  $Ce^{IV}$ /NTA oxidation. EPR conditions: as in (A), 50 scans.

Hence, a molecule with a radius of 20 Å would have a  $\tau_R$  of 8 ns in water at room temperature ( $\eta = 1$  cp at 25°C).

The lineshape of an EPR spectrum depends, among other factors, on the orientation of the paramagnetic center with respect to the applied magnetic field. In a powder, or a frozen aqueous solution, the paramagnetic centers will be fixed with a random distribution of orientations, and in the case of anisotropic  $g$ - and hfs interactions this will lead to a broadened EPR spectrum since all orientations contribute equally. In the liquid state, however, the paramagnetic centers are not fixed but undergo rotational fluctuation. In the case of fast rotation, the anisotropic interactions are thereby averaged to zero, giving rise to sharp EPR lines. If the velocity of the rotational motion decreases, the EPR spectrum will approach that of the powder spectrum. Therefore, a rotational correlation time for a paramagnetic molecule can also be determined by EPR using semiempirical formulae (Poole and Farach, 1987).

The glutathion spin adduct (GSH-PBN), which is a relatively small molecule, gives rise to a spectrum with narrow lines, typical for fast isotropic rotational motion (Figure 3-7A). For this kind of rotation, the rotational correlation time can be estimated from the intensity ratio of the low-field and high-field N-lines using a semiempirical formula (Poole and Farach, 1987, Berliner, 1976):

$$\tau' [\text{ns}] = 0.547 \Delta H_0 [(h_0/h_{-1})^{1/2} + (h_0/h_{+1})^{1/2} - 2] \quad (3.2)$$

where  $\Delta H_0$  is the peak to peak linewidth (in 0.1 mT units) of the central line, and  $h_{1,0,+1}$  are the amplitudes of the low field(+1), central(0), and high field (-1) EPR lines. This formula is valid for  $\tau$  up to 5 ns.

In large molecules, such as proteins, the rotation of the spin adduct is significantly slower leading to a broadening of the EPR lines. In this case, the rotational correlation time,  $\tau$ , is larger than 5 ns, and thus, the Formula 3.2 used for the GSH-PBN spin adduct is not applicable. The isotropic nitrogen hyperfine splitting changes to a powder like spectrum, with the peak-to-peak distance between the external peaks of the spectrum ( $2A'_{zz}(\text{N})$ ) depending on the magnitude of the rotational correlation time,  $\tau$ . Another lineshape theory for slow isotropic Brownian rotational diffusion of spin-labeled proteins has been developed by J. Freed (in Berliner, 1976). Here, an estimation of the rotational correlation time can be made by taking the ratio of the  $2A'_{zz}(\text{N})$  from the liquid state spectrum and the  $2A_{zz}(\text{N})$  from the frozen solution spectrum, which is the rigid limit of the spin adduct exhibiting the maximal possible  $2A_{zz}$  distance (see Figure 3-7 and 3-8):

$$\tau'' [\text{ns}] = a \left( 1 - \frac{A'_{zz}(\text{N})}{A_{zz}(\text{N})} \right)^b \quad (3.3)$$

where  $a$  and  $b$  are empirical constants, which are tabulated in e.g. Poole and Farach, 1987. For an EPR spectrum of a spin adduct undergoing Brownian rotational diffusion with a linewidths of 0.3 mT,  $a = 0.54$  ns and  $b = -1.36$ .

The calculated correlation times for GSH, using Equation 3.2, for BSA and R1 using Equation 3.3, and the correlation times calculated from the molecular radii by Equation 3.1 are listed in Table 3-1.

For the GSH-PBN spin adduct, the rotational correlation times lie between 0.05 and 0.2 ns, which is consistent with fast rotation as expected for a small molecule. For BSA and R1 the values are considerably larger, indicative of slow rotation. There are, however some noticeable features of the spectra. In both proteins, and most prominent in the case of oxidation by cerium, there are two different spectral parts (see Figures 3-7 and 3-8). The minor parts (marked with an asterisk in Figures 3-7 and 3-8) have a rotational correlation time of 4-5 ns, which must be regarded as fast rotation and indicate that these spin adducts are located in flexible protein chains, probably at the surface of the protein. The major parts of the spectra have correlation times of 12-15 ns calculated from the spectra of the laser photolyzed samples, and 19-22 ns calculated from the cerium-treated samples. These values are all typical for slow rotation and show that the protein-PBN spin adducts from both BSA and R1 are located in non-flexible, e.g. folded, parts of the protein. The slightly smaller rotational correlation times compared to the ones calculated using the Einstein-Debye formula (40 ns for BSA and 60 for R1) might indicate a residual mobility, which may be explained as a mobility of the protein domains. It is, however, important to note that the  $\tau$  values obtained from the EPR spectra can only be regarded as crude estimates.

**TABLE 3-1 ROTATIONAL CORRELATION TIMES OF PBN-THIYL SPIN ADDUCTS**

	Radius (Å)	$\tau_R$ (ns) Einstein- Debye	$\tau'$ (ns)	$2A_{zz}$ (N) (mT)	$2A'_{zz}$ (N) (mT)	$\tau''$ (ns)
GSH + Ce <sup>IV</sup> /NTA	8	0.05	0.2			
BSA + Ce <sup>IV</sup> /NTA	35	40		6.90	6.46	22
fast part			4			
NO-BSA	35	40		6.86	6.18	12
R1 + Ce <sup>IV</sup> /NTA	40	60		6.89	6.47	19
fast part			5			
NO-R1	40	60		6.86	6.36	15

The correlation times are calculated using Equation 3.1 for  $\tau_R$ , Equation 3.2 for  $\tau'$ , and Equation 3.3 for  $\tau''$ .

### 3.6 ACTIVITY TESTS OF ARTIFICIALLY GENERATED THIYL RADICALS

The experiments described above has shown that it is possible to generate thiyl radicals in the R1 subunit of RNR in the absence of R2. The next question arising is whether the catalytically essential thiyl radical at C439 is among these thiyl radicals, and if so, if this artificially generated radical is still able to perform catalytic activity. In this section, the first attempts to detect catalytic activity of the artificially generated thiyl radicals are described. Figure 3-13 shows the path of the radical state in RNR during catalytic turnover, which can be used as a basis for setting up experiments to mimic parts of the turnover involving the thiyl radical.

#### 3.6.1 AZIDO-CDP

2'-Azido-2'-deoxycytosine 5'-diphosphate (azido-CDP) is a substrate analogue and a suicide inhibitor for RNR. In holo RNR, azido-CDP triggers the radical transfer from the tyrosyl radical in the R2 subunit to R1, but due to its 2'-azido moiety instead of the normal 2'-hydroxy, the turnover is terminated while the radical state remains within the active site of R1 (Thelander *et al.*, 1976, Salowe *et al.*, 1993). Thereby, a sulfinylimine radical is formed at the active site that can be observed by EPR (see Section 2.1.4). Since the thiyl radical, C439, is also believed to be part of the azido-CDP inactivation scheme, the azido-CDP assay can be used to test the catalytic involvement of a possible artificial thiyl radical at C439 in a new assay leaving out the R2 subunit.

Before testing the artificially generated thiyl radicals, the azido-CDP assay was tested on the wild-type holoenzyme. EPR spectra were recorded before adding azido-CDP ( $t = 0$ ) and up to 30 minutes after mixing (Figure 3-14). During this time, the signal intensity of the tyrosyl radical (top spectrum in Figure 3-14) decreases, and a new intermediate signal appears. By subtracting the pure tyrosyl radical spectrum from the spectrum obtained after 6 minutes incubation (middle spectrum in Figure 3-14), the isolated spectrum of the new signal is obtained (lower spectrum in Figure 3-14). The  $g$ -values and nitrogen and proton hyperfine splitting of this spectrum are consistent with the sulfinylimine (R-S-N'-H) radical on C225 of the active site of R1 (van der Donk *et al.*, 1995). Figure 3-15 shows the kinetics of the biphasic decay of the Y122 radical and the formation and decay of the azido-CDP radical. The rate constants of these reactions are contained in the following expressions (from Persson *et al.*, 1997):

$$y(t) = A_{1(Y\cdot)} e^{-k_{1(Y\cdot)}t} + A_{2(Y\cdot)} e^{-k_{2(Y\cdot)}t} \quad (3.4)$$

$$y(t) = A_{(SN\cdot)} \times k_{1(SN\cdot)} / (k_{2(SN\cdot)} - k_{1(SN\cdot)}) \times (e^{-k_{1(SN\cdot)}t} - e^{-k_{2(SN\cdot)}t}) \quad (3.5)$$

where  $A_i$  is the maximum yield of the EPR signal.

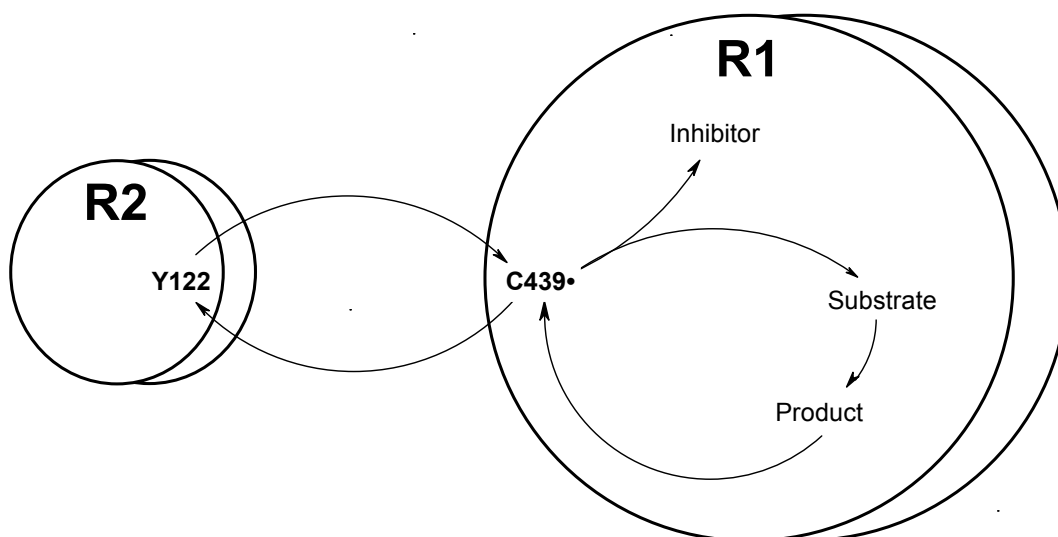


**FIGURE 3-13 POSSIBLE ROUTES OF THE RADICAL STATE IN RNR**

*The reaction of the transient thiyl radical on the cysteine C439 in the large R1 subunit of RNR, can take three different routes depending on the present environment. If a substrate is present, and the R1 disulfide bridges are reduced, the radical will attack the substrate which will thereby be reduced. If a product is present, and the disulfide bridges of R1 are oxidized, the radical will return to Y122 in R2. The radical can also be trapped on special substrate analogous inhibitors, e.g. azido-CDP (see text).*

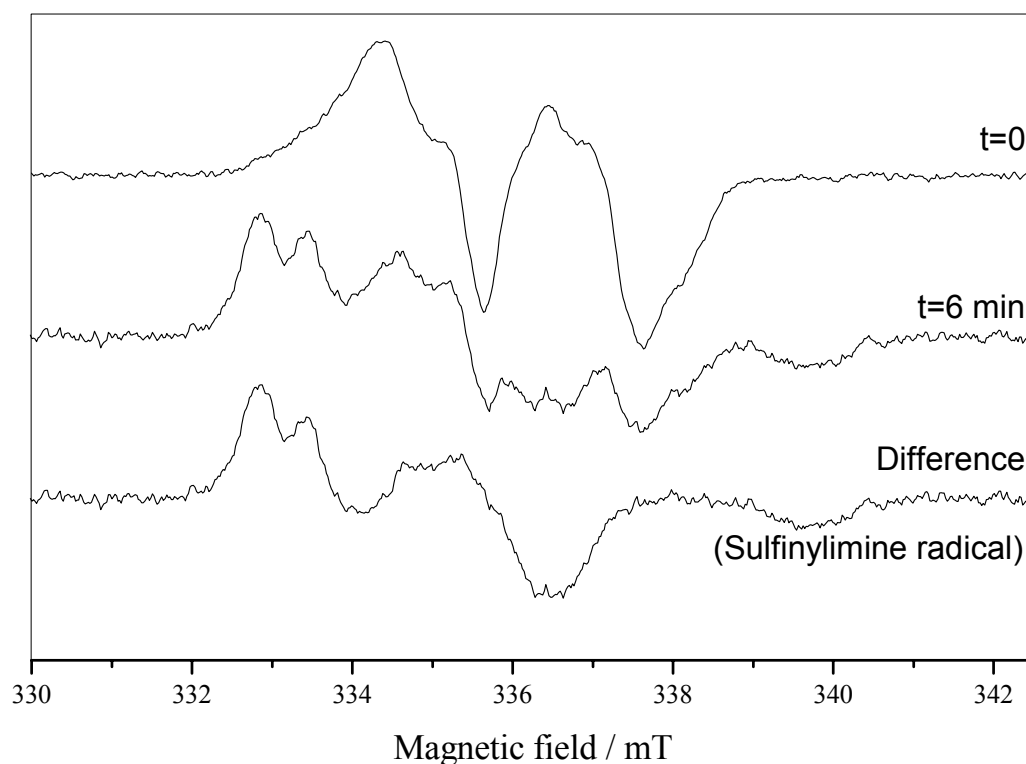


**FIGURE 3-14 EPR SPECTRA OF THE INACTIVATION OF RNR BY AZIDO-CDP**

*The upper spectrum shows a sample of 50  $\mu\text{M}$  R2 before adding R1 and azido-CDP. The middle spectrum shows a sample with 50  $\mu\text{M}$  R1, 50  $\mu\text{M}$  R2, and 1 mM azido-CDP frozen 6 minutes after mixing. The lower spectrum is the difference spectrum showing only the new radical. X-band EPR spectra recorded at 40 K, microwave power: 10  $\mu\text{W}$ , modulation amplitude: 0.1 mT, 10 scans.*

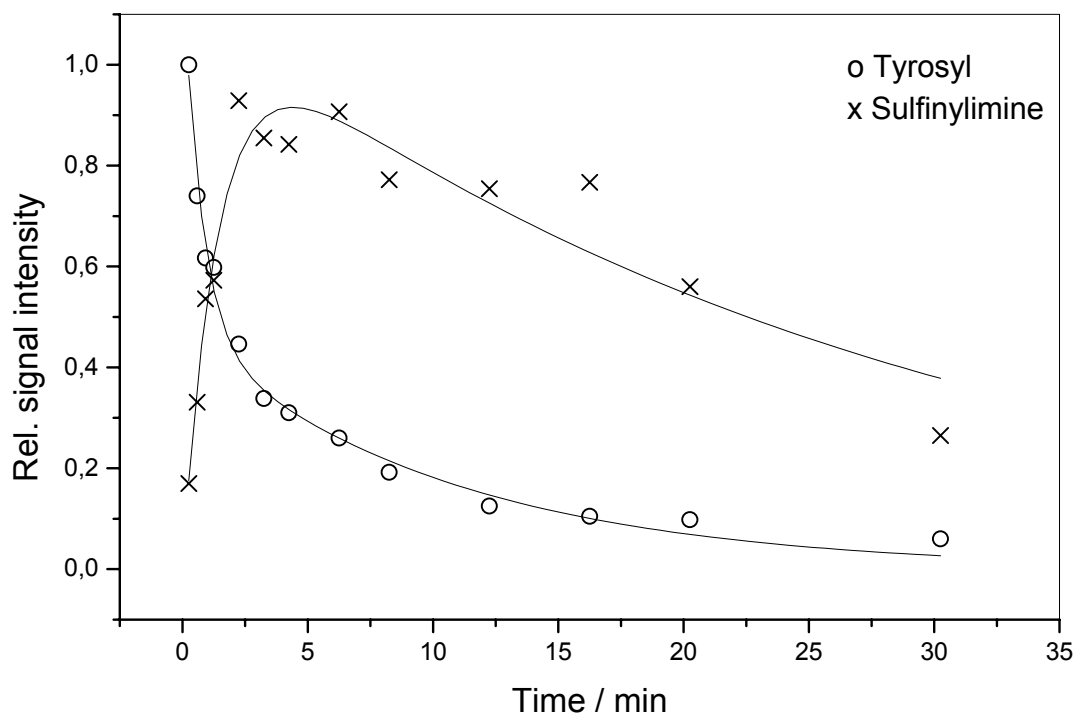


**FIGURE 3-15 KINETICS OF THE TYROSYL RADICAL AND THE SULFINYLIMINE RADICAL**

*The relative signal intensity of the two EPR signals observed at 40 K in a sample containing 50  $\mu$ M R1, 50  $\mu$ M R2, and 1 mM azido-CDP (see Figure 3-14). The different time points were obtained by thawing, incubating, freezing, and measuring the sample repeatedly. EPR parameters given in the legend of figure 3-14.*



Here, the determined rate constants using these formulae where:

$$k_1(Y^\bullet) = 1.34 \pm 0.25 \text{ min}^{-1}$$

$$k_2(Y^\bullet) = 0.95 \pm 0.15 \text{ min}^{-1}$$

for the biphasic decay of Y122<sup>•</sup>, and

$$k_1(SN^\bullet) = 0.72 \pm 0.12 \text{ min}^{-1}$$

$$k_2(SN^\bullet) = 0.036 \pm 0.007 \text{ min}^{-1}$$

for the increase and decay of SN<sup>•</sup>, respectively. This control experiment shows that our azido-CDP preparation inhibits RNR successfully in the wild-type holoenzyme.

To test the catalytic ability of the thiyl radicals generated by one-electron oxidation using cerium as oxidant, the azido-CDP assay was repeated as described in Section 2.1.4, without the R2 subunit and in presence of 8.3 mM Ce<sup>IV</sup>/NTA. The concentration of R1 was also increased to 200 μM to increase the yield of thiyl radicals able to react with azido-CDP.

In this case, however, there was no sign of the azido-CDP derived sulfinylimine radical. Similarly, in the samples with thiyl radicals generated by laser photolysis of nitrosylated R1, using 200 μM NO-R1, there was no indication of the build-up of an sulfinylimine radical.

### 3.6.2 REVERSE RADICAL TRANSFER

There are principally two possible routes for the thiyl radical on C439 in R1 to obtain its missing electron (see Figure 3-13). If a substrate, i.e. a ribonucleotide, is bound in the active site, and the cysteine pair C225/C462 is reduced, the thiyl radical will obtain an electron by abstracting the 3'-hydrogen from the substrate ribose, which is the initiation of the normal substrate turnover. However, at the end of the turnover reaction, when a product, i.e. a deoxyribonucleotide, is bound in the active site, and the cysteine pair C225/C462 is oxidized into a disulfide bridge, the electron is postulated to be obtained from Y122 in R2, thereby reforming the tyrosyl radical. This route may even be preferred if there is no substrate in R1. The state of the R2 protein during the catalytic turnover is not known, but since Y122 must provide an electron to R1, it can not be in the radical state itself, meaning that R2 must be in a redox state similar to the metR2 state (see Section 1.3.2).

Based on the assumption that the radical transfer pathway is operational in the metR2 form, we performed first attempts to visualize a reverse radical transfer from R1 with artificially generated thiyl radicals, to Y122 in metR2. The cerium-oxidation experiment was performed with 200 μM R1 and 200 μM metR2, mixed with 8.3 mM Ce<sup>IV</sup>/NTA in 1 mM DTPA and 0.5 M MOPS pH 7.0. The laser photolysis experiment was performed with 200 μM NO-R1 and 200 μM metR2. This mixture was transferred to a 4 mm EPR tube and laser flashed with 30 shots, and then frozen in cold iso-pentane.

In neither of these cases, were we able to detect formation of the stable Y122 radical with EPR.

### 3.7 DISCUSSION

In this work, three different methods for artificial generation of thiyl radicals in the protein subunit R1 of RNR have successfully been tested in the absence of the R2 subunit, which is an essential prerequisite for the generation of the catalytic thiyl radical *in vivo*.

By use of UV-irradiation, thiyl radicals were generated and detected by EPR in cysteine, BSA, and R1. The thiyl radicals observed here in the proteins BSA and R1 represents the first directly EPR detected, non-metal-associated, thiyl radicals in a protein environment in the absence of spin traps. The EPR lineshape analysis of the radical at X-band frequency revealed a strong  $g_{\perp}$  component at 2.008 and a weak and broad  $g_{\parallel}$  component at 2.17-2.30, which is typical for a thiyl radical. In the first derivative EPR spectrum, the  $g_{\parallel}$  edge is difficult to detect in proteins, but by numerical integration, the  $g_{\parallel}$  is clearly visible as a broad shoulder. There was a significant difference in the shape of the  $g_{\parallel}$  component of the axial EPR spectra in these three samples, which can be ascribed to the different electrostatic environments of the thiol groups. In cysteine, a uniformly weak hydrogen bond interacts with the sulfur atom giving rise to a distinct  $g_{\parallel}$  value of 2.29, in BSA, a larger distribution of different H-bonds, but a dominating strong H-bond give rise to a  $g_{\parallel}$ -value of 2.18, and in R1, spectral features of several different cysteines are superimposed, all with slightly different environment, so that no distinct  $g_{\parallel}$  edge can be observed. However, the  $g_{\parallel}$ -component represents a characteristic fingerprint for thiyl radicals, also in proteins. The large  $g$ -anisotropy is also reflected in the relaxation behavior of the two  $g$ -components. The  $g_{\parallel}$ -component exhibits a strong relaxation, unusual for a radical, whereas the  $g_{\perp}$ -component relaxes much slower. The broadening of the  $g_{\parallel}$ -component exhibits a considerable heterogeneity of H-bonds to the sulfur lone pair orbitals. This effect is particularly evident in the protein samples, and may contain valuable information about H-bonding of protein thiyl radicals. The stability of the thiyl radicals was investigated by annealing experiments. The thiyl radicals in frozen solutions of R1 were stable up to 150 K, at higher temperature they start to decay and at 270 K they completely disappear. The optimal conditions for successful EPR detection of protein thiyl radicals is X-band frequency, large microwave power, low temperature, and integrated first derivative spectra. Due to the resolved large  $g$ -anisotropy at X-band, high-field EPR would increase the spread of the EPR spectrum, which would be disadvantageous. EPR at lower frequencies would increase the intensity of  $g_{\parallel}$ . Spin echo detected EPR (ESE) which operates in absorption mode, has been tried, however, this technique is unsuitable for detection of the  $g_{\parallel}$ -component of the thiyl radical, due to its extreme relaxation behavior.

It was demonstrated by EPR spectroscopy and spin-trapping techniques that thiol oxidation in R1 by  $\text{Ce}^{\text{IV}}/\text{NTA}$  as well as photolytic release of NO from nitrosylated R1 led to a selective formation of thiyl radicals in R1. The spin trap PBN has been verified as an appropriate and sensitive EPR detector for thiyl radicals in R1 with a sufficient long lifetime of the spin adduct, even in presence of the strong oxidant  $\text{Ce}^{\text{IV}}/\text{NTA}$ .

Due to the small proton splitting of the thiyl-PBN spin adduct, the EPR lineshape in the immobilized case closely resembles that of nitroxide radical spin labels. Thus, the theory of lineshape of nitroxide radicals can be used completely also for determination of the dynamic properties and rotational correlation times of the protein thiyl-PBN spin adducts (Graceffa, 1983, Mullins *et al.*, 1992). In the present work, the rotational mobility of the thiyl-PBN spin adduct was determined for R1 and BSA for both the photochemically generated thiyl radicals in nitrosylated proteins and the thiyl radicals generated through oxidation using  $\text{Ce}^{\text{IV}}/\text{NTA}$ .

Although we have to take into consideration that the EPR spectrum of the spin adduct consists of the sum of different thiol positions in R1, the lineshape of the majority of the spin adducts exhibit clear properties of isotropic Brownian type rotational diffusion. The majority of the thiol-PBN spin adducts in R1 exhibit an isotropic slow-motion-type EPR lineshape, and a minority exhibit an isotropic fast-motion-type EPR lineshape. The values for the rotational correlation time in R1 and BSA,  $\tau = 12\text{-}15$  ns for the photolytically generated thiyl radicals and  $\tau = 19\text{-}22$  ns for the thiyl radical generated by oxidation (see Table 3-1), are very similar within the estimated errors, and are about 100 times larger than those for the spin adduct found in the flexible low molecular weight tripeptide GSH ( $\tau \sim 0.2$  ns). This underlines that in the proteins the majority of thiol groups carrying the spin adducts are strongly immobilized, and are therefore located in non-flexible folded regions of the protein. However, these thiols must still be accessible for both the hydrophobic PBN spin trap and the polar  $\text{Ce}^{\text{IV}}/\text{NTA}$  complex. The systematic difference between the correlation times from the  $\text{Ce}^{4+}/\text{NTA}$  treated samples, with higher  $\tau$  values, and the laser photolyzed samples, with lower  $\tau$  values could be due to the difference in pH in these samples, pH 7.0 in the cerium-oxidation assay, and 8.0 in the laser-photolysis assay. It is also possible that different cysteines contribute to the signal in these two cases, due to different accessibility of NO and the much larger  $\text{Ce}^{4+}/\text{NTA}$  complex. Hence, using  $\text{Ce}^{4+}/\text{NTA}$  a larger proportion of the thiyl radicals may be generated on the surface of the protein where the rotational mobility is larger.

In the samples that were oxidized using  $\text{Ce}^{\text{IV}}/\text{NTA}$ , a minority of the thiol groups ( $\sim 20\%$ ) displayed a faster mobility of spin adduct ( $\tau \sim 4$  ns), and seems to be localized in a more flexible protein environment, e.g. at the surface of the protein (compare Figure 3-8A with Figure 3-7B and C).

It was shown by the thiol blocking experiments that both the nitrosylation and photolysis procedure, as well as the oxidation procedure using  $\text{Ce}^{\text{IV}}/\text{NTA}$  were specific for the protein thiol groups. However, neither of these methods are specific for the thiol on C439, the proposed site for the catalytically active thiyl radical. Nitrosylation of R1 has previously been studied in the context of reversible inhibition of RNR with the result that nitrosylation is more or less uniformly distributed over the thiols in R1 (Roy *et al.*, 1995). It is therefore reasonable to assume that formation of thiyl radicals by photobleaching in R1 is also distributed over several thiol sites. By quantitation of the thiol groups using Ellman's reagent in the native R1 dimer, 10 thiols out of 22 proved to be sufficiently accessible to undergo a reaction with the reagent after 20 min incubation at room temperature. The same value was estimated for the number of R-S-NO groups in the nitrosylated R1 dimer, assuming that the optical extinction coefficient of NO-R1 is the same as for NO-BSA. The R1 dimer

has totally 22 cysteines of which 8 are capable of forming disulfide bridges. A space-filling model using standard van der Waals radii based on the crystal structure (Uhlen and Eklund, 1994, Eriksson *et al.*, 1997), reveals that most cysteines are buried in the interior of the protein. Among the more surface-exposed cysteines are both the catalytically essential C439 and C225, which are located in the active site cleft (see Figure 1-2). When a substrate is bound in the catalytic cleft, the C225 at the bottom of the cleft is covered, whereas the C439 remains accessible. Thus, it seems reasonable to assume that C439 is one target of nitrosylation and  $\text{Ce}^{\text{IV}}/\text{NTA}$  oxidation. This accessibility of the catalytic radical site of R1 may seem unfavorable for the *in vivo* enzymatic function of RNR. However, when R2 is bound to R1, the active site cleft is shielded by the C-terminal tail of R2 (Sjöberg, 1994), which would provide protection and sterical stabilization of the transient thiyl radical generated on C439 during the enzymatic turnover reaction.

Spin trapping of thiyl radicals in an oxidizing media can in some cases be troublesome, as discussed by Alberti *et al.*, 1997. Nitron spin traps such as PBN and DMPO may first be oxidized to a nitroxide cation and subsequently react with a thiolate ion ( $\text{S}^-$ ) resulting in the same spin adduct as in Scheme 2-4 in Section 2.2.8. In that case, a thiolate rather than a thiyl radical would be the spin trapped species (so called "inverted spin trapping"). In our case using  $\text{Ce}^{\text{IV}}/\text{NTA}$  as oxidant this possibility must, in principle, be considered. This situation can, however, be excluded since the presence of thiolates, which have a  $\text{pK}_a$  of 8.3 in free cysteines, is not likely for R1 in aqueous medium at neutral pH. Furthermore, the same spin adduct spectra also occur in the absence of  $\text{Ce}^{\text{IV}}/\text{NTA}$  upon laser illumination of NO-R1 samples where the scission of the S-NO bond of NO-thiols definitely leads to thiyl radicals. Another strong indication for the presence of thiyl radicals is our observation by EPR of sulfinyl radicals, which are formed from thiyl radicals in the presence of oxygen.

There were no detectable thiyl radicals under the conditions used in the two low temperature EPR studies of R1 in the absence of the spin trap PBN, where R1 was oxidized by  $\text{Ce}^{\text{IV}}/\text{NTA}$ , or the nitrosylated R1 was illuminated by laser. Instead, in both cases, we detected and assigned, for the first time, sulfinyl radicals in R1 when oxygen was present. In the case of oxidation of R1 by  $\text{Ce}^{\text{IV}}/\text{NTA}$ , the sulfinyl spectrum is absent when the thiols are chemically blocked by DTNB. We therefore interpret the observed sulfinyl radicals as successors of thiyl radicals, e.g. the reaction product of chemically or photolytically formed thiyl radicals in R1 with oxygen dissolved in the sample. This explanation is also based on prior observations of sulfinyl radicals with very similar  $g$ -values in irradiated cysteine (Sevilla *et al.*, 1987). Apparently, in absence of PBN, small concentrations of oxygen may be sufficient to react with the thiyl radicals to form sulfinyl radicals. In the presence of PBN, however, thiyl radicals react with higher affinity with the spin trap than with oxygen (Harman *et al.*, 1984). Another reason for not seeing the thiyl radicals in R1 directly by EPR may be their short lifetime. There are no data available on the lifetime of thiyl radicals in proteins. Under the conditions of our experiments – generation of thiyl radicals in the liquid state and subsequent freezing within 1 to 2 s – only long-lived protein-thiyl radicals can be observed directly by EPR. Our data

indicate that protein-thiyl radicals in R1 have lifetimes significantly shorter than 1 s at room temperature.

We were, in a first attempt, not able to detect any catalytic activity of the artificially generated thiyl radicals, neither with the azido-CDP assay in R1, nor with reverse radical transfer from R1 to Y122 in R2 in holo RNR. This tells us that either (i) no thiyl radical is generated on the catalytically essential, C439, or (ii) that the artificially generated thiyl radical C439<sup>•</sup> is too unstable to trigger catalytic activity, especially in the case without the protecting C-terminus of R2, or (iii) that the amount of C439<sup>•</sup> generated by the oxidation or photolysis reactions is too low, and hence yield of the products, i.e. the sulfinylimine radical or the tyrosyl radical, are also too low to be observed by EPR.

As discussed above, the position C439 is a very likely candidate for the artificial generation of thiyl radical due to its exposed position. This good accessibility may be fortunate for a reaction with Ce<sup>IV</sup>-complexes and the spin trap, it may, however, be unfortunate for the stability of the thiyl radical since it may react with oxygen instead of with the substrate, or with the substrate analogous inhibitor. In wild-type RNR, the cleft containing the C439 is covered by the C-terminus of R2. In a reverse radical transfer experiment (see Section 3.6.2) where metR2 is present, this could prevent the Ce<sup>IV</sup>/NTA complex from accessing C439, but in the case of laser photolysis of NO-R1 that is preloaded with nitric oxide, this should not play any role. Regarding the assay conditions for the reverse radical transfer, it is not trivial that the metR2 can function as a radical acceptor, i.e. an electron donor, for a thiyl radical on R1. In one model for radical transfer from R2 to R1, it is believed that the hydrogen bridges of the radical transfer pathway are flipped over during the time the radical is in the active site of R1 (Ehrenberg, 1999), and thus, different from the metR2 state. It may also be important to have product bound in the active site, and having the cysteine pair C225 and C462 oxidized as a disulfide bridge.

The yield of the thiyl radical generation experiments has shown that we could only detect 3 % thiyl radicals per R1 dimer. We have also shown that around 10 different cysteines are involved, reducing the probability of a visible thiyl radical on C439 further. In 200 μM R1, this could imply that we have only 1.2 μM radical on C439 if the yield is evenly distributed on all 10 cysteines, and if we count the C439 in both R1 monomers. Therefore, even with an optimally working radical pathway, this low yield alone is probably too small to be observed by EPR. The fact that probably only a fraction of the artificially generated thiyl radicals will be able to react with a substrate before they are lost, due to the short lifetime of the thiyl radical, is adding up to this problem.

This means that observation of catalytic competence of the artificially generated thiyl radicals is very difficult and needs a careful optimization of all factors involved, particularly an assay that is much more sensitive. By EPR, radical concentrations down to 10 μM can be detected, but this is not sufficient in this case.



# 4

## STABLE AND TRANSIENT PARAMAGNETIC CENTERS IN R2- Y122H

The R2 subunit in ribonucleotide reductase has several unique features which have placed it in focus of studies for more than three decades. The diiron center possesses a strong oxidation power, capable of oxidizing a tyrosine residue, Y122 in *E. coli*, to a tyrosyl radical following dioxygen activation (see Section 1.3.2). Apparently, no other amino acid radicals are formed in this reaction, which indicates that the oxidizing power of the diiron center is directed selectively to the tyrosine site in the wild-type R2 protein. The tyrosyl radical in R2 is also unusually stable for an organic radical, which is attributed to the exchange interaction with the diiron-oxygen center, as well as to its shielded position in a hydrophobic pocket within the protein, preventing the access of most radical scavengers from the surrounding medium (Ormö *et al.*, 1995). The R2 protein, in other words, seems to be an ideal system for generation of stable protein radicals.

Protein radicals are frequently involved in biological processes (Stubbe and van der Donk, 1998), however, in most cases they are only transient and difficult to trap for spectroscopic investigations. Apart from tyrosine radicals, which are also found in photosystem II (Barry and Babcock, 1987), bovine liver catalase (Ivancich *et al.*, 1997), prostaglandin H synthase (Tsai *et al.*, 1992), and possibly in dopamine  $\beta$  monooxygenase (Tian *et al.*, 1994), tryptophan radicals have been observed in cytochrom *c* peroxidase (Sivaraya *et al.*, 1989) and DNA photolyase (Kim *et al.*, 1993), glycine radicals in pyruvate formate lyase (Knappe *et al.*, 1993) and in the class III RNR (Sun *et al.*, 1993), and cysteine radicals in the class II RNR (Gerfen *et al.*, 1996b). There are also examples of radicals on modified amino acids, e.g. the joint tyrosine-cysteine residue in galactose oxidase (Gerfen *et al.*, 1996a), and possibly a tyrosine-histidine radical in cytochrom *c* oxidase (MacMillan *et al.*, 1999, Proshlyakov *et al.*, 2000). The redox potential at neutral pH ( $E_0'$ ) of tyrosine is about 0.8-1.0 mV, and for the other amino acid residues it ranges from 1.0 mV for tryptophan to 1.3 mV for cysteine (Stubbe and van der Donk, 1998) a similar value is

expected also for histidine (Lassmann *et al.*, 1999). No redox potential is known for the  $\text{Fe}^{\text{III}}\text{Fe}^{\text{IV}}$  state of R2, however, it might well be high enough to oxidize amino acid residues with a redox potential slightly higher than tyrosine.

These facts were the basis for a project started in Berlin by Dr. Günter Lassmann and Dr. Stephan Pötsch in cooperation with Prof. Astrid Gräslund and Prof. Britt-Marie Sjöberg in Stockholm, where the R2 protein was intended to be used as a test system for studies of different protein-associated amino acid radicals. A series of R2-Y122X mutants, or the equivalent R2-Y177X in the mouse protein, were generated by site directed mutagenesis, with X representing phenylalanine (F), tryptophane (W), cysteine (C), or histidine (H). These mutants should provide new information on radicals in a protein environment, and as an alternative to the tyrosine radical in wild-type R2, may even show some catalytic activity as a temporal electron acceptor during substrate turnover in the R1 subunit.

The *E. coli* mutant R2-Y122F has been known for several years to produce a stabilized high-valence diiron center, intermediate X (Bollinger *et al.*, 1991). In later studies, several other transient radical species have been observed as oxidation products of intermediate X; two of these radicals were assigned to neutral tryptophan radicals on W111 and W107, which are also located near the iron site (Sahlin *et al.*, 1994, Sahlin *et al.*, 1995). The electronic structure of W111<sup>•</sup> was characterized using ENDOR spectroscopy (Lendzian *et al.*, 1996). In the mouse R2-Y177W mutant, a tryptophan radical was actually generated at the desired position and characterized by ENDOR, but no catalytic activity could so far be detected (Pötsch *et al.*, 1999). These three different tryptophan radicals have also been studied by high-field EPR at W-band, where the *g*-tensors, and  $\beta$ -proton hf couplings are better resolved (Bleifuss *et al.*, manuscript submitted to Biochemistry).

The mutant R2-Y122H was originally designed with the aim to generate a histidine radical for EPR and ENDOR studies in the shielding hydrophobic pocket that normally hosts the tyrosyl radical, and to see if such a radical could be catalytically active. Histidine residues are often found as ligands to metal centers as well as in electron transfer pathways in proteins. The two nitrogen atoms in the imidazole ring of histidine may easily engage in hydrogen bonding, both as hydrogen donors and acceptors. It is therefore conceivable that intermediate histidine radicals occur in these systems. In fact, a histidine radical has been postulated in the plant photosystem II (Zimmermann *et al.*, 1993), but so far EPR spectroscopic evidence of any histidine radicals is missing, and almost nothing is known about their stability and spectroscopic features in a protein environment. Recently, transient cation and neutral histidine radicals in a protein-free system were generated in aqueous histidine solutions using  $\text{Ti}^{\text{III}}$  as oxidant and the hyperfine structure was characterized using continuous-flow EPR supported by DFT calculations (Lassmann *et al.*, 1999, Lassmann *et al.*, 2000).

In the R2-Y122H mutant, however, a histidine radical was not observed after the usual reconstitution reaction. Instead, the purified protein contained a small amount of a novel unusually stable paramagnetic center, named "H". The EPR and ENDOR analysis of this challenging and hitherto unknown center was done in close cooperation with the physicist Günther Bleifuss, a PhD student in the same project, who performed the spectroscopic measurements with high-field EPR and ENDOR



techniques, and the simulation of these spectra. The extensive preparations including growth of *E. coli* cells expressing the R2-mutant, protein purification, and isotope-labeling of the proteins are described in this thesis (chapter 2). The final characterization of the paramagnetic center H particularly its assignment and nature as a ligand radical coupled to the diiron center is the main topic of chapter 4.

## 4.1 THE CRYSTAL STRUCTURE OF R2-Y122H

The mutant protein R2-Y122H was crystallized by Dr. Stephan Pötsch and Dr. Derek Logan in the laboratory of Prof. Pär Nordlund, University of Stockholm, as described previously for the wild-type R2 (Nordlund *et al.*, 1989), and the X-ray structure was resolved using the Swiss-Norwegian Beam Line (SNBL) in Grenoble. The electron density derived from the X-ray structure of R2-Y122H with 1.9 Å resolution clearly confirms the mutation Tyr → His at position 122 of the R2 structure (see Figure 4-1). All ligands of the iron center are well-defined by the electron density, and their conformations are comparable to the structure of the oxidized diferric met R2 with six-coordinate iron (Nordlund *et al.*, 1990, Nordlund and Eklund, 1993). There are, however, some noticeable changes. The Fe – Fe distance in R2-Y122H is slightly longer in R2-Y122H with 3.5 Å in both chains, whereas met R2 has 3.4 and 3.3 Å in chain A and B. The bidentate carboxylate ligand D84 to Fe1 in met R2 becomes a monodentate ligand in R2-Y122H. This is similar to the reduced diferrous form of R2 (Logan *et al.* 1996), but in case of R2-Y122H the iron ligation is replaced by an extra water molecule, keeping the iron six-coordinated, different from the reduced R2 where the Fe1 is five-coordinated. The shifting of D84 in R2-Y122H is presumably favored by a hydrogen bond formed to the  $\epsilon$ -nitrogen of the mutated H122, which is separated from the D84 carboxylate oxygen by a distance of 2.7 Å. In the mammalian R2, where EPR data indicate a hydrogen bond to the tyrosyl radical (Y177') (Schmidt, *et al.* 1996), unlike the *E. coli* R2, a similar aspartate shift of D139 is observed in the crystal structure, however in this case the iron center is not present in the crystal structure. There is also a new water molecule located in the enlarged pocket around H122 adjacent to S119, to which it forms a hydrogen bond. A rotation of the side chain of H122 by 180° would cause the  $\delta$ -nitrogen atom to be hydrogen-bonded to this water molecule, but the conformation presented in Figure 4-1 is probably energetically more favorable.

Interestingly, there are also some differences between the two crystallographically independent protomer chains A and B of the R2-Y122H dimer. This effect has also been observed in the double mutant, Y122F/E238A, and in certain chemically modified wild-type samples (Logan *et al.*, 1998, Logan *et al.*, 1996). The structural differences do only appear near the diiron center, whereas the rest of the protein remains practically identical, which has been explained by a different accessibility for small molecules in the two halves due to crystal packing effects (Logan *et al.*, 1998). The main differences in R2-Y122H are on the residues E238 and F208, both close to the diiron center. E238, which is bridging Fe1 and Fe2 in reduced wild-type R2, is in the case of met R2 and chain A of R2-Y122H opened, with one carboxyl oxygen still ligated to Fe2 and the second oxygen pointing

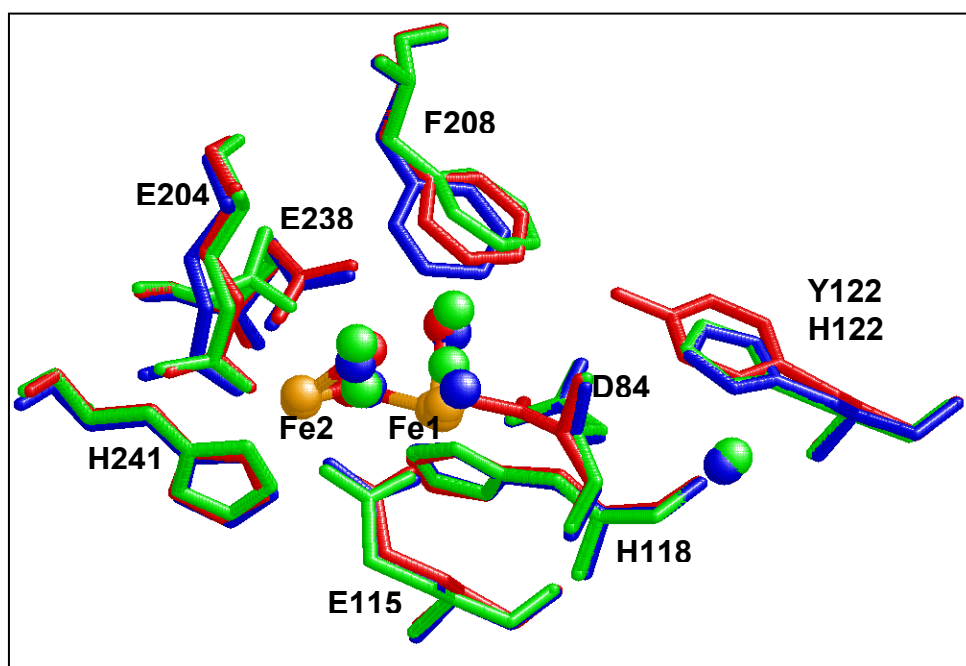


**FIGURE 4-1 SUPERIMPOSED CRYSTAL STRUCTURES OF THE DIIRON SITES OF WILD-TYPE R2 AND MUTANT R2-Y122H**

*The diiron site of both polypeptide chains of R2-Y122H (chain A in blue and chain B in green) compared with the chain A of wild-type R2 (in red, 1rib.pdb from Nordlund et al., 1990). The iron atoms of all three structures are uniformly colored in orange. The red, green and blue spheres represent the  $\mu$ -oxo bridge and water (grouped by black circles). The structures were superimposed by the program UCB Enhanced Rasmol 2.6.*

towards a water molecule ligated to Fe1. In chain B, however, we find the carboxyl group flipped 180° with one oxygen ligated to Fe2 and the second oxygen pointing away from the iron center. There is also a shift of the F208 phenyl ring. In the A chain, this is shifted towards E238 compared to the wild-type met R2, whereas the B chain is shifted in the opposite direction. A recent theoretical study concerning the iron centers in R2 and MMOH with focus on the shifting carboxylate E238 (E234 in MMOH), concluded that the shifting of the carboxylate ligands in both cases have very low energy barriers and may be essential for the oxygen activation (Torrent *et al.*, 2000).

## 4.2 THE NEW STABLE PARAMAGNETIC SPECIES – EPR DATA OF CENTER H

The purified protein R2-Y122H from cells grown in rich LB medium contains, even before the usual reconstitution procedure, a small amount of a paramagnetic species that we have named center H. This paramagnetic species displays a Gaussian shaped singlet spectrum in X-band EPR (9.7 GHz) with an isotropic  $g$ -value  $g = 2.003$  and a 2.2 mT peak-to-peak linewidth at 20 K, indicating a spin state of  $S = \frac{1}{2}$  (Figure 4-2A). Center H is remarkably stable and survives weeks at room temperature, which allows the growth of protein crystals where the signal is still measurable after two weeks. In protein crystals that were stored for three months at room temperature, however, the signal was no longer detectable. The slightly anisotropic  $g$ -tensor is completely resolved in high-field W-band EPR (94 GHz) (Figure 4-2B), and the best spectrum simulation gave  $g_x = 2.0088(1)$ ,  $g_y = 2.0040(1)$ , and  $g_z = 1.9960(1)$ , with the errors for the last digits given in parenthesis.

The spectrum linewidth increases with increasing temperature (see Figure 4-3, insert), and above 70-80 K the spectrum is too broad for EPR detection. The saturation behavior of the EPR spectrum of center H at 20 K is compared with that of the wild-type tyrosyl radical and the mixed-valence iron intermediate X in R2-Y122F in Figure 4-3. The calculated  $P_{1/2}$ -value of center H, using Equation 2.14, is 20 mW at 20 K, which is almost two orders of magnitude higher than that of the wild-type tyrosyl radical ( $P_{1/2} = 75 \mu\text{W}$ ) and the diiron intermediate X ( $P_{1/2} = 50 \mu\text{W}$ ). The inhomogeneity factor  $b$  of both intermediate X ( $b = 0.7$ ) and center H ( $b = 0.44$ ) are smaller than 1, which is indicative of an exchange coupled spin system (Galli *et al.*, 1996), whereas the tyrosyl radical can be fitted using  $b = 1$ , which is typical for an isolated radical species with  $T_1 = T_2$  (Sahlin *et al.*, 1985). The saturation behavior, temperature dependence, and the magnitude of the smallest  $g$ -value ( $g_3 < 2.0$ ), of center H is highly untypical for an organic radical, and shows similarities with a metal center.

Quantification of the EPR signal yielded only 1.5 – 3% paramagnetic spin per polypeptide dimer, R2. This means that the crystal structure presented above does not necessarily reflect the structure containing the paramagnetic center H. In the small fraction containing center H, the amino acid residues may have other orientations or be covalently modified, or, other small, non-protein, ligands may be bound to the iron center. This called for a thorough look at the properties of the metal center and the activation process in an attempt to rise the yield of H.

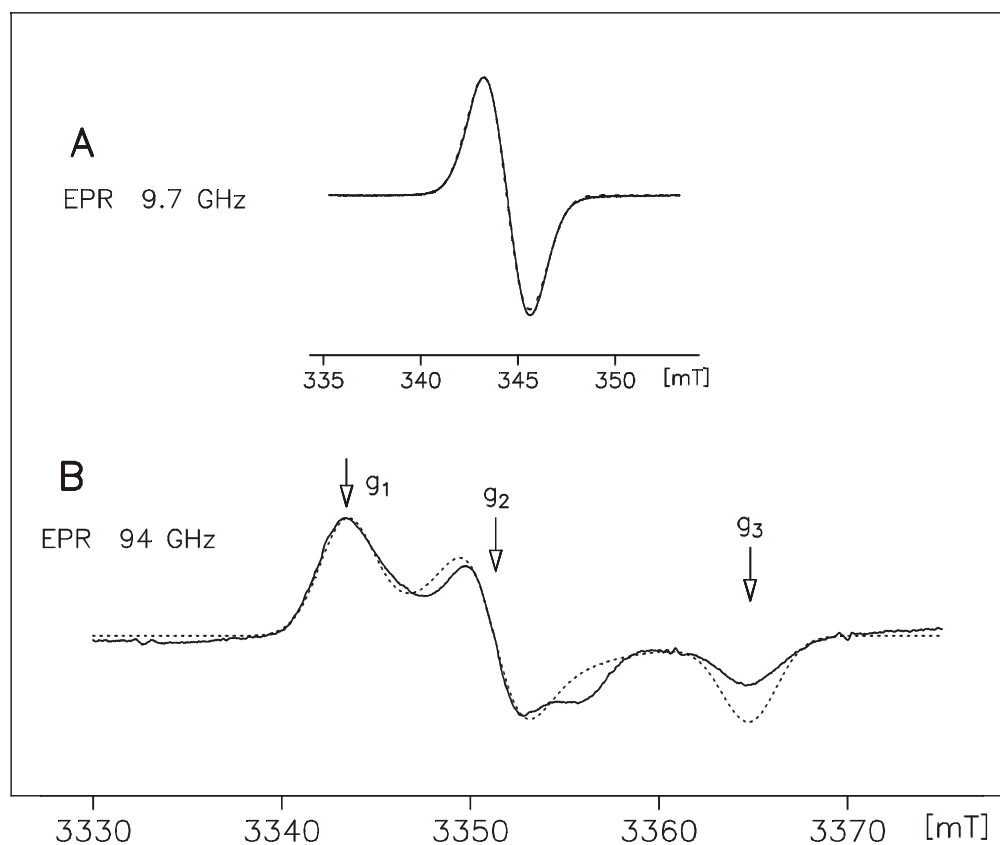


**FIGURE 4-2 CW-EPR SPECTRA OF CENTER H IN R2 Y122H**

*EPR spectrum of R2-Y122H (0.9 mM) recorded at X-band at 30 K, 1 mW microwave power, 0.7 mT modulation amplitude, and 12.5 kHz modulation frequency. In the lower spectrum R2-Y122H (3.6 mM) recorded at W-band 20 K, 1.58 mW microwave power, 0.6 mT modulation amplitude, and 100 kHz modulation frequency. Dotted lines are simulated spectra. For data see table 4-1.*

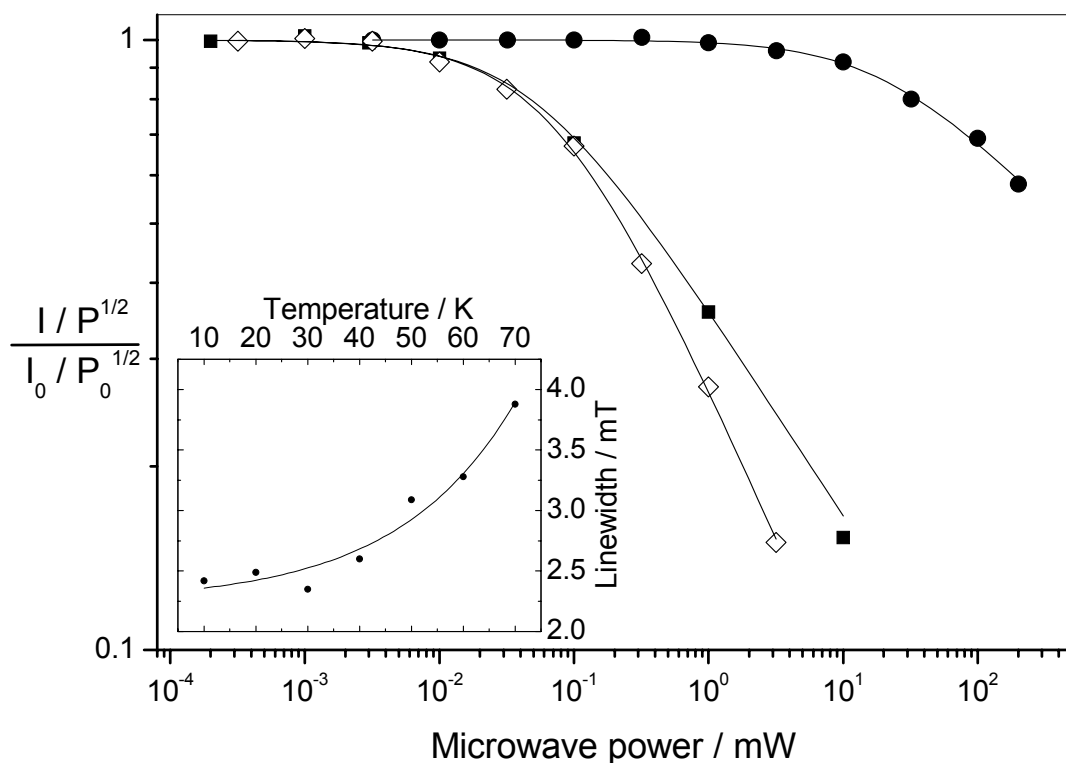


**FIGURE 4-3 SATURATION BEHAVIOR AND TEMPERATURE DEPENDENCE OF CENTER H IN R2-Y122H**

Microwave saturation curves at 20 K of the X-band EPR spectra of the wild-type tyrosine radical ( $\diamond$ ), the intermediate X from R2-Y122F( $\blacksquare$ ), and the center H from R2-Y122H ( $\bullet$ ). The best fitting curves (using Equation 2.14) of the saturation data was obtained using  $P_{1/2} = 75 \mu\text{W}$  and  $b = 1$  for Y122\*,  $P_{1/2} = 51 \mu\text{W}$  and  $b = 0.7$  for intermediate X, and  $P_{1/2} = 20 \text{ mW}$  and  $b = 0.44$  for center H. EPR conditions as in Figure 4-2A.

Insert: The temperature dependence of the peak-to-peak linewidth of center H, above 70 K the signal is no longer detectable. EPR conditions as in figure 4-2A, except that the EPR spectra were recorded at temperatures between 10 and 70 K.

## 4.3 SPECTROSCOPICAL CHARACTERIZATION OF R2-Y122H

### 4.3.1 OPTICAL PROPERTIES OF THE METAL CENTER

The wild-type protein R2 has a distinct optical absorption spectrum with a narrow peak at 410 nm and a broader structure between 350 - 400 nm resulting from the tyrosyl radical, as well as two broad absorption bands at 325 and 370 nm (Figure 4-4, top spectrum), which are typical for high-spin antiferromagnetically coupled  $\mu$ -oxo bridged diferric centers (Petersson *et al.*, 1980). The optical spectrum of R2-Y122H is identical to that of the wild-type R2 protein treated with hydroxyurea, met R2, where only the tyrosyl radical is selectively reduced and not the diiron center (Figure 4-4, middle spectra). This strongly indicates that the majority of R2-Y122H protein has a  $\mu$ -oxo bridged diferric center, which was also suggested by Mössbauer spectroscopy of the  $^{57}\text{Fe}$  labeled R2-Y122H protein (Dr. Volker Schuenemann, University of Lübeck, personal communication).

As in wild-type R2 (Atkin *et al.*, 1973), the typical optical spectrum of the diferric center in R2-Y122H is lost when the sample is treated with the strong iron chelator hydroxyquinoline under slightly denaturing conditions, which extracts the iron from the protein (see Section 2.3.1) (Figure 4-4). The colorimetric bathophenanthroline iron assay (see Section 2.3.4) revealed, analogous to the wild type, that less than 5 % of the iron initially bound to R2-Y122H was retained. Surprisingly however, the EPR spectrum of center H was still present in the treated sample, although reduced to half of the original intensity. This could imply that (i) center H is not an iron center, or (ii) the iron ions of center H are bound significantly more rigid to the protein frame than the normal diferric center and cannot be released to the chelator.

In the wild-type R2, the diferric center and the tyrosyl radical are regenerated when the sample treated with hydroxyquinoline sulfonate (HQS) is reconstituted with ferrous iron and ascorbate under aerobic conditions, after HQS has been removed by gel filtration (see Section 2.3.1). In R2-Y122H, however, only the  $\mu$ -oxo bridged diferric center reappeared, as evident from the optical spectrum, but the yield of center H remained at the same level as before the reconstitution, indicating that the center H can not be formed during the oxygen reconstitution reaction in a sample where the center has already been present.

Attempts to reconstitute the hydroxyquinoline treated R2-Y122H with copper(II), or a mixture of iron(II) and copper(II) did not increase the yield of center H, but an EPR spectrum appeared that was typical for copper coordinated to nitrogen. The optical spectrum of the copper and iron reconstituted protein was different from the iron reconstituted, as the bands at 325 and 370 nm were not resolved, indicating that copper can enter the iron site when it is added in excess over iron (data not shown). It is known for the wild-type R2 that divalent metal ions, such as manganese and cobalt, will occupy the iron site in the absence of iron (Atta *et al.*, 1992, Elgren *et al.* 1994).

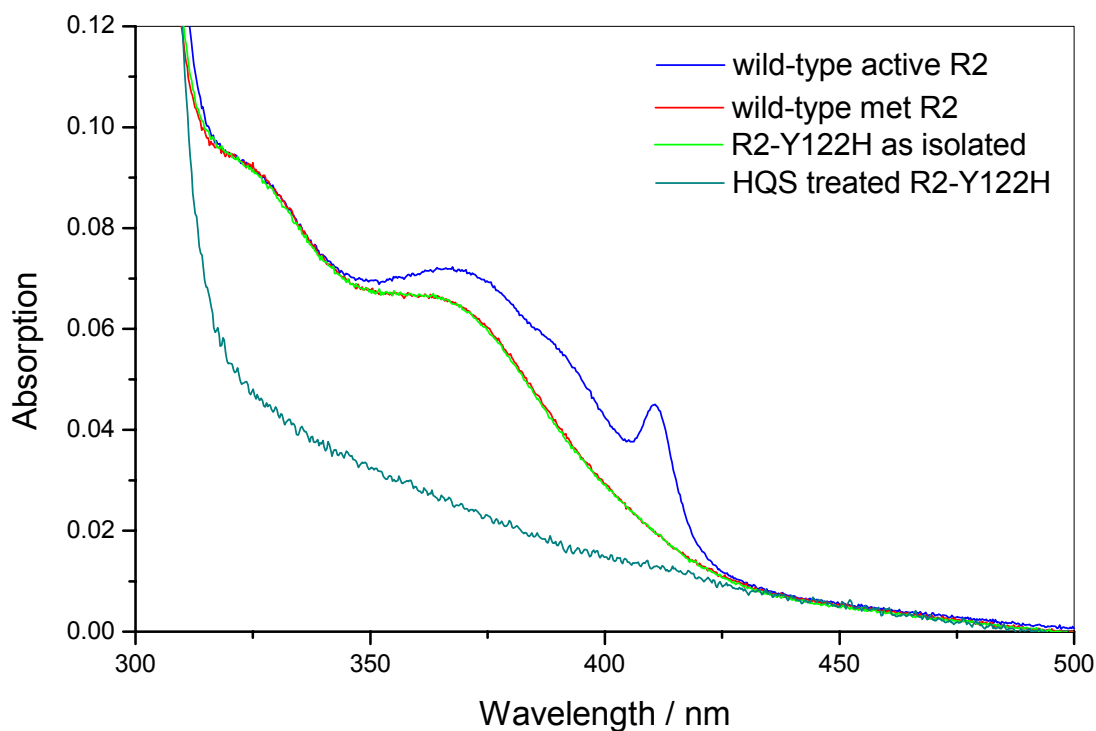


**FIGURE 4-4 OPTICAL SPECTRA OF WILD-TYPE R2 AND R2-Y122H**

*Top blue spectrum: active wt R2 with tyrosyl radical. Middle overlapping spectra: R2-Y122H as isolated (green), and hydroxyurea treated wt R2 in met R2 (red) form showing typical  $\mu$ -oxo bridged diferric center bands at 325 and 370 nm but no tyrosyl radical. Bottom spectrum: "apo" R2-Y122H after iron removal by hydroxyquinoline/imidazole (grey blue). The spectra are scaled individually to compensate for different protein concentration.*

In R2-Y122H grown in "iron free" minimal medium, the center H was already present in the purified protein, and additional iron reconstitution had only a slight positive effect on the yield. With only 3 % total yield of center H, it can however not be excluded that the minimal medium, or the glassware used for cell growth, contained traces of iron in a sufficiently large amount to generate center H.

#### **4.3.2 REDUCTION AND OXIDATION OF THE DIIRON CENTER – A MIXED VALENCE $\text{Fe}^{\text{II}}\text{-Fe}^{\text{III}}$ CENTER IN R2-Y122H**

In a ferromagnetically coupled high-spin dinuclear iron center with both irons in the same oxidation state, the unpaired spins are parallel and add up to an integer spin state, which is normally only visible in parallel mode or high-field EPR because of large zero field splitting. In the wild-type diferric R2 protein, the two high-spin  $\text{Fe}^{\text{III}}$  ( $S = 5/2$ ) are coupled antiferromagnetically so that the unpaired spins are antiparallel with a net  $S = 0$  ground state, and thus not detectable by EPR at all. On the other hand, the high-spin mixed valence centers  $\text{Fe}^{\text{II}}\text{Fe}^{\text{III}}$  and  $\text{Fe}^{\text{III}}\text{Fe}^{\text{IV}}$  have an odd number of unpaired electrons, since both  $\text{Fe}^{\text{II}}$  and  $\text{Fe}^{\text{IV}}$  have  $S = 2$ . In case of antiferromagnetic coupling, the net spin is  $S = 1/2$  and therefore readily detectable by EPR. If the center H is a pure diiron center, the oxidation levels of the two iron atoms must be different than  $\text{Fe}^{\text{III}}\text{Fe}^{\text{III}}$ . Indeed, the  $g$ -tensor values of center H are quite similar to those reported for the intermediate X, which is an  $\text{Fe}^{\text{III}}\text{Fe}^{\text{IV}}$  mixed valence species (see Table 4-1).

As shown above, the majority of R2-Y122H contains a diferric center ( $\text{Fe}^{\text{III}}\text{Fe}^{\text{III}}$ ). To generate a mixed valence state of the diiron center, the redox potential of the solution must be changed by adding a reductant for reduction to the  $\text{Fe}^{\text{II}}\text{Fe}^{\text{III}}$  state, or an oxidant for oxidation to the  $\text{Fe}^{\text{III}}\text{Fe}^{\text{IV}}$  state, as well as a redox mediator that can enter the hydrophobic interior of the protein (see Section 2.3.3). In the wild-type R2 from *E. coli*, the  $\text{Fe}^{\text{II}}\text{Fe}^{\text{III}}$  has been generated by radiolytic reduction in frozen solution at 77 K (Davydov *et al.*, 1994), and in small amounts using basic hydroxylamines or hydrazine (Gerez and Fontecave, 1992). However, in *E. coli* R2 mutants, and the wild-type R2 from other organisms, e.g. mouse, it is possible to obtain large amounts of the  $\text{Fe}^{\text{II}}\text{Fe}^{\text{III}}$  state by chemical reduction (Atta *et al.*, 1994).

Reduction of R2-Y22H with dithionite, or ascorbate, in presence of the mediator phenazine methosulfate (PMS) in liquid solution at room temperature leads to a decrease of the signal intensity of center H (Figure 4-5). Simultaneously, with an optimum at 10 minutes incubation, a new paramagnetic species is formed with  $g$ -tensor values that are resolved in X-band EPR (Table 4-1). Comparison with other mixed valence diiron centers in proteins and model systems shows that these  $g$ -tensor values agree well with an  $\text{Fe}^{\text{II}}\text{Fe}^{\text{III}}$  species. The position of the  $g$ -components are very sensitive to the electronic environment of the diiron center (Davydov *et al.*, 1999). In the radiolytically generated  $\text{Fe}^{\text{II}}\text{Fe}^{\text{III}}$  center in wild-type R2 (Davydov *et al.*, 1996), the  $g$ -tensor is far more axial than the  $g$ -tensor observed in R2-Y122H, which is more rhombic, and actually more similar to the  $g$ -tensor in of an  $\text{Fe}^{\text{II}}\text{Fe}^{\text{III}}$  center which has been observed in MMO in the presence of the dimethyl sulfoxide (DMSO) (DeRose *et al.*, 1996) (see Table 4-1). An estimation of the spin concentration of the  $\text{Fe}^{\text{II}}\text{Fe}^{\text{III}}$  species, yielded 95 %, compared to 3 % maximum intensity of center H. This clearly



**TABLE 4-1 G- AND  $^{57}\text{Fe}$  HYPERFINE TENSOR VALUES OF MIXED VALENCE DIIRON CENTERS**

Paramagnetic center	g-tensor	$^{57}\text{Fe}$ hyperfine tensors (MHz)		Ref.
Center H	2.0088(1)	72.5(2)	52.1(2)	This work
in <i>E. coli</i>	2.0040(1)	$\text{Fe}_\text{B}$ : 69.7(2)	$\text{Fe}_\text{A}$ : 47.6(2)	
RNR R2-Y122H <sup>a</sup>	1.9960(2)	66.6(2)	45.1(2)	
Reduced ( $\text{Fe}^\text{II}\text{Fe}^\text{III}$ )	1.93			This work
center in <i>E. coli</i>	1.84			
RNR R2-Y122H	1.80			
Intermediate X	2.007	– 74.2	27.5	Sturgeon <i>et al.</i> , 1996
( $\text{Fe}^\text{III}/\text{Fe}^\text{IV}$ ) in <i>E. coli</i>	1.999	$\text{Fe}^\text{III}$ : – 72.2	$\text{Fe}^\text{IV}$ : 36.8	
RNR R2-Y122F	1.994	– 73.2	36.8	
$\text{Fe}^\text{II}/\text{Fe}^\text{III}$ center in	1.950			Davydov <i>et al.</i> , 1996
radiolytically reduced	1.934			
<i>E. coli</i> RNR wt-R2	1.816			
$\text{Fe}^\text{II}/\text{Fe}^\text{III}$ center in	1.95	62	36	DeRose <i>et al.</i> , 1996
<i>M. capsulatus</i> MMO	1.87	$\text{Fe}^\text{III}$ : 68	$\text{Fe}^\text{II}$ : 38	
+ DMSO	1.82	76	<20	
$\text{Fe}^\text{II}/\text{Fe}^\text{III}$ center in <i>M.</i>	1.95	– 74	36.5	Fox <i>et al.</i> , 1993
<i>trichosporium</i> OB3b	1.86	$\text{Fe}^\text{III}$ : – 69	$\text{Fe}^\text{II}$ : 34.3	
MMO + DMSO	1.79	– 63	17.8	
Model complex	2.011			Lee <i>et al.</i> , 1999
$\text{Fe}^\text{III}\text{Fe}^\text{IV}(\mu\text{-O})_2$	1.997			
(see ref. for details)	1.986			
Model complex		– 64.5	36.5	Dong <i>et al.</i> , 1995
$\text{Fe}^\text{III}\text{Fe}^\text{IV}(\mu\text{-O})_2$		$\text{Fe}^\text{III}$ : – 64.5	$\text{Fe}^\text{IV}$ : 36.5	
(see ref. for details)		– 64.5	20	

<sup>a</sup> absolute values sorted by magnitude, numbers in parenthesis are errors in the last digit. The signs were not determined for the  $^{57}\text{Fe}$  hf data

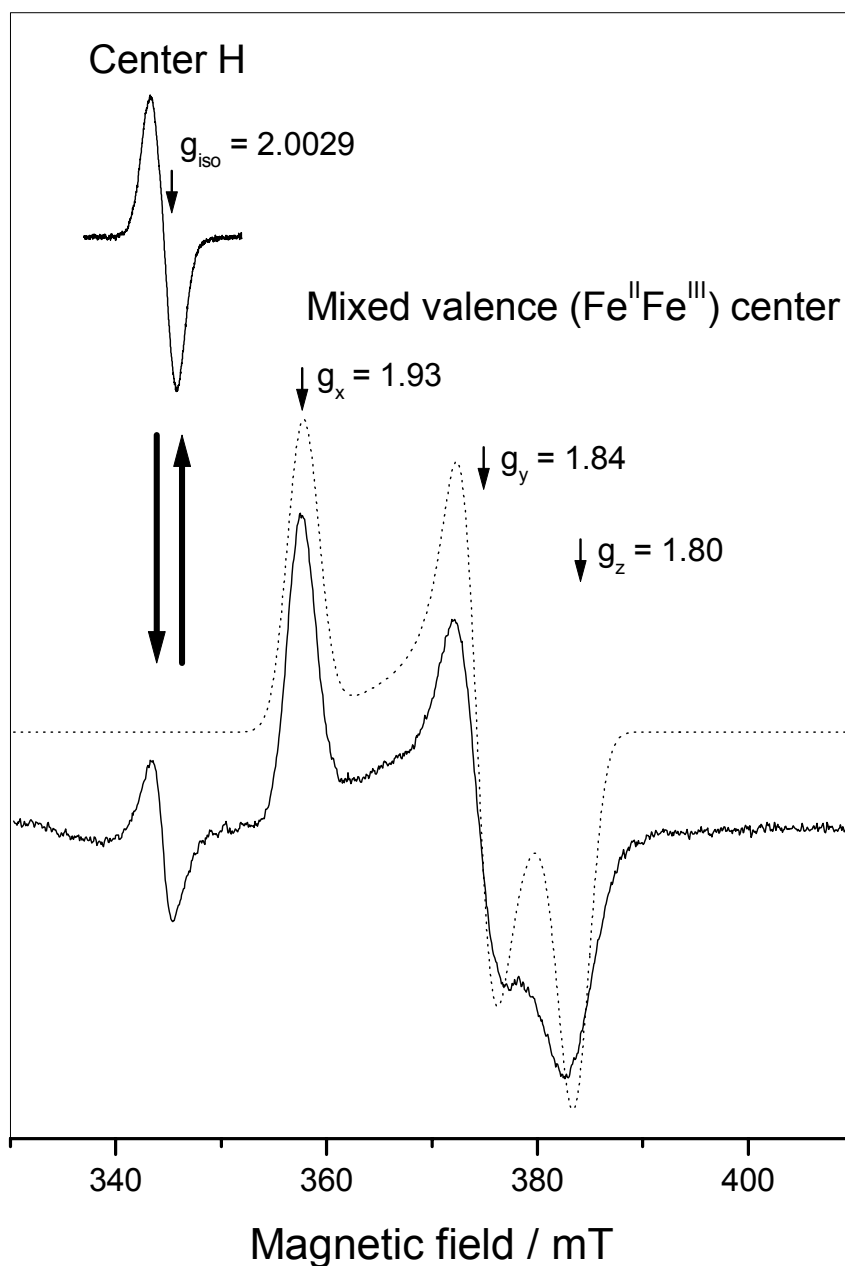


**FIGURE 4-5 REDUCTION OF THE DIIRON CENTER OF R2-Y122H**

*X-band EPR spectra at 20 K of R2-Y122H before (upper spectrum) and after (lower spectrum) reduction with dithionite and PMS. The reduction of the center H EPR signal can be reversed by adding hydrogen peroxide.*

indicates that the majority of the diiron center in the R2-Y122H protein is a diferric center, before reduction, which is independent of center H.

After 30 minutes incubation, the  $\text{Fe}^{\text{II}}\text{Fe}^{\text{III}}$  species disappears, probably due to reduction to the diferrous state, but center H is still visible with about 20 % of the original intensity. The reduction of center H is however reversible, when the reductants are removed by gel filtration, and the sample is oxidized with hydrogen peroxide, the intensity of center H is partly restored.

The distinctly different  $g$ -tensor values of center H from the mixed-valence  $\text{Fe}^{\text{II}}\text{Fe}^{\text{III}}$  species excludes that center H is an  $\text{Fe}^{\text{II}}\text{Fe}^{\text{III}}$  center, and the diminished EPR signal of center H in reduced R2-Y122H indicates that center H is an oxidized species. Oxidation of the as isolated diferric R2-Y122H sample with hydrogen peroxide, however, had no effect on the yield of center H.

## 4.4 EPR AND ENDOR SPECTROSCOPICAL CHARACTERIZATION OF CENTER H IN R2-Y122H

The chemical characterization of R2-Y122H revealed that even after treatment with strong chelators, the center H was present in almost the same quantity. All attempts to generate apo protein, and subsequently reconstitute with the  $^{57}\text{Fe}$  isotope failed to increase the EPR signal. So, if the center H is a paramagnetic species located on iron, this iron will have to be built in during the synthesis of the protein within the whole cells while growing. Therefore, a new iron containing medium was tried out, based on the "iron free" minimal medium (Åberg *et al.*, 1993) substituting the trace metal mix with 5 ppm ferric chloride. The overexpressing *E. coli* cells were then grown in both  $^{57}\text{Fe}$  and  $^{56}\text{Fe}$  medium, respectively, and the isotope labeled protein and the control were purified under the same conditions, as described in Section 2.1.2. Due to the hyperfine interactions with the nuclear spin on  $^{57}\text{Fe}$  ( $I = 1/2$ ), which are absent in  $^{56}\text{Fe}$  ( $I = 0$ ), the EPR spectra of these two proteins should reveal whether center H is associated with iron or not.

### 4.4.1 CW EPR ON $^{57}\text{Fe}$ R2-Y122H – EVIDENCE FOR AN IRON CENTER

The X-band EPR spectra of the two different iron isotope R2-Y122H samples (Figure 4-6) reveals a broadening of the peak-to-peak linewidth, from 2.2 mT observed for the  $^{56}\text{Fe}$  sample to 4.3 mT in the  $^{57}\text{Fe}$  sample, offering solid proof that significant spin density is localized on iron. In W-band EPR at ten-fold higher magnetic field (Figure 4-2B), this broadening is seen on all three principal  $g$ -tensor components, however, without giving rise to additional splittings (spectra of labeled protein not shown).

When the  $\text{Fe}^{\text{III}}\text{Fe}^{\text{IV}}$  intermediate X of the oxygen activation reaction in wild-type R2 (see Section 1.3.2) is labeled with  $^{57}\text{Fe}$ , its normal X-band EPR singlet spectrum is split into a doublet, due to hyperfine interactions with the nuclear spin of  $^{57}\text{Fe}$ . These  $^{57}\text{Fe}$  hyperfine (hf) couplings are better resolved by  $^{57}\text{Fe}$  ENDOR or Mössbauer spectroscopy (Ravi *et al.*, 1994). The  $^{57}\text{Fe}$  hf couplings of center H, however, do not give rise to a splitting, due to the large EPR linewidth. In order to obtain more information on the iron hf couplings the samples were measured in

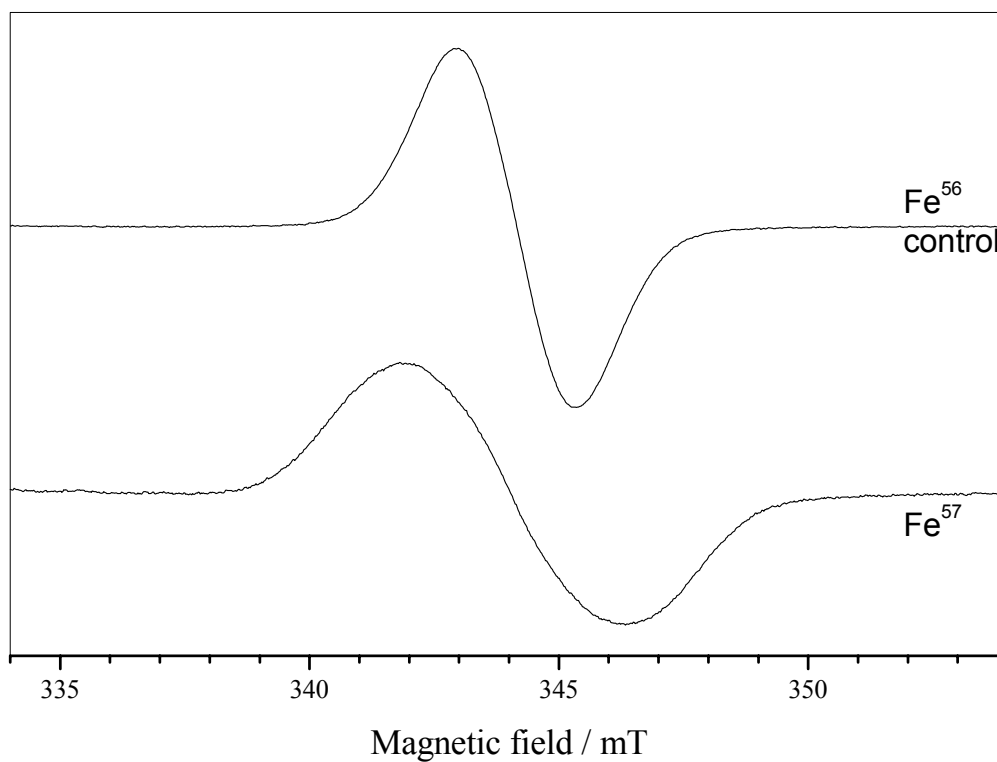


**FIGURE 4-6 EPR SPECTRA OF R2-Y122H AND R2-Y122H LABELED WITH  $^{57}\text{Fe}$**

*X*-band spectrum at  $T=30\text{ K}$  of  $^{56}\text{Fe}$  R2-Y122H (1.0 mM)(upper), and  $^{57}\text{Fe}$  R2-Y122H (0.9 mM)(lower); microwave power: 1 mW, modulation frequency: 12.5 kHz, modulation amplitude: 0.7 mT.

pulsed and CW ENDOR at X-band microwave frequency. ENDOR techniques are able to resolve hfc from unresolved EPR spectra (see Section 2.4.3).

#### 4.4.2 PULSED AND CW ENDOR ON $^{57}\text{Fe}$ R2-Y122H – EVIDENCE FOR A DIIRON CENTER

The pulse ENDOR spectra of center H with  $^{56}\text{Fe}$  exhibit resonances from protons (12-18 MHz) and  $^{14}\text{N}$  nuclei (4-10 MHz) (Figure 4-7B). The weak broad features near 26 MHz and 42 MHz result from the tyrosyl radical in residual wild-type R2 contamination ( $< 1\%$ ) (compare Figure 4-7C). In R2-Y122H substituted with  $^{57}\text{Fe}$ , two additional groups of lines appear around 25 MHz and 35 MHz (Figure 4-7A), which are absent in the  $^{56}\text{Fe}$  sample (Figure 4-7B). These two groups are fully resolved in the continuous wave (CW)  $^{57}\text{Fe}$ -ENDOR spectrum (Figure 4-7a). Each group consists of three pairs of peaks which are centered around the three  $^{57}\text{Fe}$  hyperfine (hf) tensor principal components ( $A_{1,2,3}/2$ ) and split by twice the value of the nucleus specific Larmor frequency ( $\nu^{57}\text{Fe}$ ), i.e. 0.9 MHz at X-band (see Table 2-2), which is the case when  $A/2$  is larger than the Larmor frequency (see Section 2.4.3). All three components of the two  $^{57}\text{Fe}$  hf tensors have been obtained by simulation of the CW  $^{57}\text{Fe}$ -ENDOR spectrum (see Figure 4-7a and Table 4-1).

These findings clearly show that center H is a two-iron site. The two irons are here called  $\text{Fe}_\text{A}$  and  $\text{Fe}_\text{B}$ , which can not yet conclusively be assigned to the crystallographic Fe1 and Fe2 (see Figure 4-1). The  $g$ -tensor values near  $g \sim 2$  and the small hf anisotropy of  $^{57}\text{Fe}$  suggest an antiferromagnetically coupled diiron site with an  $S = 1/2$  ground state. The ENDOR data do, however, not provide clear-cut information on the valence of the iron nuclei without comparing the  $^{57}\text{Fe}$  hf tensors of center H with data from other  $S = 1/2$  diiron centers (see Table 4-1).

The larger  $^{57}\text{Fe}$  tensor of center H ( $\text{Fe}_\text{B}$  in Figure 4-7a) has similar components to those reported for  $\text{Fe}^\text{III}$  in both the  $\text{Fe}^\text{III}\text{Fe}^\text{IV}$  center of intermediate X (values from Sturgeon *et al.*, 1996) and in the  $\text{Fe}^\text{II}\text{Fe}^\text{III}$  of MMOH (values from DeRose *et al.*, 1996), and therefore this tensor is assigned to an  $\text{Fe}^\text{III}$ . Its isotropic part, calculated from the mean value of the three components is  $A_\text{iso}(\text{Fe}_\text{B}) = 69.6$  MHz.

The smaller  $^{57}\text{Fe}$  tensor in intermediate X is assigned to  $\text{Fe}^\text{IV}$  and in MMOH to  $\text{Fe}^\text{II}$ , and in both these cases, it exhibits a significant axial symmetric anisotropy. In contrast, the smaller  $^{57}\text{Fe}$  tensor of center H ( $\text{Fe}_\text{A}$  in Figure 4-7a) is more isotropic, and the magnitude of its isotropic part ( $A_\text{iso}(\text{Fe}_\text{A}) = 48.3$  MHz) is considerably larger than those of  $\text{Fe}^\text{IV}$  in X and  $\text{Fe}^\text{II}$  in MMOH. The anisotropy of the smaller tensor is actually much more similar to the larger tensors, indicating that the second iron of center H might also be  $\text{Fe}^\text{III}$ .

The anisotropy is expected to be small in high-spin  $\text{Fe}^\text{III}$  ( $S = 5/2$ ) where the 5  $d$ -electrons are each occupying separate  $d$ -orbitals  $d_{z^2}$ ,  $d_{x^2-y^2}$ ,  $d_{xy}$ ,  $d_{xz}$ , and  $d_{yz}$ . In high-spin  $\text{Fe}^\text{II}$  and  $\text{Fe}^\text{IV}$ , which have 6 and 4  $d$ -electrons, respectively, and both  $S = 2$ , the five  $d$ -orbitals are unsymmetrically occupied leading to larger anisotropy.

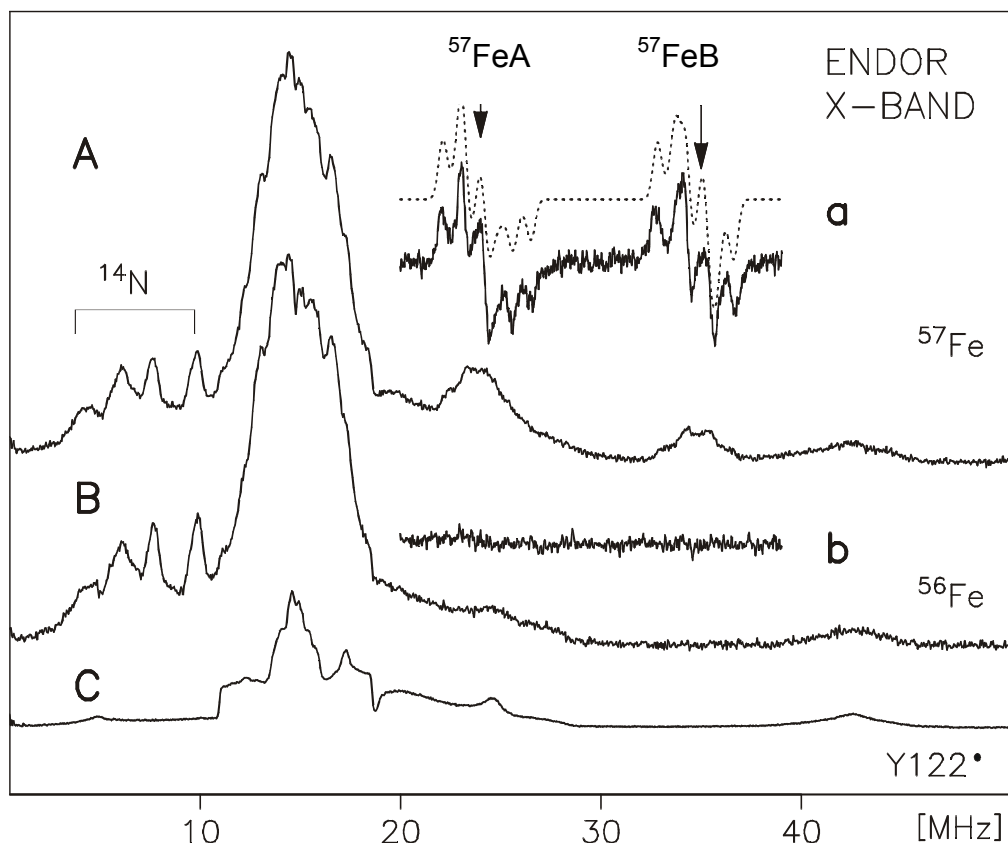
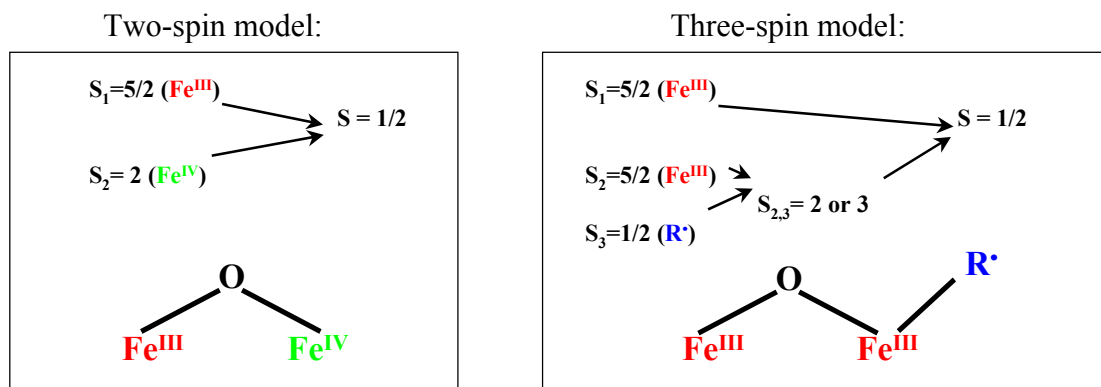


**FIGURE 4-7 PULSE DAVIES AND CW ENDOR SPECTRA OF CENTER H**

(A)  $^{57}\text{Fe}$  R2-Y122H (2.1 mM), (B)  $^{56}\text{Fe}$  R2-Y122H (1.5 mM), and (C)  $\text{Y122}^\bullet$  in wild-type R2 (1.0 mM); Radio frequency (rf) pulse:  $8\ \mu\text{s}$ ; accumulation time: 10 h (A, B), 0.5 h (C). Inserts: X-band CW ENDOR spectra (first derivative) at  $T=8\ \text{K}$  of center H; (a) in  $^{57}\text{Fe}$  R2-Y122H, and (b) in  $^{56}\text{Fe}$  R2-Y122H;  $P_{\text{mw}} = 8\ \text{mW}$ ,  $P_{\text{rf}} = 100\text{--}150\ \text{W}$ , modulation frequency = 12.5 kHz, modulation amplitude =  $\pm 150\ \text{kHz}$ ; accumulation time 3 h. Dotted trace: simulation. Data in Table 4.1.

### 4.4.3 THE SPIN DENSITY DISTRIBUTION IN CENTER H

There are in principle two possible ways for a diiron center to couple to an  $S = 1/2$  system, see Scheme 4-2. To obtain more information on the valence of the two irons, we can calculate the intrinsic hyperfine tensors for both these models and compare with other coupled iron systems.



Scheme 4-2

Center H as a two-spin system: The  $^{57}\text{Fe}$  hf tensors ( $\mathbf{A}$ ) of antiferromagnetically coupled  $S = 5/2$  and  $S = 2$  spin systems, are related to the intrinsic tensors ( $\mathbf{a}_i$ ) of the uncoupled iron by the two so-called spin projection factors (Bencini and Gatteschi, 1990). Explicitly:

$$\begin{aligned}\mathbf{A}(\text{Fe}^{\text{III}}) &= 7/3 \mathbf{a}_i(\text{Fe}^{\text{III}}) \text{ and} \\ \mathbf{A}(\text{Fe}^{\text{IV}}) &= -4/3 \mathbf{a}_i(\text{Fe}^{\text{IV}})\end{aligned}$$

For the larger coupling,  $A_{\text{iso}}(\text{Fe}_B^{\text{III}}) = 69.6$  MHz, the intrinsic value becomes  $|a_i| = 29.8$  MHz, which agrees well with the values reported for a single Fe site with octahedral coordination ( $-28$  to  $-30$  MHz) and also with the value reported for  $\text{Fe}^{\text{III}}$  in intermediate X, 31.4 MHz (Sturgeon *et al.*, 1996). However, for the smaller  $^{57}\text{Fe}$  tensor,  $A_{\text{iso}}(\text{Fe}_A^{\text{IV}}) = 48.3$  MHz, the obtained intrinsic coupling is  $|a_i| = 36.2$  MHz, which is considerably larger than the respective intrinsic value reported for X,  $|a_i| = 25.3$  MHz (Sturgeon *et al.*, 1996), meaning that  $\text{Fe}_A$  is not likely to be an  $\text{Fe}^{\text{IV}}$ .

Center H as a three-spin system: An  $\text{Fe}^{\text{III}}\text{Fe}^{\text{III}}$  center strongly coupled to a radical has earlier been suggested for intermediate X by Ravi *et al.*, 1995. In this model, the radical first couples antiferromagnetically with one iron to an intermediate spin state  $S_i = 2$ , or ferromagnetically to  $S_i = 3$ , which then couples antiferromagnetically with the second iron to  $S = 1/2$  (see Scheme 4-2), the calculated spin projection factors are:

for $S_i = 2$ :	or	for $S_i = 3$ :
$\mathbf{A}(\text{Fe}^{\text{III}}) = 7/3 \mathbf{a}_i(\text{Fe}^{\text{III}})$		$\mathbf{A}(\text{Fe}^{\text{III}}) = -5/3 \mathbf{a}_i(\text{Fe}^{\text{III}}),$
$\mathbf{A}(\text{Fe}^{\text{III}}) = -14/9 \mathbf{a}_i(\text{Fe}^{\text{III}})$		$\mathbf{A}(\text{Fe}^{\text{III}}) = 20/9 \mathbf{a}_i(\text{Fe}^{\text{III}}),$

$$A(R^{\bullet}) = 2/9 a_i(R^{\bullet})$$

$$A(R^{\bullet}) = 4/9 a_i(R^{\bullet})$$

for the three spin system  $\text{Fe}^{\text{III}}$  ( $S = 5/2$ ),  $\text{Fe}^{\text{III}}$  ( $S = 5/2$ ),  $R^{\bullet}$  ( $S = 1/2$ ) (Bencini and Gatteschi, 1990).

The obtained intrinsic hyperfine values  $|a_i|$  for  $\text{Fe}_B^{\text{III}}$  and  $\text{Fe}_A^{\text{III}}$  in center H are 29.8 and 31.05 MHz for  $S_i = 2$ , and 31.3 and 29.0 MHz for  $S_i = 3$ . In both cases, both values agree remarkably well with those for  $\text{Fe}^{\text{III}}$  in X, 31.4 MHz (Sturgeon *et al.*, 1996). This model also explains the small anisotropy of the smaller hyperfine tensor of  $\text{Fe}_A$  in center H, which is more typical for  $\text{Fe}^{\text{III}}$  and too small for  $\text{Fe}^{\text{IV}}$ .

Therefore, the calculated isotropic intrinsic  $^{57}\text{Fe}$  hyperfine values, as well as the small anisotropy of both irons, fits best with center H as an  $\text{Fe}^{\text{III}} \text{Fe}^{\text{III}}$  center with a coupled, probably ligated radical. The temperature dependence of center H reveals a strong exchange coupling since the EPR linewidth is more or less constant up to ~40 K (see Figure 4-3). The nature of the ligand radical remained open and will be elucidated in the next section.

#### 4.4.4 PULSED DAVIES ENDOR ON PHE- $d_8$ LABELED R2-Y122H – EVIDENCE FOR A LIGAND RADICAL ON F208

Before center H was identified as an iron center, Dr. Stephan Pötsch made a series of isotope labeling experiments of the ligand residues of the diiron site,  $\delta$ - $^{13}\text{C}$ -glutamate,  $\gamma$ - $^{13}\text{C}$ -aspartate, and  $\delta$ - $^{15}\text{N}$ -histidine. However, none of these preparations gave any further indications to the location of the paramagnetic spin of center H. In addition to the aspartate, glutamate, and histidine residues, there are three hydrophobic amino acids close to the diiron site: two phenylalanine residues (F208 and F121) and one isoleucine residue (I234), which together form a hydrophobic cavity (Ormö *et al.*, 1995). The F208 ring is located only 4.2 Å from the closest iron in chain A of R2-Y122H (see Figure 4-1), I234 is 4.5 Å away, and F212 is 6.7 Å away (not shown). Interestingly, F208 has been observed to be a target for oxidation by the diiron center in R2-Y122F/E238A (Logan *et al.*, 1998) (Figure 4-8) and in R2-W48F/D84E (Baldwin *et al.*, 2001) where a single hydroxylation leads to formation of *meta*-hydroxyphenylalanine. Similarly, in the mutant R2-F208Y, the Y208 can be oxidized to dihydroxyphenylalanine (DOPA) (Åberg *et al.*, 1994, Logan *et al.*, 1998) (Figure 4-8).

If we have generated a radical on F208 in the R2-Y122H mutant, e.g. a phenoxyl type radical, we can expect to observe proton ENDOR lines from the phenyl ring- and  $\beta$ -protons of F208. To find spectroscopic evidence for this, a new sample was made by growing the overproducing bacterial strain in minimal medium supplied with fully deuterated phenylalanine. Due to the different Larmor frequency of protons and deuterons (see Table 2-2) the hyperfine interactions deriving from phenylalanine should be located at a different radio frequency of the ENDOR spectrum in the labeled and non-labeled sample.

In the pulse ENDOR spectrum the Phe- $d_8$ -R2-Y122H protein (middle spectrum in Figure 4-9), two new features appear compared with the non-labeled sample (upper spectrum in Figure 4-9, see also the magnified insert). These new



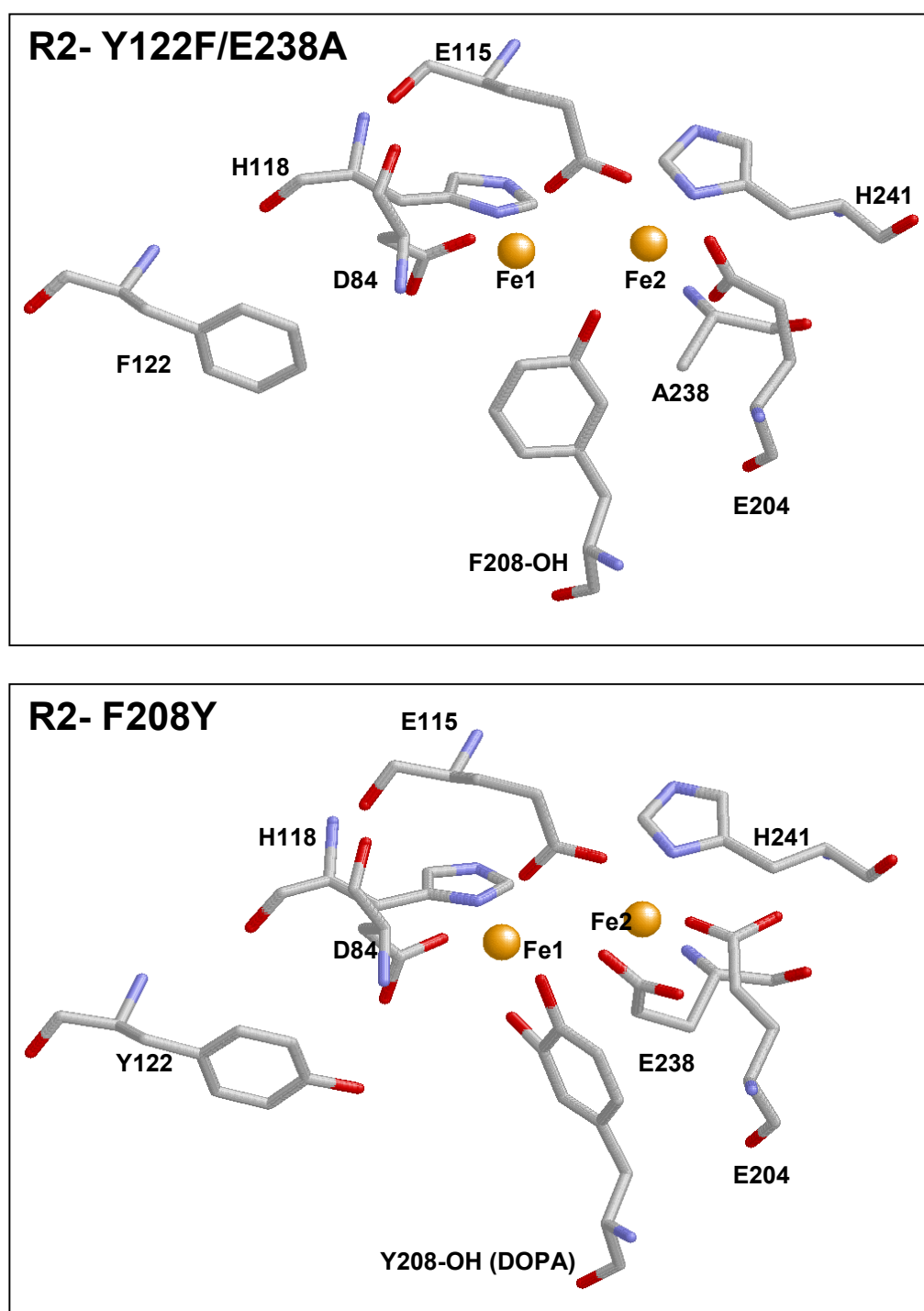


**FIGURE 4-8 SELF-HYDROXYLATING MUTANTS OF RNR R2**

Coordination of the iron centers of the R2 mutants R2-Y122F/E238A (top) and R2-F208Y (bottom). The structures are based on the x-ray crystal structures 1biq.pdb and 1rnr.pdb, respectively (Logan et al., 1998). In both cases the aromatic ring at residue 208, F208 or Y208, has been hydroxylated in the meta-position.

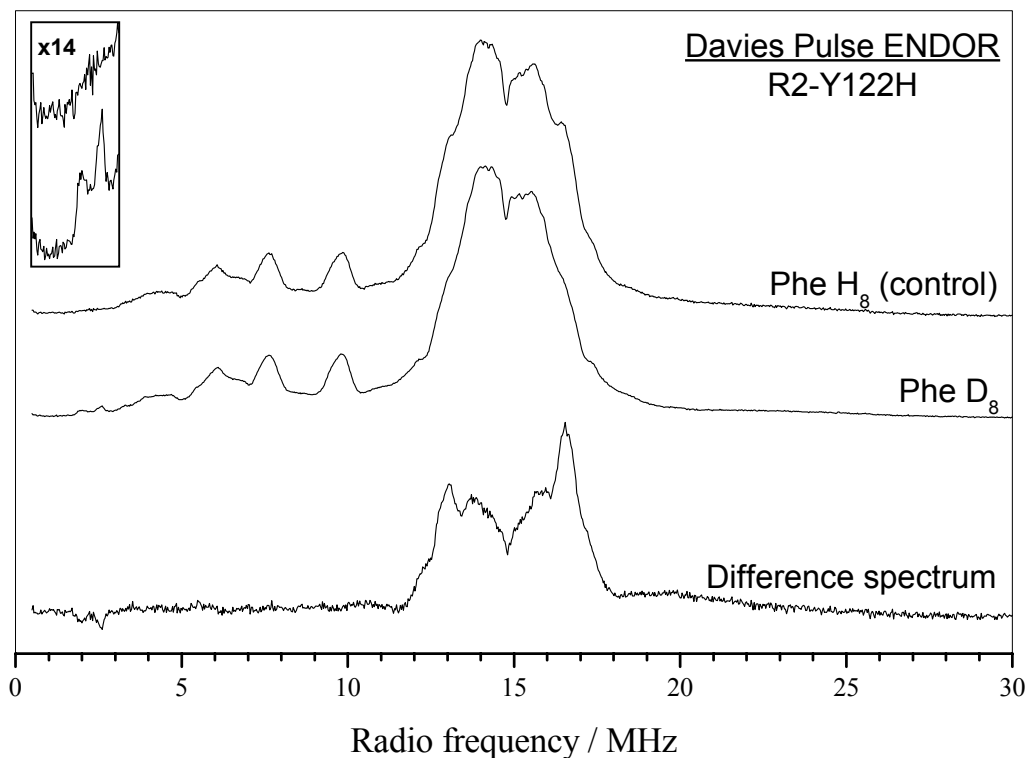


**FIGURE 4-9 PULSE DAVIES ENDOR OF R2-Y122H LABELED WITH PHE-D<sub>8</sub>**

*X*-band pulsed ENDOR spectra of 2.4 mM non-labeled R2-Y122H (upper spectrum, 347 sweeps) and 2.5 mM R2-Y122H labeled with deuterated phenylalanine, PheD<sub>8</sub> (middle spectrum, 393 sweeps). The lower spectrum is the result of subtraction of the labeled spectrum from the non-labeled spectrum. The insert of the deuterium region (0.5-3.1 MHz) is magnified 14x. The spectra were recorded at 10 K, radio frequency pulse: 8  $\mu$ s,  $\nu_{MW}$  = 9.7 GHz, magnetic field: 345.8 mT.  $\pi$ -pulse length 296 ns.

features are centered around the Larmor frequency of deuterium,  $\nu_D = 2.3$  MHz at 346 mT (calculated using the values in Table 2-2). Here, the Larmor frequency is larger than  $A/2$ , which is the opposite case as for the  $^{57}\text{Fe}$  hf couplings, so that the ENDOR transitions are positioned at  $\nu_D \pm a/2$ . Looking carefully at the proton lines, and more obviously by looking at the difference spectrum (lower spectrum in Figure 4-9), there are also couplings missing in the proton region of the spectrum ( $\nu_H = 14.7$  MHz). The deuterium lines are split by 0.54 MHz, which correspond to the lines split by 3.5 MHz in the proton region. The ratio 6.5 between these values represents exactly the theoretical difference in the Larmor frequency between protons and deuterons. In addition to the lines split by 3.5 MHz, we can also see lines split by  $\sim 5.0$  MHz and  $\sim 2.0$  MHz in the proton region, but due to the lower resolution the latter two cannot be observed in the deuterium range. These data clearly confirm that the deuterons of a labeled phenylalanine interact with the paramagnetic center H, and since F208 is located directly at the diiron site, we suggest that the deuterons on this residue is responsible for these interactions.

In the previous section, we found spin projection factors of 2/9, or 4/9, for the radical moiety of the  $\text{Fe}^{\text{III}}\text{Fe}^{\text{III}}\text{R}^{\bullet}$  center H. For phenylalanine to become the iron ligand radical, the phenyl ring needs to be oxidized to a phenoxyl radical, which is similar to the tyrosyl radical Y122 $^{\bullet}$  in wild type R2. If we accept this hypothesis, we can use the proton hyperfine couplings found for Y122 $^{\bullet}$  (Bender *et al.*, 1989) and scale these down by the spin projection factor, 2/9 or 4/9 (see Table 4-2). The numbering of the tyrosyl ring carbons with respective protons is shown in Scheme 4-3. The spin density ( $\rho$ ) of a tyrosyl radical is delocalized over the  $\pi$ -orbital system of the phenol ring as well as on the phenoxyl oxygen (Sjöberg *et al.*, 1978), see inserted table in Scheme 4-3.

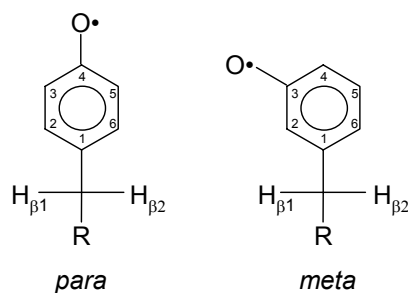
In the pulsed ENDOR spectra of center H in R2-Y122H (Figure 4-9), there are no visible proton hf couplings larger than  $\sim 6$  MHz, which means that in the case with a spin projection factor of 4/9 for the ligand radical of center H, even the [3,5]-protons would have too large hf couplings. Furthermore, the large  $\beta$ -methylene proton coupling in Y122 $^{\bullet}$ ,  $\beta_2$  in Table 4-2, is far too large even if the spin projection factor is 2/9. The magnitude of the  $\beta$ -proton couplings are, however, influenced by the orientation of the proton with respect to the aromatic ring plane. According to the McConnell relation in its simplified form:

$$A_{\text{iso}} = B_1 \rho \cos^2 \theta \quad (4.1)$$

where  $B_1$  is a proportionality factor, which has been determined to be 162 MHz for  $\beta$ -protons (Fessenden and Schuler, 1963),  $\rho$  is the spin density on  $C_1$ , and  $\theta$  is the dihedral angle between the  $\text{H}_\beta\text{-C}_\beta$  bond and the  $\pi$ -orbital axis of  $C_1$ , which is perpendicular to the plane of the phenol ring. In Figure 4-10, all the possible orientations of the two  $\beta$ -protons are plotted against the resulting magnitude of the isotropic hf coupling using  $B_1 = 162$  MHz,  $\rho = 0.49 \times 2/9$ , keeping in mind that the sum of the dihedral angles  $\theta_1$  and  $\theta_2$  must be approximately  $120^\circ$  due to the tetrahedral  $sp^3$  orbital of  $C_\beta$ . Thus, when  $\theta_1$ , and therefore also  $\theta_2$ , lies between  $55^\circ$

Spin densities ( $\rho$ ) <sup>a</sup> for the <i>para</i> -phenoxyl radical:	
C <sub>1</sub>	0.49
C <sub>2</sub> , C <sub>6</sub>	-0.07
C <sub>3</sub> , C <sub>5</sub>	0.26
C <sub>4</sub>	-0.03
O <sup>•</sup>	0.16

<sup>a</sup>From Sjöberg *et al.*, 1978



**Scheme 4-3** Spin densities and structure schematic structure of phenoxyl radicals in *para*- and *meta*- position of phenylalanine.

**TABLE 4-2** ENDOR TRANSITIONS IN Y122<sup>•</sup> AND THEIR ASSIGNED COUPLINGS

Proton	Hf tensor component	Hf coupling constant in Y122 <sup>•</sup> , <sup>a</sup> MHz	Spin projection: 2/9	Spin projection: 4/9
$\beta_1$ -methylene	$A_z$	- 1.9	- 0.4	- 0.8
$\beta_1$ -methylene	$A_x$	- 2.3	- 0.5	- 1.0
$\beta_1$ -methylene	$A_y$	+ 4.2	+ 0.9	+ 1.9
$\alpha$ -[2,6] proton	$A_1$	+ 4.8	+ 1.1	+ 2.1
$\alpha$ -[2,6] proton	$A_2$	+ 7.6	+ 1.7	+ 3.4
$\alpha$ -[3,5] proton	$A_y$	- 7.8	- 1.7	- 3.5
$\alpha$ -[3,5] proton	$A_z$	- 19.7	- 4.4	- 8.8
$\alpha$ -[3,5] proton	$A_x$	- 26.9	- 6.0	- 11.9
$\beta_2$ -methylene	$A_y$	+ 54.8	+ 12.2	+ 24.4
$\beta_2$ -methylene	$A_z$	+ 57.8	+ 12.8	+ 25.7
$\beta_2$ -methylene	$A_x$	+ 60.8	+ 13.5	+ 27.0

<sup>a</sup>Experimental values from Bender *et al.*, 1989. Similar values were obtained from a sample labeled with <sup>17</sup>O-tyrosine (Hoganson *et al.*, 1996). In the right columns, the hfc values of Y122<sup>•</sup> are scaled down by the spin projection factors 2/9 in case of an antiferromagnetic coupling to one iron, or 4/9 in case of ferromagnetic coupling to one iron of a Fe<sup>III</sup>Fe<sup>III</sup>R<sup>•</sup> system.

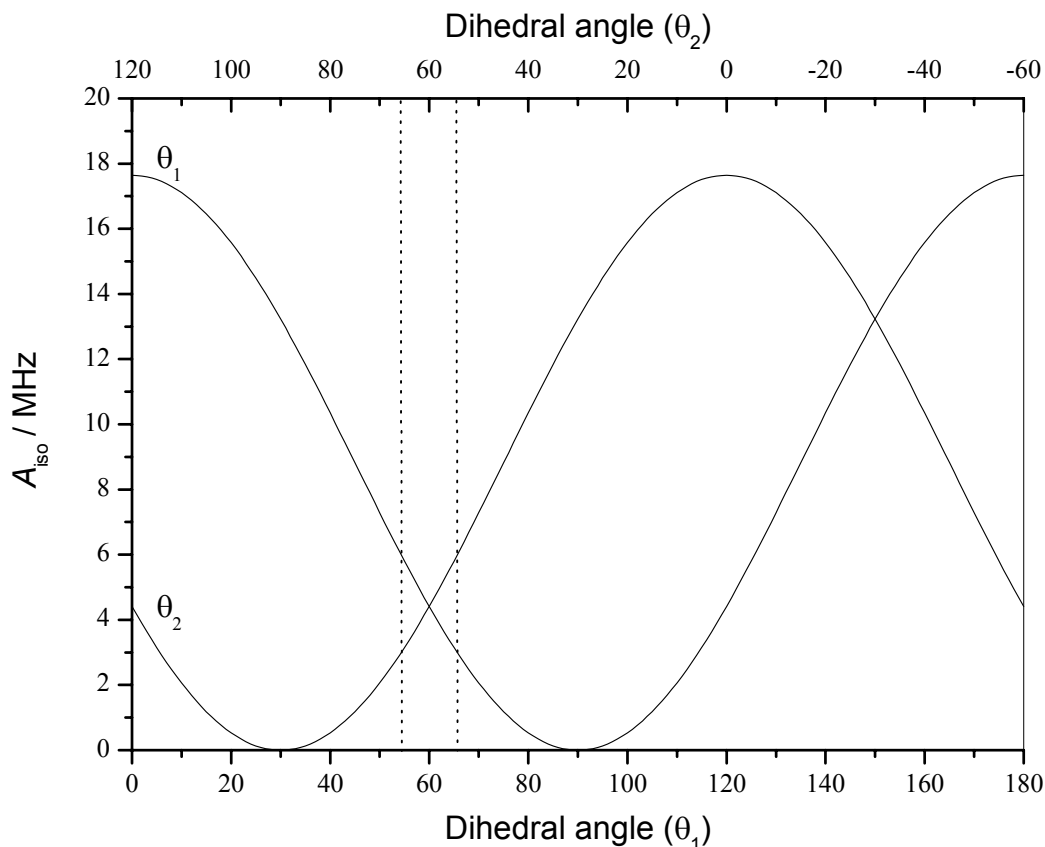


**FIGURE 4-10 ISOTROPIC HYPERFINE COUPLING OF TWO  $\beta$ -PROTONS OF A PHENOXYL RADICAL**

The curves express the effect (the McConnell relation) on the magnitude of the isotropic part of the hyperfine coupling of two  $\beta$ -protons of a para-phenoxyl (i.e. tyrosyl) radical when the phenol ring is rotated around the  $C_b$ - $C_l$  axis (see scheme 4-3). The spin projection factors  $2/9$ , calculated for the three spin system of center H, as well as the spin density  $\rho = 0.49$  on  $C_l$ , are included in the magnitude of the y-axis.  $\theta_i$  describes the dihedral angle between the  $C_\beta$ - $H_i$  bond and an axis perpendicular to the phenol ring of the phenol ring. The figure shows that the orientations of the two protons between the vertical dotted lines are the only allowed orientations if the isotropic hyperfine couplings are restricted to be smaller than 6 MHz, as observed in the pulse ENDOR spectrum of center H (see Figure 4-9). In this case, the two  $\beta$ -protons are almost equivalent.

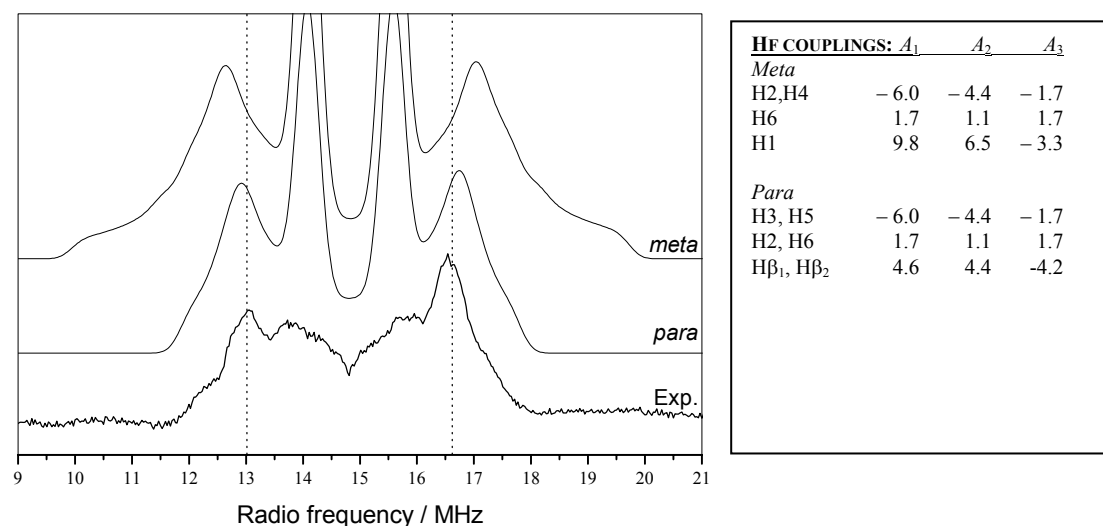


**FIGURE 4-11 SIMULATIONS AND PULSE ENDOR DIFFERENCE SPECTRUM OF THE PHE-D8 LABELED AND NON LABELED R2-Y122**

The pulsed ENDOR difference spectrum was obtained as described in Figure 4-9 (lower spectrum). The simulations were made using the  $\alpha$ -proton couplings from the tyrosyl radical Y122 $^{\bullet}$  of the wild-type R2 scaled down by the spin-projection factor 2/9 obtained for a three spin system ( $\text{Fe}^{\text{III}}\text{Fe}^{\text{III}}\text{R}^{\bullet}$ ). In addition, a new  $\alpha$ -proton hf coupling was calculated for  $\text{C}_6$ -proton of the meta-phenoxy radical (top spectrum), and a new  $\beta$ -proton hf coupling for the para-phenoxy radical (middle spectrum) assuming  $\theta = 60^\circ$  for both  $\beta$ -protons (see Figure 4-10).

and 65 the two  $\beta$ -proton hf couplings may be between 3 and 6 MHz, which is the observed region of couplings in the pulsed ENDOR spectrum of center H (Figure 4-9). In the special case where both  $\theta_1$  and  $\theta_2$  are  $60^\circ$ , both the isotropic coupling constants ( $A_{\text{iso}}$ ) are 4.4 MHz. At 10 K, hfc tensor of  $\beta$ -methylene protons (**A**) are expected to be rhombic, splitting the hf coupling constants into three components ( $A_x$ ,  $A_y$ , and  $A_z$ , or  $A_1$ ,  $A_2$ , and  $A_3$ ), as seen for the Y122 $^\bullet$  radical in Table 4-2 (Bender *et al.*, 1989). In Figure 4-11, the middle spectrum represents a simulation of the difference pulse ENDOR spectrum of non-labeled minus Phe- $d_8$  labeled R2-Y122H, using the  $\alpha$ -proton couplings with a spin projection factor of 2/9 from Table 4-2, as well as equivalent  $\beta$ -protons with  $A_{\text{iso}} = 4.4$  MHz. The magnitude of the rhombic hf tensor components of the  $\beta$ -protons in center H was obtained by assuming the same rhombicity as in the hf tensor of the  $\beta$ -protons in wild-type Y122 $^\bullet$ . The small hf couplings flanking the Larmor frequency of the protons (14.8 MHz) will appear larger in the simulation than in the experiment due to the fact that there is only one proton in the *meta*-position of the oxygen, and that Davies ENDOR is inherently weak when the hf couplings are small.

Although the spectral simulation of a *para*-phenoxyl radical in Figure 4-11 fits reasonably well with the experiment, the oxidation of the phenylalanine must not necessarily take place on C<sub>4</sub>. In fact, in the R2 mutants shown in Figure 4-9, modification of F208 (or Y208) has taken place in *meta*-position, i.e. at position C<sub>3</sub> (or the equivalent C<sub>5</sub>). A schematic structure of a *meta*-phenoxyl radical is shown next to the *para*-phenoxyl radical in Scheme 4-3. In analogy with the *para*-phenoxyl radical, the large spin densities would now be localized on C<sub>2</sub>/C<sub>4</sub> and C<sub>6</sub>. In this case there would be practically no interaction with the  $\beta$ -methylene protons due to the low spin density on C<sub>1</sub>, however, we should see a new strong hf interaction that is not present in the tyrosyl radical from the  $\alpha$ -proton on C<sub>6</sub>. Generally, the hf coupling tensor components of such  $\alpha$ -protons are known to be  $A_1 = 90$  MHz,  $A_2 = 60$  MHz, and  $A_3 = 30$  MHz, when the spin density ( $\rho$ ) on the carbon is 1 (Carrington and McLachlan, 1969). In a phenoxyl radical, we can reduce these components with the factor of 0.49 (see inserted table in Scheme 4-3) (Sjöberg *et al.*, 1978), and in center H, further with the factor 2/9 that was calculated for the Fe<sup>III</sup>Fe<sup>III</sup>R $^\bullet$  center in the previous section, giving  $A_1 = 9.8$  MHz,  $A_2 = 6.5$  MHz, and  $A_3 = 3.3$  MHz. The hf couplings from the  $\alpha$ -protons on C<sub>2</sub>/C<sub>4</sub> and C<sub>5</sub> should be the same as the C<sub>3</sub>/C<sub>5</sub> and C<sub>2</sub>/C<sub>6</sub> in Y122 $^\bullet$ , respectively. A simulated spectrum using these hf coupling components is also presented in Figure 4-11 (top spectrum). However, the large  $A_1$  hf component leads to a significant broadening, which does not fit the observed spectrum as well as the simulation based on the *para*-phenoxyl radical including the  $\beta$ -proton interactions.

## 4.5 DISCUSSION – POSSIBLE MECHANISMS FOR THE FORMATION OF CENTER H

Chapter 4 of this thesis describes the investigation of the R2 mutant Y122H of ribonucleotide reductase (RNR) from *E. coli*. In this mutant, the catalytically essential tyrosyl radical site of the wild-type protein is replaced by a histidine

residue. Based on earlier studies of other R2 mutants where the tyrosyl radical site had been modified, we expected one of two different reaction paths for the new histidine mutant, assuming that the first steps of the oxygen activation reaction are still working, including the formation of high valence iron intermediate X (see Figure 1-5). Either, (i) a histidine radical could be generated analogous to the tryptophan radical observed in the mutant R2-Y177W of the closely related RNR from mouse, or, (ii) if the iron intermediate X is not able to oxidize the new amino acid residue, as in the mutant R2-Y122F, the lifetime of intermediate X is doubled and transient tryptophan radicals in the second ligand sphere of the diiron center are observed during the decay (Sahlin *et al.*, 1994, Sahlin *et al.*, 1995, Lendzian *et al.*, 1996).

The introduction of histidine did not lead to the formation of the anticipated histidine radical, which might be explained by the significantly higher redox potential of histidine compared to tyrosine or tryptophan<sup>2</sup>. However, the characteristics of R2-Y122F are also considerably different than those observed for R2-Y122H. In contrast, we find instead a new paramagnetic species, center H, that is stable for more than two weeks at room temperature.

The <sup>57</sup>Fe ENDOR data of center H provided evidence for describing center H as a paramagnetic diiron center. However, in contrast to the Fe<sup>III</sup>Fe<sup>IV</sup> center, intermediate X, where one of the <sup>57</sup>Fe hf tensors has large anisotropy typical for Fe<sup>IV</sup>, center H has two <sup>57</sup>Fe hf tensors with relatively small anisotropy, which is in good agreement with a Fe<sup>III</sup>Fe<sup>III</sup> center. To explain that center H is still paramagnetic with an  $S = \frac{1}{2}$  ground state, a third spin needs to be coupled to the iron center. The nature of this third spin should be a ligand radical, strongly exchange coupled to the two irons.

As mentioned above, a series of isotope labeling experiments of amino acid residues in R2-Y122H was performed by Dr. Stephan Pötsch at the University of Stockholm. This series included  $\delta$ -<sup>13</sup>C-glutamate,  $\gamma$ -<sup>13</sup>C-aspartate, and  $\delta$ -<sup>15</sup>N-histidine, and the incorporation of the labeled amino acids into the protein was verified by mass spectrometry. However, none of these preparations gave rise to any isotope effects measured by EPR or ENDOR. In the case of the histidine labeled sample, the results are somewhat ambiguous. The ENDOR spectra lines (see Figure 4-7) should be altered by the incorporation of  $\delta$ -<sup>15</sup>N-histidine, due to the interactions between the electron spin on the irons and the nuclear spins on two nitrogen ligands H241 and H118. An explanation for the failure to observe an <sup>15</sup>N-effect may be that the  $\delta$ -<sup>15</sup>N-histidine was not incorporated with sufficiently high yield. In the minimal medium used for growth of the bacteria, the added labeled histidine will also be used for the purine nucleotide synthesis (Zalkin and Dalton, 1992), and the bacteria will therefore start production of their own, non-labeled, histidine. The mass difference expected for  $\delta$ -<sup>15</sup>N-histidine labeled monomeric units of the R2 protein is only 8 Da of a total of ~ 43 400 Da, which might not be detected by mass spectroscopy. In a preparation of R2-Y122H that was grown in minimal medium with <sup>15</sup>N-ammonium sulfate as the sole source of nitrogen, leading to a global <sup>15</sup>N-labeling of the protein,

---

<sup>2</sup> in an acetonitrile solution the redox potential for phenylalanine was found to be 1.8 V (Isied, 1994), whereas aqueous solutions of histidine has 1.4 V and tyrosine and tryptophan range from 0.8-1.0 V (van der Donk and Stubbe, 1998)



we did see an isotope effect on the CW and pulsed Davies ENDOR spectra. This experiment is described in the PhD thesis of Günther Bleifuss. Similar dipolar hf couplings from nitrogen are, as expected, also present in the ENDOR spectra of intermediate X (Burdi *et al.*, 1998). However, these results indicate that histidine is not a likely candidate for the localization of the third exchange coupled spin in center H.

Evidence for the actual location of the ligand radical came from the pulsed ENDOR data of the R2-Y122H labeled with Phe- $d_8$  (Figure 4-9). These data revealed a significant interaction with the protons on F208, which is the only phenylalanine residue close to the iron site. Simulations of the ENDOR difference spectrum (non-labeled minus labeled) (Figure 4-11) based on the theoretical hf couplings of a phenoxyl radical on *meta*- and *para*-position of the phenyl ring with a spin projection factor of 2/9, revealed that the *para*-phenoxyl radical with both  $\beta$ -protons having a dihedral angle of  $60^\circ$  to the phenol ring normal axis fits best with the experiment.

It should also be noted that the ring protons of phenylalanine F208 in R2-Y122H are close enough to make dipolar couplings with the two irons. An expression for the relationship between the principle values of a dipolar hf coupling tensor and the angles and distances between a binuclear metal center and a proton can be calculated using an extended point-dipole model that was developed in the research group of Prof. Lubitz (Fiege *et al.*, 1998, Schäfer *et al.*, 1998). However, the exact distances can not be taken from the crystal structure as this does not exactly reflect the situation of center H. Especially, if we assume that F208 is oxidized and forms a ligand to one iron, the Fe–H distances will be significantly shorter, and thus the dipolar hf interactions stronger.

Modification of F208 has also been observed in other R2 mutants. In R2 Y122F/E238A a new *meta*-hydroxyl group of F208 forms a ligation to Fe2, replacing the normal ligand E238 in wild-type R2 (Logan *et al.*, 1998) (see Figure 4-9). A similar hydroxylation is also observed in the R2 mutant F208Y, where the Y208 is converted to a 3-4-dihydroxyphenylalanine (DOPA) residue (Åberg *et al.*, 1994). Here, the *para*-hydroxyl group of DOPA is ligated to both iron Fe1 and Fe2, whereas the *meta*-hydroxyl group is only ligated to Fe1 (Logan *et al.*, 1998) (see Figure 4-9). Recently, a hydroxylation was also observed in the R2 mutant D84E/W48F (Baldwin *et al.*, 2001). In this case, the D84E mutation was introduced to correct the only discrepancy of the iron ligands between R2 and the structurally related enzyme methane monooxygenase (MMO). The second point mutation, W48F, serves to block the radical transfer chain, which also is not present in MMO. The hydroxylation activity observed in this mutant is similar to that of MMO, where hydroxylations of aromatic hydrocarbons can occur *in vitro*. However, the hydroxylation reactions observed in MMO and in these R2 mutants are two-electron oxidations, whereas the formation of a phenoxyl radical on phenylalanine in R2-Y122H requires abstraction of three electrons. Furthermore, the oxidation in R2-Y122H seems to have taken place on the *para*- and not the *meta*-position.

In both the mutants R2-Y122F/E238A and R2-F208Y, there are indications for the presence of a paramagnetic center with similar EPR characteristics as center H. They are, however, by far not as stable, being observable only within a few minutes after reconstituting the apo protein with iron and oxygen. In the R2-

Y122F/E238A mutant a 2.4 mT broad isotropic EPR spectrum of an unknown reconstitution intermediate was shown to be broadened to 4.3 mT after reconstitution with  $^{57}\text{Fe}$  (Bert Ove Persson, PhD thesis, Stockholm University, 1997), which is similar to the behavior of center H (see Figure 4-6).

In the mutant R2-F208, a transient paramagnetic species, called center Z, has been generated under special conditions where very high concentrations of ascorbate was present during the reconstitution reaction (Liu *et al.*, 1998). This species was described as an alternative route to the formation of DOPA described above. The CW ENDOR spectrum of center Z is remarkably similar to center H, with the exception of a proton hf coupling of  $\sim 6$  MHz in magnitude (Aimin Liu, PhD thesis, Stockholm University, 2000). This coupling has not been assigned, but as seen in Figure 4-10, any orientation of the  $\beta$ -protons of Y208 other than  $\theta \cong 60^\circ$  would lead to hf couplings larger than 6 MHz ( $\theta$  is the dihedral angle between the  $\text{H}_\beta - \text{C}_\beta$  bond and an axis perpendicular to the phenol ring plane). In fact, a  $\beta$ - $d_2$ -Tyr labeled preparation of this protein lead to a narrowing of the X-band EPR signal of center Z, but no ENDOR spectrum of this sample has been published (Liu *et al.*, 1998). However, in spite of the similarities between center Z and center H, they have a totally different lifetime, and only a very small  $^{57}\text{Fe}$  effect was observed in the X-band EPR spectra of center Z.

What could be the mechanism for the modification of F208 in the R2-Y122H mutant? We do not have evidence for when, or how, the generation of center H occurs, since center H is already present in all preparations of R2-Y122H, but it seems most likely to be an alternative route of the oxygen activation reaction leading to oxidation of a hydrophobic amino acid residue in the close vicinity of the iron.

The difference we observe between R2-Y122F, in which transient iron intermediates and tryptophan radicals are formed, and R2-Y122H, where a stable phenoxyl radical is formed, must rely on the structural differences, since they both have "non-oxidizable" amino acid residues at the normal tyrosyl radical site. Indeed, the histidine H122 in R2-Y122H forms a hydrogen bond to aspartate D84 making D84 a monodentate iron ligand, whereas in R2-Y122F, D84 is bidentately ligated to the iron, as phenylalanine is unable to form hydrogen bridges. Interestingly, D84 is found bidentately ligated to iron in the wild type metR2 from *E. coli*, whereas the corresponding aspartate in the met-R2 form of mouse RNR is monodentate, similar to the reduced diferrous form of *E. coli* RNR, indicating that this residue is rather flexible. In MMO from *M. trichosporium* OB3b the complementary E114 forms a monodentate bond to Fe1. This residue is less flexible due to the extended length of the side chain, which assures that the substrate oxidation reaction in MMO always happens directly at the iron site, and not at a more distantly located amino acid residue, as in R2. It is also important to note that in R2-Y122H, as well as in MMO, there is an extra water ligand to Fe1 at the place that is normally occupied by one of the D84 carboxyl oxygens. These structural differences, may also explain why the rhombic g-tensor of the mixed valence species,  $\text{Fe}^{\text{II}}\text{Fe}^{\text{III}}$ , of the R2-Y122H protein shows greater similarities with the g-tensor of the  $\text{Fe}^{\text{II}}\text{Fe}^{\text{III}}$  center in MMO than with the axial g-tensor of  $\text{Fe}^{\text{II}}\text{Fe}^{\text{III}}$  in wild-type R2.

In MMO, the hydroxylation of the substrate is performed by the  $\text{Fe}^{\text{IV}}\text{Fe}^{\text{IV}}$  intermediate Q, which has so far not been observed in R2 (Valentine *et al.*, 1998). In the wild-type R2, intermediate X performs the one-electron oxidation of Y122 (Bollinger *et al.*, 1994). This intermediate was originally described as a  $\text{Fe}^{\text{III}}\text{Fe}^{\text{III}}$  species with a strongly coupled hydroxyl radical ligand bound to Fe1 (Ravi *et al.*, 1994). Later, this model was changed to a formally  $\text{Fe}^{\text{III}}\text{Fe}^{\text{IV}}$  with a substantial portion of the spin delocalized to the oxygen ligands (Sturgeon *et al.*, 1996). The evidence is, however, still not clear, and the truth probably lies somewhere in the middle, or as equilibrium between the two forms. In the case of R2-Y122H, this equilibrium might be moved over to the hydroxyl radical form, which makes a nucleophilic attack on the F208 ring forming a stable phenoxyl radical. A phenoxyl type radical ligated to one of the irons could explain the stability of center H compared to X. Relatively stable phenoxyl ligand radicals have been reported for  $\text{Fe}^{\text{III}}$  model complexes (Snodin *et al.*, 1999).

In an  $\text{H}_2\text{O}/\text{D}_2\text{O}$  exchange experiment with R2-Y122H, we found a significant narrowing of the low-field side of the X-band EPR spectrum (not shown), very similar to a complimentary experiment in the intermediate X (Veselov and Scholes, 1996). Simulations of our spectra by Günther Bleifuss, indicated that a large anisotropic hyperfine coupling of an exchangeable proton with tensor components up to 1.0 mT contributes to the spectrum of center H. The coupling could result from bridging or terminal OH or from water ligands of the irons. Large exchangeable hyperfine tensor components have been observed by ENDOR of MMO (DeRose *et al.*, 1993) and of X (Willems *et al.*, 1997). Such a large anisotropic coupling is, however, difficult to detect in the ENDOR spectra and we failed to observe it, probably due to the low yield of center H (3%).

Interestingly, very recently the first EPR data from R2 of RNR of the parasite *Chlamydia trachysporium* have been presented. The RNR of this organism has been classified as Ia, based on DNA sequence alignments. There seems however not to be any tyrosyl residue at the expected position for the tyrosyl radical (Roshick *et al.*, 2000). The EPR spectra showed the build-up of intermediate X, which then decays and a new species occurs, very similar to center H (Dr. S. Fridd, personal communication). It is not clear how this RNR can work without a tyrosyl radical, but there is evidence from the mouse mutant R2-Y177F that intermediate X alone can give rise to up to 10 % substrate turnover (Henriksen *et al.*, 1994).



## 5

# SUMMARY AND OUTLOOK

This work aimed to investigate the electronic structure of catalytically relevant paramagnetic centers in the radical enzyme ribonucleotide reductase (RNR) by means of modern magnetic resonance methods. The first aim was to generate and characterize the catalytically essential thiyl radicals in the protein subunit R1 of RNR in the absence of the cofactor protein R2. The second aim was to study the electronic structure of a novel paramagnetic metal center, in particular the nature of the radical ligand, in the R2 mutant Y122H, where the normal tyrosyl radical residue has been replaced by a histidine residue.

Three different methods have successfully been tested for artificial generation of thiyl radicals in R1 of RNR. By direct UV-irradiation of frozen samples of cysteine, BSA and R1 protein-associated thiyl radicals were generated, and detected directly by EPR at low temperature without using spin traps. Thereby, the spectroscopic properties of thiyl radicals in a protein could be characterized, which have so far only been described in small molecules. The weak, broad  $g_{\parallel}$ -component and the strong, narrow  $g_{\perp}$ -component at 2.008 of the axial EPR spectrum of the thiyl radical are characteristic fingerprints for thiyl radicals. The weak, broad  $g_{\parallel}$ -component is very sensitive to the electrostatic environment, e.g. H-bonding, and varied from 2.30 in cysteine due to a weak H-bond to the sulfur, to 2.18 in BSA due to a strong hydrogen bond. In R1, only a broad shoulder but not a distinct  $g_{\parallel}$ -tensor value could be observed, due to  $g$ -strain and superposition of signals from several different cysteine residues in the protein. In all cases, however, and especially in R1, the  $g_{\parallel}$ -component was well detectable in the EPR absorption display. The spin-lattice relaxation of the two  $g$ -components is very anisotropic, which is unusual for an organic radical, but can be explained by the large spin-orbit coupling constant for sulfur.

This method of generation and direct detection of thiyl radicals allows access to the characteristic spectroscopic parameters, such as the  $g$ - and hfs tensors, lifetime, and saturation behavior of protein-associated thiyl radicals using EPR and also ENDOR spectroscopy. Furthermore, the dependency of the  $g_{\parallel}$ -component on H-bonds can be used as a probe for the electrostatic environment of the thiyl radicals.

Future experiments are planned for the estimation of the lifetime of protein-thiyl radicals under more mild conditions with laser flash photolysis of nitrosylated R1, or alternatively by thiol oxidation using  $\text{Ce}^{\text{IV}}/\text{NTA}$  and subsequent rapid freeze quench methods (RFQ) with a time resolution of up to 10 ms. The lifetime of thiyl radicals in low molecular weight thiols detected by optical methods lies in the  $\mu\text{s}$  region (Chatgililoglu and Asmus, 1990), and is therefore too short for observation by the RFQ techniques and EPR. In proteins, however, the situation is unknown, but it could be more promising since protein-based thiyl radicals may be shielded from the medium. The investigation of thiyl radicals in mono-thiol proteins would also allow investigation of *g*-strain and H-bonding without superposition of several thiyl radicals from different sites.

For generation of thiyl radicals at room temperature, a chemical and a photochemical method was used. Oxidation of thiols in R1 using  $\text{Ce}^{\text{IV}}/\text{NTA}$  as well as photolytic release of nitric oxide (NO) from nitrosylated R1 lead to the exclusive formation of thiyl radicals in R1. The spin trap phenyl-N-t-butyl nitron (PBN) was used to convert the short-lived thiyl radicals into long-lived nitroxide spin adducts, which were detected by EPR. PBN has proven to be an appropriate and sensitive EPR detector for thiyl radicals in R1 with a sufficiently long lifetime of the nitroxide spin adducts in the liquid state for EPR detection, even in the presence of the strong oxidant  $\text{Ce}^{\text{IV}}/\text{NTA}$ . The specificity of the radical generation was verified by selectively blocking the protein thiol groups using two different blocking agents. Furthermore, in aerobic sample, in absence of spin traps, we observed the characteristic EPR-spectrum of a sulfinyl radical, which is known to be the reaction product of thiyl radicals and oxygen.

The analysis of the EPR lineshape of the PBN spin adducts of the thiyl radicals in R1 yielded results about the dynamic properties (rotational motion) of the thiol-bound nitroxide radical. We have shown that the protein thiyl-PBN adduct radicals are localized predominantly in folded regions of protein R1 exhibiting EPR spectra typical for slow isotropic rotational motion. From a thiol assay using Ellman's reagent, the number of accessible cysteines was estimated to 10 out of totally 22 cysteines in the R1 dimer. The same number was obtained from quantification of NO-thiol groups from the specific optical absorption band at 340 nm.

The presented results on protein-associated thiyl radicals should be regarded as the first steps into a new field with high complexity. However, a series of suggestions for future experiments have arisen from the work so far. Further effort is necessary to find out which thiols are converted to thiyl radicals. One possible way would be the generation of thiyl radicals in specific cysteine mutants, or alternatively, by analysing the spin adducts at distinct cysteine residues after tryptic digestion of photolyzed, or  $\text{Ce}^{\text{IV}}/\text{NTA}$  treated, R1, using EPR or mass spectroscopy. A selective selenocysteine mutation of the essential thiyl radical site C439 is also planned. Selenocysteine has a 7.6 % natural occurring isotope  $^{77}\text{Se}$  with a nuclear spin  $I = \frac{1}{2}$  whose hyperfine interaction with the electron spin would discriminate a selenyl radical from other thiyl radicals in R1.

The procedures reported here for artificial generation of thiyl radicals in R1, in the absence of the R2, might open a way for mimicking partial steps of turnover in

RNR to evidence the catalytic competence of thiyl radicals in R1. Particularly the photochemical generation seems to be a suitable and mild procedure under which partial turnover can take place with the minimal risk of undesired side-effects on the R1 protein. Due to the low yield of artificially generated thiyl radicals, any detection of catalytic activity, i.e. formation of deoxyribonucleotide products, needs to be very sensitive. This can be achieved by using radioactive labeled substrate,  $^3\text{H}$ -CDP, and screening for radioactivity in the fractions containing the products,  $^3\text{H}$ -dCDP, following chromatographic separation of substrate and product (Thelander *et al.*, 1978).

In the second part of this work, a mutant of the R2 protein of RNR, R2-Y122H, was investigated. The wild-type R2 protein contains a binuclear iron complex and a stable tyrosyl radical, however, the mutant R2-Y122H contains a novel unusually stable paramagnetic center, named center H, which detailed electronic structure has been resolved here. The X-band EPR spectrum of center H revealed a single broad isotropic Gaussian shaped line at  $g = 2.003$ , typical for an  $S = \frac{1}{2}$  species. At W-band 94 GHz the  $g$ -anisotropy was fully resolved with  $g$ -tensor values 2.0088, 2.0040 and 1.9960. The  $g$ -tensor value below 2.0, the temperature dependent broadening, and the power saturation behavior indicated that center H was a strongly exchange coupled metal center. To confirm the involvement of iron, a new growth medium was developed, which allowed the incorporation of  $^{57}\text{Fe}$  into the protein during bacterial cell growth. The  $^{57}\text{Fe}$  ENDOR spectra of this sample contained signals from two  $^{57}\text{Fe}$  hf tensors, giving strong evidence for a binuclear iron center. However, the relatively small anisotropy of both the two  $^{57}\text{Fe}$  hf tensors of center H were indicative for an  $\text{Fe}^{\text{III}}\text{Fe}^{\text{III}}$  center, which has to be strongly coupled to a third spin to form an  $S = \frac{1}{2}$  ground state. By using a model for exchange coupled systems, we calculated that center H was most likely an  $\text{Fe}^{\text{III}}\text{Fe}^{\text{III}}$  center with a strongly coupled ligand radical ( $\text{R}^\bullet$ ). A main topic of this thesis is the assignment of this ligand radical, and to find out the mechanism of its formation.

A good candidate for the ligand radical was found from the Davies pulsed ENDOR data of R2-Y122H that was labeled with deuterated phenylalanine. These spectra contained deuteron hf couplings, and corresponding missing proton hf couplings, which could be assigned to phenylalanine F208, the only phenylalanine within 5.0 Å of the diiron center. However, the hydrophobic F208 phenol ring has to be modified by e.g. a hydroxylation in order to become a ligand radical coordinated to the diiron center. Based on simulations ENDOR spectra of methylene-phenoxy radicals with different positions of the phenoxy oxygen and different orientations of the  $\beta$ -methylene protons, the ligand radical is most likely a *para*-4-phenoxy radical on F208, analogous to a tyrosyl radical. The magnitude of the observed deuteron couplings, as well as the corresponding missing proton hf couplings of the Phe-*d*8 labeled R2-Y122H sample compared to the non-labeled sample, could only be explained with the spin projection factor calculated for an antiferromagnetically coupled 3-spin system.

Formally, the oxidation of phenylalanine to a phenoxy radical can be described as a three-electron oxidation. First, a two-electron hydroxylation of the phenol ring, then a single electron oxidation of the hydroxyl group to a phenoxy

radical. This means that R2-Y122H performs both monooxygenase activity, capable of hydroxylating phenylalanine similar to MMO, as well as phenoxyl radical generation, which is a similar activity to the one observed during the reconstitution reaction of wild-type R2, however on Y122 and not on F208. Hereby, the nature and the electronic structure of center H is essentially elucidated.

To obtain decisive evidence for the covalent oxygenation of F208 in future experiments, the R2-Y122H protein could be cleaved into smaller polypeptide fragments with trypsin, and these fragments could be analyzed by mass spectroscopy for a partial weight increase due to the extra oxygen. A discrimination between modification in *para*-(4) or *meta*-(3) position of the phenol ring of phenylalanine is probably only possible by complete hydrolysis of the peptide bonds, and careful chromatographic analysis of the isolated amino acids. These strategies are, however, complicated by the fact that only 3 % of the protein contains center H. Pulsed ENDOR spectra of new protein preparations with selectively deuterated phenylalanine residues, could also provide more information. The presence of deuterium interactions from an R2-Y122H protein that is labeled with  $\beta_1, \beta_2$ - $d_2$ -phenylalanine would provide conclusive evidence for a *para*-(4)-phenoxyl radical, since there would only be very weak dipolar interactions with the  $\beta$ -protons in case of *meta*-(3)-phenoxyl radical due to low spin density on  $C_1$  in this case (see Scheme 4.3), and there would practically be no dipolar interactions between these  $\beta$ -protons and the two irons.

Maybe the most promising way to obtain further information on center H is to investigate the other R2 mutants where similar, although short living, paramagnetic species have been observed with significantly higher yields. This includes the mutants R2-E238A/Y122F, R2-F208Y with its center Z, as well as the wild-type R2 from *Clamydia trachysporium*, where the normal tyrosyl radical site is missing, and replaced by phenylalanine.



# 6

## ZUSAMMENFASSUNG UND AUSBLICK

Das Ziel dieser Arbeit war, die elektronische Struktur katalytisch relevanter paramagnetischer Zentren im Radikalenzym Ribonukleotid-Reduktase (RNR) mit modernen Methoden der magnetischen Resonanz zu untersuchen. Ein Teilziel war, Thiylradikale in der R1-Proteinuntereinheit von RNR, die als katalytisch essentiell gelten, in Abwesenheit der R2-Untereinheit zu erzeugen und EPR-spektroskopisch zu charakterisieren. Ein weiteres Teilziel bestand darin, die elektronische Struktur eines neuartigen paramagnetischen Metallzentrums, und insbesondere die Natur des radikalischen Liganden, in der R2-Mutante Y122H, bei der der Tyrosinradikaltragende Aminosäurerest Y122 mit Histidin ersetzt ist, zu untersuchen.

Für die künstliche Erzeugung von Thiylradikalen in R1 von RNR, wurden drei verschiedene Methoden erfolgreich eingesetzt. Erstens wurden protein-assoziierte Thiylradikale in gefrorenen Lösungen von Cystein, Rinderserumalbumin (BSA) und R1 durch UV-Bestrahlung erzeugt, die unmittelbar mit EPR, ohne Verwendung von Spin-Traps, bei tiefer Temperatur untersucht wurden. Dadurch konnten erstmals spektroskopische Eigenschaften proteingebundener Thiylradikale mit EPR direkt bestimmt werden, die bisher nur in niedermolekularen Systemen beschrieben worden sind. Die schmale, intensive  $g_{\perp}$  Komponente bei 2,008 und die schwache, stark verbreiterte  $g_{\parallel}$ -Komponente (2,30 - 2,17) des axialen EPR-Spektrums sind charakteristische Merkmale der Thiylradikale. Der Wert der  $g_{\parallel}$ -Komponente ist sehr empfindlich gegenüber der elektrostatischen Umgebung des Schwefelatoms, und schwankt zwischen 2,30 in Cystein (schwache H-Brücke), und 2,18 in BSA infolge einer starken H-Brücke. Durch die Überlagerung von Thiylradikalen an mehreren unterschiedlichen Cysteinresten in R1, wurde hier nur eine verbreiterte  $g_{\parallel}$ -Schulter beobachtet. In allen drei Fällen, und insbesondere in R1, konnte die  $g_{\parallel}$ -Komponente jedoch zweifelsfrei im Absorptionsmodus identifiziert werden. Die Spin-Gitter-Relaxation der beiden  $g$ -Komponenten – beobachtbar im Mikrowellen-Sättigungsverhalten – zeigt eine sehr starke Anisotropie, die untypisch

für organische Radikale ist, sich aber durch die große Spinbahn-Kopplungskonstante des Schwefelatoms im Thiylradikal erklären lässt.

Die Kenntnis der EPR-Spektrengestalt der Thiylradikale erlaubt nunmehr Zugang zu charakteristischen spektroskopischen Parametern, wie z.B. g- und hfs-Tensoren, Lebensdauer und Sättigungsverhalten der Protein-Thiylradikale, mittels direkter EPR- und ENDOR Detektion. Weiterhin ist eine Charakterisierung von H-Brücken unterschiedlicher Stärke (elektrostatische Wechselwirkungen) an Thiylradikalen möglich. Für zukünftige Experimente zur Ermittlung der Lebensdauer sollen Thiylradikale durch Photolyse von nitrosyliertem R1, oder eventuell durch Oxidation mittels  $\text{Ce}^{\text{IV}}$ /NTA erzeugt werden, und durch schnelle Einfriertechniken wie z.B. "rapid-freeze-quench" (RFQ) mit einer Zeitauflösung bis 10 ms eingefangen und stabilisiert werden. Die Lebensdauer von Thiylradikalen in niedermolekularen Thiolen konnte durch optische Detektion bestimmt werden und liegt im Bereich von  $\mu\text{s}$  (Chatgililoglu und Asmus, 1990), was für einen RFQ-Nachweis zu kurzlebig ist. In Proteinen ist die Lebensdauer von Thiylradikalen unbekannt; sie könnte durch die geschützte Lage im Proteininneren jedoch sehr viel länger (wie bei Tyrosin- und Tryptophanradikalen bekannt ist) sein. Das Problem der Überlagerung von EPR-Spektren mehrerer Thiylradikale in R1, könnte durch die Radikalerzeugung im Mono-Thiolproteinen überwunden werden.

Für die Erzeugung von Thiylradikalen des R1-Protein in flüssiger Lösung bei Raumtemperatur, wurden zwei weitere Methoden eingesetzt, eine chemische und eine photochemische. Es wurde gezeigt, dass die Oxidation von Thiolgruppen ( $\text{R-SH}$ ) mittels  $\text{Ce}^{\text{IV}}$ /Nitrilotriessigsäure (NTA), bzw. eine laserphotolytische Freisetzung von Stickstoff-monoxid ( $\text{NO}$ ) von nitrosylierten Thiolgruppen ( $\text{R-SNO}$ ), zu einer spezifischen Erzeugung von Thiylradikalen führt. Die in flüssiger Phase sehr kurzlebigen Thiylradikale wurden mit Hilfe des "Spin-Trap"-Moleküls Phenyl-N-t-Butylnitron (PBN) in langlebige Nitroxid-Spinaddukte umgewandelt und dann indirekt mit EPR nachgewiesen. PBN erwies sich als ein geeigneter und empfindlicher EPR-Detektor für Thiylradikale in R1, mit einer für die EPR-Spektrenregistrierung ausreichenden Lebenszeit der Nitroxid-Spinaddukte im flüssigen Zustand, sogar in Anwesenheit des starken Oxidationsmittels  $\text{Ce}$ . Die spezifische Erzeugung von Radikalen an Thiolgruppen, konnte durch eine selektive Blockierung der Protein-Cysteinreste mit zwei verschiedenen Reagenzen belegt werden. Weiterhin wurde in aeroben R1-Proben das charakteristische EPR-Spektrum eines Sulfinylradikals bei tiefer Temperatur beobachtet, das als Reaktionsprodukt zwischen Thiylradikalen und Sauerstoff angesehen wird.

Die Analyse der EPR-Linienform der PBN-Spinaddukte von Thiylradikalen in R1 in flüssiger Phase, erbrachte Ergebnisse über dynamische Eigenschaften (Rotation-Fluktuationsbewegungen) thiolgebundener Nitroxidradikale. Es konnte anhand der EPR-Spektren, die für langsame isotrope Rotationsbewegung typisch sind, gezeigt werden, dass sich die Proteinthiyl-PBN-Adduktradikale überwiegend in gefalteten Regionen des R1-Proteins befinden. Die Zahl der zugänglichen Cysteinreste in nativem R1 wurde mit Ellmans Reagenz auf 10 von insgesamt 22 Cysteinresten im R1-Dimer bestimmt. Die gleiche Zahl wurde von der Quantifizierung der  $\text{NO}$ -Thiolgruppen von deren spezifischer optischer Absorptionsbande bei 340 nm erhalten.

Bei den vorgelegten Ergebnissen zur Charakterisierung von protein-assoziierten Thiylradikalen in R1 von RNR handelt es sich um erste Teilschritte einer komplexen bislang neuen Problematik, die trotz der zeitlichen Begrenztheit einer Dissertation bereits eine Reihe von Anregungen für künftige Schritte beinhaltet. Weitere Bemühungen sind notwendig um herauszufinden, welche von den 22 Thiolen in Thiylradikale umgewandelt werden, und ob sich insbesondere die katalytisch wichtige Position C439 unter den erzeugten Thiylradikalen befindet. Eine Möglichkeit wäre die Erzeugung von Thiylradikalen in spezifischen R1-Mutanten, wo einzelne Cysteinreste gentechnisch durch andere Aminosäurereste substituiert worden sind. Eine weitere Möglichkeit wäre, das R1-Protein mit Trypsin zu verdauen, und die daraus entstandenen Peptidfragmente mittels EPR oder Massenspektroskopie nach den kovalent gebundenen Spinaddukten abzusuchen. Ferner ist auch eine ortsgerichtete Selenocystein-Mutation, C439SeC, geplant; Selenocystein hat 7,6 % natürlichen Anteil des Isotops  $^{77}\text{Se}$  mit einem Kernspin von  $I = \frac{1}{2}$ , dessen Hyperfeinwechselwirkung ein Selenylradikal von Thiylradikalen in R1 unterscheiden würde.

Um endgültige Beweise für die Existenz eines Thiylradikals an der postulierten Position C439 und insbesondere dessen katalytischer Kompetenz zu erhalten, sind weitere gezielte Experimente unter Bedingungen eines partiellen Substratumsatzes geplant. Die photochemisch erzeugten Thiylradikale sind dafür am besten geeignet, weil diese Methode wahrscheinlich die geringsten Nebenwirkungen am R1-Protein hat. Die Detektion der Produkte des Turnovers sollte so empfindlich wie möglich sein, um auch noch geringe Mengen nachweisen zu können. Dafür sind Tritium-markierte Substrate am geeignetsten. Die Spin-Trap-Versuche bieten in geeigneten Aktivitätsassays eine prinzipielle Möglichkeit des EPR-Nachweises des katalytischen Schlüsselradikals C439 $^{\bullet}$  in R1 von RNR, das seit Jahren postuliert wurde.

In der Mutante R2-Y122H des Kofaktor-Proteins, das im nativen Zustand einen Di-Eisen-Metallkomplex und ein stabiles Tyrosinradikal am Y122 enthält, wurde ein neues, ungewöhnlich stabiles, paramagnetisches Zentrum entdeckt (Zentrum H genannt) dessen elektronische Struktur im Detail aufgeklärt wurde. Das X-Band EPR-Spektrum zeigte eine isotrope gaussförmige Einzellinie ohne Struktur bei  $g = 2,003$ , die typisch ist für ein Zentrum mit einem Grundzustand  $S = \frac{1}{2}$ . Im W-Band, bei zehnfach höherer Mikrowellenfrequenz, konnte die  $g$ -Anisotropie, mit den  $g$ -Tensorwerten 2,0088, 2,0040 und 1,9960 vollständig aufgelöst werden. Der  $g$ -Wert unterhalb 2,0, die temperaturabhängige Linienverbreiterung und das Mikrowellen-Sättigungsverhalten deuteten darauf hin, dass Zentrum H ein stark austauschgekoppelte Metallzentrum und kein Radikal ist. Zur Klärung, ob es sich um einen Eisen-Komplex handelt, wurde ein neues Wachstumsmedium entwickelt, das den Einbau von  $^{57}\text{Fe}$  während des Zellwachstums ermöglichte. Die  $^{57}\text{Fe}$ -ENDOR-Spektren enthielten eindeutige Befunde von zwei  $^{57}\text{Fe}$ -Hyperfeintensoren, ein klarer Hinweis auf ein dinukleares Eisenzentrum. Die relativ geringe Anisotropie beider  $^{57}\text{Fe}$ -Hyperfeintensoren deutete weiterhin auf dreiwertiges Eisen, d.h.  $\text{Fe}^{\text{III}}\text{Fe}^{\text{III}}$ . Das wiederum bedeutet, dass zusätzlich zu den Spins der beiden Eisenatome ein dritter Spin beteiligt sein muss, um ein Zentrum mit einem Grundzustand  $S = \frac{1}{2}$  zu

erzeugen. Der dritte Spin mit  $S = \frac{1}{2}$  legt ein Radikal im Ligandenbereich des Eisenzentrums nahe. Eine wesentliche Aufgabe dieser Dissertation bestand darin herauszufinden, welcher Natur ein solches Ligandradikal sein könnte und wie es in der Mutante entsteht.

Ein Kandidat für den dritten Spin wurde von Puls-ENDOR-Daten von einer Präparation vom R2-Y122H mit uniform deuteriertem Phenylalanin (Phe- $d_8$ ) gefunden. Diese Spektren enthielten Kopplungen, die eindeutig dem Phenylalanin F208 zugeschrieben werden konnten, da es das einzige Phenylalanin ist, das innerhalb von 5,0 Å vom Eisenzentrum entfernt liegt. Phenylalanin ist ein hydrophober Aminosäurerest, der erst nach einer Oxidation, z.B. eine Hydroxylierung, ein Eisenligand werden kann. Dieses Hydroxy-Phenylalanin könnte durch einen weiteren Oxidationschritt zu einem radikalischen Liganden werden. Durch Simulation der Puls-ENDOR-Spektren von Methylen-Phenoxyradikalen mit unterschiedlichen Positionen des Sauerstoffs, und Orientierungen der  $\beta$ -Methylenprotonen, konnte gezeigt werden, dass das Ligandradikal ein *para*-4-Phenoxyradikal, am F208 ist. Anders ausgedrückt, entspricht das Ligandradikal ein neues Tyrosinradikal am F208. Die Grösse der beobachteten Deuterium-Hyperfeinkopplungen in den Puls-ENDOR-Spektren der Phe- $d_8$ -markierten R2-Y122H-Probe zeigt, dass das Ligandradikal antiferromagnetisch zu einem der Eisenkerne gekoppelt ist.

Formal handelt es sich bei der Oxidation von F208 zu einem Phenoxyradikal, um eine Drei-Elektronen-Oxidation. Der erste Oxidationschritt wäre dann eine Zwei-Elektronen-Hydroxylierung des Phenolrings, gefolgt von einer Ein-Elektronen-Wasserstoffabstraktion. Diese Ergebnisse haben gezeigt, dass die Mutante R2-Y122H, sowohl Monooxygenase-Aktivität hat, durch die eine Hydroxylierung von Phenylalanin folgt, als auch eine Aktivität zur Phenoxyradikalerzeugung, ähnlich wie bei der Rekonstitutionsreaktion im Wildtyp-RNR bei der Y122 zum Tyrosinradikal oxidiert wird. Damit ist die Natur und die elektronische Struktur vom Zentrum H im wesentlichen aufgeklärt.

Um zusätzliche Beweise für die kovalente Modifizierung von F208 in zukünftigen Experimenten zu bekommen, wäre eine massenspektroskopische Untersuchung von Trypsinfragmenten eine Möglichkeit. Um insbesondere eine Unterscheidung zwischen *para*-(4) und *meta*-(3) Phenoxyradikalen zu treffen, ist wahrscheinlich eine vollständige Hydrolyse der Peptidbindungen und eine sorgfältige chromatographische Analyse der isolierten Aminosäuren notwendig. Allerdings sind diese Vorgehensweisen erschwert durch die geringe Ausbeute von nur 3 % Zentrum H im Gesamtprotein. Puls-ENDOR-Spektren von neuen Proteinpräparationen mit gezielt deuterierten Phenylalaninresten könnten zusätzliche Auskünfte über das Zentrum H bringen. Im Falle eines *para*-Phenoxyradikals, würde man starke Deuteriumkopplungen erwarten, wenn die Phenylalaninreste ausschließlich in  $\beta$ -Position deuteriert sind, und im Falle eines *meta*-Phenoxyradikals wären die  $\beta$ -Proton-Hyperfeinkopplungen sehr klein wegen einer sehr kleinen Spindichte am C<sub>1</sub> (siehe Schema 4-3).

Die vielleicht vielversprechendste Alternative wäre, Zentrum H mit anderen R2-Mutanten mit beobachteter Selbsthydroxylierung zu vergleichen, wo ähnliche EPR-Signale mit sehr viel höherer Ausbeute, beobachtet worden sind. Dies umfaßt

die Mutanten R2-E238A/Y122F, R2-F208Y, sowie auch Wildtyp-R2 aus *Clamydia trachysporium*, wo der normale radikalische Tyrosinrest mit Phenylalanin ersetzt ist.

Moderne Hochfeld-EPR und ENDOR-Spektroskopie kombiniert mit Isotopen-substitution hat zur Aufklärung der elektronischen Struktur eines neuartigen  $\mu$ -Oxo-Di-Eisen-Komplexes mit einem radikalischen Phenoxyl-Liganden geführt. Die erkannte Natur des Radikal-Liganden im Zentrum H, läßt Rückschlüsse über die Struktur-Wirkungs-Mechanismen durch die Mutation zu. Die Histidin-Mutation an Y122 von *E. coli* R2 bewirkt eine Monooxygenase-Aktivität, die sich in der Selbsthydroxylierung eines Phenylalanins, einer anschliessender Radikalbildung und schliesslich der Ausbildung eines neuen phenoxylischen radikalischen Liganden zu einem antiferromagnetisch gekoppelten 3-Spin-Systems,  $\text{Fe}^{\text{III}}\text{Fe}^{\text{III}}\text{R}^{\bullet}$ , mit Gesamtspin  $S = 1/2$  manifestiert.



# 7

## ABBREVIATIONS

azido-CDP.....	2'-azido-2'deoxycytosine 5'-diphosphate
BSA.....	bovine serum albumin
cP.....	centipoise
CW.....	continuous wave
DEAE.....	diethylaminoethyl
DFT.....	density functional theory
DMPO.....	5,5-dimethyl-1-pyrroline N-oxide
DOPA.....	3,4-dihydroxyphenylalanine
DTNB.....	5,5'-dithiobis (2-nitrobenzoic acid)
DTPA.....	diethylenetriaminepentaacetate
DTT.....	dithiothreitol
EDTA.....	ethylenediaminetetraacetate
ENDOR.....	electron nuclear double resonance
EPR.....	electron paramagnetic resonance
ESEEM.....	electron spin echo envelope modulation
ESR.....	electron spin resonance
EXAFS.....	extended X-ray absorption fine structure
FADH.....	flavine adenine dinucleotide
GSH.....	reduced glutathione
GSNO.....	S-nitrosoglutathione
hf.....	hyperfine
hfc.....	hyperfine coupling
hfs.....	hyperfine splitting
HQS.....	8-hydroxyquinoline sulfonate
MMO.....	methane monooxygenase
MMOH.....	the hydroxylase protein subunit of MMO
MOPS.....	3-[N-morpholino] propanesulfonate
mT.....	millitesla
NADPH.....	$\beta$ -nicotineamide adenine dinucleotide phosphate
NEM.....	N-ethylmaleimide

NMR	nuclear magnetic resonance
NTA	nitrilotriacetate
OD	optical density
PAGE	polyacrylamide gel electrophoresis
PBN	phenyl-N-t-butyl nitron
PMS	phenazine methosulfate
PMSF	phenylmethylsulfonyl fluoride
R1	the large protein subunit of RNR
R2	the small protein subunit of RNR
RFQ	rapid freeze quench
RNR	ribonucleotide reductase
RT	room temperature
SDS	sodium dodecyl sulfate
SNAP	S-nitrosoacetylpenicillamine
TEMPOL	2,2,6,6-tetramethyl-1-piperidinol
Tris	Tris(hydroxymethyl)aminomethane
TR	thioredoxin reductase
Trx	thioredoxin
UV	ultra violet light

#### Nucleotides and nucleic bases

A	adenine
C	cytosine
G	guanine
T	thymine (3-methyluracil)
U	uracil
AMP	adenosine 5'-monophosphate
CMP	cytidine 5'-monophosphate
GMP	guanosine 5'-monophosphate
TMP	thymidine 5'-monophosphate
UMP	uridine 5'-monophosphate
NMP	any 5'-monophosphate
NDP	any 5'-diphosphate
NTP	any 5'-triphosphate

#### Standard amino acids:

A	Ala	Alanine
C	Cys	Cysteine
D	Asp	Aspartic acid
E	Glu	Glutamic acid
F	Phe	Phenylalanine
G	Gly	Glycine
H	His	Histidine
I	Ile	Isoleucine
K	Lys	Lysine
L	Leu	Leucine



M	Met	Methionine
N	Asn	Asparagine
P	Pro	Proline
Q	Gln	Glutamine
R	Arg	Arginine
S	Ser	Serine
T	Thr	Threonine
V	Val	Valine
W	Trp	Tryptophan
X	xxx	Any amino acid
Y	Tyr	Tyrosine

The magnitude of the hyperfine tensor are often given in wavenumbers ( $\text{cm}^{-1}$ ), frequency (MHz), or magnetic field strength (mT or gauss ( $=0.1 \text{ mT}$ )) mostly depending on the method of determination. The correlations between these units are:

$$A [\text{MHz}] = 2.99792 \cdot 10^4 A [\text{cm}^{-1}]$$
$$A [\text{MHz}] = 28.0249 A [\text{mT}] (g / g_e)$$

where  $g$  and  $g_e$  denote the  $g$  values of the radical and of the free electron, respectively.



## 8

## REFERENCES

- Aasa, R. and Vänngård, T. (1975) EPR Signal Intensity and Powder Shapes: A Reexamination. *J. Magn. Res.*, **19**, 308-315
- Åberg, A., Hahne, S., Karlsson, M., Larsson, Å., Ormö, M., Åhgren, A., and Sjöberg, B.-M. (1989) Evidence for Two Different Classes of Redox-active Cysteines in Ribonucleotide Reductases of *Escherichia coli*. *J. Biol. Chem.*, **264**(21), 12249-12252
- Åberg, A., Nordlund, P., and Eklund, H. (1993) Unusual Clustering of Carboxyl Side Chains in the Core of Iron-Free Ribonucleotide Reductase. *Nature*, **361**, 276-278
- Åberg, A., Ormö, M., Nordlund, P., and Sjöberg, B.-M. (1993) Autocatalytic Generation of Dopa in the Engineered Protein R2 F208Y from *Escherichia coli* Ribonucleotide Reductase and Crystal Structure of the Dopa-208 Protein. *Biochemistry*, **32**(37), 9845-9850
- Alberti, A., Carloni, P., Eberson, L., Greci, L., and Stipa, P. (1997) New Insights into N-tert-Butyl- $\alpha$ -Phenylnitrone (PBN) as a Spin Trap. Part 2. The Reactivity of PBN and 5,5-Dimethyl-4,5-dihydropyrrole N-Oxide (DMPO) toward N-Heteroaromatic Bases. *J. Chem. Soc. Perkins Trans II*, 887-892
- Andersson, K. K. and Gräslund, A. (1995) Diiron-Oxygen Proteins. *Adv. Inorg. Chem.*, **43**, 359-408
- Andersson, M. E., Högbom, M., Rinaldo-Matthis, A., Andersson, K. K., Sjöberg, B.-M., and Nordlund, P. (1999) The Crystal Structure of an Azide Complex of the Diferrous R2 Subunit of Ribonucleotide Reductase Displays a Novel Carboxylate Shift with Important Mechanistic Implications for Diiron-Catalyzed Oxygen Activation. *J. Am. Chem. Soc.*, **121**(11), 2346-2352
- Askew, S. C., Barnett, J., McAninly, J., Williams, D. L. H. (1995) Catalysis by  $\text{Cu}^{2+}$  of Nitric Oxide Release from S-Nitrosothiols (RSNO). *J. Chem. Soc., Perkin Trans. 2*, 741-745
- Atherton, N. M. (1993) *Principles of Electron Spin Resonance*. Ellis Horwood PTR Prentice Hall
- Atkin, C. L., Thelander, L., Reichard, P., and Lang, G. (1973) Iron and Free Radical in Ribonucleotide Reductase. *J. Biol. Chem.*, **248**(21), 7464-7472
- Atta, M., Nordlund, P., Åberg, A., Eklund, H., and Fontecave, M. (1992) Substitution of Manganese for Iron in Ribonucleotide Reductase from *Escherichia coli*. *J. Biol. Chem.*, **267**(29), 20682-20688
- Atta, M., Andersson, K. K., Ingemarson, R., Thelander, L., and Gräslund, A. (1994) EPR Study of the Mixed-Valent  $[\text{Fe}^{\text{II}}\text{Fe}^{\text{III}}]$  Clusters Formed in the R2 Subunit of Ribonucleotide Reductase from Mouse or Herpes Simplex Virus: Mild Chemical Reduction of the Diferric Center. *J. Am. Chem. Soc.*, **116**(14), 6429-6430
- Atta, M., Debaecker, N., Andersson, K. K., Latour, J.-M., Thelander, L., and Gräslund, A. (1996) EPR and Multi-Field Magnetisation of Reduced Forms of the Binuclear Iron Centre in Ribonucleotide Reductase from Mouse. *J. Biol. Inorg. Chem.*, **1**(3), 210-220
- Baldwin, J., Krebs, C., Ley, B. A., Edmondson, D. E., Huynh, B. H., and Bollinger, J. M., Jr. (2000) Mechanism of Rapid Electron Transfer during Oxygen Activation in the R2 Subunit of

- Escherichia coli* Ribonucleotide Reductase. 1. Evidence for a Transient Tryptophan Radical. *J. Am. Chem. Soc.*, **122**(49), 12195-12206
- Baldwin, J., Voegtli, W. C., Khidekel, N., Moënne-Loccoz, P., Krebs, C., Pereira, A. S., Ley, B. A., Huynh, B. H., Loehr, T. M., Riggs-Gelasco, P. J., Rosenzweig, A. C., and Bollinger, J. M., Jr. (2001) Rational Reprogramming of the R2 Subunit of *Escherichia coli* Ribonucleotide Reductase into a Self-Hydroxylating Monooxygenase. *J. Am. Chem. Soc.*, **123**(29), 7017-7030
- Bar, G., Bennati, M., Nguyen, H.-H. T., Ge, J., Stubbe, J., and Griffin, R. G. (2001) High-Frequency (140 GHz) Time Domain EPR and ENDOR Spectroscopy: The Tyrosyl Radical-Diiron Cofactor in Ribonucleotide Reductase from Yeast. *J. Am. Chem. Soc.*, **123**(15), 3569-3576
- Barnett, D. J., McAninly, J., and Williams, D. L. H. (1994) Transnitrosylation between Nitrosothiols and Thiols. *J. Chem. Soc., Perkin Trans. 2*, 1131-1133
- Barry, B. A., and Babcock, G. T. (1987) Tyrosine Radicals are Involved in the Photosynthetic Oxygen-evolving System. *Proc Natl Acad Sci U S A.*, **84**(20), 7099-7103
- Becker, D., Swarts, S., Champagne, M., Sevilla, M. D. (1988) An ESR Investigation of the Reactions of Glutathione, Cysteine and Penicillamine Thiyl Radicals: Competitive Formation of  $\text{RSO}\bullet$ ,  $\text{R}\bullet$ ,  $\text{RSSR}\bullet$ , and  $\text{RSS}(\bullet)$ . *Int. J. Radiat. Biol.* **53**(5), 767-786
- Bencini, A., and Gatteschi, D. (1990) *EPR of Exchange Coupled Systems*, Springer Verlag, Berlin/Heidelberg
- Bender, C. J., Sahlin, M., Babcock, G. T., Barry, B. A., Chandrashekar, T. K., Salowe, S. P., Stubbe, J., Lindström, B., Petersson, L., Ehrenberg, A., and Sjöberg, B.-M. (1989) An ENDOR Study of the Tyrosyl Free Radical in Ribonucleotide Reductase from *Escherichia coli*. *J. Am. Chem. Soc.*, **111**(21), 8076-8083
- Berardi, M. J., Pendred, C. L., and Bushweller, J. H. (1998) Preparation, Characterization, and Complete Heteronuclear NMR Resonance Assignments of the Glutaredoxin (C14S)-Ribonucleotide Reductase B1 737-761 (C754S) Mixed Disulfide. *Biochemistry*, **37**(17), 5849-5857
- Berliner, L. J. (1976) *Spin Labeling, Theory and Application*, Academic Press, New York, NY
- Bertini, I., and Luchinat, C. (1996) NMR of Paramagnetic Substances. *Coordination Chemistry Reviews.*, **150**, 1-28
- Bianchi, V., Borella, S., Calderazzo, F., Ferraro, P., Bianchi, L. C., and Reichard, P. (1994) Inhibition of Ribonucleotide Reductase by 2'-Substituted Deoxycytidine Analogs: Possible Application in AIDS Treatment. *Proc. Natl. Acad. Sci. USA*, **91**, 8403-8407
- Bollinger, J. M., Jr., Edmondson, D. E., Huynh, B. H., Filley, J., Norton, J. R., and Stubbe, J. (1991) Mechanism of Assembly of the Tyrosyl Radical-Dinuclear Iron Cluster Cofactor of Ribonucleotide Reductase. *Science*, **253**, 292-298
- Bollinger, J. M., Jr., Tong, W. H., Ravi, N., Huynh, B. H., Edmondson, D. E., and Stubbe, J. (1994a) Mechanism of Assembly of the Tyrosyl Radical- Diiron(III) Cofactor of *E. coli* Ribonucleotide Reductase. 2. Kinetics of the Excess  $\text{Fe}^{2+}$  Reaction by Optical, EPR, and Mössbauer Spectroscopies. *J. Am. Chem. Soc.*, **116**(18), 8015-8023
- Bollinger, J. M., Jr., Tong, W. H., Ravi, N., Huynh, B. H., Edmondson, D. E., and Stubbe, J. (1994b) Mechanism of Assembly of the Tyrosyl Radical- Diiron(III) Cofactor of *E. coli* Ribonucleotide Reductase. 3. Kinetics of the Limiting  $\text{Fe}^{2+}$  Reaction by Optical, EPR, and Mössbauer Spectroscopies. *J. Am. Chem. Soc.*, **116**(18), 8024-8032
- Bollinger, J. M., Jr., Krebs, C., Vicol, A., Chen, S., Ley, B. A., Edmondson, D. E., and Huynh, B. H. (1998) Engineering the Diiron Site of *Escherichia coli* Ribonucleotide Reductase R2 to Accumulate an Intermediate Similar to Hperoxo, the Putative Peroxodiiron(III) Complex from the Methane Monooxygenase Catalytic Cycle. *J. Am. Chem. Soc.*, **120**(5), 1094-1095
- Bonazzola, L., Fackir, L., LeRay, N., and Roncin, J. (1984) ESR Study of Some Sulfur Centered Radicals Formed in Irradiated Cysteamine and 1,4-Dithiane Single Crystals. *Radiat. Res.*, **97**, 462-467
- Box, H. C., Freund, H. G., and Budzinski, E. E. (1966) Free Radical Formation by Ultraviolet Irradiation in Single-Crystals of Cysteine HCl. *J. Chem. Phys.*, **45**, 809-811
- Brudvig, G. W. (1995) Electron Paramagnetic Resonance Spectroscopy. *Meth. Enzymol.*, **246**, 536-554

- Buettner, G. R. (1985) Thiyl Free Radical Production with Hematoporphyrin Derivative, Cysteine and Light: a Spin Trapping Study. *FEBS Letters*, **177**(2), 295-299
- Buettner, G. R. (1987) Spin Trapping: ESR Parameters of Spin Adducts. *Free Rad. Biol. Med.*, **3**, 259-303
- Burdi, D., Sturgeon, B. E., Tong, W. H., Stubbe, J., and Hoffman, B. M. (1996) Rapid Freeze-Quench ENDOR of the Radical X Intermediate of *Escherichia coli* Ribonucleotide Reductase Using  $^{17}\text{O}_2$ ,  $\text{H}_2^{17}\text{O}$ , and  $^2\text{H}_2\text{O}$ . *J. Am. Chem. Soc.*, **118**(1), 281-282
- Burdi, D., Willems, J.-P., Riggs-Gelasco, P., Antholine, W. E., Stubbe, J., and Hoffman, B. M. (1998) The Core Structure of X Generated in the Assembly of the Diiron Cluster of Ribonucleotide Reductase:  $^{17}\text{O}_2$  and  $\text{H}_2^{17}\text{O}$  ENDOR. *J. Am. Chem. Soc.*, **120**(49), 12910-12919
- Burghaus, O., Plato, M., Rohrer, M., Möbius, K., MacMillen, F., and Lubitz, W. (1993) 3-mm High-Field EPR on Semiquinone Radical Anions  $\text{Q}^{\bullet-}$  Related to Photosynthesis and on the Primary Donor  $\text{P}^{++}$  and Acceptor  $\text{Q}_\text{A}^{\bullet-}$  in Reaction Centers of *Rhodobacter sphaeroides* R-26. *J. Phys. Chem.*, **97**(29), 7639-7647
- Carrington, A., and McLachlan, D. M. (1969) *Introduction to Magnetic Resonance*, Harper and Row, New York, NY
- Carson, D. A., Wasson, D. B., Esparza, L. M., Carrera, C. J., Kipps, T. J., and Cottam, H. B. (1992) Oral Antilymphocyte Activity and Induction of Apoptosis by 2-Chloro-2'-arabino-fluoro-2'-deoxyadenosine. *Proc. Natl. Acad. Sci. USA*, **89**, 2970-2974
- Chatgililoglu, C., and Asmus, K.D. (1990) *Sulfur-Centered Reactive Intermediate in Chemistry and Biology*, Plenum Press, New York, NY
- Clark, W. M. (1960) *Oxidation-Reduction Potentials of Organic Systems*. Waverly Press, Baltimore MD
- Cory, J. G., Downes, D. L., and Cory, A. H. (1996) Differences in the Properties of Mammalian Ribonucleotide Reductase toward Its Substrates. *Adv. Enzyme Regul.*, **36**, 3-15
- Covès, J., deFallos, L. L. H., Le Pape, L., Décout, J.-L., and Fontecave, M. (1996) Inactivation of *Escherichia coli* Ribonucleotide Reductase by 2'-Deoxy-2'-Mercaptouridine 5'-Diphosphate Electron Paramagnetic Resonance Evidence for a Transient Protein Perthiyl Radical. *Biochemistry*, **35**(26), 8595-8602
- Covès, J., Laulhère, J.-P., and Fontecave, M. (1997) The Role of Exogenous Iron in the Activation of Ribonucleotide Reductase from *Escherichia coli*. *J. Biol. Inorg. Chem.*, **2**(4), 418-426
- Davies, M. J., Gilbert, B. C., and Haywood, R. M. (1993) Radical-Induced Damage to Bovine Serum Albumin: Role of the Cysteine Residue. *Free Rad. Res. Comms.*, **18**(6), 353-367
- Davydov, R., Kuprin, S., Gräslund, A., and Ehrenberg, A. (1994) Electron Paramagnetic Resonance Study of the Mixed-Valent Diiron Center in *Escherichia coli* Ribonucleotide Reductase Produced by Reduction of Radical-Free Protein R2 at 77 K. *J. Am. Chem. Soc.*, **116**(24), 11120-11128
- Davydov, R., Sahlin, M., Kuprin, S., Gräslund, A., and Ehrenberg, A. (1996) Effect of the Tyrosyl Radical on the Reduction and Structure of the *Escherichia coli* Ribonucleotide Reductase Protein R2 Diferric Site as Probed by EPR of the Mixed-Valent State. *Biochemistry*, **35**(17), 5571-5576
- DeGray, J. A. and Mason, R. P (1995) Biothiyls: Free Radical Chemistry and Biological Significance. In: Packer, L. and Cadenas, E. (eds.) *Biothiols in Health and Disease*, Marcel Dekker, Inc., **270**(33), 20655-20658
- DeRose, V. J., Liu, K. E., Kurtz, D. M., Jr., Hoffman, B. M., and Lippard, S. J. (1993) Proton ENDOR Identification of Bridging Hydroxide Ligands in Mixed-Valent Diiron Centers of Proteins: Methane Monooxygenase and Semimet Azidohemerythrin. *J. Am. Chem. Soc.*, **115**(14), 6440-6441
- DeRose, V. J., Liu, K. E., Lippard, S. J., and Hoffman, B. M. (1996) Investigation of the Dinuclear Fe Center of Methane Monooxygenase by Advanced Paramagnetic Resonance Techniques: On the Geometry of DMSO Binding. *J. Am. Chem. Soc.*, **118**(1), 121-134
- Davies, E. R. (1974) A New Pulse ENDOR Technique. *Phys. Letters A*, **47**, 1-2
- Dong, Y., Que, L. Jr., Kauffmann, K., and Münck, E. (1995) An Exchange-Coupled Complex with Localized High-Spin FeIV and FeIII Sites of Relevance to Cluster X of *Escherichia coli* Ribonucleotide Reductase. *J. Am. Chem. Soc.*, **117**(45), 11377-11378

- Dutton, L. (1978) Redox Potentiometry: Determination of Midpoint Potentials of oxidation-reduction Components of Biological Electron-Transfer Systems. *Meth. Enzymol.*, **55**, 411-435
- Ehrenberg, A. (1998) Protein Dynamics, Free Radical Transfer and Reaction Cycle of Ribonucleotide Reductase. *Proceedings of "Third International Symposium on Biological Physics", Santa Fé*
- Ehrenberg, A., and Reichard, P. (1972) Electron Spin Resonance of the Iron-containing Protein B2 from Ribonucleotide Reductase. *J. Biol. Chem.*, **247**(11), 3485-3488
- Ekberg, M., Pötsch, S., Sandin, E., Thunnissen, M., Nordlund, P., Sahlin, M., and Sjöberg, B.-M. (1998) Preserved Catalytic Activity in an Engineered Ribonucleotide Reductase R2 Protein with a Nonphysiological Radical Transfer Pathway. *J. Biol. Chem.*, **273**(33), 21003-21008
- Eklund, H. and Fontecave, M. (1999) Glycyl Radical Enzymes: A Conservative Structural Basis for Radicals. *Structure*, **7**, r257-2262
- Elgren, T. E., Ming, L.-J., and Que, L., Jr. (1994) Spectroscopic Studies of Co(II)-Reconstituted Ribonucleotide Reductase R2 from *Escherichia coli*. *Inorg. Chem.*, **33**(5), 891-894
- Ellman, G. L. (1959) Tissue Sulfhydryl Groups. *Arch. Biochem. Biophys.*, **82**, 70-77
- Eriksson, L. A. (1998) Sulfinylimine Radical in Azido-CDP- and Azido-UDP-Inhibited Ribonucleotide Reductase. *J. Am. Chem. Soc.*, **120**(32), 8051-8054
- Eriksson, M., Uhlin, U., Ramaswamy, S., Ekberg, M., Regnström, K., Sjöberg, B.-M., and Eklund, H. (1997) Binding of Allosteric Effectors to Ribonucleotide Reductase Protein R1: Reduction of Active-Site Cysteines Promotes Substrate Binding. *Structure*, **5**, 1077-1092
- Feher, G. (1956) Observation of Nuclear Resonance via the Electron Spin Resonance Line. *Phys. Rev.*, **103**, 834-835
- Feig, A. L. and Lippard, S. J. (1994) Reactions of Non-Heme Iron(II) Centers with Dioxygen in Biology and Chemistry. *Chem. Rev.*, **94**, 759-805
- Fessenden, R. W., and Schuler, R. H. (1963) *J. Chem. Phys.*, **39**, 2147
- Fiege, R., Zwegart, W., Bittl, R., Adir, N., Renger, G., and Lubitz, W. (1996) EPR and ENDOR Studies of the Water Oxidizing Complex of Photosystem II. *Photosynth. Res.*, **48**, 227-237
- Fontecave, M., Gerez, C., Atta, M., and Jeunet, A. (1990) High Valent Iron Oxo Intermediates might be Involved During Activation of Ribonucleotide Reductase: Single Oxygen Atom Donors Generate the Tyrosyl Radical. *Biochem. Biophys. Res. Commun.*, **168**(2), 659-664
- Fox, B. G., Hendrich, M. P., Surerus, K. K., Andersson, K. K., Froland, W. A., Lipscomb, J. D., and Münck, E. (1993) Mössbauer, EPR, and ENDOR Studies of the Hydroxylase and Reductase Components of Methane Monooxygenase from *Methylosinus trichosporium* OB3b. *J. Am. Chem. Soc.*, **115**(9), 3688-3701
- Frey, P. A. (1997) Radicals in Enzymatic Reactions. *Curr. Op. Chem. Biol.*, **1**, 347-356
- Galli, C., Innes, J. B., Hirsch, D. J., and Brudwig, G. W. (1996) Effects of Dipole-Dipole Interactions on Microwave Progressive Power Saturation of Radicals in Proteins. *J. Magn. Res.*, **B110**, 284-287
- Gaston, B. (1999) Nitric Oxide and Thiol Groups. *Biochim. Biophys. Acta*, **1411**, 323-333
- Gerez, C. and Fontecave, M. (1992) Reduction of the Small Subunit of *Escherichia coli* Ribonucleotide Reductase by Hydrazines and Hydroxylamines. *Biochemistry*, **31**(3), 780-786
- Gerfen, G. J., Bellew, B. F., Griffin, R. G., Singel, D. J., Ekberg, C. A., Whittaker, J. W. (1996a) High-Frequency Electron Paramagnetic Resonance Spectroscopy of the Apogalactose Oxidase Radical. *J. Phys. Chem. A*, **100**(41), 16739-16748
- Gerfen, G. J., Licht, S., Willems, J.-P., Hoffman, B. M., and Stubbe, J. (1996b) Electron Paramagnetic Resonance Investigations of a Kinetically Competent Intermediate Formed in Ribonucleotide Reductase: Evidence for a Thiyl Radical-Cob(II)alamin Interaction. *J. Am. Chem. Soc.*, **118**(35), 8192-8197
- Gessner, C., Stein, M., Albracht, S. P. J., and Lubitz W. (1999) Orientation-Selected ENDOR of the Active Center in *C. vinosum* [NiFe]-Hydrogenase in the Oxidized, 'Ready' State. *J. Biol. Inorg. Chem*, **4**, 379-389
- Gilbert, B. C., Lane, H. A. H., Norman, R. O. C., and Sealy, R. C. (1975) Electron Spin Resonance Studies. Part XLVI. Oxidation of Thiols and Disulfides in Aqueous Solution: Formation of  $RS\cdot$ ,  $RSO\cdot$ ,  $RSO_2\cdot$ ,  $RSSR\cdot$ , and Carbon Radicals. *J. Chem. Soc. Perkin Trans. II*, 892-900
- Glasoe, P. K., and Long, F. A. (1960) *J. Chem. Soc. A.*, 188-190

- Graceffa, P. (1983) Spin Labeling of Protein Sulfhydrylgroups by Spin Trapping a Sulfur Radical: Application to Bovine Serum Albumin and Myosin. *Arch. Biochem. Biophys.*, **225**(2), 802-808
- Gräslund, A. and Sahlin, M. (1996) Electron Paramagnetic Resonance and Nuclear Magnetic Resonance Studies of Class I Ribonucleotide Reductase. *Annu. Rev. Biophys. Biomol. Struct.*, **25**, 259-286
- Gordy, W., Ard, W. B., and Shields, H. (1955) Microwave Spectroscopy of Biological Substances. II. Paramagnetic Resonance in X-irradiated Amino Acids and Proteins. *Proc. Natl. Acad. Sci. USA*, **41**, 983-996
- Guittet, O., Roy, B., and Lepoivre, M. (1999) Nitric Oxide: a Radical Molecule in Quest of Free Radicals in Proteins. *Cell. Mol. Life Sci.*, **55**, 1054-1067
- Guittet, O., Decottignies, P., Serani, L., Henry, Y., Le Maréchal, P., Laprévote, O., and Lepoivre, M. (2000) Peroxynitrite-Mediated Nitration of the Stable Free Radical Tyrosine Residue of the Ribonucleotide Reductase Small Subunit. *Biochemistry*, **39**(16), 4640-4648
- Harman, L. S., Mottley, C., and Mason, R. P. (1984) Free Radical Metabolites of L-Cysteine Oxidation. *J. Biol. Chem.*, **259**(9), 5606-5611
- Haskin, C. J., Ravi, N., Lynch, J. B., Münck, E., and Que, L., Jr. (1995) Reaction of NO with the Reduced R2 Protein of Ribonucleotide Reductase from *Escherichia coli*. *Biochemistry*, **34**(35), 11090-11098
- Hazebrouck, S., Camoin, L., Faltin, Z., Strosberg, A. D., and Eshdat, Y. (2000) Substituting Selenocysteine for Catalytic Cysteine 41 Enhances Enzyme Activity of Plant Phospholipid Hydroperoxide Glutathione Peroxidase Expressed in *Escherichia coli*. *J. Biol. Chem.*, **275**(37), 28715-28721
- Hendrich, M. P., Elgren, T. E., and Que, L., Jr. (1991) A Mixed Valent Form of the Iron Cluster in the B2 Protein of Ribonucleotide Reductase from *Escherichia coli*. *Biochem. Biophys. Res. Commun.*, **176**(2), 705-710
- Henriksen, M. A., Cooperman, B. S., Salem, J. S., Li, L.-S., and Rubin, H. (1994) The Stable Tyrosyl Radical in Mouse Ribonucleotide Reductase Is Not Essential for Enzymatic Activity. *J. Am. Chem. Soc.*, **116**(21), 9773-9774
- Hoganson, C. W., Sahlin, M., Sjöberg, B.-M., and Babcock, G. T. (1996) Electron Magnetic Resonance of the Tyrosyl Radical in Ribonucleotide Reductase from *Escherichia coli*. *J. Am. Chem. Soc.*, **118**(19), 4672-4679
- Holmgren, A. (1988) Thioredoxin and Glutaredoxin: Small Multi-functional Redox Proteins with Active-site Disulphide Bonds. *Biochem. Soc. Trans.*, **16**, 95-96
- Isied, S. S. (1994) in *Metals in Biological Systems* (Siegel, H., and Siegel, A., Eds) Marcel Dekker, Inc., New York, NY, pp 10-50
- Ivancich, A., Jouve, H. M., Sartor, B. and Gaillard, J. (1997) EPR Investigation of Compound I in *Proteus mirabilis* and Bovine Liver Catalases: Formation of Porphyrin and Tyrosyl Radical Intermediates. *Biochemistry*, **36**(31), 9356-9364.
- Ivancich, A., Mattioli, T. A., and Un, S. (1999) Effect of Protein Microenvironment on Tyrosyl Radicals. A High-Field (285 GHz) EPR, Resonance Raman, and Hybrid Density Functional Study. *J. Am. Chem. Soc.*, **121**(24), 5743-5753
- Johnson, (1998) Iron-sulfur Proteins: New Roles for Old Clusters. *Curr. Op. Chem. Biol.*, **2**, 173-181
- Jordan, A. and Reichard, P. (1998) Ribonucleotide Reductases. *Annu. Rev. Biochem.*, **67**, 71-98
- Kalyanaraman, B. (1994) Thiyl Radicals in Biological Systems: Significant or Trivial?. *Biochem. Soc. Symp.*, **61**, 55-63
- Karlsson, M., Sahlin, M., and Sjöberg, B.-M. (1992) *Escherichia coli* Ribonucleotide Reductase. Radical Susceptibility to Hydroxyurea is Dependent on the Regulatory State of the Enzyme. *J. Biol. Chem.*, **267**(18), 12622-12626
- Katchalski, E., Benjamin, G. S., and Gross, V. (1957) The Availability of the Disulfide Bonds of Human and Bovine Serum Albumin and of Bovine  $\gamma$ -Globulin to Reduction by Thioglycolic Acid. *J. Am. Chem. Soc.*, **79**, 4096-4099
- Kennedy, M. C., Antholine, W. E., and Beinert, H. (1997) An EPR Investigation of the Products of the Reaction of Cytosolic and Mitochondrial Aconitases with Nitric Oxide. *J. Biol. Chem.*, **272**(33), 20340-20347

- Kim, S. T., Sancar, A., Essenmacher, C., and Babcock, G. T. (1993) Time-resolved EPR Studies with DNA Photolyase: Excited-state FADH<sup>0</sup> Abstracts an Electron from Trp-306 to Generate FADH<sup>-</sup>, the Catalytically Active Form of the Cofactor. *Proc. Natl. Acad. Sci. U.S.A.*, **90**(17), 8023-8027
- Knappe, J., Elbert, S., Frey, M., and Wagner, A. F. V. (1993) Pyruvate Formate-Lyase Mechanism Involving the Protein-Based Glycyl Radical. *Biochem. Soc. Trans.*, **21**, 731-734
- Kolberg, M., Bleifuss, G., Pötsch, S., Gräslund, A., Lubitz, W., Lassmann, G., and Lendzian, F. (2000) A New Stable High-Valent Diiron Center in R2 Mutant Y122H of *E. coli* Ribonucleotide Reductase Studied by High-Field EPR and <sup>57</sup>Fe-ENDOR. *J. Am. Chem. Soc.*, **122**(40), 9856-9857
- Kou, W. W. H., and Box, H. C. (1976) Primary Radiation Products in Cysteine Hydrochloride. *J. Chem. Phys.*, **64**(7), 3060-3062
- Krauth-Siegel, R. L., Jacoby, E. M., and Schirmer, R. H. (1995) Trypanothione and N<sup>1</sup>-Gluthathionylspermidine: Isolation and Determination. *Meth. Enzymol.*, **251**, 287-294
- Krebs, C., Chen, S., Baldwin, J., Ley, B. A., Patel, U., Edmondson, D. E., Huynh, B. H., and Bollinger, J. M., Jr. (2000) Mechanism of Rapid Electron Transfer during Oxygen Activation in the R2 Subunit of *Escherichia coli* Ribonucleotide Reductase. 2. Evidence for and Consequences of Blocked Electron Transfer in the W48F Variant. *J. Am. Chem. Soc.*, **122**(49), 12207-12219
- Kunkel, T. A. (1985) Rapid and Efficient Site-specific Mutagenesis without Phenotypic Selection. *Proc. Natl. Acad. Sci. USA*, **82**, 488-492
- Kurreck, H., Kirste, B., and Lubitz, W. (1988) *Electron Nuclear Double Resonance Spectroscopy in Solution*. VCH, Weinheim
- Kurtz, D. M., Jr. (1997) Structural Similarity and Functional Diversity in Diiron-oxo Proteins. *J. Biol. Inorg. Chem.*, **2**(2), 159-167
- Laemmli, (1970) Cleavage of Structural Proteins During the Assembly of the Head of Bacteriophage T4. *Nature*, **227**, 680-685
- Larsson, Å., Karlsson, M., Sahlin, M., and Sjöberg, B.-M. (1988) Radical Formation in the Dimeric Small Subunit of Ribonucleotide Reductase Requires Only One Tyrosine 122. *J. Biol. Chem.*, **263**(33), 17780-17784
- Lassmann, G., Eriksson, L. A., Himo, F., Lendzian, F., and Lubitz, W. (1999) Electronic Structure of a Transient Histidine Radical in Liquid Aqueous Solution: EPR Continuous-Flow Studies and Density Functional Calculations. *J. Phys. Chem. A*, **103**(9), 1283-1290
- Lassmann, G., Eriksson, L. A., Lendzian, F., and Lubitz, W. (2000) Structure of a Transient Neutral Histidine Radical in Solution: EPR Continuous-Flow Studies in a Ti3+/EDTA-Fenton System and Density Functional Calculations. *J. Phys. Chem. A*, **104**(40), 9144-9152
- Lawrence, C. C., Bennati, M., Obias, H. V., Bar, G., Griffin, R. G., and Stubbe, J. (1999) High-Field EPR Detection of a Disulfide Radical Anion in the Reduction of Cytidine 5'-diphosphate by the E441Q R1 Mutant of *Escherichia coli* Ribonucleotide Reductase. *Proc. Natl. Acad. Sci. USA*, **96**, 8979-8984
- Lee, D. and Lippard, S. J. (1998) Structural and Functional Models of the Dioxygen-Activating Centers of Non-Heme Diiron Enzymes Ribonucleotide Reductase and Soluble Methane Monooxygenase. *J. Am. Chem. Soc.*, **120**(46), 12153-12154
- Lendzian, F., Sahlin, M., MacMillan, F., Bittl, R., Fiege, R., Pötsch, S., Sjöberg, B.-M., Gräslund, A., Lubitz, W., and Lassmann, G. (1996) Electronic Structure of Neutral Tryptophan Radicals in Ribonucleotide Reductase Studied by EPR and ENDOR Spectroscopy. *J. Am. Chem. Soc.*, **118**(34), 8111-8120
- Lenz, R. and Giese, B. (1997) Studies on the Mechanism of Ribonucleotide Reductase. *J. Am. Chem. Soc.*, **119**(12), 2784-2794
- Lepoivre, M., Fieschi, F., Coves, J., Thelander, L., and Fontecave, M. (1991) Inactivation of Ribonucleotide Reductase by Nitric Oxide. *Biochem. Biophys. Res. Commun.*, **179**(1), 442-448
- Licht, S., Gerfen, G. J., and Stubbe, J. (1996) Thiyl Radicals in Ribonucleotide Reductases. *Science*, **271**, 477-481



- Lin, A.-N. I., Ashley, G. W., and Stubbe, J. (1987) Location of the Redox Active Thiols of Ribonucleotide Reductase: Sequence Similarity between the *Escherichia coli* and *Lactobacillus leichmannii* Enzymes. *Biochemistry*, **26**(22), 6905-6909
- Ling, J., Sahlin, M., Sjöberg, B.-M., Loehr, T. M., and Sanders-Loehr, J. (1994) Dioxygen is the Source of the  $\mu$ -Oxo Bridge in Iron Ribonucleotide Reductase. *J. Biol. Chem.*, **269**(8), 5595-5601
- Liu, A., Sahlin, M., Pötsch, S., Sjöberg, B.-M., and Gräslund, A. (1998) New Paramagnetic Species Formed at the Expense of the Transient Tyrosyl Radical in Mutant Protein R2 F208Y of *Escherichia coli* Ribonucleotide Reductase. *Biochem. Biophys. Res. Commun.*, **246**(3), 740-745
- Logan, D. T., Su, X.-D., Åberg, A., Regnström, K., Hajdu, J., Eklund, H., and Nordlund, P. (1996) Crystal Structure of Reduced Protein R2 of Ribonucleotide Reductase: the Structural Basis for Oxygen Activation at a Dinuclear Site. *Structure*, **4**(9), 1053-1064
- Logan, D. T., deMaré, F., Persson, B. O., Slaby, A., Sjöberg, B.-M., and Nordlund, P. (1998) Crystal Structure of Two Self-Hydroxylating Ribonucleotide Reductase Protein R2 Mutants: Structural Basis for the Oxygen-Insertion Step of Hydroxylation Reactions Catalysed by Diiron Proteins. *Biochemistry*, **37**(30), 10798-10807
- Ludwig, W. and Follmann, H. (1978) Inhibition of Bacterial Ribonucleotide Reductases by Arabinonucleotides. *Eur. J. Biochem.*, **91**, 493-499
- MacMillan, F., Kannt, A., Behr, J., Prisner, T., and Michel, H. (1999) Direct Evidence for a Tyrosine Radical in the Reaction of Cytochrome *c* Oxidase with Hydrogen Peroxide. *Biochemistry*, **38**(29), 9179-9184
- Mao, S. S., Holler, T. P., Bollinger, J. M., Jr., Yu, G. X., Johnston, M. I., and Stubbe, J. (1992a) Interaction of C225SR1 Mutant Subunit of Ribonucleotide Reductase with R2 and Nucleoside Diphosphates: Tales of a Suicidal Enzyme. *Biochemistry*, **31**(40), 9744-9751
- Mao, S. S., Holler, T. P., Yu, G. X., Bollinger, J. M., Jr., Booker, S., Johnston, M. I., and Stubbe, J. (1992b) A Model for the Role of Multiple Cysteine Residues Involved in Ribonucleotide Reduction: Amazing and Still Confusing. *Biochemistry*, **31**(40), 9733-9743
- Mao, S. S., Yu, G. X., Chalfoun, D., and Stubbe, J. (1992c) Characterization of C439SR1, a Mutant of *Escherichia coli* Ribonucleotide Diphosphate Reductase: Evidence That C439 Is a Residue Essential for Nucleotide Reduction and C439SR1 Is a Protein Possessing Novel Thioredoxin-like Activity. *Biochemistry*, **31**(40), 9752-9759
- Maples, K. R., Kennedy, C. H., Jordan, S. J., and Mason, R. P. (1990) *In Vivo* Thiyl Free Radical Formation from Hemoglobin following Administration of Hydroperoxides. *Arch. Biochem. Biophys.*, **277**(2), 402-409
- Massey, V. (1957) Studies on Succinic Dehydrogenase. *J. Biol. Chem.*, **229**, 763-770
- Meyer, D. J., Kramer, H., Özer, N., Coles, B., and Ketterer, B. (1994) Kinetics and Equilibria of S-Nitrosothiol-Thiol Exchange between Glutathione, Cysteine, Penicillamines and Serum Albumin. *FEBS Letters*, **345**, 177-180
- Miller, M. A., Gobena, F. T., Kauffmann, K., Münck, E., Que, L., Jr., and Stankovich, M. T. (1999) Differing Roles for the Diiron Clusters of Ribonucleotide Reductase from aerobically Grown *Escherichia coli* in the Generation of the Y112 Radical. *J. Am. Chem. Soc.*, **121**(5), 1096-1097
- Moënné-Loccoz, P., Baldwin, J., Ley, B. A., Loehr, T. M., and Bollinger, J. M., Jr. (1998) O<sub>2</sub> Activation by Non-Heme Diiron Proteins: Identification of a Symmetric  $\mu$ -1,2-Peroxide in a Mutant of Ribonucleotide Reductase. *Biochemistry*, **37**(42), 14659-14663
- Mullins, M. E., Stamler, J. S., Osborne, J. A., Loscalzo, J., and Singel, P. J. (1992) EPR Spectroscopic Characterization of Biological Thiyl Radicals as PBN Spin-Trap Adducts. *Appl. Magn. Reson.*, **3**, 1021-1032
- Musci, G., Di Marco, S., di Patti, M. C. B., and Calabrese, L. (1991) Interaction of Nitric Oxide with Ceruplasmin Lacking an EPR-Detectable Type 2 Copper. *Biochemistry*, **30**, 9866-9872
- Nelson, D. and Symons, M. C. R. (1975) The Detection of Thiyl Radicals by ESR Spectroscopy. *Chem. Phys. Lett.*, **36**(3), 340-341
- Nelson D. J., Petersen, R. L., Symons, M. C. R. (1977) *J. Chem. Soc. Perkins Trans. II*, 2005-2014

- Nicovich, J. M., Kreutter, K. D., van Dijk, C. A., and Wine, P. H. (1992) Temperature Dependent Kinetics  
Studies of the Reactions  $\text{Br}(\text{}^2\text{P}_{3/2}) + \text{H}_2\text{S} \rightarrow \text{SH} + \text{HBr}$  and  $\text{Br}(\text{}^2\text{P}_{3/2}) + \text{CH}_3\text{SH} \rightarrow \text{CH}_3\text{S} + \text{HBr}$ .  
Heats of Formation of SH and  $\text{CH}_3\text{S}$  Radicals. *J. Phys. Chem.*, **96**, 2518
- Nilsson, O., Åberg, A., Lundquist, T., and Sjöberg, B.-M. (1988) Nucleotide Sequence of the Gene  
Coding for the Large Subunit of Ribonucleotide Reductase of *Escherichia coli*. Correction.  
*Nucleic Acid Res.*, **16**, 4174-4175
- Nocentini, G. (1996) Ribonucleotide Reductase Inhibitors: New Strategies for Cancer Chemotherapy.  
*Crit. Rev. Oncol. Hematol.*, **22**, 89-126
- Nordlund, P. and Eklund, H. (1993) Structure and Function of the *Escherichia coli* Ribonucleotide  
Reductase Protein R2. *J. Mol. Biol.*, **232**, 123-164
- Nordlund, P., Uhlin, U., Westergren, C., Joelsen, T., Sjöberg, B.-M., and Eklund, H. (1989) New  
Crystal Forms of the Small Subunit of Ribonucleotide Reductase from *Escherichia coli*.  
*FEBS Letters*, **258**(2), 251-254
- Nordlund, P., Sjöberg, B.-M., and Eklund, H. (1990) Three-Dimensional Structure of the Free Radical  
Protein of Ribonucleotide Reductase. *Nature*, **345**, 593-598
- Ohnishi, T. (1987) *Curr. Top. Bioenerg.* **15**, 37-65
- Ormö, M. and Sjöberg, B.-M. (1990) An Ultrafiltration Assay for Nucleotide Binding to  
Ribonucleotide Reductase. *Analyt. Biochem.*, **189**(2), 138-141
- Ormö, M. and Sjöberg, B.-M. (1996) The Cys292-Ala Substitution in Protein R1 of Class I  
Ribonucleotide Reductase from *Escherichia coli* has a Global Effect on Nucleotide Binding  
at the Specificity-Determining Allosteric Site. *Eur. J. Biochem.*, **241**, 363-367
- Ormö, M., Regnström, K., Wang, Z., Que, L. Jr., Sahlin, M., and Sjöberg, B.-M. (1995) Residues  
Important for Radical Stability in Ribonucleotide Reductase from *Escherichia coli*. *J. Biol.  
Chem.*, **270**(12), 6570-6576
- Parast, C. V., Wong, K. K., Kozarich, J. W., Peisach, J., and Magliozzo, R. S. (1995) Electron  
Paramagnetic Resonance Evidence for a Cysteine-Based Radical in Pyruvate Formate-Lyase  
Inactivated with Mercaptopyruvate. *Biochemistry*, **34**(17), 5712-5717
- Parkin, S. E., Chen, S., Ley, B. A., Mangravite, L., Edmonson, D. E., Huynh, B. H., and Bollinger, J.  
M., Jr. (1998) Electron Injection through a Specific Pathway Determines the Outcome of  
Oxygen Activation at the Diiron Cluster in the F208Y Mutant of *Escherichia coli*  
Ribonucleotide Reductase Protein R2. *Biochemistry*, **37**(4), 1124-1130
- Penefsky, H. (1979) A Centrifuged-Column Procedure for the Measurement of Ligand Binding by  
Beef Heart  $\text{F}_1$ . *Meth. Enzymol.*, **56**, 527-530
- Persson, A., Eriksson, M., Katterle, B., Pötsch, S., Sahlin, M., and Sjöberg, B.-M. (1997) A New  
Mechanism-based Radical Intermediate in a Mutant R1 Protein Affecting the Catalytically  
Essential Glu441 in *Escherichia coli* Ribonucleotide Reductase. *J. Biol. Chem.*, **272**(50),  
31533-31541
- Persson, A., Sahlin, M., and Sjöberg, B.-M. (1998) Cysteinylyl and Substrate Radical Formation in  
Active Site Mutant E441Q of *Escherichia coli* Class I Ribonucleotide Reductase. *J. Biol.  
Chem.*, **273**(47), 31016-31020
- Persson, B. O., Karlsson, M., Climent, I., Ling, J., Sanders Loehr, J., Sahlin, M., and Sjöberg, B.-M.  
(1996) Iron Ligand Mutants in Protein R2 of *Escherichia coli* Ribonucleotide Reductase. *J.  
Biol. Inorg. Chem.*, **1**(3), 247-256
- Petersson, L., Gräslund, A., Ehrenberg, A., Sjöberg, B.-M., and Reichard, P. (1980) The Iron Center  
in Ribonucleotide Reductase from *Escherichia coli*. *J. Biol. Chem.*, **255**(14), 6706-6712
- Pilbrow, J. R. and Hanson, G. R. (1993) Electron Paramagnetic Resonance. *Meth. Enzymol.*, **227**, 330-  
353
- Poole, C. P., Jr., and Farach, H. A. (1987) in *Theory of Magnetic Resonance*, John Wiley & Sons,  
New York, NY, pp 319-321
- Pötsch, S., Drechsler, H., Liermann, B., Gräslund, A., and Lassmann, G. (1994) p-Alkoxyphenols, a  
New Class of Inhibitors of Mammalian R2 Ribonucleotide Reductase: Possible Candidates  
for Antimelanotic Drugs. *Mol Pharmacol.*, **45**(4), 792-796

- Pötsch, S., Lendzian, F., Ingemarson, R., Hörnberg, A., Thelander, L., Lubitz, W., Lassmann, G., and Gräslund, A. (1999) The Iron-Oxygen Reconstitution Reaction in Protein R2-Tyr-177 Mutants of Mouse Ribonucleotide Reductase. *J. Biol. Chem.*, **274**(25), 17696-17704
- Proshlyakov, D. A., Pressler, M. A., DeMaso, C., Leykam, J. F., DeWitt, D. L., and Babcock, G. T. (2000) Oxygen Activation and Reduction in Respiration: Involvement of Redox-Active Tyrosine 244. *Science*, **290**(5496), 1588-1591
- Rao, D. N. R., Fischer, V., and Mason, R. (1990) Glutathione and Ascorbate Reduction of the Acetaminophen Radical Formed by Peroxidase. Detection of the Glutathione Disulfide Radical Anion and the Ascorbyl Radical *J. Biol. Chem.*, **265**(2), 844-847
- Ravi, N., Bollinger, J. M., Jr., Huynh, B. H., Edmondson, D. E., and Stubbe, J. (1994) Mechanism of Assembly of the Tyrosyl Radical- Diiron(III) Cofactor of *E. coli* Ribonucleotide Reductase. 1. Mössbauer Characterization of the Diferric Radical Precursor. *J. Am. Chem. Soc.*, **116**(18), 8007-8014
- Reddy, S. G., Wong, K. K., Parast, C. V., Peisach, J., Magliozzo, R. S., and Kozarich, J. W. (1998) Dioxygen Inactivation of Pyruvate Formate-Lyase: EPR Evidence for the Formation of Protein-Based Sulfinyl and Peroxyl Radicals. *Biochemistry*, **37**(2), 558-563
- Reichard, P. (1997) The Evolution of Ribonucleotide Reductases. *TIBS*, **22**, 81-85
- Riggs-Gelasco, P. J., Shu, L., Chen, S., Burdi, D., Huynh, B. H., Que, L., Jr., and Stubbe, J. (1998) EXAFS Characterization of the Intermediate X Generated During the Assembly of the *Escherichia coli* Ribonucleotide Reductase R2 Diferric Tyrosyl Radical Cofactor. *J. Am. Chem. Soc.*, **120**(5), 849-860
- Robins, M. J. and Ewing, G. J. (1999) Biomimetic Modeling of the First Substrate Reaction at the Active Site of Ribonucleotide Reductases. Abstraction of H3' by a Thiyl Free Radical. *J. Am. Chem. Soc.*, **121**(24), 5823-5824
- Roshick, C., Iliffe-Lee, E. R., and McClarty, G. (2000) Cloning and Characterization of Ribonucleotide Reductase from *Chlamydia trachomatis*. *J. Biol. Chem.*, **275**(48), 38111-38119
- Roy, B., Lepoivre, M., Henry, Y., and Fontecave, M. (1995) Inhibition of Ribonucleotide Reductase by Nitric Oxide Derived from Thionitrites: Reversible Modifications of Both Subunits. *Biochemistry*, **34**(16), 5411-5418
- Sahlin, M., Gräslund, A., and Ehrenberg, A. (1985) Determination of Relaxation Times for a Free Radical from Microwave Saturation Studies. *J. Magn. Res.*, **67**, 135-137
- Sahlin, M., Gräslund, A., Petersson, L., Ehrenberg, A., and Sjöberg, B.-M. (1989) Reduced forms of the Iron-Containing Small Subunit of ribonucleotide Reductase from *Escherichia coli*. *Biochemistry*, **28**(6), 2618-2625
- Sahlin, M., Sjöberg, B.-M., Backers, G., Loehr, T., and Sanders-Loehr, J. (1990) Activation of the Iron-Containing B2 Protein of Ribonucleotide Reductase by Hydrogen Peroxide. *Biochem. Biophys. Res. Commun.*, **167**(2), 813-818
- Sahlin, M., Lassmann, G., Pötsch, S., Slaby, A., Sjöberg, B.-M., and Gräslund, A. (1994) Tryptophan Radicals Formed by Iron/Oxygen Reaction with *Escherichia coli* Ribonucleotide Reductase Protein R2 Mutant Y122F. *J. Biol. Chem.*, **269**(16), 11699-11702
- Sahlin, M., Lassmann, G., Pötsch, S., Sjöberg, B.-M., and Gräslund, A. (1995) Transient Free Radicals in Iron/Oxygen Reconstitution of Mutant Protein R2 Y122F. *J. Biol. Chem.*, **270**(21), 12361-12372
- Salowe, S., Bollinger, J. M., Jr., Ator, M., and Stubbe, J. (1993) Alternative Model for Mechanism-Based Inhibition of *Escherichia coli* Ribonucleotide Reductase by 2'-Azido-2'-deoxyuridine 5'-Diphosphate. *Biochemistry*, **32**(47), 12749-12760
- Saxeboel, G., and Herskedal, Ø. (1975) Electron Spin Resonance Studies of Electron-Irradiated Peptides. A Single Crystal of N-Acetyl-L-Cysteine at 77 K. *Radiat. Res.*, **62**, 395-406
- Schäfer, K. O., Bittl, R., Zwegart, W., Lendzian, F., Haselhorst, G., Weyhermüller, T., Wieghardt, K., and Lubitz, W. (1998) Electronic Structure of Antiferromagnetically Coupled Dinuclear Manganese (Mn<sup>III</sup>Mn<sup>IV</sup>) Complexes Studied by Magnetic Resonance Techniques. *J. Am. Chem. Soc.*, **120**(50), 13104-13120

- Schmidt, P. P., Andersson, K. K., Barra, A.-L., Thelander, L., and Gräslund, A. (1996) High Field EPR Studies of Mouse Ribonucleotide Reductase Indicate Hydrogen Bonding of the Tyrosyl Radical. *J. Biol. Chem.*, **271**(39), 23615-23618
- Schmidt, P. P., Rova, U., Katterle, B., Thelander, L., and Gräslund, A. (1998) Kinetic Evidence That a Radical Transfer Pathway in Protein R2 of Mouse Ribonucleotide Reductase Is Involved in Generation of the Tyrosyl Free Radical. *J. Biol. Chem.*, **273**(34), 21463-21472
- Sevilla, M. D., Becker, D., Swartz, S., and Herrington, J. (1987) Sulfinyl Radical Formation from the Reaction of Cysteine and Glutathione Thiyl Radicals with Molecular Oxygen. *Biochem. Biophys. Res. Commun.*, **144**(2), 1037-1042
- Sevilla, M. D., Yan, M., and Becker, D. (1988) Thiol Peroxyl Radical Formation from the Reaction of Cysteine Thiyl Radical with Molecular Oxygen: an ESR Investigation. *Biochem. Biophys. Res. Comm.*, **155**, 405-410
- Sexton, D. J., Muruganandam, A., McKenney, D. J., and Mutus, B. (1994) Visible Light Photochemical Release of Nitric Oxide from S-Nitrosoglutathione: Potential Photochemotherapeutic Applications. *Photochem. Photobiol.*, **59**(4), 463-467
- Sheu, F.-S., Zhu, W., and Fung, P. C. W. (2000) Direct Observation of Trapping and Release of Nitric Oxide by Glutathione and Cysteine with Electron Paramagnetic Resonance Spectroscopy. *Biophys J.*, **78**(3), 1216-1226
- Siegbahn, P. E. M. (1998) Theoretical Study of the Substrate Mechanism of Ribonucleotide Reductase. *J. Am. Chem. Soc.*, **120**(33), 8417-8429
- Silva, D. J., Elgren, T. E., Que, L., Jr., and Stankovich, M. T. (1995) Electron Transfer Properties of the R2 Protein of Ribonucleotide Reductase from *Escherichia coli*. *Biochemistry*, **34**(43), 14093-14103
- Singh, R. J., Hogg, N., Joseph, J., and Kalyanaraman, B. (1996) Mechanism of Nitric Oxide Release from S-Nitrosothiols. *J. Biol. Chem.*, **271**(31), 18596-18603
- Sivaraja, M., Goodin, D. B., Smith, M., and Hoffman, B. M. (1989) Identification by ENDOR of Trp191 as the Free-Radical Site in Cytochrome c Peroxidase Compound ES. *Science*, **245**(4919), 738-740
- Sjöberg, B.-M. (1995) Structure of Ribonucleotide Reductase from *Escherichia coli*. *Nucl. Acids Mol. Biol.*, **9**, 192-221
- Sjöberg, B.-M., Reichard, P., Gräslund, A., and Ehrenberg, A. (1978) The Tyrosine Free Radical in Ribonucleotide Reductase from *Escherichia coli*. *J. Biol. Chem.*, **253**(19), 6863-6865
- Sjöberg, B.-M., Hahne, S., Karlsson, M., Jörnvall, H., Göranson, M., and Uhlin, B. E. (1986) Overproduction and Purification of the B2 Subunit of Ribonucleotide Reductase from *Escherichia coli*. *J. Biol. Chem.*, **261**(12), 5658-5662
- Sjöberg, B.-M., Karlsson, M., and Jörnvall, H. (1987) Half-site Reactivity of the Tyrosyl Radical of Ribonucleotide Reductase from *Escherichia coli*. *J. Biol. Chem.*, **262**(20), 9736-9743
- Snodin, M. D., Ould-Moussa, L., Wallmann, U., Lecomte, S., Bachler, V., Bill, E., Hummel, H., Weyhermüller, T., Hildebrandt, P., and Wieghardt, K. (1999) The Molecular and Electronic Structure of Octahedral Tris(phenolato)iron(III) Complexes and Their Phenoxyl Radical Analogues: A Mössbauer and Resonance Raman Spectroscopic Study. *Chem. Eur. J.*, **5**(9), 2554-2565
- Solomon, E. I., Brunold, T. C., Davis, M. I., Kemsley, J. N., Lee, S.-K., Lehnert, N., Neese, F., Skulan, A. J., Yang, Y.-S., and Zhou, J. (2000) Geometric and Electronic Structure/Function Correlations in Non-Heme Iron Enzymes. *Chem. Rev.*, **100**, 235-349
- Stamler, J. S., Simon, D. I., Osborne, J. A., Mullins, M. E., Jaraki, O., Michel, T., Singel, D. J., and Loscalzo, J. (1992a) S-Nitrosylation of Proteins with Nitric Oxide: Synthesis and Characterization of Biologically Active Compounds. *Proc. Natl. Acad. Sci. USA*, **89**, 444-448
- Stamler, J. S., Singel, D. J., and Loscalzo, J. (1992b) Biochemistry of Nitric Oxide and Its Redox-Activated Forms. *Science*, **258**, 1898-1902
- Stamler, J. S. and Feelisch, M. (1996) Preparation and Detection of S-Nitrosothiols. In: *Feelisch, M. and Stamler, J.S. (eds.) Methods in Nitric Oxide Research*, Wiley, New York, 521-539
- Stesmans, A. and van Gorp, G. (1989) Novel Method for Accurate g Measurements in Electron-Spin Resonance. *Rev. Sci. Instrum.*, **60**(9), 2949-2952

- Stubbe, J. and Ackles, D. (1980) On the Mechanism of Ribonucleoside Diphosphate Reductase from *Escherichia coli*. *J. Biol. Chem.*, **255**(17), 8027-8030
- Stubbe, J. and van der Donk, W. A. (1995) Ribonucleotide Reductases: Radical Enzymes with Suicidal Tendencies. *Chem. Biol.*, **2**, 793-801
- Stubbe, J. and van der Donk, W. A. (1998) Protein Radicals in Enzyme Catalysis. *Chem. Rev.*, **98**, 705-762
- Stubbe, J. and Riggs-Gelasco, P. (1998) Harnessing Free Radicals: Formation and Function of the Tyrosyl Radical in Ribonucleotide Reductase. *TIBS*, **23**, 438-443
- Stubbe, J., Ge, J., and Yee, C. S. (2001) The Evolution of Ribonucleotide Reduction Revisited. *TIBS*, **26**(2), 93-99
- Sturgeon, B. E., Burdi, D., Chen, S., Huynh, B.-H., Edmondson, D. E., Stubbe, J., and Hoffman, B. M. (1996) Reconsideration of X, the Diiron Intermediate Formed during Cofactor Assembly in *E. coli* Ribonucleotide Reductase. *J. Am. Chem. Soc.*, **118**(32), 7551-7557
- Sun, X., Ollagnier, S., Schmidt, P. P., Atta, M., Mulliez, E., Lepape, L., Eliasson, R., Gräslund, A., Fontecave, M., Reichard, P., and Sjöberg, B.-M. (1996) The Free Radical of the Anaerobic Ribonucleotide Reductase from *Escherichia coli* Is at Glycine 681. *J. Biol. Chem.*, **271**(12), 6827-6831
- Tabor, S., and Richardson, C. C. (1985) A Bacteriophage T7 RNA Polymerase/Promoter System for Controlled Exclusive Expression of Specific Genes. *Proc. Natl. Acad. Sci. USA.*, **82**(4), 1074-1078
- Thelander, L. (1974) Reaction Mechanism of Ribonucleoside Diphosphate Reductase from *Escherichia coli*. *J. Biol. Chem.*, **249**(15), 4858-4862
- Thelander, L. and Reichard, P. (1979) Reduction of Ribonucleotides. *Annu. Rev. Biochem.*, **48**, 133-158
- Thelander, L., Larsson, B., Hobbs, J., and Eckstein, F. (1976) Active Site of Ribonucleoside Diphosphate Reductase from *Escherichia coli*. *J. Biol. Chem.*, **251**(5), 1398-1405
- Thelander, L., Sjöberg, B. M., and Eriksson, S. (1978) Ribonucleoside Diphosphate Reductase (*Escherichia coli*). *Meth. Enzymol.*, **51**, 227-237
- Tian, G., Berry, J. A., Klinman, J. P. (1994) Oxygen-18 Kinetic Isotope Effects in the Dopamine beta-Monooxygenase Reaction: Evidence for a New Chemical Mechanism in Non-Heme Metallomonooxygenases. *Biochemistry*, **33**(1), 226-234
- Tong, W., Chen, S., Lloyd, S. G., Edmondson, D., Huynh, B. H., and Stubbe, J. (1996) Mechanism of Assembly of the Diferric Cluster-Tyrosyl Radical Cofactor of *Escherichia coli* Ribonucleotide Reductase from the Diferrous Form of the R2 Subunit. *J. Am. Chem. Soc.*, **118**(8), 2107-2108
- Tong, W., Burdi, D., Riggs-Gelasco, P., Chen, S., Edmondson, D., Huynh, B. H., Stubbe, J., Han, S., Arvai, A., and Tainer, J. (1998) Characterization of Y122F R2 of *Escherichia coli* Ribonucleotide Reductase by Time-Resolved Physical Biochemical Methods and X-ray Crystallography. *Biochemistry*, **37**(17), 5840-5848
- Torchinski, Y. M. (1974) in *Thiol and Disulfide Groups of Proteins* (Dixon, H. B. F., ed) p. 24, Consultants Bureau, New York, NY
- Torrent, M., Musaev, D. G., and Morokuma, K. (2000) The Flexibility of Carboxylate Ligands in Methane Monooxygenase and Ribonucleotide Reductase: A Density Functional Study. *J. Phys. Chem. B*, **105**(1), 322-327
- Tsai, A. L., Palmer, G., and Kulmacz, R. J. (1992) Prostaglandin H Synthase. Kinetics of Tyrosyl Radical Formation and of Cyclooxygenase Catalysis. *J. Biol. Chem.*, **267**(25), 17753-17759
- Twitchett, M. B., Dobbing, A. M., and Sykes, A. G. (2000) New Mechanistic Insight into the Reactivity of the R2 Protein of *E. coli* Ribonucleotide Reductase (RNR). *J. Inorg. Biochem.*, **79**, 59-65
- Uhlin, U. and Eklund, H. (1994) Structure of Ribonucleotide Reductase Protein R1. *Nature*, **370**, 533-539
- Un, S., Gerez, C., Elleingand, E., and Fontecave, M. (1996) 245 GHz High-Field EPR Study of Tyrosine-D° and Tyrosine-Z° in Mutants of Photosystem II. *Biochemistry*, **35**(3), 679-684
- Valentine, A. M., Tavares, P., Pereira, A. S., Davydov, R., Krebs, C., Hoffman, B. M., Edmondson, D. E., Huynh, B. H., and Lippard, S. J. (1998) Generation of a Mixed-Valent Fe(III)Fe(IV)

- Form of Intermediate Q in the Reaction Cycle of soluble Methane Monooxygenase, an Analog of Intermediate X in Ribonucleotide Reductase R2 Assembly. *J. Am. Chem. Soc.*, **120**(9), 2190-2191
- van der Donk, W. A., Stubbe, J., Gerfen, G. J., Bellew, B. F., and Griffin, R. G. (1995) EPR Investigation of the Inactivation of *E. coli* Ribonucleotide Reductase with 2'-Azido-2'-deoxyuridine 5'-Diphosphate: Evidence for the Involvement of the Thiyl Radical of C225-R1. *J. Am. Chem. Soc.*, **117**(35), 8908-8916
- Veselov, A. and Scholes, C. P. (1996) X-Band ENDOR of the Liganding Environment from the Radical X Intermediate of *Escherichia coli* Ribonucleotide Reductase. *Inorg. Chem.*, **35**(12), 3702-3705
- Voegtli, W. C., Khidekel, N., Baldwin, J., Ley, B. A., Bollinger, J. M., Jr., and Rosenzweig, A. C. (2000) Crystal Structure of the Ribonucleotide Reductase R2 Mutant that Accumulates a  $\mu$ -1,2-Peroxodiiron(III) Intermediate during Oxygen Activation. *J. Am. Chem. Soc.*, **122**(14), 3255-3261
- Walker, F. A. (1999) Magnetic Spectroscopic (EPR, ESEEM, Mössbauer, MCD and NMR) Studies of Low-Spin Ferriheme Centers and Their Corresponding Heme Proteins. *Coord. Chem. Rev.*, **185-186**, 471-534
- Willems, J.-P., Lee, H.-I., Burdi, D., Doan, P. E., Stubbe, J., and Hoffman, B. M. (1997) Identification of the Protonated Oxygenic Ligands of Ribonucleotide Reductase Intermediate X by Q-Band 1,2H CW and Pulsed ENDOR. *J. Am. Chem. Soc.*, **119**(41), 9816-9824
- Wood, P. D., Mutus, B., and Redmond, R. W. (1996) The Mechanism of Photochemical Release of Nitric Oxide from S-Nitrosoglutathione. *Photochem. Photobiol.*, **64**(3), 518-524
- Zalkin, H., and Dalton, J. E. (1992) *De novo* Purine Nucleotide Biosynthesis. *Prog. Nucl. Acid. Res. Mol. Biol.*, **42**, 259-285
- Zimmermann, J. L., Boussac, A., and Rutherford, A. W. (1993) The Manganese Center of Oxygen-evolving and Ca(2+)-Depleted Photosystem II: a Pulsed EPR Spectroscopy Study. *Biochemistry*, **32**, 4831-4841
- Zweygart, W., Thanner, R., and Lubitz, W. (1994) An Improved TM110 ENDOR Cavity for the Investigation of Transition Metal Complexes. *J. Magn. Reson. A*, **109**, 172-176

# ACKNOWLEDGEMENTS

I would like to express my gratitude and thanks to my doctoral advisors, Dr. habil. Günter Laßmann and Dr. Friedhelm Lendzian, for all their support during the course of my doctoral work. Their great enthusiasm and knowledge, as especially expressed in our fruitful discussions, inspired me in my work. I would also like to thank Dr. Günther Bleifuß, my friend and fellow doctoral student in this project, who gave me a warm welcome and introduction to Germany and contributed work on EPR and ENDOR spectroscopy and simulations, which served as a basis for his dissertation and were also vital to my work. I would also like to extend my thanks to Prof. Dr. Wolfgang Lubitz for providing me with the opportunity to work in his most knowledgeable and exciting interdisciplinary team. I am also indebted to all the members of his team, and the whole of the Max-Volmer-Laboratory for their professional help as well as many enjoyable lunches in the TU refectory and other social occasions, particularly Dr. Wulf Hofbauer, who lent his expertise in high-field EPR as well as his companionship, Dr. Rafael Jordan and Irene Geisenheimer for their useful tips on the job and their friendship off the job, Stefanie Foerster for the indispensable anaerobic line and taking care of our sample pools, Uwe Fink for giving helpful tips on chromatography, Dr. Frank Müh, who joined our group and helped with fermentor growth and optical spectroscopy, and Dr. Stephan Pötsch, who as a postdoc at the University of Stockholm started the work on R2-Y122H by making this mutant and doing the first EPR analyses as well as mass-spectroscopic analyses of our isotope labeled samples.

My thanks also go out to our cooperation partners, Prof. Dr. Astrid Gräslund, Dep. of Biochemistry and Biophysics, and Prof. Dr. Britt-Marie Sjöberg, Dep. of Molecular Biology and Functional Genomics, University of Stockholm, for their great interest and helpful suggestions and corrections for our manuscripts. Prof. Sjöberg and her team also taught me how to prepare the RNR proteins and let me use their facilities on several occasions. I am also indebted to Dr. Derek Logan, who provided the crystal structure of R2-Y122H at the Swiss-Norwegian-Beam-Lines, ESRF, Grenoble, while he was working in Prof. Dr. Pär Nordlunds lab at the Dep. of Biochemistry and Biophysics, University of Stockholm.

Dr. Thomas Eitingner at the Dep. of Microbiology, Humboldt University, for his valuable help with protein expression under minimal and anaerobic growth conditions, Dr. Rainer Zocher and his group at the Dep. of Biochemistry, TU-Berlin, for allowing me to perform experiments in their lab that could not have been carried out in our own lab.

I would also like to thank Prof. Dr. Kristoffer Andersson, University of Oslo, who first introduced me to the field of radical and metallo-enzymes, and provided the initial contacts to Berlin.

Finally, I want to thank Taryn Ann Galloway for her care and support, and her admirable patience.



# CURRICULUM VITAE

**Name:** Matthias Kolberg  
**Date of birth:** January 2, 1971  
**Place of birth:** Oslo  
**Marital status:** Single

## Education:

1976 - 1982	Primary school	Sofiemyr skole, Oppegård
1982 - 1986	Secondary school	Fløisbonn ungdomsskole, Oppegård
1986 - 1989	High school	Oppegård videregående skole, Oppegård
1989	Examen philosophicum	University of Oslo (UiO)
1989 - 1994	Cand. Mag.-degree	UiO
1994 - 1997	Cand. Scient.-degree	Department of Biochemistry, UiO
12/1997	Study for PhD degree (Dr. rer. nat.)	Technical University of Berlin
		Dept. of Biophysical chemistry and Biochemistry

## Military service:

1991 - 1992	Airport terminal assistant	Fornebu military airport, Oslo
01 - 05/1992	Representative for the conscripted personnel in Oslo	Headquarters Defence Command, Huseby, Oslo

## Professional experience:

1991 - 1996	Storehouse employee	A/S Jernia, Oppegård
1992 - 1996	Leader in a weekend relief home for disabled children	Ås commune, Ås
1995 - 1997	Course assistant KJB 200 - General Biochemistry KJB 220 - Biochemical Methods	Department of Biochemistry, UiO
08 - 11/1997	High school teacher 70 %, science	Nesodden videregående skole
08 - 11/1997	Technical assistant 50 %	Dept. of Anatomy, UiO